UNIVERSITÉ DE NANTES
FACULTÉ DES SCIENCES ET DES TECHNIQUES

———

ÉCOLE DOCTORALE 3MPL

Année 2014

Electrode formulation of Si and $LiNi_{0.5}Mn_{1.5}O_4$ for Li-ion battery applied to electric traction

———

THÈSE DE DOCTORAT
Discipline : Science des matériaux
Spécialité : physicochimie et électrochimie

Présentée
et soutenue publiquement par

Binh Phuong Nhan NGUYEN

Le 20 juin 2014, devant le jury ci-dessous

Président	M. Guy OUVRARD, professeur, Université de Nantes
Rapporteurs	Mme Séverine JOUANNEAU SI LARBI, docteur, CEA-LITEN
	Mme Laure MONCONDUIT, directeur de recherche, Université Montpellier 2
Examinateurs	M. Torbjörn GUSTAFSSON, assistant-professor, Uppsala University
	M. Dominique GUYOMARD, directeur de recherche, Université de Nantes
	M. Bernard LESTRIEZ, maître de conférences, Université de Nantes
Invité	M. Erik KELDER, assistant-professor, Technische Universiteit Delft

Directeur de thèse : M. Bernard LESTRIEZ

Encadrant de thèse : Mme Manuella CERBELAUD

Co-encadrant de thèse : M. Dominique GUYOMARD

Table of Contents

Résumé long en Français

La récente escalade des coûts des combustibles fossiles qui fournissent plus de 80% de l'énergie primaire, et une augmentation des préoccupations quant à la pollution de notre environnement ont tourné l'attention des chercheurs vers les systèmes d'énergie propre et de meilleure qualité. De plus, les réserves de combustibles fossiles sont limitées et ces ressources pourraient être consommées en moins de 100 ans, s'il n'y a pas de développement de ressources en énergies alternatives.

L'énergie durable est définie une énergie qui répond aux besoins des humaines et dont la production ne compromet pas la capacité des générations futures à répondre à leurs besoins. Les sources d'énergie durables comprennent toutes les sources d'énergie renouvelables et il y a une grande variété de choix, comme l'énergie marémotrice, l'énergie éolienne, l'énergie des vagues, l'énergie géothermique, l'hydroélectricité, l'énergie solaire, et la bio-énergie. Cependant, les sources d'énergie durable sont intermittentes (par exemple : éolienne, solaire et hydroélectrique) ou restreinte dans un endroit (par exemple, l'énergie géothermique) et nécessitent donc l'utilisation de technologies appropriées pour le stockage de l'énergie.

Les besoins en systèmes de stockage d'énergie ont continué d'augmenter de façon significative chaque année pendant la dernière décennie et resteront sans doute l'un des défis majeurs du 21e siècle. Les technologies de stockage de l'énergie, tels que les piles à combustible, supercondensateurs, piles rechargeables, etc ... ont joué un rôle important pendant les 20 dernières années. Parmi ces systèmes, la batterie lithium-ion rechargeable (LIB) est l'une des technologies de stockage d'énergie les plus prometteuses et occupe une position importante, car elle présente des densités d'énergie gravimétrique et volumétrique plus élevées et une plus grande longévité que les technologies de batteries rechargeables traditionnelles comme le plomb-acide, nickel-cd, etc. La LIB permet à le développement d'une gamme variée de transports propres (véhicules électriques hybrides, véhicules électriques, plug-in véhicules électriques hybrides) qui sont essentiels pour réduire la dépendance au pétrole fossile et d'améliorer la qualité de vie humaine.

Une batterie Li-ion est composée de plusieurs cellules électrochimiques montées en série et/ou en parallèle. Une cellule électrochimique conventionnelle se compose d'une électrode positive et négative séparées par un séparateur imbibé d'un électrolyte (sel de lithium dans un solvant organique) qui interdit le contact entre les deux électrodes. La plupart

des LIB commerciales sont basées sur des composés d'intercalation qui peuvent accueillir réversiblement des ions Li^+ dans leur structure au niveau des électrodes positives et négatives. L'électrode à potentiel plus élevé est désignée comme l'électrode positive et est généralement à base d'un oxyde de métal de transition contenant du lithium (par exemple, $LiCoO_2$, $LiMnO_4$, $LiNi_{1/3}Co_{1/3}Mn_{1/3}O_2$, $LiFePO_4$ ...), alors que les matières carbonées sont utilisées comme électrodes négatives. Cependant, ces matériaux présentent des limitations (par exemple en termes de densité d'énergie, de limitation des ressources, de coût élevé, de sécurité ...).

Table 1. Caractéristiques des matières utilisées pour les électrodes des batteries lithium-ion commerciales. Adapté de Kinson et al. [1].

Électrode	**Potentiel moyen vs. Li/Li+ (V)**	**Capacité spécifique, (mAh/g)**	**Avantages**	**Désavantages**
Les électrodes positives				
$LiCoO_2$	3.9	140	Meilleur compromis (capacité, tension, cyclabilité, densité, durée de vie, sécurité) [2]	Limites de ressources et coût de Co, faible capacité
$LiNi_{0.8}Co_{0.15}Al_{0.05}O_2$	3.8	180–200	Hautes capacité et tension	Limites de ressources et coût de Co et de Ni, sécurité
$LiNi_{1/3}Mn_{1/3}Co_{1/3}O_2$	3.8	160–170	Haute tension, sécurité modérée	Limites de ressources et coût de Co et de Ni
$LiMn_2O_4$ et dérivés	4.1	100–120	Faible coût et abondance de Mn, haute tension, sécurité modérée	Durée de vie limitée, faible capacité
$LiFePO_4$	3.45	170	Excellente sécurité, cyclabilité, faible coût et abondance de Fe, faible toxicité	Tension et capacités modérées (faible densité énergétique)
Les électrodes négatives				
Graphite	0.1	372	Cyclabilité, abondance	Faible densité d'énergie; irréversibilité au 1er cycle due à la formation de l'interface électrolyte solide
$Li_4Ti_5O_{12}$	1.5	175	Matériau "Zéro variation de volume", bonne cyclabilité	Tension et capacité modérées (faible densité énergétique)

Ce travail de thèse s'inscrit dans le cadre d'un projet européen de collaboration (EuroLiion, coordonné par E. Kelder de l'Université Technique de Delft), qui vise à développer une nouvelle cellule Li-ion pour la traction avec une densité d'énergie élevée (> 200Wh/kg), à faible coût (par exemple, <150Euro/kWh) et sécuritaire. Bien que les cellules Li-ion aient déjà de bonnes performances, des recherches approfondies pour les optimiser sont

[1] Kinson C. Kam and Marca M. Doeff, Material Matters, 2012 (7) 4.
[2] S. Levasseur, « Matériaux d'électrode positive pour batteries Li-ion : récents développements industriels », GFECI 2008.

encore nécessaires. De nombreux matériaux utilisés sont trop chers et ne répondent pas aux critères de sécurité pour l'application automobile, aux critères des normes environnementales (par exemple, $LiCoO_2$), ne peuvent pas atteindre des critères de densité d'énergie (par exemple, le graphite), ou sont brevetés de telle façon que leur commercialisation dans le monde est entravée (par exemple, $LiFePO_4$). Par conséquence, un *shift* du carbone au silicium de capacité beaucoup plus élevée à l'électrode négative, et des composés à base de cobalt ou de fer au $LiNi_{0.5}Mn_{1.5}O_4$ (LNMO) qui fonctionne à un potentiel plus élevé, sont proposés. Cependant, il existe un problème important qui est la grande variation de volume du silicium lors de son alliage et de-alliage avec le lithium, ce qui conduit à de fortes contraintes mécaniques et la perte subséquente de contacts électriques dans l'électrode composite. Cela nécessite une nouvelle formulation de l'électrode quant au liant, et de l'électrolyte. Un autre problème crucial est l'existence de réactions parasites qui se produisent en permanence au cours du cyclage des deux matériaux, le silicium et LNMO.

$LiPF_6$ est le sel commercial standard des batteries lithium-ion actuelles. Parmi ses inconvénients les plus importants, on note la formation d'acide fluorhydrique (HF). HF est responsable de réactions délétères sur les solvants de l'électrolyte, de la corrosion des matériaux d'électrodes conduisant à des problèmes de sécurité avec l'émission de produits chimiques toxiques. En ce qui concerne l'aspect de la sécurité, 4,5-dicyano-2-(trifluorométhyl) imidazolate de lithium (LiTDI) apparait être l'un des candidats les plus intéressants pour remplacer $LiPF_6$ en raison de sa stabilité thermique supérieure (jusqu'à 250°C), sa stabilité dans les conditions humides, sa stabilité électrochimique (jusqu'à 4.6 V vs Li/Li^+) et de son moindre coût. En outre, le nombre de transport du lithium plus élevé devraient permettre de meilleures performances en puissance. Gagner sur toutes ces propriétés est particulièrement important pour les applications à haute énergie, telle que les véhicules électriques.

Ce travail a commencé en 2011 dans ce contexte. Les objectifs de cette thèse sont de (i) définir les formulations optimisées, d'abord avec du silicium nanométrique puis avec du LNMO micrométrique, tous les deux étant produits par l'Université Technologique de Delft, (ii) de fabriquer des électrodes pragmatiques pour l'industrie, c'est à dire avec une grande capacité de surface de ~3 mAh cm^{-2}. Ces formulations doivent posséder de bonnes performances électrochimiques et des compositions autorisant leur fabrication sur les machines d'enduction semi-industrielles du CEA, qui était le partenaire en charge de la production de cellules prototypes silicium/LNMO pour une évaluation plus approfondie de cette technologie par d'autres partenaires. Pour atteindre ces objectifs, le procédé d'élaboration (broyage à billes, agitation magnétique, enduction, séchage, calandrage) a été étudié, les

suspensions d'électrodes ont été caractérisées (évaluation du comportement rhéologique, mesure de la distribution de taille des particules, du potentiel zêta, essais de décantation), les électrodes ont été caractérisées (analyse de la texture par SEM-EDX, mesures de porosité, analyse des comportements mécanique, électrique et électrochimique). Dans les formulations obtenues, le silicium est couplé avec la carboxyméthylcellulose (CMC), l'acide poly (acrylique-co-maléique) (PAMA) et un graphène de faible coût; et le LNMO micrométrique est couplé avec du poly(fluorure de vinylidène) (PVDF) et des nanofibres de carbone (CNF). Dans les deux cas, des essais d'enduction de ces formulations d'électrodes ont été réalisés sur les lignes de production à l'échelle pilote au CEA, ce qui a conduit à des évolutions dans la composition des formulations.

Cette thèse est divisée en trois chapitres qui décrivent les travaux effectués; les résultats obtenus, et sont ensuite résumés dans les conclusions finales. Un bref aperçu des différents chapitres est donnée ci-dessous.

Le chapitre 1 donne une vue générale sur les LIB et décrit les principaux composants d'une batterie. Les matériaux pour électrodes positives et négatives connus sont décrits et leurs avantages et inconvénients sont mis en évidence. Dans ce chapitre, une attention particulière a été consacrée au deux matériaux actifs du projet, le silicium (couplé couplé avec de la CMC dans une électrode positive) et le $LiNi_{0.5}Mn_{1.5}O_4$.

Le chapitre 2 donne les appareillages et méthodes utilisés au cours du travail expérimental, la caractérisation des matières premières. Les procédés de préparation d'électrodes sont aussi décrits.

Le chapitre 3 donne une description historique et concise de tous les efforts réalisés visant à atteindre les objectifs du projet EuroLiion. Les principales étapes et réalisations sont présentées. Cependant, ils sont scientifiquement examinés et interprétés dans les quatre articles suivants :

I. Manufacturing of industry-relevant silicon negative composite electrodes for lithium ion-cells, B. P. N. Nguyen, S. Chazelle, M. Cerbelaud, W. Porcher and B. Lestriez, Journal of Power Sources, 262 (2014) 112-122.
II. Nanosilicon-Based Thick Negative Composite Electrodes for Lithium Batteries with Graphene as Conductive Additive, B. P. N. Nguyen, N. A. Kumar, J. Gaubicher, F. Duclairoir, T. Brousse, O. Crosnier, L. Dubois, G. Bidan, D. Guyomard and B. Lestriez., Adv. Enery Mater., 3 (2013) 1351.

III. Analogy between electrochemical behaviour of thick silicon granular electrodes for lithium batteries and fine soils micromechanics, B. P. N. Nguyen, J. Gaubicher and B. Lestriez, Electrochimica Acta, 120 (2014) 319–326.

IV. Manufacturing of industry-relevant $LiNi_{0.5}Mn_{1.5}O_4$ positive composite electrodes for lithium ion-cells, B. P. N. Nguyen, N. Mariage, R. Fredon, E. Kelder, and B. Lestriez, written and to be submitted.

Le travail a repris dans cette thèse vise à définir les formulations optimisées, d'abord avec nanométrique Si puis pour LNMO micrométrique afin de fabriquer des électrodes pertinentes pour l'industrie avec une cible capacité de ~ 3mAh/cm². Ces formulations doivent posséder de bonnes performances électrochimiques et des propriétés satisfaisantes pour le traitement sur les machines de couvert semi-industrielles du CEA, qui étaient le partenaire en charge de la production de cellules prototypes LNMO/Si pour une évaluation plus approfondie de cette technologie par d'autres partenaires au sein du projet de EuroLiion. Les résultats acquis peuvent être résumés en trois points :

1. Formulation optimisée d'électrode négative à base de silicium (Si)

Il n'a pas été possible de réaliser par enduction des électrodes de capacité surfacique ~3mAh/cm² avec le silicium commercial (70-80m²/g, 10-150nm, Alfa Aesar) en raison de sa surface spécifique élevée, contrairement ai silicium fourni par le CEA (14m²/g, 150nm). Par ailleurs, les suspensions d'électrode à base de ce silium et avec les formulations optimisées sont stables et leurs des propriétés rhéologiques convenables par rapport aux paramètres du procédés au CEA. Les bandes présentent une bonne adhésion/cohésion et une bonne homogénéité à toutes les échelles (quelques microns jusqu'à quelques cm).

En accord avec des travaux antérieurs [3,4] une bien meilleure performance électrochimique pour les électrodes préparées dans un tampon pH 3 par rapport à l'eau est obtenue avec le liant carboxyméthyle cellulose (CMC). Deux formulations d'électrodes optimisées ont été identifiées :

- La 1ère formulation est à base noir de carbone et d'acide Poly(acrylique-co-maléique) (PAMA) qui joue le rôle de dispersant. Cette formulation permet à une électrode de fonctionner plus de 400 cycles à 1200mAh/g_Si (800mAh/g_electrode) (CE 99.3%) et

[3] D. Mazouzi, B. Lestriez, L. Roué, D. Guyomard, J. Electrochem. Solid-State Lett. 12 (2009) A215.
[4] B. Lestriez, S. Bahri, I. Sandu, L. Roué, D. Guyomard, Electrochem. Commun., 9 (2007) 2801.

à la capacité surfacique ~ 2.1mAh/cm^2. En outre, le rôle de l'agent dispersant PAMA a été étudié. Celui-ci contribue à l'obtention d'une homogénéité élevée pour l'électrode préparée au laboratoire, en particulier en ce qui concerne la distribution du carbone noir qui est plus uniforme, ce qui conduit à une amélioration de la cyclabilité et du rendement faradique en demi-cellule, mais également facilite l'incorporation de l'additif conducteur à l'échelle pilote. Cependant, la quantité de PAMA a été optimisée à 1.7wt% dans la composition de l'électrode sèche, car une adsorption compétitive se produit entre PAMA et CMC par rapport aux particules de carbone noir, avec une exclusion de la CMC qui est préjudiciable au pontage mécanique des particules. Lorsque cette première formulation a été transférée à l'échelle pilote, il a été constaté l'obligation d'ajouter un liant élastomère (un copolymère de caoutchouc styrène-co-butadiène (SBR) et de calandrer l'électrode pour atteindre une tenue mécanique de l'électrode suffisante. L'ajout de SBR joue un rôle important pour atteindre la longévité en cyclage, mais le calandrage est très préjudiciable et réduit la durée de vie significativement.

- La 2ème formulation utilise le graphène au lieu du noir de carbone comme additif conducteur, ce qui permet une amélioration significative des performances électrochimiques, quelles que soient les conditions de cyclage. La capacité surfacique de 3.1mAh.cm^{-2}_electrode est maintenue après 200 cycles (CE 99.5 +/- 0.4%) quand le cyclage est réalisée avec une limitation de la capacité. Sans limiter la capacité, la capacité de décharge est stabilisée à 1800mAh/g^{-1} _Si après 200 cycles (~3.1mAh.cm^{-2}). Les propriétés électrochimiques n'ont pas été améliorées lors du mélange de nanofibres de carbone avec le graphène. SBR a été ajouté quand la 2ème formulation a été traitée à l'échelle pilote.

Pour les deux formulations préparées au CEA, une moins bonne performance électrochimique a été obtenue par rapport à celle préparée à l'IMN. Ce résultat pourrait être attribué aux différentes échelles concernées. A l'IMN, les électrodes sont préparées à l'échelle du laboratoire qui implique de petites quantités et un enchaînement des opérations mélange/coulée rapide ainsi qu'un séchage lent, tandis qu'au CEA les électrodes sont préparées à une plus grande échelle, qui implique des quantités beaucoup plus grandes avec un temps d'attente entre la fin du mélangeage qui est préjudiciable à la stabilité et par conséquent l'homogénéité des suspensions. Par ailleurs, sur la ligne pilote le séchage est beaucoup plus rapide, ce qui peut avoir une conséquence quant à l'organisation dans l'électrode.

2. Formulation optimisée de l'électrode positive sur la base de LNMO

L'influence de la formulation de l'électrode composite sur la cyclabilité des électrodes LNMO a été étudiée. Le meilleur résultat est une rétention de la capacité de 80% après 300 cycles à la capacité surfacique de ~3mAh.cm^{-2}. La chute de la capacité due à des réactions parasites à haut potentiel est ralentie en augmentant la quantité d'additifs du conducteurs ou par substitution d'une partie du noir de carbone par des nanofibres de carbone. Cependant, la cyclabilité des électrodes avec une capacité surfacique élevée est fortement diminuée, ce qui pourrait être attribué à l'existence d'un plus grand nombre de défauts en termes de percolation électronique ou d'adhésion et de cohésion avec des électrodes épaisses. En outre, les électrodes préparées dans de l'eau avec la CMC comme liant montrent une cyclabilité plus faible que celles préparées dans de la N-méthyl-pyrrolidone (NMP) avec le PVDF.

3. La conception de Li-ion cellule complète - des tests préliminaires

Les résultats préliminaires de cellules complètes assemblées avec les électrodes optimisées dans ce travail sont prometteurs. Trois cellules ayant une capacité de surface différente (1.0, 1.5 et 2.0mAh/cm²) peuvent fonctionner avec l'électrolyte 90wt% LP30 10wt% FEC. La longévité a été améliorée de manière significative si l'électrode de silicium est entièrement lithié/delithiée dans une cellule contenant une contre électrode de lithium métal avant l'assemblage dans une cellule contenant l'électrode de LNMO : plus de 100 cycles avec une capacité réversible de 100mAh/g_LNMO (CE 99.1%).

General introduction

Nowadays, energy production and consumption that rely on the combustion of fossil fuels have had severe impacts on world economics and ecology. All the areas such as greenhouse gases, global warming, pollution, the environment, etc. are affected and must be seriously considered when producing energy for our daily demands, especially from the transport sector. Our common sources of energy including coal, oil, and natural gas are non-renewable. Once a deposit or source of these is depleted it cannot be readily replenished.

The recent cost escalation of fossil fuels which supply over 80 percent of primary energy, and increased concern over pollution from these combustible power sources, have turned the attention of researchers towards clean and better energy systems. In addition, fossil fuels reserves are finite and these resources could be consumed in less than 100 years if there is no development of alternative resources. This is the only way to preserve world's economic efficiency and more importantly, to save our living environment.

Sustainable energy is defined as the provision of energy that meets the needs of the present without compromising the ability of the future generations to meet their needs. Sustainable energy sources include all renewable energy sources and there is a wide variety of choices, such as tidal power, wind energy, wave power, geothermal energy, hydroelectricity, solar energy, and bio-energy. However, the sources of sustainable energy are intermittent (e.g., wind, solar and hydro) or restricted in location (e.g., geothermal) and therefore require the use of suitable technologies for energy storage.

The needs for advanced energy storage systems has kept growing significantly each year for the past decade and will doubtlessly remain one of the major challenges of the 21st century. Energy storage technologies, such as fuel cells, supercapacitors, rechargeable batteries, etc… have played an important role for the last 20 years. Among these systems, rechargeable lithium-ion battery (LIB) is one of the most promising energy storage technologies and occupies a major position because it exhibits higher gravimetric and volumetric energy density and longer lifespan than traditional rechargeable batteries technologies like lead-acid, Ni-Cd, etc. LIB could enable a various range of clean transportations (hybrid electric vehicles, electric vehicles, Plug-in Hybrid Electric Vehicles)

which are essential to reduce the fossil oil dependency and improve quality of our living environment.

A Li-ion battery is composed of several electrochemical cells connected in series and/or in parallel. A conventional electrochemical cell is composed of a positive and negative electrode separated by a separator soaked with an electrolyte (lithium salt in an organic solvent) which prohibits contact between two electrodes. Most of the commercial LIBs are based on intercalation compounds that can reversibly host Li^+ ions in their structure at both negative and positive electrodes. The electrode with higher potential is referred to as the positive electrode and generally it consists of a lithium containing transition metal oxide (e.g., $LiCoO_2$, $LiMnO_4$, $LiNi_{1/3}Co_{1/3}Mn_{1/3}O_2$, $LiFePO_4$…) whereas carbonaceous materials are used as negative electrodes which have lower potential. However, these materials are still facing some drawbacks (e.g., energy density criterion, environmental issues, resource limitations, high cost, safety…).

Table 1. Characteristics of Commercial Battery Electrode Materials. Adapted from Kinson et al. [1].

Electrode	Average Potential vs. Li/Li^+ (V)	Specific Capacity, (mAh/g)	Advantages	Disadvantages
Positive Electrodes				
$LiCoO_2$	3.9	140	Best compromise (capacity, voltage, cyclability, density, shelf life, security) [2]	Cost and resource limitations of Co, low capacity
$LiNi_{0.8}Co_{0.15}Al_{0.05}O_2$	3.8	180–200	High capacity and voltage, excellent rate performance	Safety, cost and resource limitations of Ni and Co
$LiNi_{1/3}Mn_{1/3}Co_{1/3}O_2$	3.8	160–170	High voltage, moderate safety	Cost and resource limitations of Ni and Co
$LiMn_2O_4$ variants	4.1	100–120	Low cost and abundance of Mn, high voltage, moderate safety, excellent rate performance	Limited cycle life, low capacity
$LiFePO_4$	3.45	170	Excellent safety, cycling, and rate capability, low cost and abundance of Fe, low toxicity	Low voltage and capacity (substituted variants), low energy density
Negative Electrodes				
Graphite	0.1	372	Long cycle life, abundant	Relatively low energy density; inefficiencies due to Solid Electrolyte Interface formation
$Li_4Ti_5O_{12}$	1.5	175	"Zero strain" material, good cycling and efficiencies	High voltage, low capacity (low energy density)

A. Average

[1] Kinson C. Kam and Marca M. Doeff, Material Matters, 2012 (7) 4.

[2] S. Levasseur, « Matériaux d'électrode positive pour batteries Li-ion : récents développements industriels », GFECI 2008.

This PhD work is part of an European collaborative project (EuroLiion, coordinated by E. Kelder from Delft Technical University), which aims to develop a new Li-ion cell for traction purposes with high energy density (>200Wh/kg), low cost (e.g., <150Euro/kWh) and safety improvement. Although Li-ion cells have already good performances, extensive research and development is still required. Many materials used before are too expensive, do not meet current safety, environmental standards (e.g., $LiCoO_2$), cannot reach the energy density criterion (e.g., graphite), or to be patented hindering worldwide commercialization (e.g., $LiFePO_4$). As a result, a shift from carbon to much higher capacity silicon-based anode and from cobalt or iron-based to higher voltage $LiNi_{0.5}Mn_{1.5}O_4$ (LNMO) cathode is proposed. However, a crucial problem is the large volume changes undergone upon alloying and de-alloying of silicon with lithium, which results in strong mechanical strains and subsequent loss of electrical contacts in the composite electrode. This requires a new electrode formulation with respect to the binder, electrolyte salt, solvent and composition. Another crucial problem is the parasitic reactions that continuously occur upon cycling the two materials, silicon and LNMO.

$LiPF_6$ is the commercial standard salt of lithium ion batteries today. Among the most important drawbacks of the $LiPF_6$ used in electrolyte system is the formation of hydrogen fluoride (HF). HF is responsible for deleterious reaction on carbonate solvents, corrosion of electrode materials leading to safety problems then release to toxic chemicals. As for the safety aspect, Lithium 4,5-dicyano-2-(trifluoromethyl)imidazolate (LiTDI) shows one of the most interesting candidate in stead of $LiPF_6$ due to its superior thermal stability (up to 250°C), stability in case of moisture presence, electrochemical stability (up to 4.6 V vs. Li/Li^+) and possible material savings when used in electrolyte. In addition, higher transference numbers of LiTDI should provide higher charge-discharge cycle yield. That is especially beneficial for high-energy applications, such as EVs or grid energy storage. [3,4,5]

This work has started in 2011 in this context. The scope of this thesis was to define the optimized formulations, first with nanometric Si and then for micrometric LNMO, both produced by the Delft Technical University, to make industry-relevant electrodes, i.e. with high surface capacity of ~3 mAh cm^{-2}. These formulations must possess good electrochemical performance and satisfactory properties for processing on semi-industrial coating machines of

[3] L. Niedzicki, G.Z. Zukowska, M. Bukowska, P. Szczecinski, S. Grugeon, S. Laruelle, M. Armand, S. Panero, B. Scrosati, M. Marcinek, W. Wieczorek, Electrochim. Acta 55 (2010) 1450.
[4] L. Niedzicki, M. Kasprzyk, K. Kuziak, G.Z. Zukowska, M. Armand, M. Bukowska, M. Marcinek, P. Szczecinski, W. Wieczorek, J. Power Sources 192 (2009) 612.
[5] L. Niedzicki, S. Grugeon, S. Laruelle, P. Judeinstein, M. Bukowska, J. Prejzner, P. Szczecinski, W. Wieczorek, M. Armand, J. Power Sources 196 (2011) 8696.

the CEA, which was the partner in charge of producing silicon/LNMO prototype-cells for further evaluation of this technology by other partners. In order to achieve this purpose, elaboration process (ball milling, magnetic stirring) and characterization of electrode slurries (e.g., rheological behaviour, particle size distribution, zeta potential measurements, settling tests) was investigated together with elaboration (e.g., tape casting, calendaring, drying) and characterization of the electrodes (e.g., texture analysis through SEM, EDX observations, measurements of porosity, mechanical, electrical and electrochemical behaviours). In the achieved formulations, silicon is coupled with carboxymethyl cellulose (CMC), poly (acrylic-co-maleic) acid (PAMA) and a cheap graphene at the negative side; and micrometric LNMO material is coupled with polyvinylidene fluorine (PVdF) and carbon nanofibres (CNF) at the positive side. In both cases, trials were done to coat electrodes with these formulations on the pilot producing line at the CEA, which led to some evolutions in the composition of the formulations for further production at semi-industrial level.

This thesis is divided into 3 chapters that describe the work carried out; the results obtained, and are then summarized in the final conclusions. A brief outline of the different chapters is given below.

Chapter 1 provides a general overview on LIBs and describes the main components in a battery. Materials for positive and negative electrodes studied so far are described and their advantages and drawbacks are pointed out. In this chapter, a special attention has been devoted to silicon negative electrodes couped with carboxymethyl cellulose (CMC) as a binder and $LiNi_{0.5}Mn_{1.5}O_4$ positive electrodes.

Chapter 2 summarizes the materials and methods used during the experimental work, characterization of raw materials and the electrode preparation processes are described.

Chapter 3 gives a historical, factual and concise description of all efforts intended in this work to reach the objectives of the EuroLiion project. The main steps and achievements are reported. However, they are scientifically discussed and interpreted in four articles.

The following papers written in the frame of this thesis are referred to in the text by their Roman numerals, I-IV.

I. Manufacturing of industry-relevant silicon negative composite electrodes for lithium ion-cells, B. P. N. Nguyen, S. Chazelle, M. Cerbelaud, W. Porcher and B. Lestriez, Journal of Power Sources, 262 (2014) 112-122.

II. Nanosilicon-Based Thick Negative Composite Electrodes for Lithium Batteries with Graphene as Conductive Additive, B. P. N. Nguyen, N. A. Kumar, J. Gaubicher, F. Duclairoir, T. Brousse, O. Crosnier, L. Dubois, G. Bidan, D. Guyomard and B. Lestriez., Adv. Enery Mater., 3 (2013) 1351.

III. Analogy between electrochemical behaviour of thick silicon granular electrodes for lithium batteries and fine soils micromechanics, B. P. N. Nguyen, J. Gaubicher and B. Lestriez, Electrochimica Acta, 120 (2014) 319–326.

IV. Manufacturing of industry-relevant $LiNi_{0.5}Mn_{1.5}O_4$ positive composite electrodes for lithium ion-cells, B. P. N. Nguyen, N. Mariage, R. Fredon, E. Kelder, and B. Lestriez, written and to be submitted.

Chapter 1. General aspects on lithium-ion batteries

1.1 Brief historical development of battery systems

Batteries are energy storage systems that convert chemical energy stored in electrodes to electrical energy via electrochemical reduction-oxidation (redox) reactions. The term battery often refers to a single electrochemical cell, particularly in the case of the primary systems but it can equally well refer to a multiple of electrochemical cells that are connected in series and/or in parallel. An electrochemical cell consists of two coupling electrodes for energy storage (positive and negative electrodes), and a conductive electrolyte (either solid or liquid) in which the two electrodes are electrically connected. When a battery is connected to a load, the electrochemical potential between the two electrodes drives electrons from negative electrode to the positive electrode, and induce redox reactions within the electrodes for continuous electron release. There are two types of battery systems: the primary batteries which are discharged once and then discarded and secondary (or rechargeable) batteries, which have reversible redox reactions and are capable of restoring their original chemical composition after charge and discharge for over hundreds of thousands of cycles. [1,2]

The first primary battery was made in 1800 by Alessandro Volta (voltaic cell) by assembling a pile of alternate silver (or brass or copper) and zinc (or tin) discs, with each pair of dissimilar metals separated from the next by a piece of cloth which was saturated with brine. The next step was the invention of the well-known Daniell cell in 1836 by John Daniell. The cell consists of a copper pot filled with a copper sulfate solution in which an unglazed earthenware container filled with sulfuric acid and a zinc electrode was immersed (Figure 1-1). A subsequent major advance was made by the French chemist Georges

[1] Butterworlth-Heinemann, Rechargeable Batteries Applications Handbook, Elsevier, 1998
[2] R. M. Dell and D. A. J. Rand, Understanding batteries, RCS, 2011

Leclanché in 1866. Leclanché cell is a battery that consisted of a zinc anode and a manganese dioxide cathode wrapped in a porous material, dipped in a jar of ammonium chloride solution. The first rechargeable battery, which is still widely used in automobiles, was lead – acid battery (Pb/PbO_2 in H_2SO_4) invented by Gaston Planté in 1859.

After these inventions, many studies were performed to develop electrochemical systems with different electrodes using various combinations of materials. The 20th century has seen major advances in battery science and technology. Primary zinc (Leclanché) batteries have been greatly improved by the invention of alkaline batteries; while advances in materials technology and cell design have revolutionized the performance of the lead-acid battery. Entirely new secondary batteries have been developed and commercialized, notably the nickel-metal-hydride battery and the lithium ion battery.

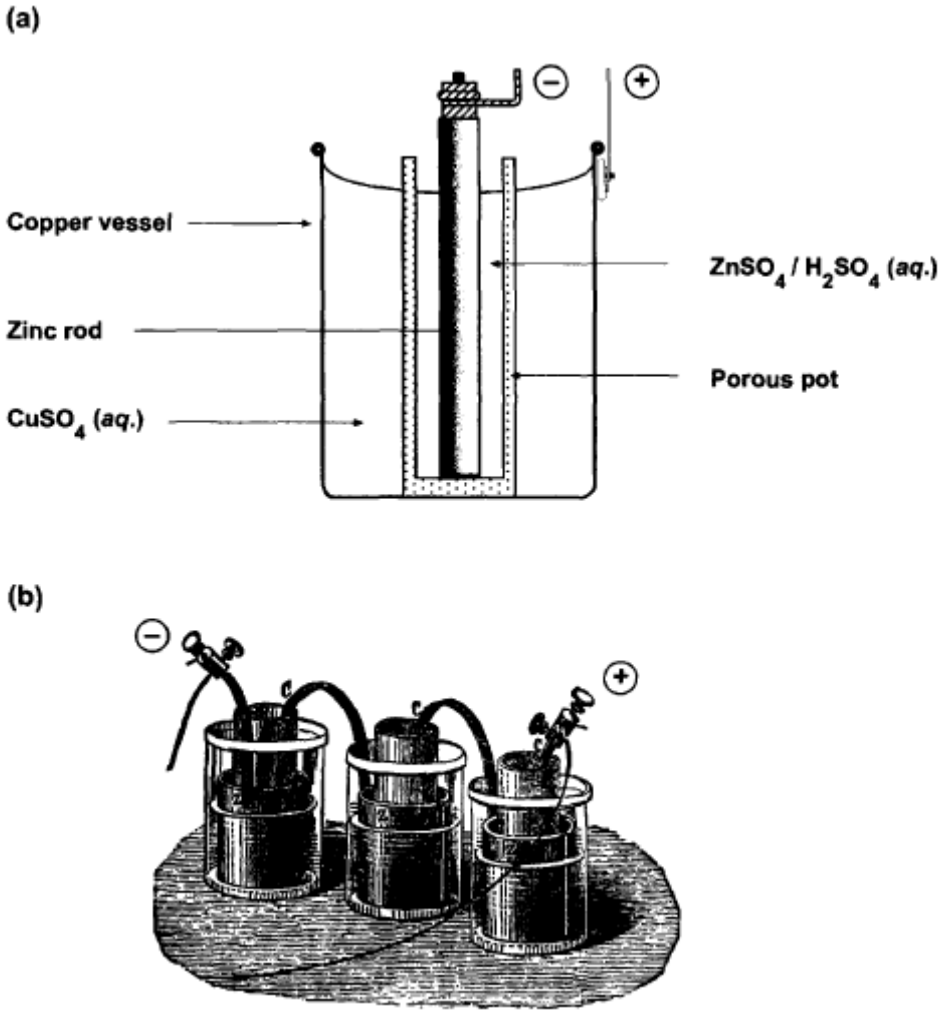

Figure 1-1. (a) Construction of a Daniell cell; (b) early illustration of Daniell cells [2]

1.2 Li-ion battery

Lithium is an interesting element because it is the lightest metallic element with atomic weight M_w= 6.941 g.mol^{-1} thereby, it presents the lowest density of 0.54g.cm^{-3}. It has also the smallest electrochemical equivalent weight at 3.86Ah.g^{-1}, as well as the lowest standard electrode potential at -3.04V versus standard hydrogen electrode. All of these characteristics make lithium as a negative electrode material with high specific energy and low voltage. Lithium batteries have both the highest volumetric and gravimetric energy density among known technologies applied, including lead-acid, nickel-cadmium, nickel metal hydroxide and other systems as plotted in Figure 1-2 [3].

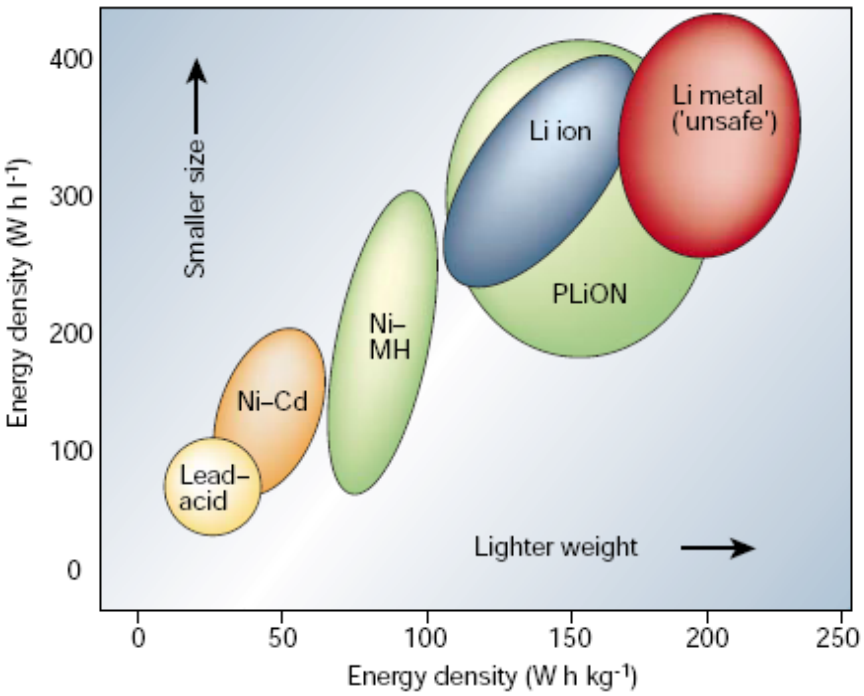

Figure 1-2. Comparison of different battery technologies in terms of volumetric and gravimetric energy density [3]

However, the main drawback of these systems was associated to the use of the highly reactive metallic lithium as the negative electrode and the formation of dendrites upon cycling, thus leading to safety problem because of internal short circuits.

The development of LIBs has resulted from the use of lithium anode material, and the safety problems in the application of lithium batteries promoted the great development of lithium-ion batteries. LIBs are different from lithium batteries. In contrast to lithium batteries, which

[3] J. M. Tarascon, M. Armand, Nature, 414 (2001) 359-367

contain metallic lithium as negative electrode and present severe security issues during operation, LIBs contain no metallic lithium. Lithium is found only in ionic form in electrolytes and in atomic scale in oxide cathode materials and when intercalated into carbon anodes [4].

The main working principle of LIBs is the reversible electrochemical reaction leading to insertion/extraction of lithium ions in the electrode materials along with parallel electron addition/removal which flows through the external circuit.

The structure of a conventional LIB consists of a positive active material, mainly lithium transition metal oxide, a carbon based negative active material, an electrolyte consisting of a solution of a lithium salt in a mixed organic solvent (e.g. $LiPF_6$ in a mixture of ethylene carbonate and dimethyl carbonate) and a porous polymeric separator soaked in electrolyte to avoid electrical contact between the electrodes. A typical LIB configuration is represented in Figure 1-3. The battery voltage is derived from the electrochemical potential difference between the positive and negative electrode. The performance of LIBs depends on the intrinsic properties of the materials used for the cell assembly. When a Li-ion cell is charged, an external electrochemical force is applied and the positive material is oxidized while, correspondingly, the negative one is reduced. In this process, lithium ions are de-intercalated from the positive material and intercalated into the negative material. Simultaneously, the compensating electrons travel in the external circuit and are accepted by the host to balance the reaction. The discharge reverses this process and the electrons pass around the external circuit to power various systems. A general reaction scheme during charging/discharging of a conventional LIB with $LiCoO_2$ cathode and graphite anode is presented below [5,6].

[4] R. J. Brodd, K. R. Bullock, R. A. Leising, R. L. Middaugh, J. R. Miller, E. Takeuchi, J. Electrochem. Soc. 151, K1-K11 (2004)
[5] J. O. Besenhard, Handbook of battery materials, Wiley, 1999
[6] D. S. Ginley, D. Cahen, Fundamentals of Materials for Energy and Environmental Sustainability, Cambridge University Press, 2012

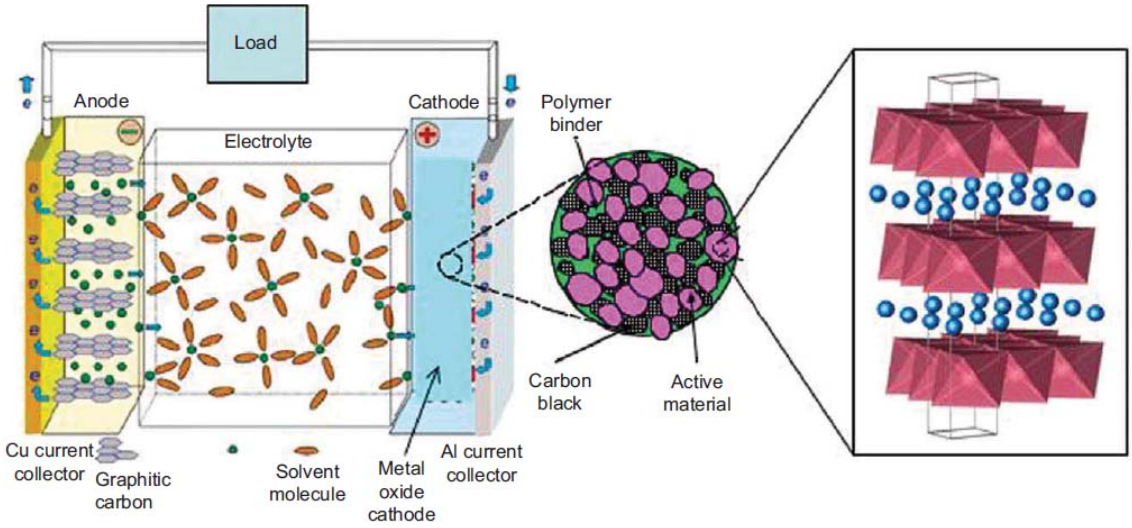

Figure 1-3. Schematic representation of a lithium-ion battery based on intercalation reactions [6]

$$\text{Positive electrode} : LiCoO_2 \underset{\text{discharge}}{\overset{\text{charge}}{\rightleftharpoons}} Li_{1-x}CoO_2 + xLi^+ + xe^-$$

$$\text{Negative electrode} : C + xLi^+ + xe^- \underset{\text{discharge}}{\overset{\text{charge}}{\rightleftharpoons}} Li_xC$$

$$\text{Overall cell} : LiCoO_2 + C \underset{\text{discharge}}{\overset{\text{charge}}{\rightleftharpoons}} Li_xC + Li_{1-x}CoO_2$$

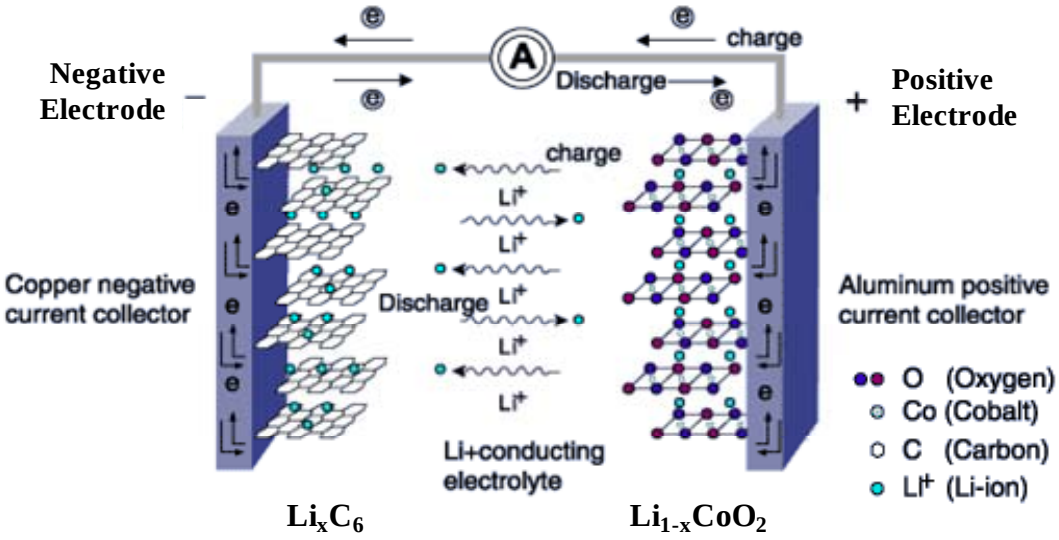

Figure 1-4. Scheme of the electrochemical process in a Li-ion cell

1.3 The composition of the composite electrode

The composite electrodes usually consist of a mixture of active material (AM) grains with non-electro active additives. This additive is generally composed of a conducting agent (C) of electrons and a polymeric binder (B). This system allows an effective electronic and ionic transfer in the electrode. The polymer ensures a good mechanical ability of the electrode and the porosity inside the electrode must be sufficient to allow a good circulation of the Li^+ ions of the liquid electrolyte toward the AM and vice versa. The composite electrode must, moreover, be chemically and electrochemically stable in order to provide an acceptable lifespan. It is essential that the current collectors and the interfaces between the various solid phases of the composite prematurely do not lose their properties by film formation of passivation which harms the quality of the electrical contacts inside the battery. The composite electrode must also have a good mechanical cohesion and adherence with respect to the collector current in the presence of liquid electrolyte and the changes of volume which happens at the time of the insertion and the deinsertion of lithium in the AM. [7]

The choice of the non-electroactive additives and the processing of the composite electrode are both very important to reach optimal performance of the composite electrode. For battery optimum energy density, the amount per unit mass and the volume of the non-electroactives need to be minimized. In order to meet the preset targets, a very efficient AM, an optimum formulation and a very good processing condition are obligatory.

1.3.1 The non-electroactive conducting agents

Electro-conductive additives are employed to compensate for the low intrinsic conductivity of AM to allow them to perform effectively. They contribute to an increase in the capacity, the charge-discharge rate and the cycle life of LiB. Conductive carbon particulates, such as acetylene black (AcB), ketjen black (KB), super P (SP) and graphite (G) are usually employed for this purpose. However, since these additives have relatively large surface area, their reactivity with electrolyte and organic solvents can be high, causing parasitic reactions [8,9].

For high power performance it is also reported that the type of conducting additive plays a role. The addition of vapour grown carbon nanofibres (VGCF) reduces the electron

[7] B. Lestriez, C. R. Chimie 13 (2010) 1341-1350.
[8] I. Fransson, T. Eriksson, K. Edstrom, T. Gustafsson, J. O. Thomas, J. Power Sources, 101 (2001) 1.
[9] P. P. Prosini, S. Passerini, 2001, Eur. Polym. J., 37 (2001) 65.

conducting resistance, hence increases the utilization of active materials during high-current discharge [10]. By substituting carbon nanotubes (CNTs) for AcB or VGCF, much conductive additives and binder could be saved, and the cathode with only a small amount of conductive additives shows excellent rate capacity [11]. More recently, graphene has attracted a lot of interest [12,13] and by using reduced graphene oxide (rGO) instead of CB as the conductive additive for nano silicon based negative composite electrodes, a significant improvement of the electrochemical performance was confirmed, whatever the cycling conditions [14,15].

1.3.2 The binder

The binder additive brings its mechanical strength to the electrode. It must bind the active material and conductive additive particles altogether and with current collector for long battery cycle life. It allows for a good electric contact between the electrode and the current collector, and it ensures the electrode a sufficient liquid electrolyte uptake to provide internal ionic percolation. Furthermore, it also has to be chemically and electrochemically stable in the operating potential window. From the viewpoint of energy density, it is necessary to minimize the amount of binder. Insuring the right quantity of the binder is also very important. In addition to the type of binder and non electroactive conducting additive, the ratio of the binder and the conductive agent is reported to play an important role in high rate performance of the composite electrodes. [7]

Polymers with large electrochemical stability (up to 5V vs. Li^+/Li) such as polytetrafluoroethylene (PTFE) or PVdF based have been most widely adopted as a binder for composite electrodes in LiB. Remarkable improvement resulted from the use of a copolymer of vinylidene fluoride with hexafluoropropylene (PVdF-HFP), which lead to the widely accepted polymer Li-ion technology [16].

A new trend is now being developed to substitute the PVdF-based binders. Reasons brought up include high cost, insufficient mechanical properties (strong binding strength, but low flexibility) and safety aspects. Suitable alternative binders such as silica, poly(acrylonitrile-methyl methacrylate), poly(methyl methacrylate) (PMMA), aromatic

[10] Mao-Sung Wu, Jyh-Tsung Lee, Pin-Chi Julia Chiang, Jung-Cheng Lin, J Mater Sci., 42 (2007) 259
[11] Wang Guoping, Zhang Qingtang, Yu Zuolong, Qu MeiZheng, Solid State Ionics, 179 (2008) 263
[12] Sun, Y., Wu, Q., Shi, G., Energy and Environmental Science, 4 (2011) 1113-1132
[13] G. Kucinskis, G. Bajars, J. Kleperis, J. Power Sources 240 (2013) 66-79
[14] B. P. N. Nguyen, N. A. Kumar, J. Gaubicher, F. Duclairoir, T. Brousse, O. Crosnier, L. Dubois, G. Bidan, D. Guyomard, B. Lestriez, Adv. Energy Mater., 3 (2013) 1351
[15] B. P. N. Nguyen, J. Gaubicher, B. Lestriez, Electrochimica Acta, 120 (2014) 319–326
[16] J. M. Tarascon, A. S. Gozdz, C. Schmutz, F. Shokoohi, P. C. Warren, Solid State Ionics, 86 (1996) 49-54

polyimides, and polypyrrole have been identified. The combination of several binders has also been found interesting [17,18,19,20,21].

1.3.3 Active materials for Li-ion batteries

Rechargeable LIB is one of the most promising energy storage technologies to enable a various range of clean transportations. To meet requirements of these automotive applications, it is necessary to find suitable electrode materials for LIBs which satisfy several conditions: (i) high specific capacity ($Ah.kg^{-1}$) and volumetric capacity ($Ah.L^{-1}$); (ii) high difference of potential between positive and negative electrodes; (iii) high safety and environmental standards.

A wide range of materials for both negative and positive electrodes is displayed in Figure 1-5. In this scheme, the x axis shows the capacity ($Ah.kg^{-1}$) while the y axis represents the potential (Volt) of each material compared to metallic Lithium which has the most electropositive standard potential compared to hydrogen (-3.04V vs SHE). For the negative materials, the lower the potential (vs. Li/Li^{+}) the better, and the opposite is true for positive materials. It's obvious that there are huge differences in capacity between Li metal and the other negative materials, while the safety problem caused by dendrite growth is serious. Another issue is that the capacities of negative materials are generally much higher than those of positive materials, the real specific capacities of negative materials in commercial use are lower. As a result, extensive research and development on both positive and negative materials are equally important. [3]

[17] D. Aurbach, M. D. Levi, O. Lev, J. Gun, L. Rabinovich, J. Appl. Electrochem., 28 (1998) 1051
[18] S. S. Zhang, T. R. Jow, J. Power Sources, 109 (2002) 422
[19] N. Ohta, T. Sogabe, K. Kuroda, Carbon, 39 (2001) 1434
[20] Y. H. Huang, K. S. Park, J. B. Goodenough, J. Electrochem. Soc., 153 (2006) A2282
[21] D. Guy, B. Lestriez, D. Guyomard, Adv. Mater., 16 (2004) 553

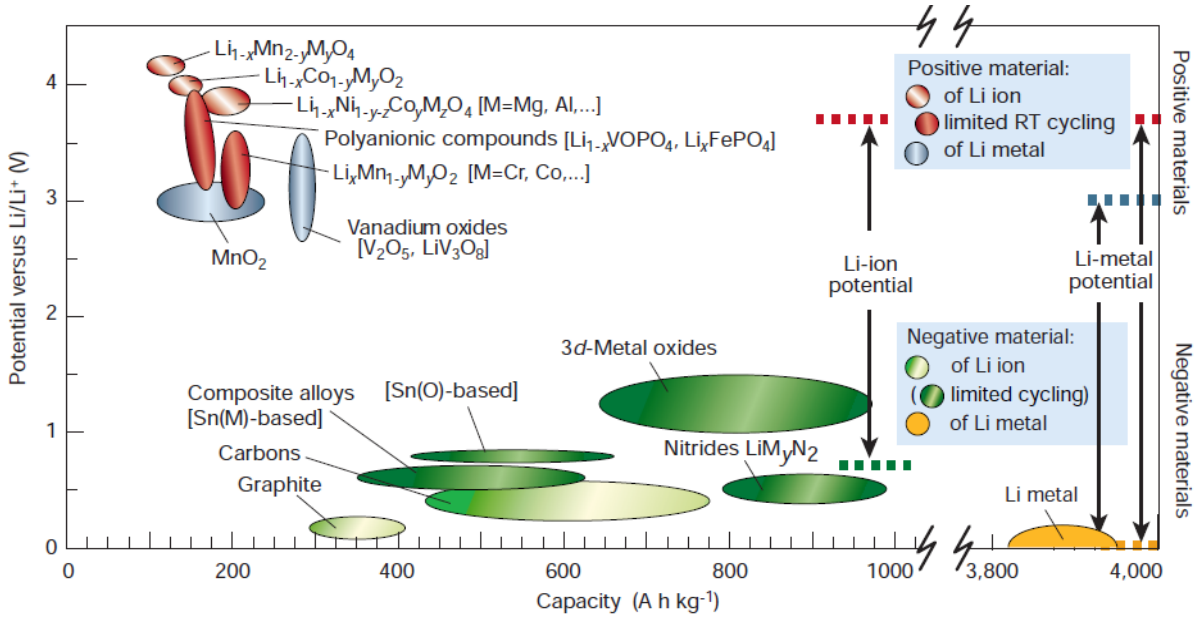

Figure 1-5. Voltage versus capacity for positive and negative electrode materials [3]

To successfully be used as negative or positive electrodes in a Li-ion battery, the active material (AM) has to fulfill following conditions [22]:

Negative electrode AM	Positive electrode AM
The material should contain a readily reducible/oxidizable ion	
The material should have reversible reaction with Li and possess minimal or reversible structures changes upon insertion/extraction of the Li leading to a good cycle life	
The insertion/extraction process has to be fast to achieve high power density	
The material may host several Li-ions per formula unit in order to deliver high capacity	
Low operating potential and close to potential of Li/Li^+ to obtain a wide cell voltage	High operating potential to obtain a wide cell voltage
The AM must have good compatibility with electrolyte solution	
The AM must have good electronic and lithium-ion conductivity	
The raw materials must be abundant, the synthesis must be simple and low cost	
The AM must be thermally and chemically stable, and environmentally benign.	

However, the existing AM rarely or never meet all the above requirements at the same time.

1.3.3.1 Active materials for negative electrodes

Metallic lithium was always seen as the first choice as negative electrode material in lithium batteries during the 1970s and early 1980s due to its high specific capacity of 3860 $mAh.g^{-1}$. However, safety issues due to dendrite formation upon cycling could lead to short circuiting.

[22] M. S. Whittingham, Chem. Rev. 2004, 104, 4271- 4301

This made researchers turned to alternative negative materials that could store lithium at low potentials vs. Li/Li^+. [3] The successful commercial application of LIBs is mainly attributed to the use of lithium compounds instead of Li metal as negative material.

Research on negative materials addresses a wide variety of compounds able to support the reversible storage of lithium. They can be classified into three main families according to their reaction mechanism with Lithium: [23]

(1) Intercalation/de-intercalation materials, such as carbon based materials, porous carbon, carbon nanotubes, graphene, TiO_2, $Li_4Ti_5O_4$, etc;

(2) Alloying/de-alloying materials such as Si, Ge, Sn, Al, etc;

(3) Conversion materials like transition metal oxides (TMOs) (Mn_xO_y, NiO, Fe_xO_y, CuO, Cu_2O, MoO_2 etc.), metal sulphides, metal phosphides and metal nitrides (M_xX_y; here X=S, P, N).

Table 1-1. Most common negative materials used for LIBs [23]

Active anode material	Theoretical capacity ($mAh.g^{-1}$)	Advantages	Common issues
Insertion/de-insertion materials			
A. Carbonaceous			
a. Hard carbon	200-600	➢ Good working potential	❖ Low coulombic efficiency
b. CNTS	1116	➢ Low cost	❖ High voltage hysteresis
c. Graphene	780/1116	➢ Good safety	❖ High irreversible capacity
B. Titanium oxides		➢ Extreme safety	❖ Very low capacity
a. $LiTi_4O_5$	175	➢ Good cycle life	❖ Low energy density
b. TiO_2	330	➢ Low cost	
		➢ High power capability	
Alloying materials			
a. Silicon	3579	➢ High specific capacity	❖ Large irreversible capacity
b. Germanium	1624	➢ High energy density	❖ Huge capacity fading
c. Tin	993	➢ Good safety	❖ Poor cycling
d. Antimony	660		
e. Tin oxide	790		
f. SiO	1600		
Conversion materials			
a. Metal oxides (Fe_2O_3, Fe_3O_4, CoO, Co_3O_4, Mn_xO_y, Cu_2O/CuO, NiO, Cr_2O_3, RuO_2, MoO_2/MoO_3 etc.)	500-1200	➢ High capacity ➢ High energy ➢ Low cost ➢ Environmentally compatibility	❖ Low coulombic efficiency ❖ Unstable SEI formation ❖ Large potential hysteresis ❖ Poor cycle life
b. Metal phosphides/sulfides/nitrides (MX_y; M=Fe, Mn, Ni, Cu, Co etc. and X=P, S, N)	500-1800	➢ High specific capacity ➢ Low operation potential & Low polarization than counter oxides	❖ Poor capacity retention ❖ Short cycle life ❖ High cost of production

Currently graphite is used as a negative electrode in the commercial LIBs. There are ongoing efforts to increase the capacity of carbon. Different chemical and mechanical preparation and modification methods, such as pyrolytic processes, mechanical milling etc. are employed on

[23] S. Goriparti, E. Miele, F. D. Angelis, E. D. Fabrizio, R. P. Zaccaria, C. Capiglia, J. Power Sources, 257 (2014) 421-443

the carbon negative electrodes for improving their electrochemical properties. The capacities of 450 $mAh.g^{-1}$ are now achievable, as compared to conventionally used graphite which has a practical capacity of 350 $mAh.g^{-1}$. [3]

Another commonly used negative electrode material is the spinel $Li_4Ti_5O_{15}$ which shows attractive characteristics in terms of extremely high safety, high power capability and no volume change but having disadvantages such as low theoretical capacity of 175$mAh.g^{-1}$ and higher operating voltage (1.55V vs. metallic lithium). Besides, transition metal oxides (TMOs) are also alternative materials to carbon. Although they have large capacities (from 500-1200$mAh.g^{-1}$, depending on the TMO), there are still a number of shortcomings, such as limited cycle life, low coulumbic efficiency and large potential hysteresis. [23]

Lithium-metal alloys are the most promising negative materials because they can store a large amount of lithium which results in higher specific capacities compared to graphite. There are numerous elements studied that can be alloyed with lithium and they are mainly in group IIIA (B, Al, Ga, In), group IVA (Si, Sn, Ge, Pb) and group VA (As, Sb, Bi) of the periodic table. Among them, much attention has been devoted to Si because of its promising electrochemical performances (large capacity, moderate operating potential) as well as its intrinsic characteristics (abundance, cost, toxicity, etc). However, poor performance of Si based electrodes is a major issue due to dramatic volume expansion and shrinkage during lithiation and delithiation, respectively. This volumetric variation results in conduction network breakage. [23,24]

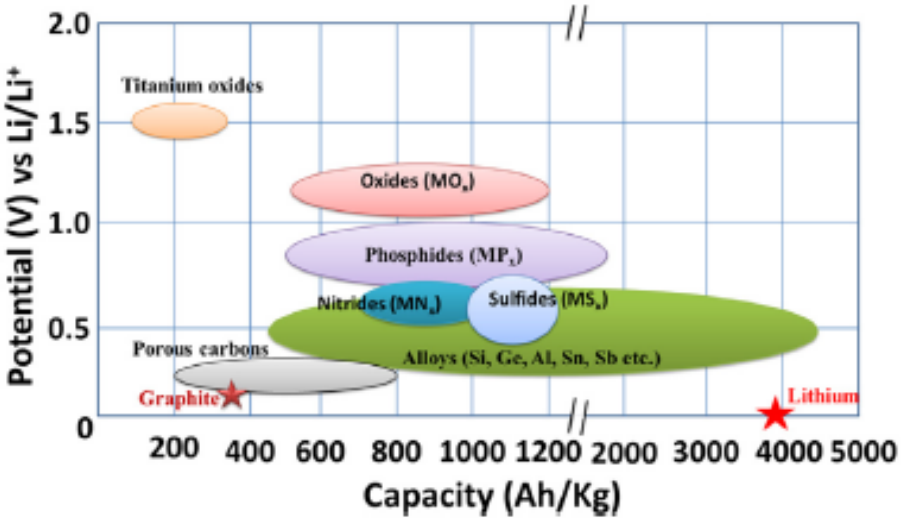

Figure 1-6 . Schematic illustration of negative materials for LIBs [23]

[24] W.J. Zhang, J Power Sources. 196 (2011) 13-24.

Several strategies have been undertaken to overcome large volume changes upon insertion and extraction of lithium ions into Si such as modification of Si morphologies/structures, use of additional phase to buffer the volume expansion, limitation of the capacity etc.[24] The main research of this work is to define the optimized formulations coupled with carboxymethyl cellulose (CMC) in order to cope at the molecular scale with the expansion and contraction of Si upon cycling. This will be exhaustively studied in the following section.

1.3.3.2 Active materials for positive electrodes

The choice of the positive electrode material is crucial in terms of cost, safety, specific energy and energy density of the battery. The energy density is determined by the reversible capacity and operating voltage, which are mostly determined by intrinsic chemistry of the materials, such as the effective redox couples and maximum lithium ion concentration in the active material.

Conventional positive electrode materials include layered compounds $LiMO_2$ (M=Co, Ni, Mn, etc.), spinel compounds LiM_2O_4 (M=Mn, Fe, etc.), and olivine compounds $LiMPO_4$ (M=Fe, Co, Mn, etc.). Figure 1-7 compares the gravimetric energy densities of different cathode materials that are currently under investigations. While some materials such as $LiFeBO_3$ and $LiFeSO_4F$ are already approaching their theoretical energy densities, for other materials including conventional layered and spinel compounds, significant gaps are still present between their theoretical and practical energy densities. These materials with promising theoretical properties have high potentials as the candidates of future generation LIB cathode, however, their rate capacity and cycling performances still need much improvement before they can be commercialized. [25]

[25] B. Xu, D. Qian, Z. Wang, Y. S. Meng, Mater. Sci. Eng. R 73 (2012) 51

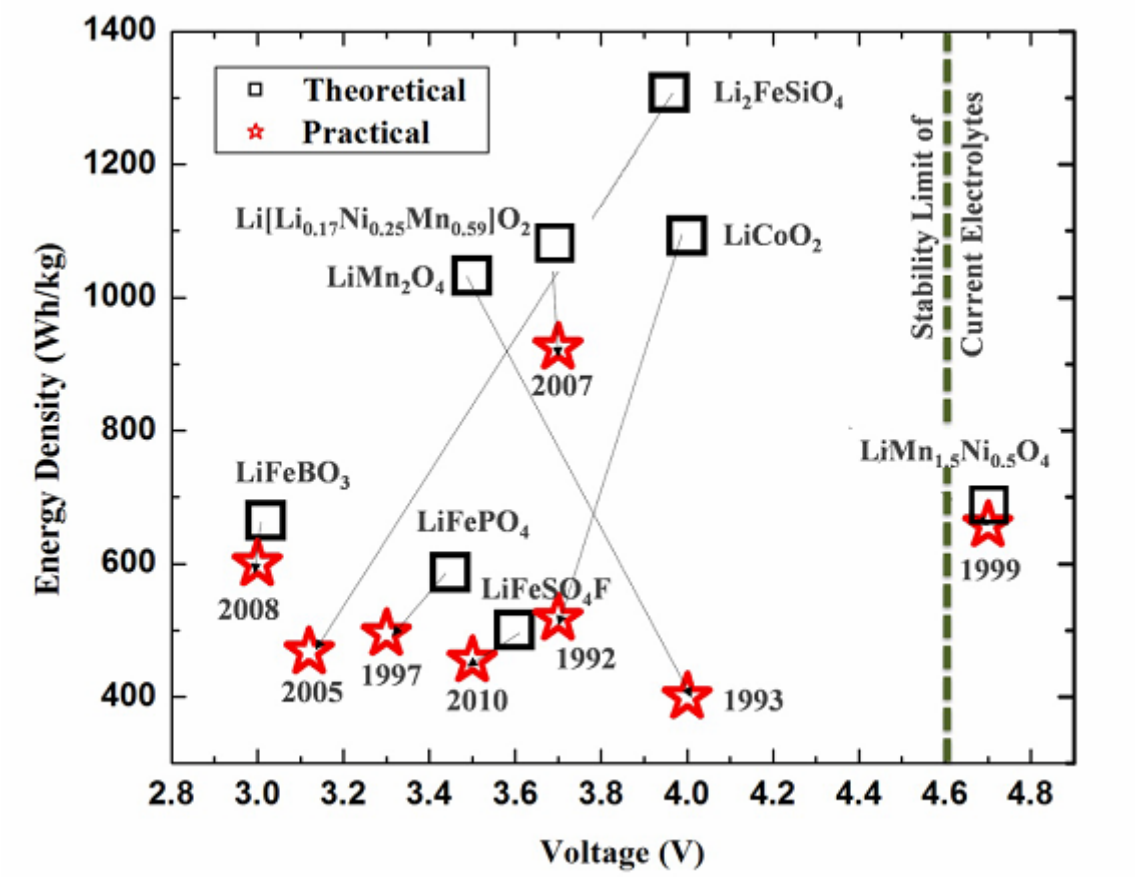

Figure 1-7. Theoretical and practical gravimetric energy densities of different positive electrode materials [25]

The ideal structure of layered compound $LiMO_2$ is shown in Figure 1-8. [25] The oxygen anions (omitted for clarity in the figure) form a close-packed fcc lattice with cations located in the 6-coordinated octahedral crystal site. The MO_2 slabs and Li layers are stacked alternatively. Although the conventional layered oxide $LiCoO_2$ has been commercialized as the LIB cathode for twenty years, it can only deliver about 140mAh/g capacity which is half of its theoretical capacity. Such limitation can be attributed to the intrinsic structural instability of the material when more than half of the Li ions are extracted. On the other hand, the presence of toxic and expensive Co ions in $LiCoO_2$ has introduced the environmental problem as well as raised the cost of the LIB.

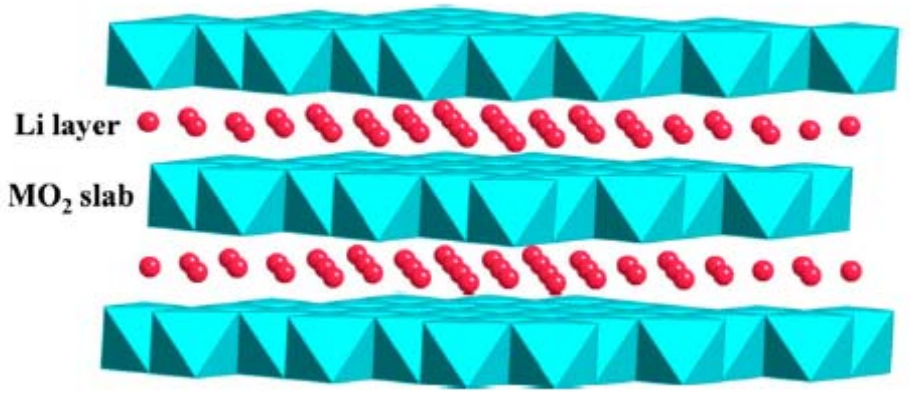

Figure 1-8. Crystal structure of layered $LiMO_2$ (blue: transition metal ions; red: Li ions) [25]

For improvement, Co ions in $LiCoO_2$ can be substituted by other transition metal ions such as Ni and Mn. The new substitutions can reduce the cost of the materials and make the materials more environmentally friendly by eliminating the use of Co ions which are expensive and toxic. One of the most promising candidates is so called Li excess nickel manganese layer oxides $Li[Ni_xLi_{1/3-2x/3}Mn_{2/3-x/3}]O_2$. The compounds were first reported in 2001 [26] and can be expressed as a composite of two end members of $Li[Li_{1/3}Mn_{2/3}]O_2$ and $LiNi_{1/2}Mn_{1/2}O_2$. A reversible capacity of 250mAh.g^{-1} can be obtained routinely [27]

The structure of olivine compound $LiMPO_4$ (typically $LiFePO_4$) is shown in Figure 1-9. It consists of a distorted hexagonal close-packed (hcp) framework containing lithium and iron in octahedral sites and phosphorous in tetrahedral sites. There are two distinct octahedral positions in the lattice: the M1 site on an inversion centre and the M2 site on a mirror plane. Li usually occupies M1 sites and Fe occupies M2 site whereas P occupies tetrahedral sites. The FeO_6 octahedra are linked together by corner sharing in the b, c plane. The FeO_6 octahedra share edges with PO_4 tetrahedra, while lithium is located in a second set of octahedral sites, with LiO_6 octahedra chain sharing edges. It generates preferential pathways for rapid one-dimensional lithium ion conductivity [28,29], as shown in Figure 1-9.

[26] Z. Lu, D.D. MacNeil, and J.R. Dahn, Electrochemical and Solid-State Letters, 2001. 4(11) A191-A194
[27] C. R. Fell, K. J. Carroll, M. Chi, and Y. S. Meng, Journal of The Electrochemical Society, 157 (11), A1202-A1211
[28] C. Delacourt, P. Poizot, J. M. Tarascon, C. Masquelier, *Nature Materials*, 4 (2005) 254
[29] D. Morgan, A. Van der Ven, G. Ceder, *Electrochemical and Solid-State Letters*, 7 (2004) A30

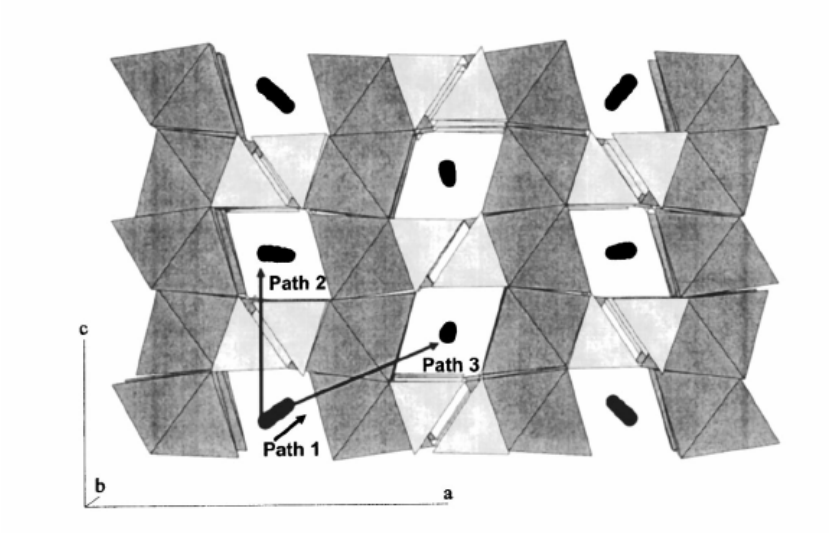

Figure 1-9. The olivine structure. The Fe octahedral are dark gray, the P tetrahedral are light gray, and the Li atoms are black. Back lines show candidate diffusion paths for Li ions [29].

Lithium metal phosphate ($LiMPO_4$) has a very stable structure [30,31], due to covalent bonding between oxygen and phosphor, and $LiFePO_4$ was developed as a response to economic and environmental concerns. $LiFePO_4$ offers several advantages, such as a theoretical specific capacity of $170mAh.g^{-1}$ and a high flat voltage versus charge characteristic at 3.4 V vs. lithium. However, the major issue with $LiFePO_4$ is the poor lithium ion and electronic conduction.

The structure of LiM_2O_4 spinel is shown in Figure 1-10. [25] The oxygen framework of LiM_2O_4 is the same as that of $LiMO_2$ layered structure. M cations still occupy the octahedral site but 1/4 of them are located in the Li layer, leaving 1/4 of the sites in transition metal layer vacant. Li ions occupy the tetrahedral sites in Li layer that share faces with the empty octahedral sites in the transition metal layer. The structure is based on a three dimensional MO_2 host and the vacancies in transition metal layer ensure the three dimensional Li diffusion pathways.

[30] M. Armand et al. U.S Patent No. US7457018B2
[31] A.K. Padhi, K.S. Nanjundaswamy, J.B. Goodenough, *J. Electrochem. Soc*. 144 (1997) 1188

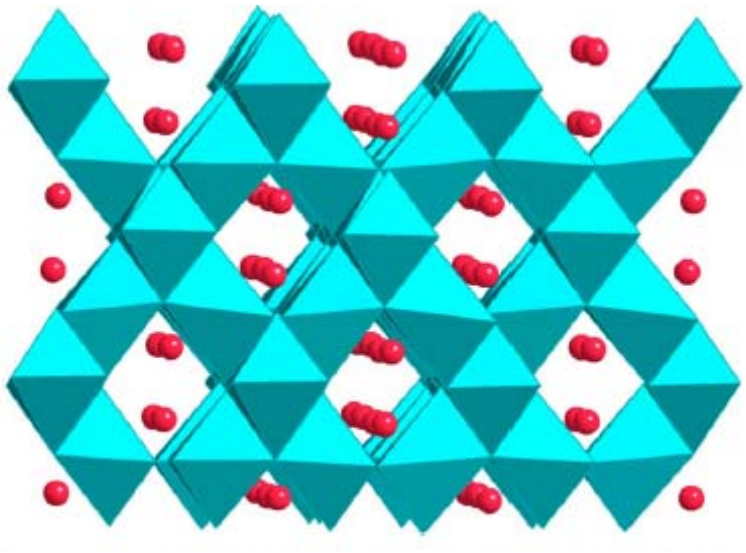

Figure 1-10. Crystal structure of spinnel LiM_2O_4 (blue: transition metal ions; red: Li ions)

The spinel $LiMn_2O_4$ was proposed as the cathode of the lithium ion battery by Thackeray et al. in 1983 [32,33,34], but the material was found to encounter sever capacity fading problems. Its three dimensional cubic spinel structure provides wider 3D-pathways for Li [35], but it also presents intrinsic disadvantages in terms of structural changes and limited cycle life, as well as Mn dissolution due to disproportionation of Mn^{3+} into Mn^{4+} and Mn^{2+} at high potentials [36,37].

Substituting Mn with other metal ions has been used as an important approach to improve cycling performance of spinel materials. Multiple dopants including inactive ions such as Mg, Al, Zn etc. [38,39,40], first row transition metal ions such as Ti, Cr, Fe, Co, Ni, Cu, etc. [41,42,43,44,45] and rare earth metal ions such as Nd, La, etc. [46,47,48] have been

[32] M. Thackeray, W.I.F. David, P.G. Bruce, and J.B. Goodenough, Materials Research Bulletin, 1983 18 (4) 461-472.
[33] J.B. Goodenough, M. Thackeray, W.I.F. David, and P.G. Bruce, Revue de Chimie Minerale, 1984. 21 (4) 435-455.
[34] W.I.F. David, M. Thackeray, P.G. Bruce, and J.B. Goodenough, Materials Research Bulletin, 1984. 19 (1) 99-106.
[35] M. Thackeray, L. de Picciotto, A. de Kock, P. Johnson, V. Nicholas, K. Adendorff, Journal of Power Sources, 1987 21 (1) 1-8.
[36] R. Gummow, A. de Kock, and M. Thackeray, Solid State Ionics. 1994 69 (1) 59-67.
[37] D. Jang, Y. Sin and S. Oh, 1996, Journal of Electrochemical Society, 148 (7) 2204-2211.
[38] R.J. Gummow, A. Dekock, and M.M. Thackeray, Solid State Ionics, 1994. 69 (1) 59-67.
[39] K.-S. Lee, S.-T. Myung, H.J. Bang, S. Chung, and Y.-K. Sun, Electrochimica Acta, 2007. 52 (16) 5201-5206.
[40] Y.J. Lee, S.H. Park, C. Eng, J.B. Parise, and C.P. Grey, Chemistry of Materials, 2002. 14 (1) 194-205.
[41] L. Hernan, J. Morales, L. Sanchez, and J. Santos, Solid State Ionics, 1999. 118 (3-4) 179-185.
[42] J.H. Kim, S.T. Myung, C.S. Yoon, S.G. Kang, and Y.K. Sun, Chemistry of Materials, 2004. 16 (5) 906-914.

investigated and $LiNi_{0.5}Mn_{1.5}O_4$ shows the best overall electrochemical performances among the above. $LiNi_{0.5}Mn_{1.5}O_4$ could meet the above requirements for LIB applications such as high potential, high energy density, good cycle life and high rate capability. The theoretical capacity of the $LiNi_{0.5}^{II}Mn_{1.5}^{IV}O_4/Ni_{0.5}^{IV}Mn_{1.5}^{IV}O_4$ redox system is $146.7mAhg^{-1}$, which corresponds to the oxidation of nickel (II) to nickel (IV) at 4.7–4.75V vs. Li^+/Li (Figure 1-11). This high potential gives a specific energy equivalent to $700Wh\ kg^{-1}$ of active material, referring to Li metal (in comparison with conventional materials such as $LiCoO_2$, $LiMn_2O_4$ and $LiFePO_4$). [49]

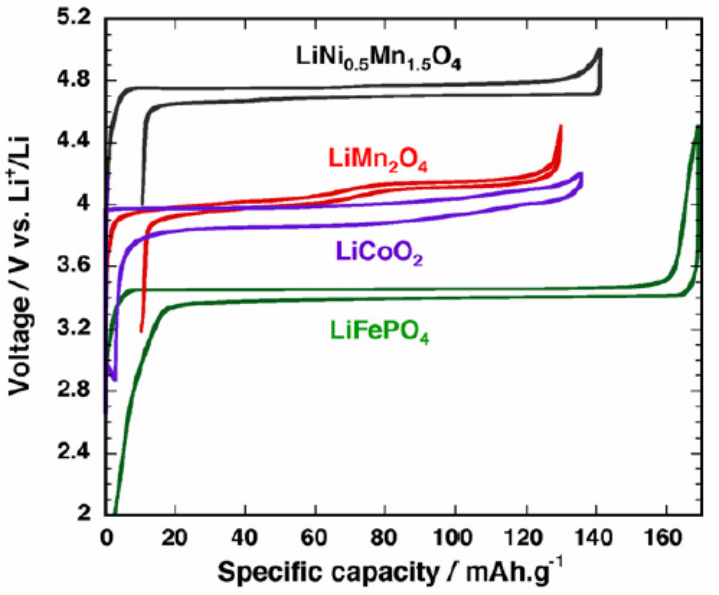

Figure 1-11. Voltage vs. capacity for several positive electrode materials, obtained under normal cycling conditions (20°C, C/5 rate) [49]

[43] G.H. Li, H. Ikuta, T. Uchida, M. Wakihara, Journal of The Electrochemical Society, 1996. 143 (1) 178-182
[44] J. Molenda, J. Marzec, K. Swierczek, W. Ojczyk, M. Ziemnicki, M. Molenda, M. Drozdek, and R. Dziembaj, Solid State Ionics, 2004. 171 (3-4) 215-227
[45] T. Ohzuku, S. Takeda, and M. Iwanaga, Journal of Power Sources, 1999. 81-82 90-94
[46] R. Singhal, S.R. Das, M.S. Tomar, O. Ovideo, S. Nieto, R.E. Melgarejo, and R.S. Katiyar, Journal of Power Sources, 2007. 164(2) 857-861
[47] J. Tu, X.B. Zhao, D.G. Zhuang, G.S. Cao, T.J. Zhu, and J.P. Tu, Physica B-Condensed Matter, 2006. 382 (1-2) 129-134
[48] T. Yang, J.H. Jia, L. Ding, and M.C. Zhang, Electrochimica Acta, 2003. 48 (5) 569-573
[49] S. Patoux, L. Daniel, C. Bourbon, H. Lignier, C. Pagano, F. Le Cras, S. Jouanneau, S. Martinet, Journal of Power Sources, 189 (2009) 344–352

1.4 The formulation of silicon-based negative electrodes: how mitigating volume variations

1.4.1 Carboxymethylcellulose (CMC) as a potential binder for Si-based electrodes

Most studies of Si anodes have involved the use of carboxymethylcellulose (CMC) and poly vinylidene fluoride (PVDF) binders. The most conventional binder PVDF used for the batteries is likely attached to Si particles via weak Van der Waals forces only (between its fluorine atoms and hydrogen atoms). [7] It fails to accommodate large changes in spacing between the particles during battery cycling. It quickly becomes incompetent in keeping the particles together and maintaining electrical conductivity within the anode, which is required for battery operation. Until now, the use of PVDF or CMC-based binders as well as their modifications were the focus of numerous studies. Noteworthy amounts of data have been achieved for CMC binders, which typically display a better performance and can be considered to be the state of the art in this field.

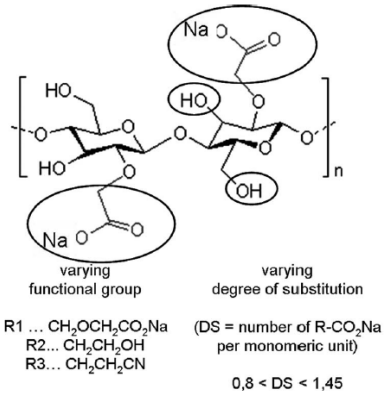

Figure 1-12. Structure of CMC with centres for modification [54]

CMC is a linear polymeric derivative of cellulose, consisting of β-linked glucopyranose residues with various degree of substitution (DS) of OH groups by CH_3COO^- carboxy-methyl groups. Because there are three OH groups per C_6 ring, the maximum DS being equal to 3 since each monomeric unit hangs three hydroxyl groups. As a salt (sodium for example), the substituting groups are dissociated in water forming anionic groups responsible for the aqueous solubility of Na-CMC in contrast with insoluble cellulose.

A few works by Lee et al. and Drofenik et al. demonstrated that Na-CMC could perform as an efficient binder for the graphite negative electrodes. [50,51] Moreover, these

[50] J.-H. Lee, U. Paik, V. A. Hackney, and Y.-M. Choi, J. Electrochem. Soc., 152, A1763 (2005).

studies suggested that the reducible OH groups do not contribute to irreversible capacity and eventually participated in the formation of more favourable SEI layer than PVdF. More recently, a specific reactivity of CMC towards the electrolyte ($LiPF_6$ in a mixture of carbonate solvents) could be evidenced by El Ouatani et al., resulting in the formation of new species that contribute to the surface film composition. [52] Based on these previous works, CMC was investigated as a potential binder for Si-based electrodes. [53,54,55]

Buqa et al. and Liu et al. reported that the cycle life of Si-based electrodes was improved by using an aqueous binder containing the elastomeric styrene butadiene rubber (SBR) and Na-CMC. [53,54] However, Li et al. showed that the use of the stiffer CMC binder resulted in better capacity retention than the SBR + CMC combination and PVdF. [55] Li et al. compared the performance of CMC (2200, Daicel, Japan) and SBR/CMC (1:1) binders for micro-Si (7-8 μm, 325 mesh) powder with carbon black as conductive additive (Si:C:binder with the composition ratio 80:12:8, active mass loading ~1.4mg cm^{-2}). In order to minimize anode degradation, they limited the lower potential to 170 mV (vs Li/Li^+). Better performance was obtained with the pure CMC binder; however with electrode deintercalation capacity decreasing from 1600 to 700 mAh/g (~56%) after 80 cycles.

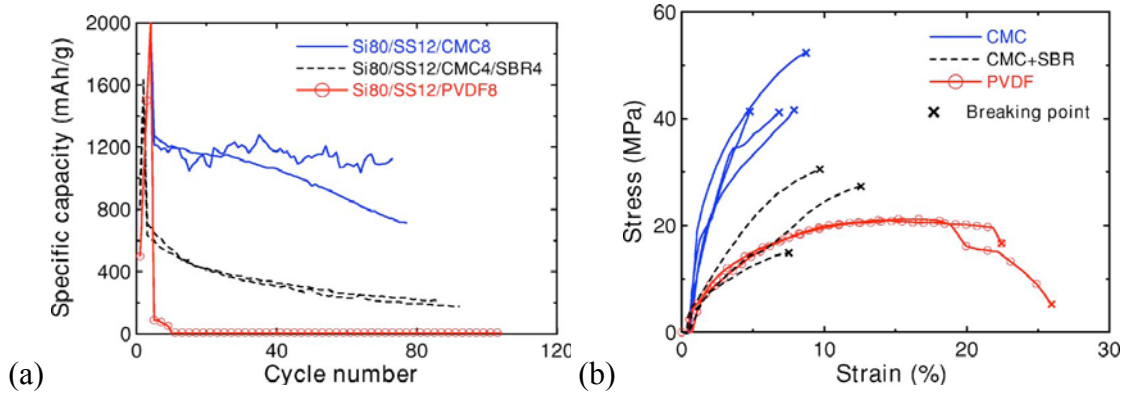

Figure 1-13. (a) Specific capacity vs. cycle number for two cells each having electrodes with 80wt% Si, 12wt% carbon black and 8wt% of CMC or PVdF or 4wt% of CMC and 4wt% of SBR. Cells were charged and discharged at 150 mA/g between 0.17 and 0.9 V. (b) Stress vs strain for CMC, CMC–SBR, and PVDF films. The × at the end of each curve indicates the breaking point [55].

[51] J. Drofenik, M. Gaberscek, R. Dominko, F. W. Poulsen, M. Morgensen, S. Pejovnik, and J. Jamnik, Electrochim. Acta, 48, 883 (2003).
[52] L. El Ouatani, R. Dedryvère, J.-B. Ledeuil, C. Siret, P. Biensan, J. Desbrières, D. Gombeau, J. Power Sources 189 (2009) 72.
[53] H. Buqa, M. Holzapfel, F. Krumeich, C. Veitc, P. Nov´ak J. Powers Sources 161 (2006) 617
[54] W.R. Liu, M.H. Yang, H.C. Wu, S.M. Chiao, N.L. Wu, Electrochem. Solid-State Lett. 8 (2005) A100.
[55] J. Li, R. B. Lewis, and J. R. Dahn, J. Electrochem. Solid-State Lett. 10 (2007) A17.

1.4.2 Searching for the reasons of the CMC efficiency

Lestriez et al. showed that CMC favours both (i) a much more homogeneous distribution of the carbon black conductive additive particles and (ii) an efficient networking process of the carbon black and Si particles in the composite electrode slurry, due to its extended conformation in solution that enables the formation of bridges between particles. [56] Moreover, it was discovered at that time that adjusting the processing conditions with use of a buffered water solution at pH 3 resulted in very significant performance improvement in the case of micro-Si (Si:C:binder with the composition ratio 80:12:8, active mass loading ~0.5mg cm^{-2}; CMC Mw 90,000g mol^{-1}, DS 0.7) cycled on the full capacity in the 1 V - 0 V vs. Li^+/Li operating voltage window.

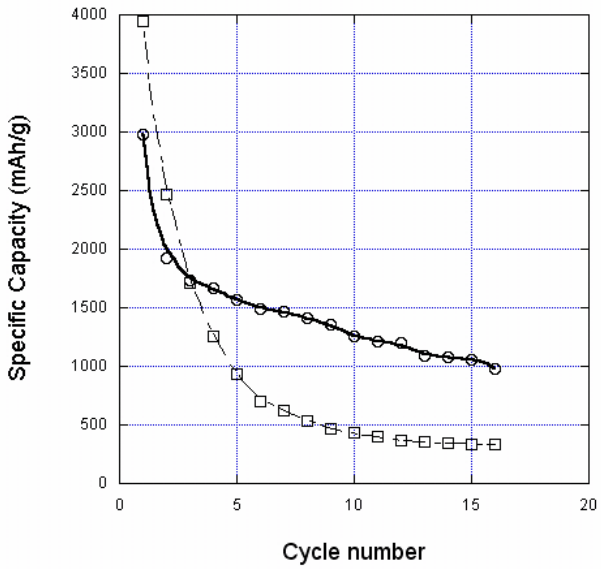

Figure 1-14. Specific discharge capacity vs. cycle number for cells having CMC based electrodes prepared with different pH 3 (-○-) and 7 (-□-) [56].

[56] (a) B. Lestriez, S. Bahri, I. Sandu, L. Roué, D. Guyomard J. Electrochem. Commu. 9 (2007) 2801. (b) B. Lestriez, S. Pedneault, L. Roué and D. Guyomard, oral 26 presented at the 2008 International Meeting for Lithium Batteries (IMLB2008).

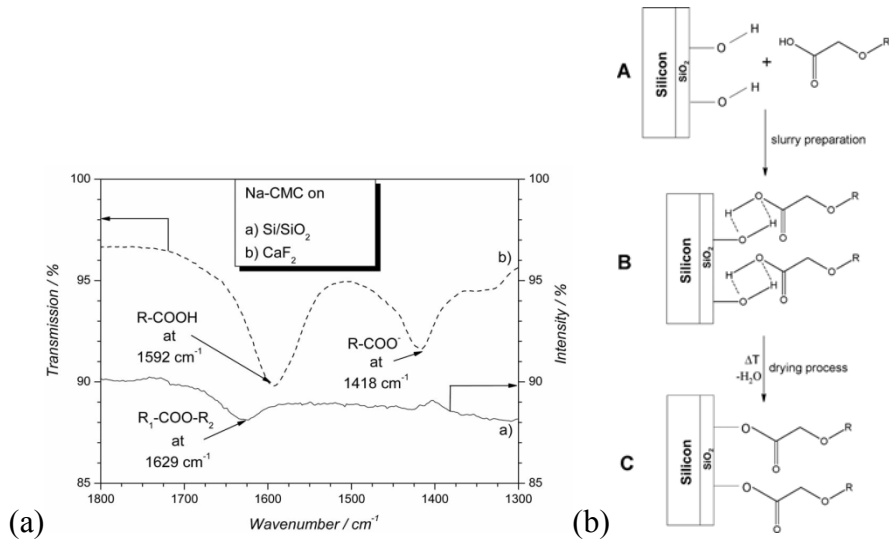

Figure 1-15. (a) IR spectrum of CaF_2 and Si/SiO_2 covered with a Na–CMC layer. (b) Possible reaction mechanism, condensation of the free carboxylic acid group of Na–CMC and the partially hydrolysed SiO_2 layer that covers a Si particle [57].

Hochgatterer et al. showed that compared to the flexible PVdF–hexafluoropropylene (HFP) PVdF-HFP, hydroxyethylcellulose (CH_2CH_2OH is the substitution group) also significantly improves cyclability, but to a lesser extent than CMC. They demonstrated (attenuated total reflection–Fourier transform infrared spectroscopy) the formation of a chemical bond between the carboxylate function (COO^-) of the binder and silicon dioxide layer present at the surface of a silicon wafer. This result suggested that the setup of a chemical bond between the binder and the active masses could be the major claim leading to long-lasting reversibility of lithium uptake/release for Si–C-composite anodes. They also found that the electrode's cycling stability is influenced by the degree of substitution on the CMC-molecule, a higher degree of substitution (⇔ a higher concentration of COO^- function) being more favourable. [57].

In two independent studies, Ding et al. and Mazouzi et al. emphasized the role played by the pH of the aqueous electrode slurry. [58,59] In the study of Ding et al. (electrode composition: 40 wt.% nano-Si Aldrich, 98%, average particle size: 50 nm, 40 wt.% CB and 20 wt.% Na-CMC), formic acid was used to adjust the pH values in the range 2-5.4. They found that the best capacity retention was achieved for electrodes prepared in acidic

[57] N. S. Hochgatterer, M. R. Schweiger, S. Koller, P. R. Raimann, T. Wöhrle, C. Wurm, and M. Winter, J. Electrochem. Solid-State Lett. 11 (2008) A76.
[58] N. Ding, J. Xu, Y. Yao, G. Wegner, I. Lieberwirth, C. Chen, J. Powers Sources 192 (2009) 644.
[59] D. Mazouzi, B. Lestriez, L. Roué, D. Guyomarda, J. Electrochem. Solid-State Lett. 12 (2009) A215.

conditions. It was also found that drying the electrode at 150°C decreased its cyclability, likely due to the CMC decomposition.

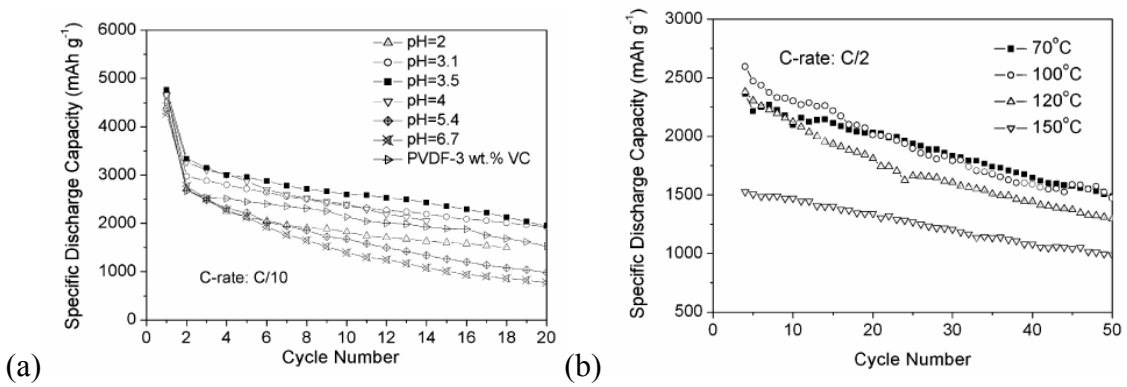

Figure 1-16. (a) Cycling performance of micro-Si with CMC binders at different pH values and with PVdF binder; (b) Cycling performance of micro-Si, nano-Si and carbon-coated nano-Si with Na-CMC binder (pH 3.5). [58].

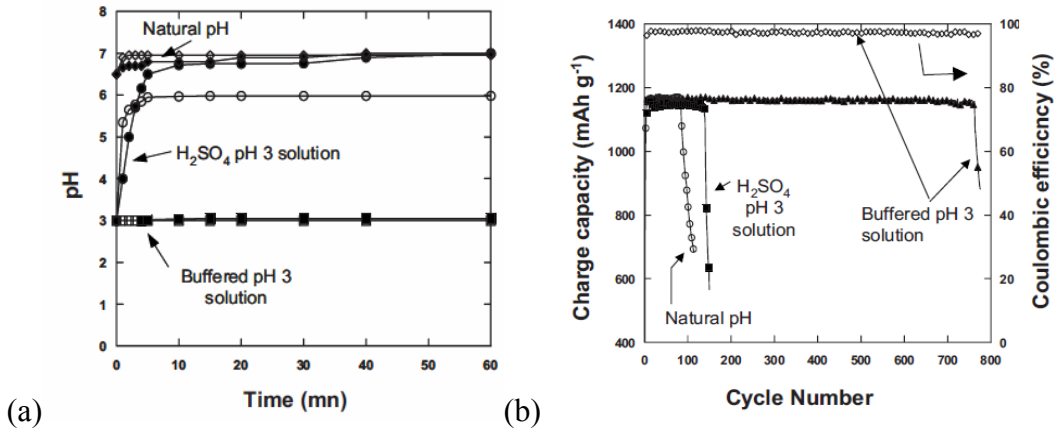

Figure 1-17. (a) pH as a function of time for Si suspension (full symbols) or CMC solution (open symbols) prepared in deionized water (◇,◆) or a buffered solution at pH 3 (□,■). The pH of deionized water was also modified by addition of 10^{-3} M of H_2SO_4 before experiment started (○,●). (b) Charge specific capacity and Coulombic efficiency vs cycle number for electrodes prepared in (O) DI water, (■) aqueous H_2SO_4 pH = 3 solution, and (▲) buffered solution at pH = 3. [59]

Mazouzi et al. showed the buffering of the aqueous solution is mandatory to promote covalent bonding (Si-OCO-R) between Si particles and the CMC binder. When a pH 3 buffer solution is used for the electrode preparation, i.e. at a pH value near to the IEP of Si particles and pKa of CMC, then full neutralization of both the SiO^- and COO^- groups into SiOH and COOH groups, respectively, can be achieved thus favouring the esterification reaction. A fairly impressive 700 cycles could be achieved when they optimized the pH of the CMC binder solution and minimized the stresses and volume changes in Si by employing Li insertion capacity limited to 960 $mAhg^{-1}$, about one-third of the full Si capacity (electrode

composition: 80 wt.% nano-Si Alfa aesar, 98%, average particle size: 50 nm, 12 wt.% CB and 8 wt.% Na-CMC: Mw 90,000g mol^{-1}, DS 0.7, active mass loading 0.5mg.cm^{-2}).

Bridel et al. confirmed the lack of electrochemical reactivity of CMC at low potential. This study also confirmed the model dealing with the conformation effect of Lestriez et al., highlighting improved capacity retention for CMC with longer chains. However, they proposed that hydrogen bonding between carboxyl groups in CMC and hydroxyl groups on Si surface exhibits self-healing behaviour that allows for the long-term cycling stability. [60] As a matter of fact, they demonstrated that: (i) the absence of binding (COOH) groups or the presence of strong binding groups (NH_2) have a very negative effect on the cycling performances; (ii) Si particles OH free (grafted with nonpolar propyltriethoxy silane) unable to interact with the CMC chains, and Si particles strongly and covalently bonded to CMC chains (through peptidic bonds with grafted 3-aminopropyltrialkoxysilane onto Si) both have very poor capacity retention. Thus, suggesting that weak Si-polymer bonding is a mandatory parameter to ensure an optimum reversibility of the reaction with Li. For a 1/1/1 (Si:C:binder) composition, they observed much poorer capacity retention for an electrode prepared in acidic conditions, Figure 1-18.

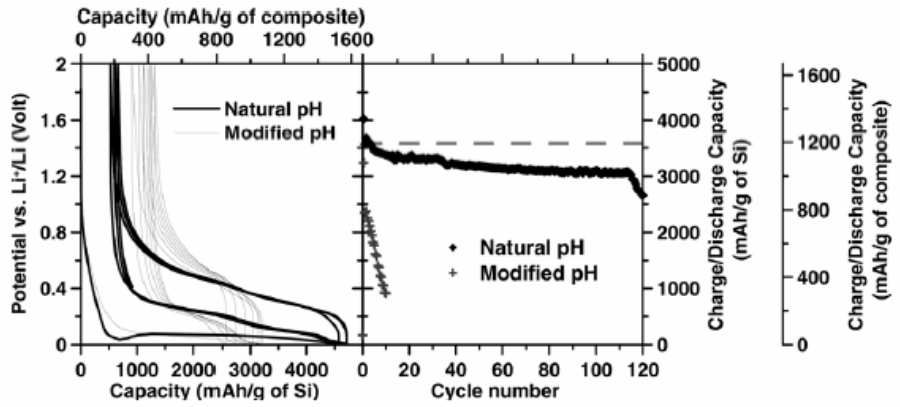

Figure 1-18. Voltage-Composition galvanostatic signatures (1 Li / 7.5 h, 25°C, 1 M $LiPF_6$ in EC-DMC) (left) and capacity as a function of cycle number (right) for Si/C/CMC (1/1/1 wt) composite electrodes prepared from suspensions having natural (NP) or modified (MP) pH conditions. The horizontal dashed line (right panel) shows the capacity value for full Si lithiation ($Li_{15}Si_4$). [60]

In their follow-up study, Bridel et al. confirmed (by means of solid state Nuclear Magnetic Resonance spectroscopy) that CMC chains can bind to Si via covalent or hydrogen bonding depending upon the pH of the mother suspension. [61] They also showed through in-situ SEM observations that the Si/C network (mother suspension pH = 7) can sustain the

[60] J.S. Bridel, T. Azaïs, M. Morcrette, J.M. Tarascon, D. Larcher, Chem. Mat. 22 (2010) 1229
[61] J.S. Bridel, T. Azaïs, M. Morcrette, J.M. Tarascon, D. Larcher, J. Electrochem. Soc 158 (2011) A750

electrode expansion and shrinking during discharging/charging. Moreover, live in-situ SEM observations revealed a two-step change in electrode volume. Up to 1.7–2 Li/Si, the electrode porosity totally buffers the Si expansion. Beyond this limit, the internal organization of the electrode has to adapt in response to the particles swelling, resulting in either a progressive loss of particles contact and reversibility because of definitive breaking of the Si-CMC covalent bond, or in a preservation of the networking thanks to a supposedly self healing behaviour of the CMC-Si hydrogen bonding. This accounts for the beneficial effect of limiting the capacity for such covalently bound electrodes to maintain their reversibility (Figure 1-19). Indeed, an uptake of 1.7 Li/Si is equivalent to a 125% particle volume increase, meaning 12% increase in the particle radius, and thus a 12% increase in the distance between two fixed points lying at the surface of two adjacent fixed Si particles, when taking into account the volumetric contribution of carbon black. This value (12%) only slightly exceeds the maximum CMC stretching value before breaking. Beyond this critical Li/Si stoechiometry, the CMC chains thus exceed their maximal stretching, and the CMC-Si covalent bonds should be definitively broken, whereas the relatively loose and weaker CMC-Si hydrogen interaction would adapt this stress by being temporarily broken but then reformed step by step from one anchorage site to the neighboring ones, thanks to the self-healing character of the polymer-Si interaction with the end result being the preservation of both the percolation network and the electrode integrity.

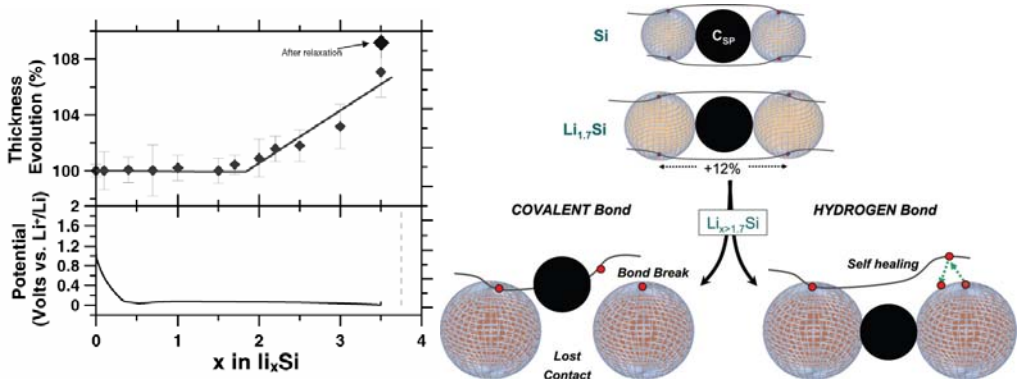

Figure 1-19. (left) In situ (SEM) variations in thickness (top panel) and first reduction potential (vs $Li^+/Li°$, 1 Li in 3.5 h, 25°C, 1 M $LiPF_6$ in PC) (bottom panel) of a Si/C/CMC electrode. (right) Schematic model showing the evolution in the CMC-Si bonding as the Li uptake proceeds, from top to bottom. Up to around 1.7 Li/Si, both covalent and hydrogen bondings can sustain the particles volume changes, the overall swelling being buffered by the electrode porosity. Beyond 1.7 Li/Si, the maximum CMC stretching ability is reached, and only the hydrogen-type Si-CMC interaction allows preservation of the efficient network through a proposed self-healing phenomenon [61]

Maver et al. used the atomic force microscopy to probe the interaction between silicon and CMC, depending on pH condition preparation. [62] Their results indicate that the type of bonding between the binder (CMC) and the active particles (silicon) has influence on the force and on the interaction range between the particle–binder complex and the nearby solid phase (in their case silicon wafer). Covalent Si–CMC bonding results in up to an order of magnitude bigger forces and longer interaction distances if compared to Si–CMC adsorption complexes (Figure 1-19). This suggests that a covalent bonding between CMC and Si particles produces much tougher (stronger) electrode composites. In both cases, adsorption and covalent bonding, the reversibility of the adhesion was observed.

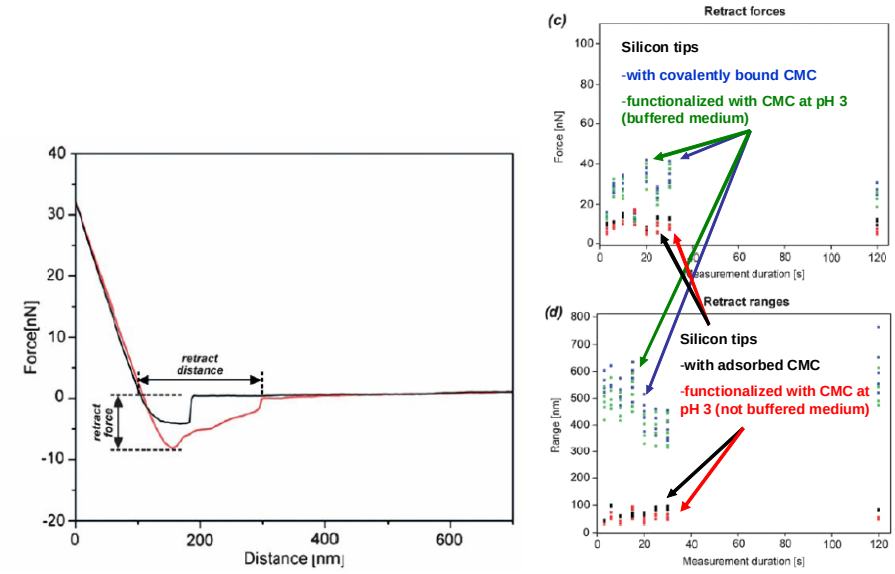

Figure 1-20. Left: typical force curve (black—approach curve and red—retract curve) between an AFM silicon tip functionalized with CMC and a silicon wafer. Right: plots of (c) the retracting force and (d) the retracting ranges in propylene carbonate for different kind of probe functionalization [62]

1.4.3 Discussion on the role(s) played by the CMC binder

In their studies, Bridel et al. propose a very elegant and unifying understanding of the Si/CMC system and compare the performance of two electrodes differing in their compositions (Si:C:CMC):

- the 33/33/33, prepared from a slurry at natural pH
- the 80/12/8, prepared from a slurry buffered at pH 3

[62] U. Maver, A. Znidarsic and M. Gaberscek, J. Mater. Chem., 2011, 21, 4071

Interestingly, both electrodes display good cyclability and close capacity if expressed in mAh per g of composite electrode. However, the cycling conditions are different also:

- the 33/33/33 is cycled at full capacity
- the 80/12/8 is cycled with constrained capacity (1200 mAh per g of Si)

Their modelling is summarized in Figure 1-19 of this report and is not repeated here. Several comments can be made however.

#1: Part of their demonstration relies upon the very poor electrochemical performance of Si particles strongly and covalently bonded to CMC chains (through peptidic bonds with grafted 3-aminopropyltrialkoxysilane onto Si). However, when very strong bonding is favoured before processing the slurry, preferential wrapping of the Si particles due to strong interactions with the polymeric chains is likely favoured, thus preventing the bridging mechanism when processing the slurry. In contrary, acidification of the slurry allows both (i) the bridging mechanism to occur and (ii) the establishments of hydrogen bonds between Si-OH and COOH groups, then favouring their subsequent condensation during the drying step (after having processed the slurry).

#2: another part of the demonstration relies upon the very poor electrochemical performance of the 33/33/33 electrode when prepared in acidic conditions. However, acidification of the slurry favours the adsorption of CMC at the surface of the Si particles (this phenomenon occurs in much lesser extent at natural pH due to electrostatic repulsion). As a consequence, with the 33/33/33 composition, thus with a fairly large binder content, a poor electronic wiring of the active mass is very likely. Indeed, the initial capacity of the pH modified sample is smaller and the polarization larger (Figure 1-18). Moreover, in the study of Ding et al., with a 40/40/20 composition, i.e. with less binder, better performance are obtained for an electrode prepared from a mother slurry at pH 3, compared to natural pH.

#3: bridges formed by covalently bounded CMC chains couldn't support the volume expansion of Si particles above the critical $Li_{1.7}Si$ composition, while thanks to a self-healing process, adsorbed CMC chains could. However, in the case of covalently bonded CMC chains, the self-healing mechanism is also possible though COOH groups not engaged into ester bonds with SiOH groups. The schematic in Figure 1-19 which described a single CMC chain simultaneously bounded to two Si particles might be an unrealistic view far from the details of the microstructure at this scale. At least two studies report that NaCMC (and HCMC) form a gel in aqueous solution, i.e. a 3D network of threads of several chains with

thickness of tenths of nanometres (e.g. 20-30nm), Figure 1-21. [63,64] The maximum stretching value before breaking of threads of a few chains could be different from the one of a massive (bulky film).

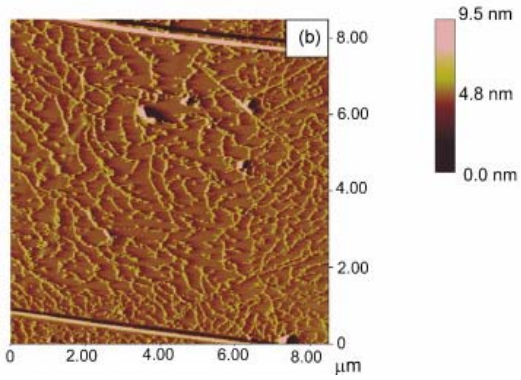

Figure 1-21. Left: AFM image of CMC on the surface of an highly oriented pyrolytic graphite (HOPG). HOPG was dipped into 1 wt.% of CMC solution. Right: visualization of the gel structure of a Na-CMC solution after freeze-fracturing [62]

#4: finally, why is observed a poor cycling for electrodes prepared without acidification of the slurry, when limiting the capacity in the study of Mazouzi et al, if the deformation at break of the CMC bridges, whatever the bound (covalent or hydrogen), is larger than the deformation resulting from the Si volume expansion?

The study of Oumellal et al. strongly suggests that the main cause of capacity fade of Si-based negative electrodes, in the case of nano Si-particles formulated with the carboxymethyl cellulose (CMC) binder, is the continuous liquid electrolyte degradation. This degradation results in the formation of a continuously growing blocking layer on the active mass. This layer fills the electrode porosity and further inhibits lithium diffusion through the composite electrode. [65] The recent study of E. Radvanyi fully confirm this end-of-life model. [66] In agreement, a recent study by Key et al. suggests CMC stabilizes the surface of silicon particles with respect to some unfavorable irreversible electrolyte reduction that might be another reason for better cycling performance of CMC-based silicon electrodes. [67] Then,

[63] T. Müller, H. Hakert, and Th. Eckert, Colloid Polym. Sci. 267 (1989) 267
[64] S. Pejovnik, R. Dominko, M. Bele, M. Gaberscek, J. Jamnik, J. Power Sources 184 (2008) 593
[65] Y. Oumellal, N. Delpuech, D. Mazouzi, N. Dupré, J. Gaubicher, P. Moreau, P. Soudan, B. Lestriez and D. Guyomard, J. Mater. Chem., 2011, 21, 6201
[66] E. Radvanyi, "Compréhension des mécanismes de (dé)lithiation et de dégradation d'électrodes de silicium pour accumulateur Li-Ion et étude de facteurs influents", PhD at the University of Grenoble (2014).
[67] B. Key, R. Bhattacharyya, M. Morcrette, V. Seznec, J.-M. Tarascon, C.P. Grey, J. Am. Chem. Soc., 131 (2009) 9239.

CMC could act as a preformed SEI layer at the surface of the Si particles. If true, the optimum amount of binder (⇔ the optimal electrode composition) could depend on the pH of the mother slurry, as the pH is known to modify the Si/CMC interactions and the extent of adsorption of the binder on the particles. Moreover, it is known that $LiPF_6$ forms HF with H_2O. Same kind of salt degradation could be envisioned with SiOH groups. Passivation of these SiOH groups after reaction with CMC could be the reason for the much better cyclability of 80/12/8 electrodes prepared in acidic conditions. [68] In the case of the 33/33/33 electrodes, it can be postulated that the amount of adsorbed binder is too high for good electronic and/or ionic wiring.

1.4.4 Design of the electrode architecture: porosity, conductive additives, current collector

Beattie et al. suggested using large amount of binder to dilute the volume expansion of the Si particles (270%) and prevent their displacements, rearrangements and thus the composite electrode disintegration. A simple model was proposed. It uses geometrical considerations to design an electrode that can accommodate large changes in volume due to particle lithiation and delithiation. The experimental results agreed well with the theoretical approach. Nano-Si-based electrodes (100nm) with a relatively low Si content and high binder content (electrode composition: Si:C:binder = 1:1:1, CMC Mw = 700,000 DS = 0.9) cycled at large capacities (660 mAh/g_electrode) for 150 cycles (gravimetric loading 1-3 mg/cm² total electrode, C/7.5 rate). [69] The follow-up study of Bridel et al. demonstrated further improved stability of the anode with this optimum composition (Si:C:binder = 1:1:1), Figure 1-18. [60]

With the same goal in mind of alleviating the deformation of the CMC binder during cycling, Guo and co-worker reported a porous CMC scaffold structure as binder for Si anodes. The slurry (electrode composition: 52 wt% Si nano-particles, 12 wt% carbon black, 36 wt% CMC) was sprayed onto the heated copper foil, and water evaporated instantly upon contact with the copper foil. The scaffold electrodes have higher porosity (0.216 cm^3/g total pore volume compared to 0.111 cm^3/g, majority of pores ranges from 50 to 120nm). The scaffold CMC–NanoSi electrode showed distinctly superior cyclability compared to the corresponding conventional electrode. The advantage of this scaffold binder would be that the intentionally introduced cavities (pores) allow the Si particles to expand without deformation

[68] N. Delpuech, D. Mazouzi, N. Dupré, P. Moreau, M. Cerbelaud, J.S. Bridel, J-C. Badot, E. De Vito, D. Guyomard, B. Lestriez, B. Humbert, submitted to J. Phys. Chem. C.
[69] S.D. Beattie, D. Larcher, M. Morcrette, B. Simon, J.M. Tarascon, J. Electrochem. Soc 155 (2008) A158.

of the electrode structure. Moreover, the porous structure likely increases ion transport in electrodes. Carbon coating on the Si nano-particles further enhanced the cycling stability of the electrodes. According to SEM, the carbon coating on the Si surface seems to largely reduce the formation of the SEI film. The carbon coated Si nanoparticles could maintain capacity of 1685 mAh/g after 150 cycles at 250 mAg^{-1} charge/discharge current. [70]

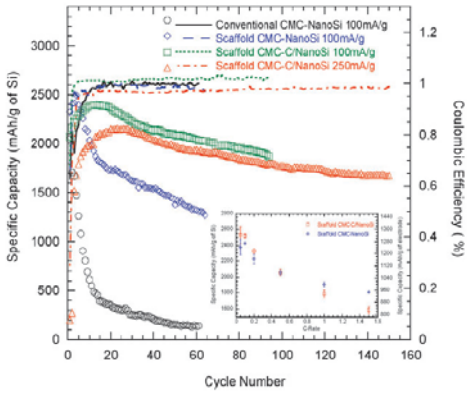

Figure 1-22. Cycle stabilitities of Si nano-particle electrodes with CMC scaffold binder [70]

Gómez Cámer et al. reported a composite electrode made in a ratio 34:66% w/w Si/cellulose fibers and containing no other additive (neither carbon black nor a binder) can exhibit specific capacity of ca. 1400 mAh/g after 50 cycles with a coulombic efficiency approaching 100%. Nanometric Si (Aldrich) and cellulose fibers were mixed in isopropanol and continuously stirred under soft heating until all liquid was evaporated. Upon mixing with cellulose, the particles tended to adhere onto the fiber surface. No Si agglomerates were observed. It is believed that the dispersive effect of the fibers on the nanoparticles minimized the macroscopic mechanical stress arising during the insertion and removal of Li. [71] Performance of the Si/cellulose electrodes could be enhanced by the addition of conductive carbon black. This beneficial effect is not only a result of the improvement of electrical conductivity and inter-particle contacts, but also due to a reduction of the expansion and shrinkage undergone by the electrode when Li is inserted into Si or extracted from Li_xSi, as revealed by in situ electrochemical dilatometry measurements. [72]

[70] J. Guo and C. Wang, J. Chem. Commun. 46 (2010) 1428
[71] J. L. Gómez Cámer, J. Morales, and L. Sánchez, Electrochem. Solid-State Lett., 11 (2008) A101
[72] J.L. Gómez Cámera, J. Morales, L. Sánchez, P. Ruch, S.H. Ng, R. Kötz, P. Novák, Electrochimica Acta 54 (2009) 6713

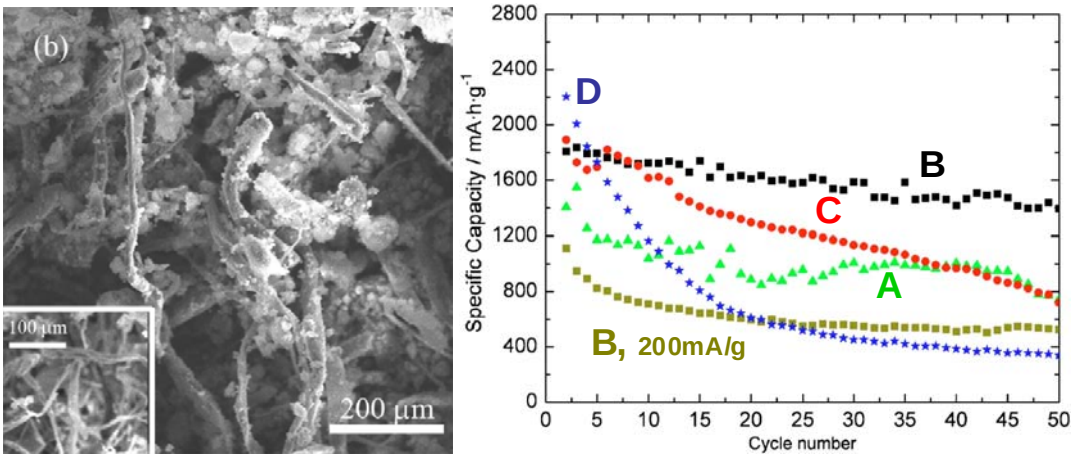

Figure 1-23. Left: SEM image of a mixture of Si-cellulose fibers. The inset shows pure cellulose fibers. Right: Capacity delivered by the cells as a function of the number of cycles . Electrodes with Si/cellulose weight percent ratio, 15:85 (A), 34:66 (B), 66:34 (C), and 100:0 (pure Si electrode). Unless noted, all measurements were made at a current of 100 mA/g [71]

With respect to the role played with the conductive additives, Lestriez et al. reported that combining carbon nanotubes (multiwall carbon nanotubes (MWNTs)) and nanofibers (vapor-grown carbon nanofibers (VGCFs)) allows building a hierarchical and resilient 3D conductive network, which strongly improves the cyclability of micron-size Si in Si/C/CMC composite electrodes. [73] However, in the case of nano-size Si, no improvement was found by using these carbon additives when compared to the standard carbon black. [65]

The expansion of the Si/C/CMC composite electrode is constrained at the interface with the current collector. Here, the resulting shear stress might cause the debonding of the composite electrode from the copper current collector and subsequent rise of the electrode polarization and capacity fade. Hu et al. proposed fabricating the silicon electrode by adding a 20 µm carbon (90% CB 10% PVdF) layer between current collector and active coating (60wt.% 1µm-Si 16wt.% AcB 24wt.% PVDF dried at 120°C for 10h under vacuum, then pressed at 20MPa, then further annealed at 230°C for 3 h in Ar gas). The prepared silicon electrode exhibit high reversible capacity of 2500mAhg^{-1} for 30 cycles at 100mA/g, which is much higher than that of bare silicon electrode with normal structure. However, the coulombic efficiency is not improved. The electrochemical impedance spectroscopy and electrode morphologies characterizations show that the improved performance of modified electrode can be attributed to the carbon layer, which enhances the electric conductivity at the

[73] B. Lestriez, S. Desaever, J. Danet, P. Moreau, D. Plée, D. Guyomard, Electrochem. Solid-State Lett. 12 (2009) A76

current collector/active coating interface (the contact resistance) but also likely release the stress caused by volume change of silicon. [74]

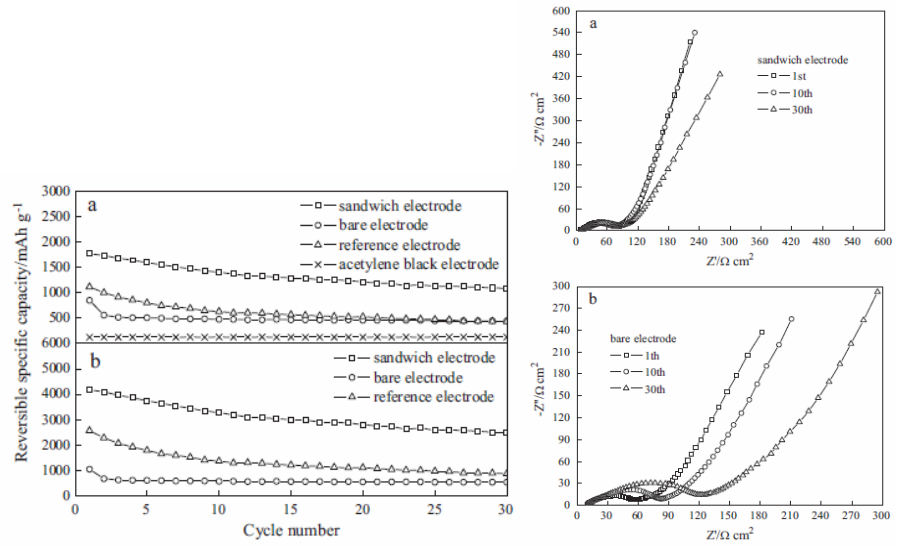

Figure 1-24. Left: Cycle performance of the prepared silicon electrodes (reversible capacity is presented). (a) Capacity is scaled to weights of silicon and acetylene black; (b) capacity is rescaled to weight of pure silicon. Right: Nyquist plots of (a) sandwich electrode; (b) bare electrode; electrode at the charged state [74].

1.4.5 Alternative binders

Whereas Na-CMC shows excellent performance with Si anodes, it suffers from some restrictions. First, CMC is not soluble in organic solvents. While the use of water as a solvent is advantageous for the environment, it may cause the surface oxidation of Si and may affect the columbic efficiency and long-term stability of Si-based anodes. This hypothesis has however not been demonstrated. Second, the mechanical properties of CMC are fixed, and therefore cannot be optimized.

Zaidi and co-workers investigated the influence of CMC and carboxymethylcellulose-formate (CMC-f) on MgH_2 anodes which show volume variation of the electrode during the repeating charge/discharge cycles. The results showed that the use of CMC and CMC-f binder had an interesting effect on the capacity retention. The capacities of 240mAhg^{-1} for CMC and 542mAhg^{-1} for CMC-f binders were indeed obtained after 40 cycles comparing to a value of 174mAhg^{-1} without any binder. An advantage of CMC-f could be that it can be solubilised in organic solvent. [75]

[74] YuHong Xu, GePing Yin, XinQun Cheng, PengJian Zuo, Electrochimica Acta 56 (2011) 4403
[75] W. Zaidi, Y. Oumellal, J.-P. Bonnet, J. Zhang, F. Cuevas, M. Latroche, J.-L. Bobet, L. Aymard, J. Powers Sources 196 (2011) 2854.

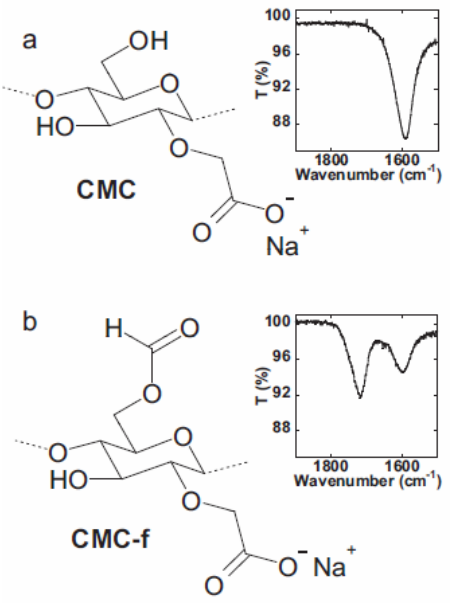

Figure 1-25. Molecular structure and corresponding IRTF spectra of sodium carboxymethylcellulose (CMC) (a) and carboxymethylcellulose-formate (CMC-f) (b) [75]

Recently, in order to replace CMC, Magasinki et al. investigated the use of poly(acrylic acid) (PAA), which offers tuneable properties. The electrodes contained ~15wt% of the binder, 43wt% of Si and 42wt% of C and the commercial electrolyte was used is 1M $LiPF_6$ salt in ethylene carbonate-diethyl carbonate-dimethyl carbonate mixture (EC:DEC:DMC = 1:1:1 vol%). The electrodes with both PAA and CMC binders showed capacities close to 3300-3700 $mAhg^{-1}$ for about 20 cycles at the C/20 rate, whereas the capacity of PVdF based anodes was much lower. The authors proposed that pure poly(acrylic acid) (PAA), possessing certain mechanical properties comparable to those of CMC but containing a higher concentration of carboxylic functional groups, may offer superior performance as a binder for Si anodes. They also found that carbon coatings on the surface of Si nanoparticles could improve the stability for all the binders studied. [76]

[76] A. Magasinski,B. Zdyrko, I. Kovalenko, B. Hertzberg, R. Burtovyy, C. F. Huebner, T. F. Fuller, I. Luzinov, G. Yushin, J. Applied Materials and Interfaces 2 (2010) 3004

1.4.6 Conclusion

In summary, for the binder, Na-CMC binder exhibits a better performance than PVdF due to its extended conformation in solution that enables the formation of bridges between particles [56] and the esterification between hydroxyl on Si surface and carboxyl in CMC. [59] The bridges allow the maintaining of the Si/C/CMC structure upon cycling. [61] The esterification allows the passivation to some extent of the Si surface. [68]

Although the practical capacity of silicon material today, is about 1000 mAh/g_electrode, [59,61] which is more than two times higher than the state of the art carbonaceous materials, the volumetric capacity is lower because the volume fraction of the active mass in the electrodes must be kept at low values (high porosity of the electrode or high non-electroactive additives contents). [69-71] At the battery level, the volumetric energy density is even more decreased because the actual silicon-based electrodes have low active mass loading (1 to 3mg/cm²). Addressing the volumetric issue requires the improvement of the mechanical properties of the composite electrode and of its attachment to the current collector.

Nevertheless, the actual lack of stability of the solid electrolyte interphase layer formed from the liquid electrolyte still remains the stumbling block. [65,66,68] Such instability is the consequence of the volume variation of the silicon particles upon (de)alloying [66].

1.5 Toward the formulation of $LiNi_{0.5}Mn_{1.5}O_4$-based positive electrodes

$LiMn_2O_4$-based oxides are good candidates to replace the $LiCoO_2$, due to their low cost and environment friendliness. [77,78] However, $LiMn_2O_4$ suffers from structural degradation such as disproportionation reaction and Jahn-Teller distortion, which results from the Mn valence change to Mn^{3+} on discharge. [79]

To improve the electrochemical performance of the $LiMn_2O_4$-based positive electrodes, doping with metallic cations has been the most followed strategy. The $LiNi_{0.5}Mn_{1.5}O_4$ (LNMO) is the most studied $LiMn_2O_4$-doped spinel [80,81] since Zhong et al. showed that LNMO can de-/insert Li^+-ions at very high potential, ca. 4.7 V vs. Li^+/Li. Furthermore, the structural stability of LNMO is superior to the $LiMn_2O_4$, because the Mn valence remains 4+ because only the nickel ions are active with two-electron redox reaction ($Ni^{2+} \leftrightarrow Ni^{4+}$). Thus, LNMO, which is free from disproportionation reaction and Jahn-Teller distortion, shows very good structural stability upon cycling. [82,83,84,85,86,87] As a positive electrode active material, its large reversible capacity of ca 135 mAh/g and high working voltage results in higher specific energy than that of $LiFePO_4$, undoped-$LiMn_2O_4$ and $LiCoO_2$. Moreover, both experiment and calculation suggest that LNMO can be a high rate electrode material even in the form of micron-size particles (Figure 1-26). [88] LNMO is thus envisioned for EVs as it meets the performance/cost requirements needed.

---

[77] M.R. Palacín, Recent advances in rechargeable battery materials: a chemist'sperspective, Chemical Society Review 38 (2009) 2565–2575.
[78] B.G. Pollet, I. Staffell, J.L. Shang, Current status of hybrid, battery and fuel cellelectric vehicles: from electrochemistry to market prospects, Electrochimica Acta 84 (2012) 235–249.
[79] D. Kim, S. Park, O. B. Chae, J. H. Ryu, Y. U. Kim, R. Z. Yin, and S. M. Oh, J. Electrochem. Soc., 159, A193 (2012)
[80] Q. Zhong, A. Bonakclarpour, M. Zhang, Y. Gao, J.R. Dahn, Synthesis and electro-chemistry of LiNixMn2−xO4, Journal of the Electrochemical Society 144 (1997) 205–213.
[81] J.C. Arrebola, A. Caballero, M. Cruz, L. Hernán, J. Morales, E. Rodríguez Castellón, Crystallinity control of a nanostructured LiNi0.5Mn1.5O4spinel viapolymer-assisted synthesis: A method for improving its rate capability andperformance in 5 V lithium batteries, Advanced Functional Materials 16 (2006) 1904–1912.
[82] M. Kunduraci, G. G. Amatucci, J. Electrochem. Soc. 2006, 153, A1345
[83] S. Patoux, L. Sannier, H. Lignier, Y. Reynier, C. Bourbon, S. Jouanneau, F. Le Cras, S. Martinet, Electrochim. Acta 2008, 53, 4137.
[84] E. S. Lee, K. W. Nam, E. Y. Hu, A. Manthiram, Chem. Mater. 2012, 24, 3610.
[85] J. Cabana, M. Casas-Cabanas, F. O. Omenya, N. A. Chernova, D. L. Zeng, M. S. Whittingham, C. P. Grey, Chem. Mater. 2012, 24, 2952.
[86] J. Xiao, X. L. Chen, P. V. Sushko, M. L. Sushko, L. Kovarik, J. J. Feng, Z. Q. Deng, J. M. Zheng, G. L. Graff, Z. M. Nie, D. W. Choi, J. Liu, J. G. Zhang, M. S. Whittingham, Adv. Mater. 2012, 24, 2109.
[87] L. Wang, H. Li, M. Courty, X. Huang, E. Baudrin, J. Power Sources 2013, 232, 165.
[88] X. H. Ma, B. Kang, and G. Ceder, J. Electrochem. Soc., 157, A925 (2010).

(a) 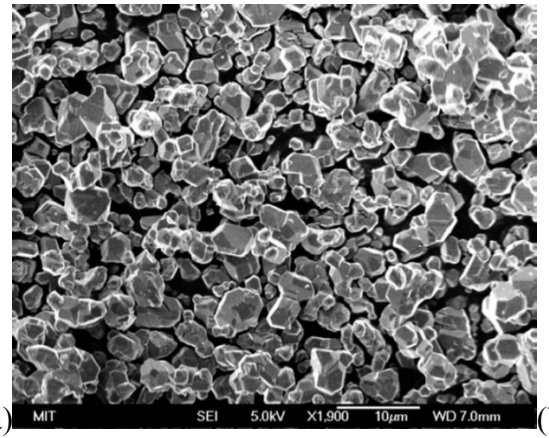

(b) 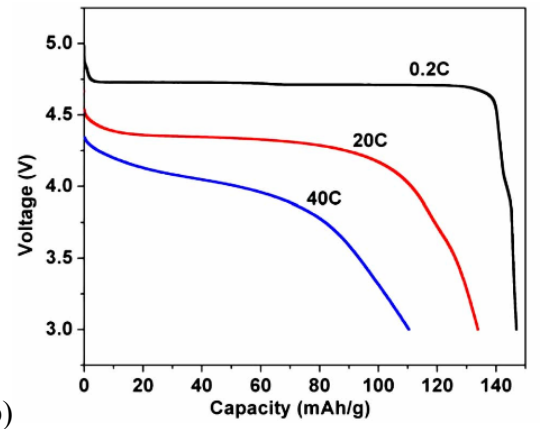

Figure 1-26. (a) SEM of LNMO prepared by a solid-state reaction from Li_2CO_3, $NiCO_3$, and MnO_2. A stoichiometric amount of these starting materials was ballmilled for 6 h at 300 rpm with 5 mm diameter yttrium-stabilized zirconia balls. After drying, the mixture was ground and pressed into a pellet. The pellet was calcined in air at 900°C for 12 h and slowly cooled down. The product was ground and repelletized. The pellet was annealed at 700°C in air for 48 h and slowly cooled down. (b) Discharge rate performance of this LNMO. The electrode density is 3 mg/cm², and the electrode contains 15 wt% carbon. Charge rate is 0.5C. Voltage window is 3–5 V. [88]

1.5.1 Instability of several of the cell constituents at the high working voltage

Its advantages are, however, largely offset by the instability of several of the cell constituents at the high working voltage of this positive electrode. Indeed, the working voltage of LNMO is beyond the thermodynamic stability window of common organic electrolytes. As a consequence, parasitic reactions occur at the surface of the active material with the electrolyte that decompose and form surface films deposit including lithium salts and organic carbonates. [89] As a result, large irreversible capacity at the first cycle and low coulombic efficiency are usually observed for LNMO with conventional electrolytes, which prohibit the use of LNMO in commercial lithium-ion cells. [90]

Through accurate measurements, Dahn and co-workers showed the CE decreases proportionally to the increase in charge-discharge cycle time indicating that parasitic reactions at the positive electrode occur at a fixed rate at a given temperature. Time and temperature, not the cycle count, impact the parasitic reactions as well as calendar life for LNMO-based cells. The CE decreased with increasing temperature showing that the parasitic reactions increased with temperature. [91] One can note that in most papers, the cyclability of LNMO-

[89] Y. Talyosef, B. Markovsky, R. Lavi,G. Salitra, D. Aurbach, D. Kovacheva, M. Gorova, E. Zhecheva, and R. Stoyanova, J. Electrochem. Soc., 154, A682 (2007).
[90] S. R. Li, C. H. Chen, X. Xia, J. R. Dahn, J. Electrochem. Soc., 160 (2013) A1524-A1528.
[91] S. R. Li, C. H. Chen, J. Camardese, and J. R. Dahn, J. Electrochem. Soc., 160, A1517-A1523 (2013)

based electrodes is done at high rate, typically 1C, which makes less pronounced the influence of parasitic reactions.

Several efforts have been devoted with a partial success to mitigate the electrolyte decomposition/film deposition. For example, alternative electrolytes with wider electrochemical potential windows [92,93] and additives decreasing the decomposition of the electrolyte [94,95,96,97,98] such as succinic anhydride-SA, 1,3-propane sultone-PS, Lithium difluoro(oxalate)borate-LiDFOB, Tris (pentafluorophenyl) phosphine-TPFPP, Lithium bis(oxalato)borate-LiBOB have been developed. Alternatively, various surface coatings on LNMO have been explored, including inert metal oxides (Al_2O_3,[99] ZnO,[100] Bi_2O_3,[99] $AlPO_4$,[101] $FePO_4$[102]), solid electrolyte (lithium phosphorus oxynitride, Lipon), [103] or polymers (polyimide) [104,105]. Optimization of either particle morphology or size has also been tried to minimize the electrolyte decomposition. [89,91,106,107] The trend that is systematically observed is a decrease in the extent of electrolyte degradation, decrease of first cycle irreversible loss and increase of the coulombic efficiency with a decrease in the surface area/increase of the particle size (Figure 1-27). Upon cycling, the surface film formed from the electrolyte degradation becomes thicker, which leads to the resistance increase. [108] The charge/discharge reaction becomes sluggish due to polarization increase, which eventually leads to capacity fading.

[92] V. Borgel, E. Markevich, D. Aurbach, G. Semrau, M. Schmidt, J. Power Sources 2009, 189, 331.
[93] A. Abouimrane, I. Belharouak, K. Amine, Electrochem. Commun. 2009, 11, 1073.
[94] H. Lee, S. Choi, S. Choi, H. J. Kim, Y. Choi, S. Yoon, J. J. Cho, Electrochem. Commun. 2007, 9, 801.
[95] Q. Wu, W. Lu, M. Miranda, T. K. Honaker-Schroeder, K. Y. Lakhsassi, D. Dees, Electrochem. Commun. 2012, 24, 78.
[96] Y. Zhu, Y. Li, M. Bettge, D. P. Abraham, J. Electrochem. Soc. 2012, 159, A2109.
[97] M. Q. Xu, Y. L. Liu, B. Li, W. S. Li, X. P. Li, and S. J. Hu, Electrochem. Commun., 18, 123 (2012).
[98] S. Dalavi, M. Q. Xu, B. Knight, and B. L. Lucht, Electrochem. Solid-State Lett., 15, A28 (2012).
[99] J. Liu and A. Manthiram, J. Electrochem. Soc., 156, A833 (2009).
[100] Y. K. Sun, K. J. Hong, J. Prakash, and K. Amine, Electrochem. Commun., 4, 344 (2002).
[101] J. Liu, A. Manthiram, Chem. Mater. 2009, 21, 1695.
[102] D. L. Liu, Y. Bai, S. Zhao, W. F. Zhang, J. Power Sources 2012, 219, 333.
[103] J. Li, L. Baggetto, S. K. Martha, G. M. Veith, J. Nanda, C. Liang, and N. J. Dudney, Adv. Energy Mater. 2013, 3, 1275–1278.
[104] J.-H. Cho, J.-H. Park, M.-H. Lee, H.-K. Song, and S.-Y. Lee, Energy Environ. Sci., 5, 7124 (2012).
[105] M. C. Kim, S. H. Kim, V. Aravindan, W. S. Kim, S. Y. Lee, and Y. S. Lee, J. Electrochem. Soc., 160, A1003-A1008 (2013).
[106] J. Cabana, H. H. Zheng, A. K. Shukla, C. Kim, V. S. Battaglia, and M. Kunduraci, J. Electrochem. Soc., 158, A997 (2011).
[107] J. Mao, K. Dai, Y. Zhai, Electrochim. Acta 63 (2012) 381– 390.
[108] T. Yoon, D. Kim, K. H. Park, H. Park, S. Jurng, J. Jang, J. H. Ryu, J. J. Kim, and S. M. Oh, J. Electrochem. Soc., 161 (4) A519-A523 (2014).

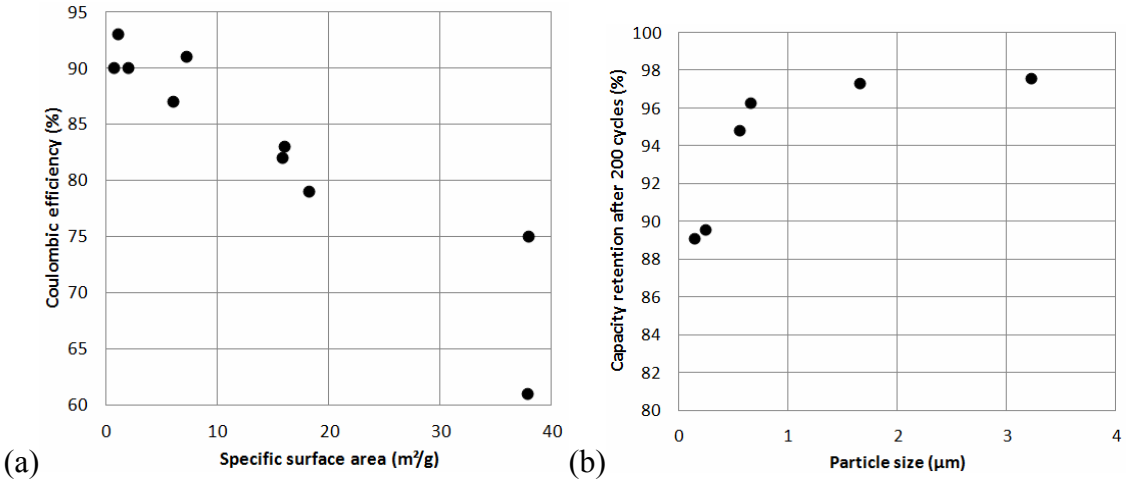

Figure 1-27. (a) First cycle Coulombic efficiency vs. Specific surface area for different LNMO powders 1 M $LiPF_6$ in EC:DEC with 1:2 weight ratio as electrolyte. The ratio of LNMO:carbon:PVDF was 80:10:10. The active material loadings in the electrodes were approximately 3.5 mg/cm². Adapted from 88. (b) Capacity retention at RT after 200 cycles vs. Particle size for different LNMO powders. The ratio of LNMO:carbon:PVDF was 80:10:10. The active material loadings in the electrodes were approximately 6 mg/cm², and a compression density of 3.0±0.1 g cm^{-3} was achieved by adjusting the calendaring pressure. The cycling performance tests were conducted under a 0.5 C/1 C (1 C = 148 mA g^{-1}) charge/discharge rate between 3.5 and 5.0 V in 1 mol L^{-1} $LiPF_6$ in 3:5:2 ethylene carbonate/dimethyl carbonate/tetramethylene sulfone. [107]

The stability of inactive components electrodes upon exposure to high potentials can affect cell performance. Lucht and co-workers [109] studied the influence of storage at high potential on half-cells prepared with positive electrodes composed of different inactive components (aluminum current collector, carbon black, and graphite but without active materials). Storage at 4.6 or 4.9 V in the presence of $LiPF_6$ in 3:7 ethylene carbonate (EC) and ethyl methyl carbonate (EMC) electrolyte results in limited decomposition on conductive carbon and greater decomposition on graphite. For an electrode with 40wt% PVdF and 60wt% carbon Super P, 1.32mg, after a week the cell stored at 4.9V showed a total accumulated capacity of 0.1mAh/cm². For an electrode with 10wt% PVdF and 90wt% SFG 6 graphite, 1.69mg, after a week the cell stored at 4.9V showed a total accumulated capacity of 0.8mAh/cm². The surfaces of carbon Super P and SFG-6 graphite electrodes were covered with a mixture of compounds from electrolyte decomposition including lithium alkyl carbonates, LiF, and $Li_xPF_yO_z$. The higher surface area of conductive additives leads to more parasitic reactions. [110] Moreover, for the low surface area carbon such as Super P, PF_6^- anions reversibly intercalate into carbon structure at around 4.7 V. For high surface area carbons, in addition to the electrolyte decomposition, the oxidation of functional groups at

[109] X. Li, Y. Chen, C. C. Nguyen, M. Nie, and B. L. Lucht, J. Electrochem. Soc., 161 (4) A576-A582 (2014)
[110] J. Zheng, J. Xiao, W. Xu, X. Chen, M. Gu, X. Li, J.-G. Zhang, Journal of Power Sources 227 (2013) 211-217

high voltage further increases the irreversible capacity and Li^+ ion consumption. For KB and graphene, surface functional groups are concurrently oxidized at high voltages in addition to the decomposition of electrolyte, generating a thick passivation film on the electrode surface and deteriorating the cell performances. The irreversible electrolyte oxidation processes on the carbon conductive additive may have quite severe implications for the lifetime of high-voltage Li-ion battery systems. Indeed, the carbon black (CB) additives constitute typically 80-98% of the composite electrode surface area.

Furthermore, graphitic carbons show an electrochemical activity at high potentials. PF_6^- intercalation into graphitic carbons occurs at potentials above 4.5 V, and the extent of the electrochemical intercalation increases with decreasing d_{002} interplanar distance. In other words, the capacity depends on the crystallinity of graphitic-carbons, and the highest value of 90 mAh g^{-1} was obtained for an almost ideal graphitic structure. [111] However, large expansion of d_{002} interplanar distance from 3.35 to 4.5Å upon PF_6^- intercalation and non-uniform mass transport rate in polycrystalline graphite induces a significant stress in the graphite crystalline lattice, which leads to gradual structural degradation upon cycling. [112] Kostecki and co-workers finely studied the electrochemical activity of carbon blacks (CB) in $LiPF_6$-based organic electrolytes. [113] Shawinigan Black, Acetylene Black and Super P appear to be electrochemically active toward $LiPF_6$-based organic carbonate electrolytes at high potentials. PF_6^- anion intercalation into different types of CB was observed in 1M $LiPF_6$ EC/DEC (3:7 vol.) electrolyte (Figure 1-28a). The PF_6^- intercalation into CB occurs at potentials (~4.2 V) significantly lower than for PF_6^- intercalation in graphite (~4.5 V), which is assigned to larger d_{002} spacing in CB than in graphite. In situ X-ray diffraction, Raman spectroscopy, and ex situ scanning electron microscopy and FTIR spectroscopy showed that this process is not fully reversible and induces morphological and structural changes of carbon material (Figure 1-28b), leading to possible changes in its electronic properties. In particular, the half-width of the carbon d_{002} reflection increased upon cycling by ca. 83%, indicating possible fracture of carbon grains, presence of graphitic domains with significantly higher (002) spacing and induced stress. The spectro-electrochemical investigations also reveal electrolyte oxidation processes on carbon black at high electrochemical potentials.

[111] T. Ishihara, M. Koga, H. Matsumoto, M. Yoshio, Electrochem. Solid-State Lett. 10 (2007) A74
[112] J. A. Seel and J. R. Dahn, J. Electrochem. Soc., 147, 892 (2000)
[113] J. Syzdek, M. Marcinek, R. Kostecki, J. Power Sources, 245 (2014) 739-744

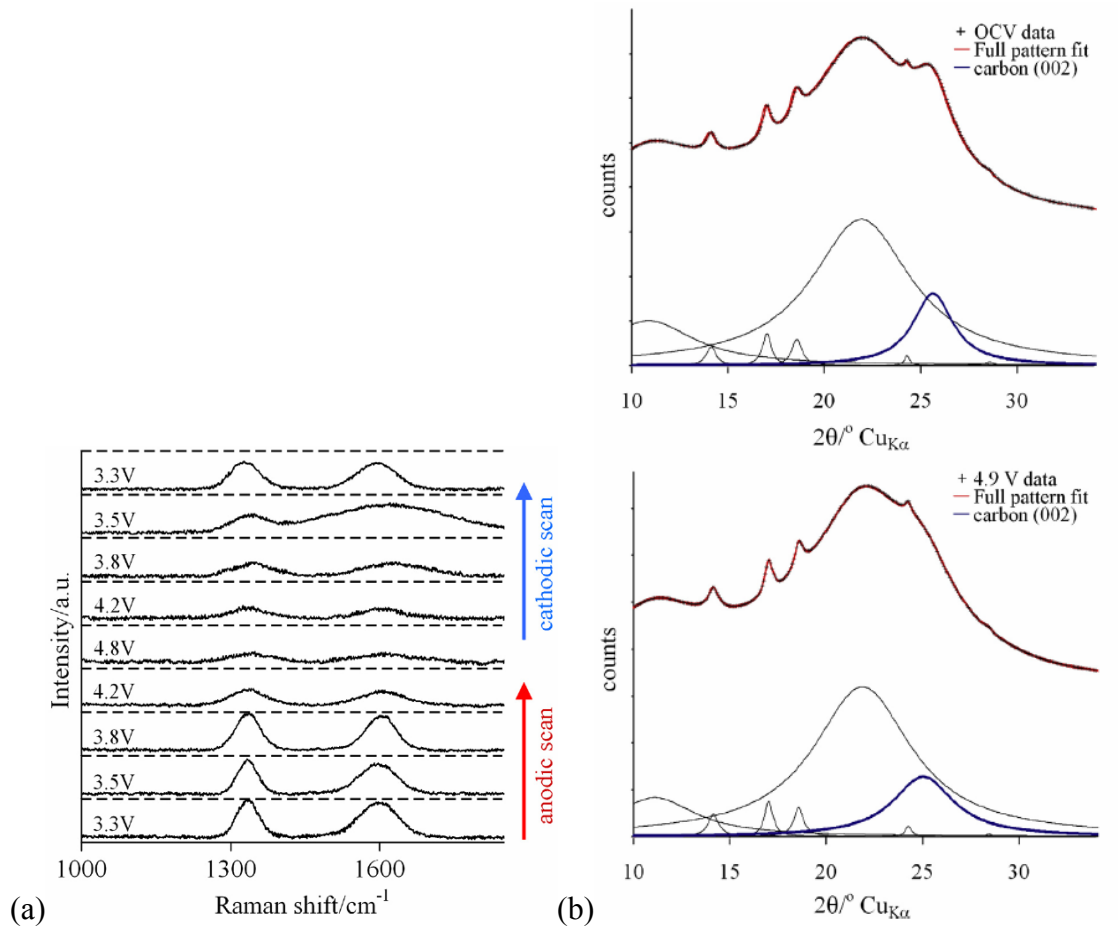

Figure 1-28. (a) In situ Raman spectra of the Shawinigan Black electrode during the first CV scan between 2.5 and 4.9 V at 1 mV s^{-1}. (b) In situ XRD patterns of fresh (top) and cycled (bottom) Shawinigan Black (2000 cycles between 2.5 and 4.9 V at 1 mV s^{-1} at room temperature), and the corresponding experimental data fitting (black traces in (b) and (c) correspond to contributions from cell components i.e., steel case, polymer separator, liquid electrolyte etc.) [113].

Such structural changes of carbon material might be a significant cause of carbon particles decrepitation and/or loss of conductivity, allowing residual interparticle resistance to dominate positive electrode impedance and resulting in an overall gradual loss of cell power and capacity loss. [114] In complement, the precipitation of the electrolyte degradation products at the surface of CB, should contribute to the buildup of ionic and electronic barriers within the electrode. It likely leads to impedance rise of composite electrodes as a consequence of increased contact resistance between CB and active material. As a conclusion, the structural properties and distribution of carbon conductive additives for high voltage positive electrodes must be carefully optimized and matched to expect cycling potential range and electrolyte chemistry in order to provide reliable long-term electrochemical performance and safe operation.

[114] R. Kostecki and F. McLarnon, Electrochem. Solid-State Lett., 7, A380 (2004)

Systematic investigations of the inactive materials in batteries (including coin cell positive cans and separators) indicates that every component used in conventional Li-ion batteries have to be re-examined when high voltage (i.e., >4.5 V) cathodes such as LNMO are used. [115,116] Commercial lithium-ion cells use aluminum current collectors, not stainless steel, on the positive electrode side. Dahn and co-workers found some corrosion of the coin cell hardware occurs at high voltages (Figure 1-29). [115] Most coin cells are made of stainless steel because it naturally forms a passive layer of (Cr, Fe) oxide on the surface that yields good corrosion resistance. However, the (Cr, Fe)-oxide components of the passive layer on stainless steel most likely react with the HF [117] generated from $LiPF_6$ decomposition and reaction with traces of water present in the electrolyte, [118,119] according to

$$LiPF_6 \rightarrow LiF + PF_5,$$

$$PF_5 + H_2O \rightarrow POF_3 + 2HF$$

$$Cr_2O_3 + 6HF \rightarrow 2\ CrF_3 + 3H_2O \text{ or}$$

$$Fe_2O_3 + 6HF \rightarrow 2\ FeF_3 + 3H_2O$$

By contrast, aluminum-sputtered cases demonstrated a stable behavior and no corrosion due to their passivation by dense surface films (Figure 1-29).

[115] N.N. Sinha, J.C. Burns, R.J. Sanderson, J. Dahn, J. Electrochem. Soc 158 (2011) A1400
[116] X. Chen, W. Xu, J. Xiao, M.H. Engelhard, F. Ding, D. Mei, D. Hu, J. Zhang, J.-G. Zhang, J. Power Sources 213 (2012) 160
[117] S. T. Myung, Y. Sasaki, T. Saito, Y. K. Sun, and H. Yashiro, Electrochim. Acta, 54, 5804 (2009)
[118] D. Aurbach, J. Electrochem. Soc., 136, 906 (1989)
[119] K. Edstrom, T. Gustafsson, and J. O. Thomas, Electrochim. Acta, 50, 397 (2004)

(a)

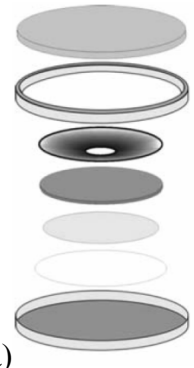

Casing Top (Negative Terminal)

Gasket

Disk Spring

Stainless Steel Spacer

Counter/Reference Li Electrode

Separator

Casing Bottom (Positive Terminal)

Working Electrode

(b)

Table I. – Composition of alloy #304 and alloy #444 Stainless Steel (weight percent).

	Alloy #304	Alloy #444
Element	Percentage	Percentage
C	0.08 max	0.025 max
Mn	2.00 max	1.00 max
P	0.045 max	0.040 max
S	0.030 max	0.030 max
Si	0.75 max	1.00 max
N	0.10 max	0.035 max
Cr	18.0 – 20.0	17.5–19.5
Ni	8.0–12.0	1.00 max
Mo	-	1.75–2.5
Ti + Nb	-	0.4–0.8 max
Fe	Balance	Balance

(c)

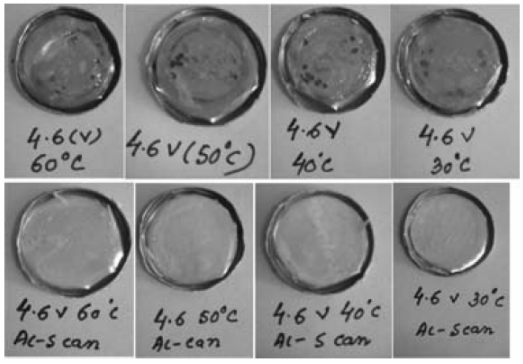

Figure 1-29. (a) Schematic of a 2325 coin cell. (b) The compositions of the alloys used in 2325-size coin cells: alloy #304 stainless steel (annealed – Kaga Steel, Japan) for the negative electrode side and alloy #444 stainless steel (annealed – Kaga Steel, Japan) for the positive electrode side. (c) Photographs of the normal and Al-sputtered coin cell cans after 200 hours of electrochemical testing (Potentiostatic chronoamperometry in 1 M $LiPF_6$ in ethylene carbonate/diethyl carbonate (1:2 v/v). The testing protocol for each cell is written next to each photograph. The photographs show one wet separator layer on top of the coin cell can. Brown dots on the separator of the normal coin cell can are visible at all temperatures after holding at 4.6 V. The brown dots could be due to localized corrosion products of stainless steel. [115]

Luchts and co-workers found that upon storage at 4.9V, the aluminum is stable due to the formation of a AlF_3 passivation film (Figure 1-30). [109]

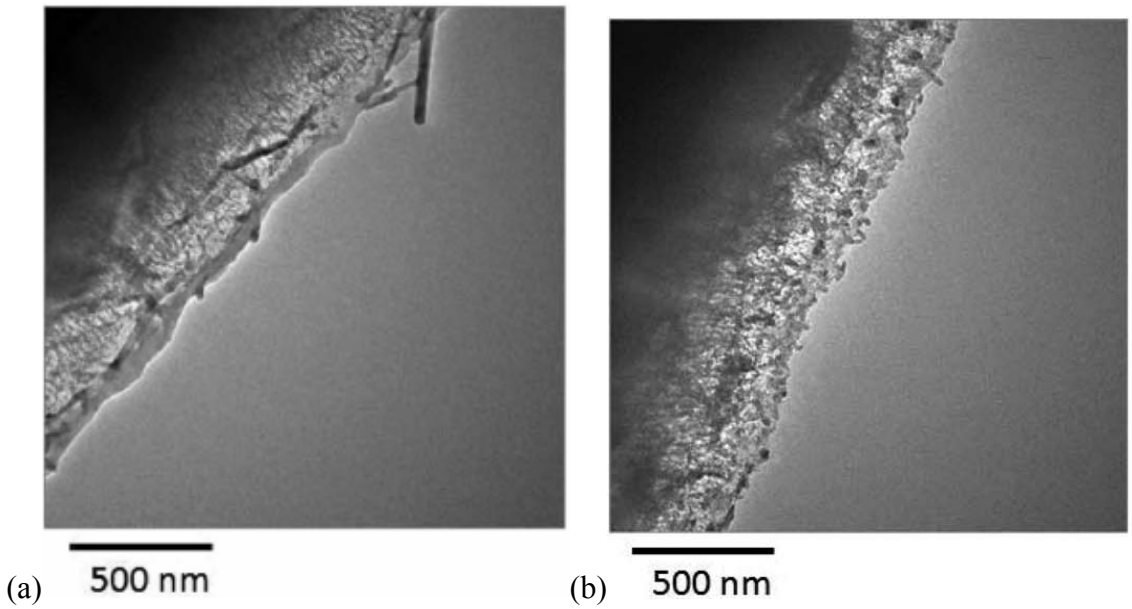

(a) (b)

Figure 1-30. TEM images of (a) fresh aluminum and aluminum stored at (b) 4.9 V.

Because most commercially available separators have been used extensively in Li-ion batteries with voltages less than 4.5 V, their stabilities at higher voltages (e.g., 5 V) need to be examined before they are used in high voltage Li-ion batteries. Results show PE-based separator are very stable while PP-based one are not and the half-cell using the latter exhibit faster capacity fading. [116]

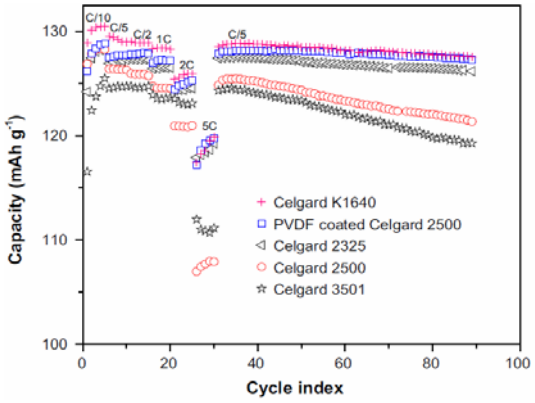

Figure 1-31. Rate performance and long-term cycling stability of Li/LNMO half cells using Al-clad SS-316 positive cans and various separators, including Celgard K1640 (monolayer PE membrane), Celgard 2325 (trilayer PP/PE/PP membrane), Celgard 2500 (monolayer PP membrane), Celgard 3501 (surface modified PP membrane), and PVDF-coated Celgard 2500.

1.5.2 Role of the electrode formulation or engineering

Very few works studied the role of the electrode formulation or engineering on the cyclability and rate capability of LNMO-based positive electrodes. As can be observed from the Table 1-2, the amount of AM can vary from 80wt%-90wt%, of binder (polyvinyldenefluoride -

PVdF or polytetrafluoroethylene - PTFE) is about 10wt% and of conductive additive from 5wt%-13wt%. In all experiments, the solvent used to prepare the slurry is NMP. There is no information about solid loading and preparation condition of the composite slurry.

Table 1-2. Recap of electrode formulation of $LiNi_{0.5}Mn_{1.5}O_4$, current collector, electrolyte and cycling conditions

Electrode formulation wt%			Solvent	Current collector	Electrolyte	Cycling condition	Reference
AM	Binder	Conductive Additive					
80%	10% PVdF	10% CB	NMP	Aluminum (Al)	1M $LiPF_6$ in EC:PC:DEC 1:1:3 (w/w)	C/5	[120]
80%	7% PTFE	13% CB	-	Stainless Steel	1M $LiPF_6$ in PC	3.5-4.9V Different C rates	[121]
80%	10% PVdF	10% CB	NMP	Al	1M $LiPF_6$ in EC:EMC:DMC 1:1:1 (in volume)	3.5-4.95V C and C/10	[122]
80%	10%PVdF	10% CB	NMP	Al	1M LiBOB in EC:DMC 1:1 (w/w)	3.5-4.9V C/10	[123]
85%	10%PVdF	5% CB	NMP	Al	#1 1M $LiPF_6$ in EC:DMC 1:1 (w/w) #2 1M LiBOB EC:DMC 1:1 (w/w)	3.5-4.85V Different C rates	[124]
90%	(Product from LG Chem)			Al	1.5M $LiPF_6$ DMC:EC (2:1) (w/w)	3.5-4.9V C/5	[125,126,127]

E. Vidal et al., studied LNMO (particle size less than 0.5μm)-based electrodes formulated with a blend of graphite and carbon black as conductive additives and either polyvinyldenefluoride (PVDF) or a blend of PVDF with a small amount of Teflon®(1 wt%). [128] Composition is 78wt% LNMO, 10wt% conductive additives and 12wt% binder. Composites electrodes with weight up to 17 mg/cm^2 were prepared. Application of sonication treatment to the electrode slurries and compaction under 2tons/cm^2 of the dry electrode/aluminum assemblies remarkably enhanced the electrode rate capabilities. At 5C rate, capacity retentions of 80% are found for electrode with weight of 17 mg/cm^2. The

[120] S. Patoux, L. Daniel, C. Bourbon, H. Lignier, C. Pagano, F. Le Cras, S. Jouanneau, S. Martinet, Journal of Power Sources, 189 (2009) 344–352.
[121] X. Wu, S. B. Kim, Journal of Power Sources, 109 (2002) 53-57.
[122] SUN Qiang, WANG Zhi-xing, LI Xin-hai, GUO Hua-jun, PENG Wen-jie, Trans. Nonferrous Met. Soc. China 17 (2007) s917-s922.
[123] J.C. Arrebola, A. Caballero, J.L. Gómez-Cámer, L. Hernán, J. Morales, L. Sánchez, Electrochemistry Communications 11 (2009) 1061–1064.
[124] J. C. Arrebola, A. Caballero, L. Hernan, J. Morales, Journal of Power Sources 183 (2008) 310–315.
[125] B. Markovsky, Y. Talyossef, G. Salitra, D. Aurbach, H. J. Kim, S. Choi, Electrochemistry Communications 6 (2004) 821–826.
[126] D. Aurbach, B. Markovsky, Y. Talyossef, G. Salitra, H. J. Kim, S. Choi, Journal of Power Sources 162 (2006) 780–789.
[127] Y. Talyosef, B. Markovsky, G. Salitra a, D. Aurbach, H.-J. Kimb, S. Choi, Journal of Power Sources 146 (2005) 664–669.
[128] E. Vidal, J. M. Rojo, M. C. García-Alegre, D. Guinea, E. Soto, J. M. Amarilla, Electrochimica Acta 108 (2013) 175–181.

electrode porosity was ca.60% for all the non-compacted electrodes and ca. 25% for all the 2tons/cm^{2}compacted ones.

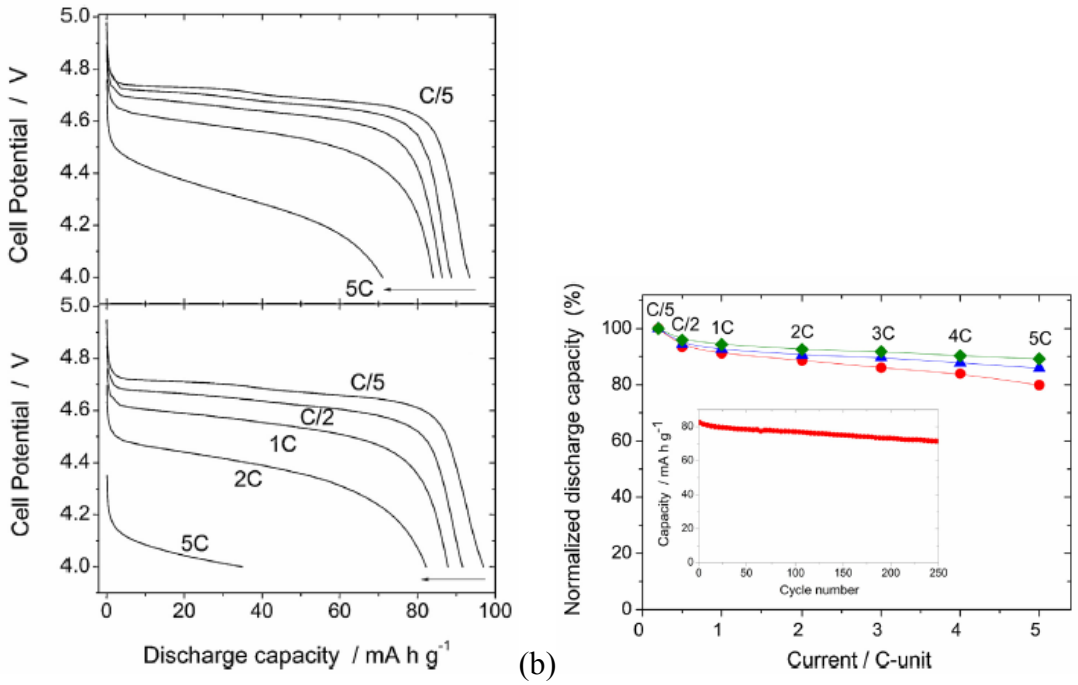

Figure 1-32. (a) Discharge galvanostatic profiles recorded at C/5, C/2, 1C, 2C and 5C rates for electrodes with 14 mg/cm² weight that were compacted at several pressures. (top) 2 tons/cm² and (bottom) non-compacted electrode. In both cases the electrode slurries were sonicated. (b) Normalized discharge capacity vs. current for electrodes having several weights: 2.7 mg/cm² (diamonds), 7.3 mg/cm² (triangles) and 16.8 mg/cm² (circles).The three electrodes have the same sonication treatment and they were compacted under the same pressure (2tons/cm²). The inset shows the long-cycling behavior of 16.8 mg/cm² electrode (circles). The voltage region explored was: 4–5 V and 1C = 147 mA/g. The electrolyte was 1 M $LiPF_6$ solution in anhydrous ethylene carbonate and dimethyl carbonate (1:1 weight ratio).

Chapter 2. Experimental

2.1 Experimental

In this chapter, a brief description of the experimental techniques utilized for characterization of the Li-ion cell components, composite slurries, composite electrodes and preparation of composite electrodes are summarized here. Particular conditions for each circumstance during this work will be specified and the results will be discussed in the following chapter.

2.2 Materials

All materials used in this work are classified with their information in Table 2-1 below

Table 2-1. Recap of all materials with different data (e.g., particle size, specific surface area, supplier…)

Components	Name	Source	Particle size	Surface area (m^2/g)	Comments
Active material	Silicon (Si)	Alfa Aesar (AA)	10-150nm	70-80	-
		CEA	150nm	13.8	-
	$LiNi_{0.5}Mn_{1.5}O_4$ (LNMO)	Delft University	1-10µm	0,32	-
	Lithium foils	Sigma-Aldrich	-	-	-
Conductive additive	Super P carbon black (CB)	Timcal	10-50nm	62	
	Carbon nanofibres (VGCF-H)	Showa Denko	-	16	-
	Carbon nanofibres (VGCF-S)	Showa Denko	-	35	-
	Graphene nanoplatelets (GM15)	XG Science	15µm	120-150	-
	Multiwalled carbon nanotube (MWNTs)	Nanostructure & Amorphous Materials Inc.		$110 m^2/g$	
	Graphene oxide (GO)	-	-	-	Collaboration with Ashok from CEA-LINAC
	Reduced graphene oxide (rGO)	-	-	-	
Binder	Carboxylmethyl cellulose (CMC)	Sigma-Aldrich	-	-	DS=0.9, M_w=700.000 g/mol
					DS=0.7, M_w=250.000 g/mol
					DS=0.7, M_w=90.000 g/mol
	Polyvinylidene fluoride (PVDF) type I	Arkema	-	-	reference number Kynar HSV 900
	Polyvinylidene fluoride (PVDF) type II	Arkema	-	-	reference number Kynar ADX 161
	Plextol X4020	PolymerLatex	-	-	-
	Plextol X6010	PolymerLatex	-	-	-
	Styrene-co-Butadiene rubber copolymer (SB)	-	-	-	
	Poly acrylic acid (PAA)	Sigma-Aldrich			M_w= 450.000
Dispersant	Poly (acrylic-co-maleic) acid (PAMA)	Sigma-Aldrich	-	-	M_w=3000g/mol
	Poly ethylene imine (PEI)	Sigma-Aldrich	-	-	M_w=2000g/mol
Electrolyte	Lithium hexafluorophosphate ($LiPF_6$)	Sigma-Aldrich	-	-	-
	Lithium 4,5-dicyano-2-(trifluoromethyl)imidazolate (LiTDI)	Lab. of Technological Processes – Warsaw (LPT)	-	-	-
	Ethylene carbonate (EC)	Novolyte	-	-	-
	Dimethyl carbonate (DMC)	Novolyte	-	-	-
	Vinylene carbonate (VC)	Sigma-Aldrich	-	-	-
	Fluoroethylene carbonate (FEC)	Sigma-Aldrich	-	-	-
Solvent	N-Methylpyrrolidone (NMP)	Sigma-Aldrich	-	-	-
	Buffer solution (0.1M, pH=3)	-	-	-	Prepared in IMN

2.3 Techniques of analysis

Different techniques were used to characterize active materials, composite slurries and composite electrodes.

Zeta potential measurement - this technique was used to investigate the charge density on the surface of Si particles in solution at different pH (3mg/15ml solvent, solid loading 2.10^{-4} wt%). The zeta potentials of the Si particles were measured by Malvern Zetasizer Nano-ZS instrument coupled with MPT-2 accessory on diluted suspensions in DI water (Figure 2-1). Mobility measurements were performed at 25°C with different pH values by adding small quantities of HCl and NaOH. Zeta-potential values were calculated automatically according to the Smoluchowski theory. [1] The isoelectric point (IEP) was determined as the pH value for which the zeta potential is equal to 0.

Figure 2-1. Image of Zetasizer Nano machine with MPT-2 accessory

Specific surface area - The specific surface area was determined by multipoint Brunauer-Emmett-Teller treatment (BET method) from the volumetric adsorption isotherms at 77K of nitrogen gas (instrument ASAP 2010 Physisorption Analyzer). The amount of powder used is from 0.8-1.2g for each measurement

The scratch testing - This method was used to evaluate the relative adhesive properties of the tape after drying and based on the achievement of a scratch on the sample under moving point which is placed in contact with the tape under a gradual load. [2] The scrapping load

[1] J. Israelachvili, Intermolecular and surface forces. Academic Press, 1991
[2] Yoo, M., Frank, C.W., Mori, S., and Yamaguchi, S. 2003, Polymer, 44, 4197

obtained is the critical load at which the tape is removed completely from the copper current collector.

Figure 2-2. The device of scratch test

Sedimentation test – this measurement was used to study the stability of the materials in different conditions. The process of settling was observed visually as a function of time.

Rheological measurements - Rheological properties were measured on a controlled-stress rotating rheometer (Anton Paar, MCR 101) with a 50mm diameter plane-and-plane geometry and the sample gap between the Pelletier plane and the geometry was fixed at 0.6mm. Several types of rheological measurements were carried out: (i) Two measurements were done with continuous shear: a rate sweep measurement from 0.1 to 1000s^{-1} to determine the viscosity of the slurries and sequence at constant rate measurement 10s^{-1} for 900s to simulate and follow what happens upon gentle mixing as in the reservoir of the slot die machine. (ii) The evolution of moduli at a frequency of 1Hz and a strain of 1% after a preshear at 100s^{-1} for 60s to simulate and follow what occurs after casting.

Study of electrode texture - Scanning electron microscopy (SEM) and Energy dispersive x-ray (EDX) imaging was performed by using a JEOL JSM 7600 to investigate textural properties of composite electrodes.

Study of structure – The crystalline structure of material was identified by X-ray diffraction (XRD) using Bruker AXS D8 Advance system, equipped with Cu Kα1.

Electrical measurements - Electronic resistivity measurements were carried out by impedance spectroscopy on dry Si electrode/current collector samples sandwiched in between two metallic plungers in a standard swagelok cell, using a VMP automatic cycling/data recording system (Biologic). The frequency range was scanned from 10 mHz to 189 kHz.

Several compositions were studied at different thicknesses. Six samples were evaluated for each composition. The measurement was repeated three times on each sample. The impedance diagrams corresponded in all cases to a single point on the real axis. The electrode resistivity, ρ, was determined from the well-known equation $\rho = (R \times S)/t$, where S is the contact surface area between the probe (metallic plunger) and the sample, 0.283cm².

In complement, a mapping of the electronic resistivity of dry Si composite tapes prepared on plastic film was also measured by using four-point probe mapping system (model 280SI-Microword) with computer controlled stepping motors to move the four-point probe. The spacing between each probe is 1mm. Each probe has a contact area radius of 100μm and the load applied on each probe is 60g. The current source is a fixed-output, range-programmable constant-current generator, and provides an appropriate amount of test current to the sample under test. It is automatically selected by the measurement board during the measurement sequence.

Cyclic voltametry – this technique was used to study electrochemical processes occurring in the potential range considered, which allows identifying parasitic reactions happen or stability of substance. Two-electrode Swagelok™ cells were used with lithium metal as counter and reference electrode, working electrode will be described in the following chapter.

Electrochemical testing – This test gives information about the reversibility of the electrochemical process during cycling, the long-term cycling behaviour and rate capability, measuring the amount of charge passed through the cell in the charge and discharge of each cycle

Half cells: two-electrode Swagelok™ test cells or coin cells comprise (i) a 0.78 cm^2 disc of composite positive electrode (ii) a porous glass paper as separator soaked in an electrolyte and (iii) a 0.78 cm^2 Li metal disc as the negative and reference electrode.

Full cells: two-electrode Swagelok™ test cells comprise (i) a 0.78 cm^2 disc of composite positive electrode (ii) a porous glass paper as separator soaked in an electrolyte and (iii) a 0.78 cm^2 of composite negative, also as a reference electrode.

The cells were assembled in the glove box under argon atmosphere. Cell cycling was performed at 20°C, monitored by a VMP™ system (Biologic) in a galvanostatic mode. The composition of the electrolyte, the voltage range and cycling conditions will be specified depending on each particular case in the following chapter.

2.4 Preparation of the composite electrode

Most of the composite electrode slurries were prepared by ball milling. Composite electrodes were made of active material (AM), conductive additive (C), binder (B) and/or dispersant (D). All powders were introduced in a silicon nitride vial. Then, the solvent was added to composite electrode materials. The ranges of typical quantities used are from 0.5 to 1.5ml. Three silicon nitride balls (9.5mm diameter) served as mixing media. A Fritsch Pulverisette 7 mixer was used to mill the slurry.

Figure 2-3. Planetary ball mill "Pulverisette 7"

The slurry was tape casted directly after ball milling by using an automatic doctor blade onto current collector in tape casting machine (Figure 2-4). The height of tape casting blade can be controlled by micrometer adjustable film.

Figure 2-4. Automatic Thick Film / Tape Casting Coater with Vacuum chuck and Micrometer adjustable Film Applicator.

Chapter 3. Results and Discussion

Based on the industrial state-of-the-art, 3mAh/cm² is typical surface capacity in high energy batteries. Reaching such a surface capacity has been an objective of my work to be competitive with current technology in terms of gravimetric energy density. Considering typical performance in the literature on silicon negative electrodes, e.g. 1200 mAh/g_Si with ~70wt% Si in the dried electrode composition, or 3000 mAh/g_Si with 33wt% of Si in composition, I looked for Si active mass loadings of more than 2.5mg/cm². Considering typical performance of LNMO electrodes, e.g. 120 mAh/g_LNMO, I looked for LNMO active mass loadings of more than 25mg/cm².

3.1 Negative electrode formulation based on Si

To design the formulation of the Si-based negative electrode, starting with the composition initially proposed by Dahn and co-workers [1], and modified by the group through the introduction of pH 3 buffered processing [4,6], I searched in two directions. The previous works in the group show that preparing the electrode at buffer pH 3 is mandatory to achieve the grafting of the CMC binder, which strongly improves the cycle life [4]. However, at pH 3, the zeta potential of the Si particles is equal to zero and the CMC has poorer dispersing properties as a consequence of the neutralization of carboxylate groups into carboxylic ones. As a consequence the slurries are not stable and easily flocculate through the attractive Van der Waals interactions. [2] Although this flocculation phenomenon can be managed at the laboratory scale when working on small quantities with short casting durations, it becomes a significant problem at the pilot or semi-industrial scale where the stability of electrode slurries is mandatory to achieve homogeneous tape cast electrodes [10]. Different dispersants (Poly (acrylic-co-maleic) acid-PAMA and Polyethyleneimine-PEI) were tested to improve the stability of the electrode slurries for large scale processing. It resulted in 1st optimized electrode formulation using PAMA dispersant with carbon black (CB) as a conductive additive (paper I). In the second direction I

[1] J. Li, R.B. Lewis, J.R. Dahn, Electrochem. Solid-State Lett. 10 (2007) A17.
[2] M. Cerbelaud, B. Lestriez, D. Guyomard, A. Videcoq, R. Ferrando, Langmuir, 28 (2012) 10713.

searched for other conductive additive than CB. Previous work in the group, but realized on micrometric silicon, showed other conductive additives than CB (carbon nanofibers and/or carbon nanotubes) result in significant improvement of the cyclability of silicon-based electrodes [3]. This way, I tested different conductive additives, carbon nanofibers, carbon nanotubes and graphene. It resulted in 2nd optimized electrode formulation with graphene as a conductive additive (paper II). In the end, putting everything together and trying to analyse the results as a whole, we went to propose an analogy between electrochemical behaviour of thick silicon granular electrodes for lithium batteries and fine soils micromechanics (paper III).

At the beginning of my work, many constituents were studied to check the morphology, working condition (for Si), solubility and stability during processing (for latex) before slurry preparation as stated below:

- Active materials: two types of Silicon were used, one supplied from Alfa Aesar (AA) (the oxygen content is 3-4wt%) and another from CEA (the oxygen content is 0.7wt%) with different characteristics. In the context of EuroLiion I was supposed to work on the formulation of nanosilicon material synthesized at Faculty of Applied Sciences, Delft University of Technology (TUD). The particle size of the latter material is very low, ~20nm. Waiting for receiving from TUD their silicon I made trials with the silicon from Alfa Aesar, which is also a nanosilicon material although with larger particle size, ~50nm. I also made some trials with another nanosilicon supplied by the CEA, which has the largest particle size of the three, ~150nm. In the end we decided to focus on silicon from CEA, as explained later.
- Binders: searching for the best mechanical strength of the electrodes, different types of CMC binder with different degree of substitution (DS) and molecular weight (M_w) were investigated: DS=0.9 (M_w= 700,000), DS=0.7 (M_w= 250,000 and M_w= 90,000).
- Latex: in order to improve mechanical strength of the thick Si based composite electrode to the copper current collector in complement to CMC binder, polymer latex binders were evaluated. Two polymer latex, Plextol X6100 (pH 2.5) as an

[3] B. Lestriez, S. Desaever, J. Danet, P. Moreau, D. Plée, D. Guyomard, Electrochem. Solid-State Lett., 12 (2009) A76.

aqueous dispersion of a self-crosslinking acrylic polymer based on ethylacrylate and Plextol X4020 (pH 7.0-9.0) as an aqueous dispersion of a copolymer of styrene, n-butylacrylate, were supplied from PolymerLatex. According to their technical specifications, both Plextol X6100 and Plextol X4020 can be used in both acidic and neutral pH conditions.

- Two different solutions were used in order to prepare the composite slurries, following previous works at the IMN [4]: (i) Buffer solution pH 3 (0.1M) prepared with citric acid and KOH and (ii) Distilled water pH 7.

3.2 Characterization of constituents

3.2.1 Zeta potential measurement of Si CEA

According to the results of Mazouzi et al. [4], it is favourable to prepare the electrode with aqueous slurry buffered at pH 3, in the case of Si from AA, because at such pH a grafting esterification of the CMC chains at the surface of Silicon particles is greatly enhanced (see bibliographical part). Zeta potential measurement of Silicon from CEA was carried out to identify the appropriate pH which must be used for electrode preparation in order to favour the grafting esterification. Figure 3-1 displays zeta potential as a function of different pH for Silicon from CEA. At pH > 3, the zeta potential is negative which corresponds to the negative charges ($-O^-$ groups) covering the surface of Silicon particles. When concentration of H^+ increases, the negative charges are gradually neutralised with decrease of zeta potential and reaches 0 at pH 3 where there is no charge (mostly –OH groups) on the surface of Silicon. When pH < 3, the zeta potential becomes positive related to positive charges ($-OH_2^+$ groups) at the surface of Silicon. The isoelectric (IEP) point obtained for Si from CEA is 3.03. Both Si from CEA and AA have the similar value of IEP. It's thus suitable to use buffer solution at pH 3 as a solvent to prepare slurry for both Silicons. In addition, I also tried to prepare the slurries at pH 7 to confirm for Si CEA the influence of the pH of the electrode slurry on the electrochemical performance of the resulting electrodes.

[4] D. Mazouzi, B. Lestriez, L. Roué, D. Guyomard, J. Electrochem. Solid-State Lett. 12 (2009) A215.

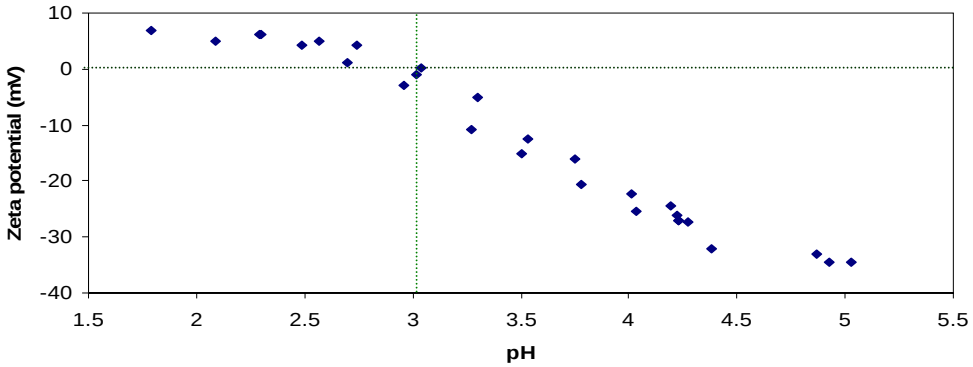

Figure 3-1. Zeta potential as a function of pH (Si from CEA)

3.2.2 The morphology and particle size of Si CEA and AA

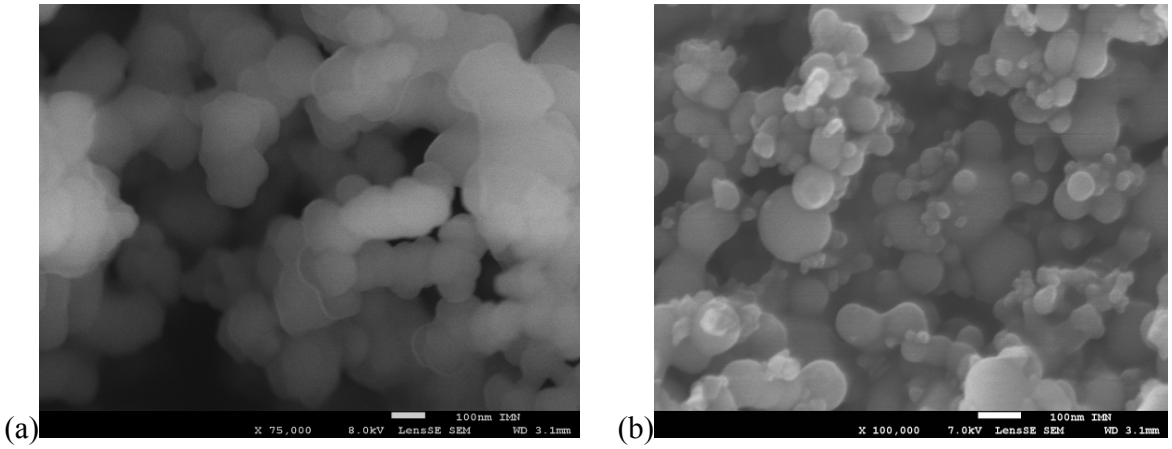

Figure 3-2. SEM pictures of Si particles supplied from (a) CEA and (b) Alfa Aesar.

As can be observed from SEM images (Figure 3-2), particle size distribution of Si CEA is rather homogeneous and its size is around 150nm while Si AA shows different properties. It has inhomogeneous particle size distribution (10-150nm) and the average size is 50nm.

Table 3-1. Specific surface area of different Si

Sample	Calculated BET $S_{tsa}=6/D\times\rho$ (m^2/g)	BET (m^2/g)
CEA – 150nm	17.2	13.8
AA – 50nm	51.5	70-80

with the theoretical surface area is calculated from the following equation:

$$S_{theoretical\ surface\ area} = \frac{S_{sphere}}{V_{sphere} \cdot \rho} = \frac{4\pi R^2}{\frac{4}{3}\pi R^3 \cdot \rho} = \frac{3}{R \cdot \rho} = \frac{6}{D \cdot \rho}\ (m^2/g)$$

where D is the diameter of the grains (m) and ρ is the density ($g.cm^{-3}$).

Table 3-1 shows the BET measurements along with the theoretically calculated BET value from the mean particle size determined on SEM pictures. A good agreement is found between calculated and measured values for Si CEA. For Si AA the calculated BET is lower than the measured one, which can be attributed to the broader particle size distribution, the smaller particles contributing the more on the BET surface.

3.2.3 Solubility and stability of the latex

Before adding the latex into the electrode formulation I studied its stability in the processing conditions. Small amount (40mg) of Plextol was dispersed in 10ml of different solutions by using stirring or ball milling at 500rpm in 60min. After that, the solution was observed visually as a function of time. Plextol X6100 formed white agglomerates upon stirring in buffer solution while in other solutions (HCl, H_2SO_4 at pH 3 0.1M), it disperses completely and remains stable during more than 24hours as a milky homogeneous solution (Figure 3-3).

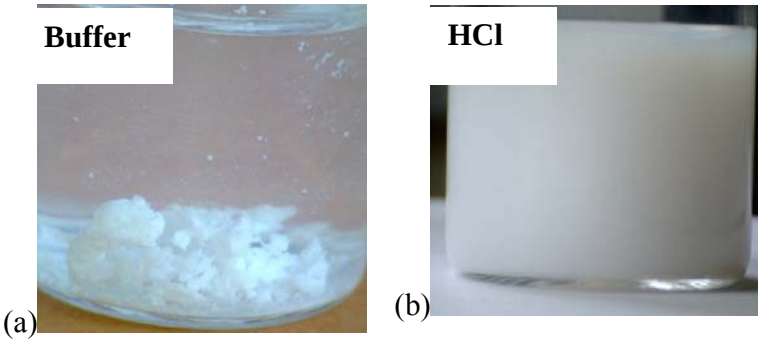

Figure 3-3. Camera images of solution with Plextol X6100 in different solvents at pH=3
(a) Buffer and (b) HCl

More experiments were carried out to investigate the effect of pH and different ions such as K^+, Li^+, H^+ Cl^-, SO_4^{2-}…etc, on the stability of Plextol X6100. We found that each component such as H^+, Cl^-, SO_4^{2-}, citric acid, or citrate and also pH conditions don't induce precipitation. However, the presence of ion K^+ or Li^+ is the reason which causes this process. As a result, Plextol X6100 is not suitable to use in the process of making the Si composite electrode with the standard citric acid/KOH or /LiOH buffers.

The solubility and stability of Plextol X4020 was studied in different pH conditions (pH3 buffer and H_2O) and for two mixing methods. By stirring, it disperses well in both buffer and H_2O and solutions and is stable more than 24hours. However, under high energy milling Plextol X4020 is only stable in water while it forms white agglomerates in acidic buffer (Figure 3-4). Unfortunately, high energy milling is mandatory for dispersing nanopowders at the lab-scale.

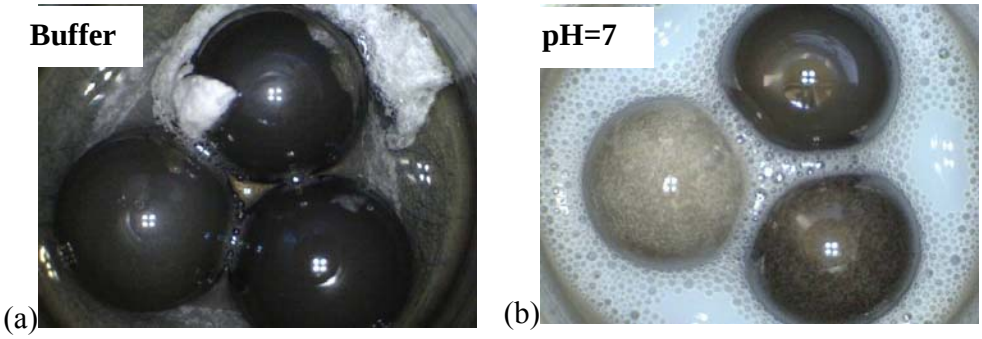

Figure 3-4. Camera images of stability of Plextol X4020 in different solvents after ball milling (a) Buffer pH 3 and (b) Distilled water pH 7

In summary, Plextol X6100 is unstable with presence of ion K^+ and Plextol X4020 is unstable under high mechanical energy in buffer solution. As a result, both couldn't be used in process of making Si based electrode in buffer solution pH 3. However, Plextol X4020 could be used in preparation of Si based electrode at pH 7 (and also in aqueous processing of LNMO based electrodes).

3.3 Preparation of slurries – preliminary results based on Si AA

The standard electrode composition to start with at the beginning was 80wt% Si 12wt% CB and 8wt% CMC (Mw 90,000 and DS = 0.7) [4] based on previous study of D. Mazouzi et al. in our group. Their nanosilicon-based composite electrode when processed in buffer solution pH 3 could achieve more than 700 cycles at a high capacity of 960 mAh/g of electrode but with a low active mass loading of about 0.5mg/cm². In my preliminary studies, 200mg of composite electrode materials was dispersed in different solvents with variation of quantities (0.5 to 1.5ml of buffer at pH 3 or distilled water pH 7) and Si AA was used as active material. During tape casting process, the thickness of blade gap was fixed at 250µm in order to obtain thick Si based electrodes (>2mg Si/cm^2).

Table 3-2. Recap of the preliminary experiments of Si AA with different type of CMC binder, solid loading, and scrapping load on dried electrodes

CMC binder	Volume of solvent (ml)	Solid loading (wt%)	Scrapping load (g)	
			pH 7	pH 3
M_w=90,000 DS=0.7	0.5	28.5	0	0
	1.0	16.7	10-20	10-20
M_w=250,000 DS=0.7	0.75	21.1	10-20	0-10
	1.25	13.8	30-40	10-20
M_w=700,000 DS=0.9	1.0	16.7	20-30	30-40
	1.5	11.8	30-40	0

Table 3-2 recaps the influence of different types of CMC binders, along with different solid loadings used in the process of making the slurry based on Si AA, on scrapping loads of the electrodes after drying. Most of the composite tapes after drying or after punching (for cell assembly) detached completely from the copper current collector. They also shown lots of severe cracks (Figure 3-5) on the surface which is consistent with low values of scratch test obtained (0-20g). Among them, the electrode formulation prepared with CMC (M_w=700,000, DS=0.9) in buffer solution pH 3 (solid loading 16.7%) shows better adhesion with highest scrapping load (30-40g), which allows to punch some electrodes without detaching although many cracks observed after drying on the surface of the tape. In addition, the Si loading after drying is higher than 2mg/cm^2. At pH 7, the electrodes which have same mechanical properties (30-40g of scrapping load) could be produced with CMC M_w=250,000, DS 0.7 and CMC M_w=700,000, DS 0.9; however at lower solid loading (13.8 wt% and 11.8 wt%, respectively). After drying, the Si loading of these formulations is lower than 2mg/cm^2. According to the study of Bridel et al. [5] and my results, CMC binder with highest M_w=700.000 & DS=0.9 was chosen for the optimization of electrode formulation because it has better mechanical strength thanks to bridging mechanism [6] and the solid loading was fixed at ~17wt% to satisfy the AM loading (> 2mgSi/cm^2).

[5] J.S. Bridel, T. Azaïs, M. Morcrette, J.M. Tarascon, D. Larcher, Chem. Mat. 22 (2010) 1229.
[6] B. Lestriez, S. Bahri, I. Sandu, L. Roué, D. Guyomard, Electrochem. Commun., 9 (2007) 2801.

(a)  (b) 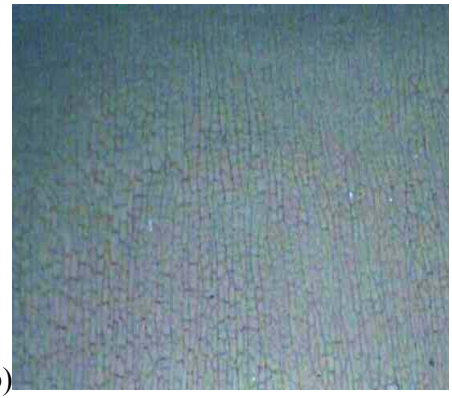

Figure 3-5. Camera pictures of composite tape after drying at (a) pH 3 and (b) pH 7 with CMC binder M_w=700,000 DS 0.9 (solid loading 16.7%)

3.4 Efforts to optimize the adhesion and eliminate the cracks at pH 3

In order to achieve composite electrodes firstly with good mechanical properties (strong adhesion, cohesion and elimination of the cracks after drying), many efforts were carried out. The dispersion of CMC was improved by different ways:

- Increasing energy mixing from 500rpm to 700rpm in order to have better mixing of CMC, Si and CB particles.
- Pre-dissolving measured amount of CMC in buffer solution (before adding measured amount of Si and CB into the milling vial) by various mixing methods:
    - ✓ Using ball milling at 700rpm in 1hour
    - ✓ Using rolling machine in 24 hours
    - ✓ Using magnetic stirrer in 24 hours
    - ✓ Combination of magnetic stirrer with heating at 50-70^{o}C in 24 hours

In summary, all above methods couldn't solve the issues with the mechanical strength and cracks still appeared on the tape after drying. We then considered the surface area of Si AA that is so large (70-80 m^2/g) that the amount of binder used might be insufficient to obtain good adhesion and connect all particles together to eliminate the cracks. Therefore, the quantity of CMC binder was increased from 8 to 10wt% and then 16wt% along with the decrease of the amount of Si from 80 to 78% and 72%, respectively, while the amount of conductive additive was unchanged. Typically, Figure 3-6 shows pictures of composite tapes (10wt% and 16wt% of CMC binder) with still poor mechanical properties. With 16wt% CMC binder, the appearance of the tape is better with fewer cracks. It suggests however that the amount of binder is still not high enough to achieve satisfactory mechanical properties. However, I haven't tried with larger CMC quantities

because the electrode slurries with 16wt% CMC were already very viscous. A strategy would have been to decrease the solid loading of the slurry; however, it is known that it is difficult to make thick electrodes from dilute slurries as a consequence of significant shrinkage upon volatile solvent removal upon drying.

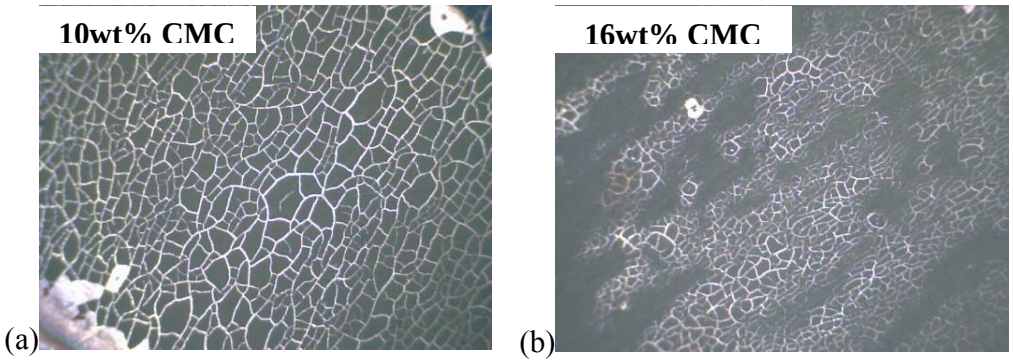

Figure 3-6. Camera images of the tapes with different amount of CMC binder
(a) 10wt% and (b) 16wt%

In addition, during experiments I observed that the quality of Si AA varies from batch to batch supplied by producer (Figure 3-7). It also can be proved by scratching test with two measurements: 1st measurement for old batch (in May 2011) and 2nd measurement for new batch (in October 2011) (Table 3-3).

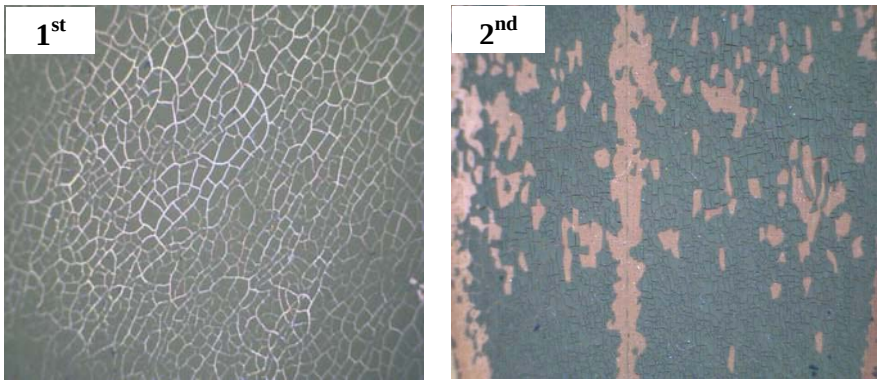

Figure 3-7. Camera image of the tapes of Si with different batches
(80wt%Si 12wt%AcB 8wt%CMC in buffer pH=3, solid loading 16,7%)

Table 3-3. Scrapping load of different tapes at different pH

Electrode formulation	Solid loading (%)	pH	Scrapping load (g)	
			1st measurement	2nd measurement
80wt%Si 12wt%CB 8wt%CMC	16.7	3	30-40	0-10
		7	20-30	0-10

In summary, I couldn't succeed to obtain the optimized formulation for Si AA with high active mass loading. It could be ascribed to very small particle size (~50nm) and large surface area of

Si AA, thus the amount of CMC binder is insufficient to achieve good connection of all the particles and high mechanical strength in composite electrode. This will be discussed more in the following part with optimized formulation based on Si CEA. In addition, the quality of Si AA varies from batch to batch leading to lack of reproducibility. As a result, Si AA was replaced by using Si CEA to work on the electrode formulation.

3.5 Preparation of composite electrodes with Si CEA

The electrode formulation applied was 80wt%Si 12wt%CB 8wt%CMC with the active material based on Silicon CEA (BET 13.8m²/g) and conductive agent (acetylene black CB), CMC as binder (DS=0.9, M_w=700,000). The solid loading is ~17wt% (200mg/1ml). The composite tapes after drying are shown in Figure 3-8. With Si CEA, we successfully achieved good tapes prepared in both pH 3 buffer solution and in pH7 distilled water with satisfactory Si loading. Basically, the tapes obtained have only few small cracks on the surface and the Si loading is higher than 2mg/cm^2.

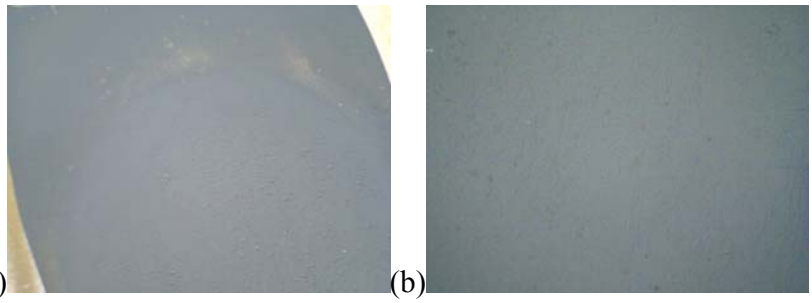

Figure 3-8. Camera images of the tape with formulation 80%Si:12%AcB:8%CMC at (a) pH 3 and (b) pH 7

The question here is why I couldn't prepare electrode with same formulation using Si AA? In previous studies, Azmach Toleza [7] and I [8] optimized the formulation of a C-$LiFePO_4$ (LFP) based composite electrode with different particle sizes and carbon coatings (50nm-4wt%C, 150nm-2.8wt%C, 400nm-2.1wt%C). The optimized electrode compositions are shown in Table 3-4.

[7] A. Toleza, "Modeling and optimization the positive Electrode of lithium ion batteries based on $LiFePO_4$", master thesis report (2009).
[8] B.P.N. Nguyen, "Design of the formulation of $LiFePO_4$-based positive electrode as a function of the particle size", master thesis report (2010).

Table 3-4. Optimized composition of different composite electrodes with C-$LiFePO_4$ as an AM.

Particle size (nm)	$LiFePO_4$ (wt%)	CB (wt%)	PVdF (wt%)
LFP - 50nm	76	10	14
LFP - 150nm	87.5	5	7.5
LFP - 400nm	86.5	8.5	5

BET measurements of different active materials and conductive additive are shown in Table 3-5:

Table 3-5. Specific surface area of different materials

Sample – particle size	BET (m^2/g)
LFP - 50nm	54.8
LFP - 150nm	29.3
LFP - 400nm	18
Si CEA - 150nm	13.8
Si AA - 50nm	75
CB	77

The ratio Γ (mg/m^2) between the amount of binder in the electrode composition and the total surface area of the powder (AM + CB), taking into account the amount of both powders and their specific surface area is calculated and shown in the Table 3-6.

Table 3-6. The ratio Γ between the amount of binder in the electrode composition and the total surface area of the powder (AM + CB) for different active materials

Active material	Total surface area (AM+CB) in 100mg composite electrode (m^2)	Amount of binder in 100mg composite electrode (mg)	The ratio Γ (mg/m^2)
LFP - 50nm	4.93	14	2.8
LFP - 150nm	2.95	7.5	2.5
LFP - 400nm	2.21	5	2.3
Si CEA - 150nm	2.03	8	3.9
Si AA - 50nm	6.92	8	1.16
Si Delft – 20nm	12.12	8	0.66

According to Table 3-6, sufficient adhesion to the current collector could be obtained for Γ values higher than 2.3 mg/cm^2. Contrarily, for Γ lower than 1.16 (i.e. the case of Si AA with the same electrode formulation of Si CEA) poor adhesion was obtained. The values between different active materials are slightly different because of different morphology of the surface and different type of binder. The theoretical quantity of CMC which is necessary to reach the critical order of value of Γ to achieve good adhesion with Si AA is calculated ~27mg of binder (if considering here the same ratio Γ of Si CEA) that is more than 3 times higher than the amount

used in formulation of Si CEA. This explains why I couldn't succeed in preparing thick electrodes based on Si AA with good mechanical properties.

In summary, we couldn't succeed to obtain the optimized electrode formulation based on Si AA with AM loading higher than 2mg/cm^2. It could be explained that Si AA contains small particle size (50nm and less) and high specific surface area, thus the amount of CMC binder up to 16wt% is insufficient to achieve good mechanical properties. In addition, the quality of Si AA doesn't have the same properties from different batches, which leads to lack of reproducibility. Hence, we decided to move from Si AA to Si CEA for optimizing the negative electrode formulation. Preliminary tests of composite slurries prepared both in buffer solution pH 3 and in de-ionized water pH 7 show good mechanical properties with high Si CEA loading (>2mg/cm^2).

Based on our results, we decided to not make electrode formulation trials with Si from TUD. Indeed, this Silicon has very low particle size (~20nm and ~140m^2/g). We can also calculate the theoretical quantity of CMC which would be necessary to reach the critical order of value of Γ~3.9. It gives 47.3wt%. According to the state-of-the-art and our background, it is not possible to prepare electrodes with such high binder content by ball milling and tape casting to reach significant active mass loading. However, other processing techniques such as spray coating could allow to prepare composite electrodes with such nanomaterial and reasonable binder content [9]. Nevertheless, the processing method available at CEA for large-scale manufacturing is slot die coating, a derivative of tape-casting.

3.6 Preparation of composite electrodes based on Si CEA in distilled water pH 7

In order to validate the previous results achieved in the group about the influence of the pH of the aqueous electrode slurry on the electrochemical performance of the electrode, I made some investigations on the influence of this parameter (pH) for Si CEA. Plextol X4020 was used in pH 7 in order to eventually improve the mechanical properties of the tape. The amount of Si and CB was kept constant while decreasing the amount of CMC (from 6wt% to 2wt%) and increasing the amount of Plextol X4020 (from 2wt% to 6wt%) respectively (Table 3-7).

[9] D. Munao et al., "Si based nano-composites electrodes and strategies to reduce the irreversible capacity loss", oral presentation at ALISTORE ERI meeting in Warsaw (2011).

Table 3-7. Composition, scraping load and AM loading of composite electrodes prepared in distilled water pH 7

Electrode name	Si (wt%)	CB (wt%)	CMC (wt%)	Latex (wt%)	Scrapping load (g)	AM loading (mgSi/cm^2)
X1	80	12	8	-	300	2.4-2.6
X2	80	12	6	2	500	2.3-2.5
X3	80	12	4	4	400	2.4-2.9
X4	80	12	2	6	200	2.1-3.0

Plextol X4020 helps to increase the adhesion of the tape with small quantity (2wt%). The scrapping load starts increasing when latex is used and reaches the maximum at 2wt% for X2 then decreases for X3 and X4. It confirms that Plextol X4020 could help to improve the mechanical strength of the tapes. SEM images of X1 electrode show the particles are fairly well dispersed at micro scale (Figure 3-9a). However, when the amount of latex increases, the homogeneity of the electrode degrades with agglomeration of latex (Figure 3-9c) and inhomogeneous distribution of particles (Figure 3-9b,c,d). The electrodes with high amount of latex (X3 and X4) exhibit more area which has rich carbon or Si particles than the electrodes without or with less latex (X1 and X2). This is quite consistent with the poorer reproducibility of the active mass loading along the length of the dried tape of these less homogeneous X3, X4 electrodes compared to the others (Figure 3-10 and Table 3-7). Therefore, it can be concluded that CMC binder favors homogeneity, as already shown in previous work [6]. The lower content of CMC in X3 and X4 than in X2 and X1 likely explains the poor homogeneity of X3 and X4. The decreasing mechanical strength of X3 and X4 versus X2 could be explain by both the lack of homogeneity as well as the lack of CMC that plays a role on the mechanical strength through the bridging of the particles at the molecular scale [10].

[10] B. Lestriez, C. R. Chimie, 137 (2010) A1341.

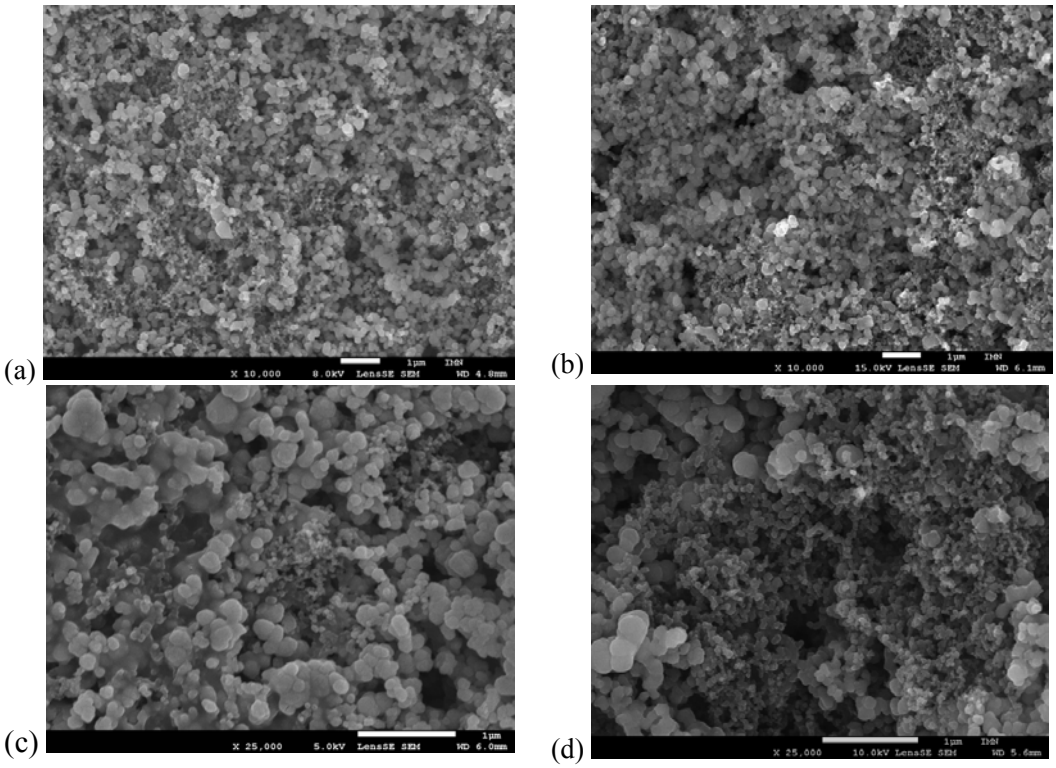

Figure 3-9. SEM images for electrode X1 (a), X2 (b), X3 (c) and X4 (d).

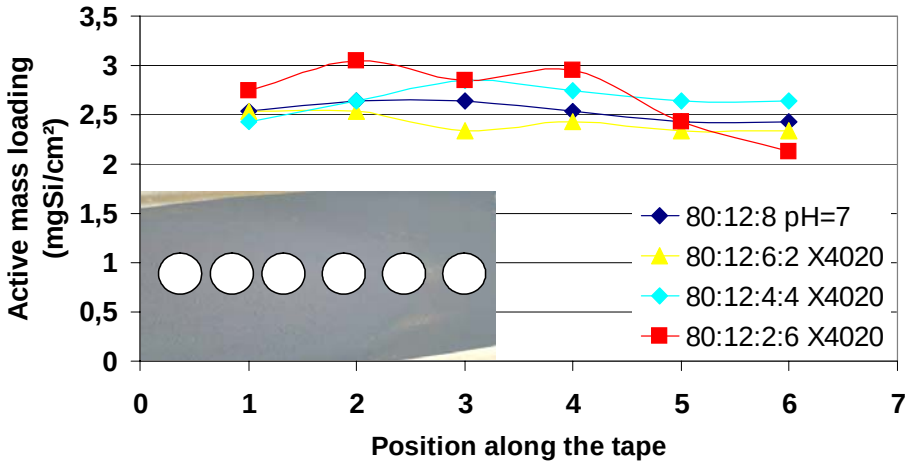

Figure 3-10. Evolution of active mass of different tapes (pH 7) at different positions along the tape

Electrochemical studies were done with X1 and X2 electrodes which show better properties (homogeneity, mechanical strength) than the others. Before battery assembly, a further drying at 100°C in 2 hours under dynamic vacuum was done. Two-electrode Swagelok™ test cells using Si-based composite electrodes were assembled in the glove box under argon atmosphere with lithium metal as counter electrode, porous glass paper as separator soaked in different electrolytes:

- 1M $LiPF_6$ solution in an EC-DMC (1:1) mixture (LP30).
- 88 wt% LP30 2wt% VC 10wt% FEC (LP30 VCFEC).

The voltage range used was 0.01-1.0V. The batteries were cycled with discharge capacity limitation to 1200mAh/g_Si. Electrochemical performance is done first at C/20, D/20 then at C/2, D/2 where C and D implies charge and discharge rate respectively.

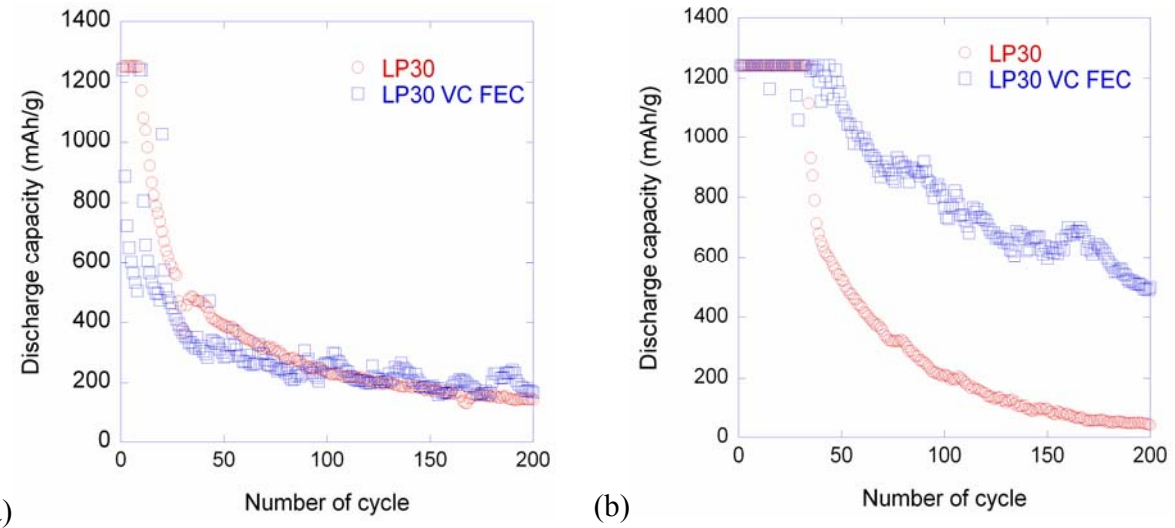

Figure 3-11. Discharge capacity as a function of number of cycle of electrode formulation X1 (a) and X2 (b) with different electrolyte composition

Figure 3-11 shows poor electrochemical behaviours with fast capacity drop and low cyclability for both electrodes prepared at pH 7. X2 electrodes display better performance than X1 electrodes. It might be due to better adhesion of the X2 electrode upon cycling. Some improvement in capacity retention was observed with addition of VC FEC additives. Nevertheless, the performance is much poorer than the one I obtained when preparing the electrodes in pH 3buffer solution in preliminary tests (see next part). Neither X1 nor X2 electrodes could meet EuroLiion's target of a cycle life of more than 500 cycles. As a result, I stopped working on the preparation of electrodes at pH 7 and fully investigated the electrode formulation prepared in pH 3 buffer solution.

3.7 Optimized 1st electrode formulation with CB as a conductive additive (paper I)

PEI and PAMA were selected as possible dispersants for pH 3 buffered aqueous silicon-based electrode slurries as they could retain enough charged functional groups at pH 3 to work as dispersant according to the electro-steric mechanism described by Li and co-workers [11,12]. Indeed, PEI is a cationic polyelectrolyte, which –NH2 functional groups are charged as –NH3+ in acidic conditions. PAMA has shown some favourable interaction with carbon black conductive additive in acidic conditions with zeta potential values of carbon black/PAMA particles at pH 3 of -20mV [13].

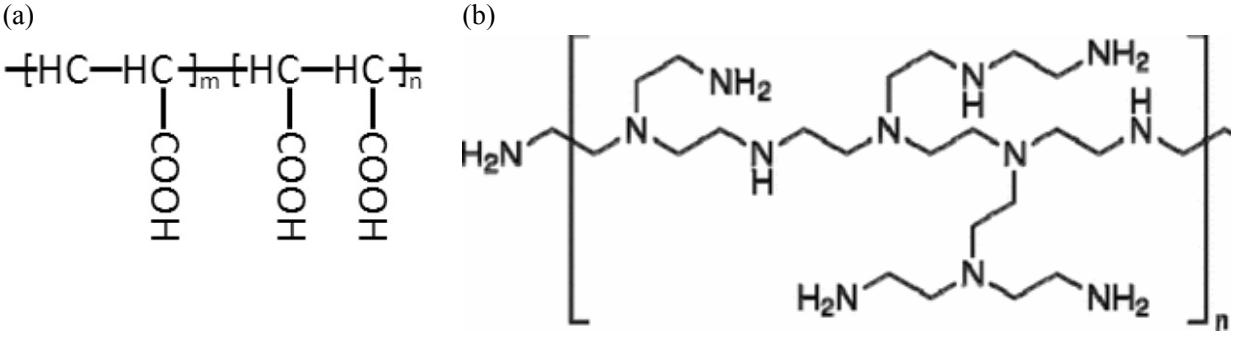

Figure 3-12. Diagram showing chemical structure of (a) PAMA and (b) PEI [14]

3.7.1 Electrode preparation

Composite electrodes were made of nanometric Si CEA as an active material (AM), Super P carbon black (CB) as a conductive additive (C), Carboxylmethyl cellulose (CMC, DS=0.9, M_w=700,000 g/mol) and a Styrene-co-Butadiene rubber copolymer latex (SB) as a binder (B) and Poly (acrylic-co-maleic) acid (PAMA M_w=3000 g/mol) Polyethyleneimine (PEI M_w=2000 g/mol) as a dispersant (D).

At the lab scale, powders were introduced in a silicon nitride vial according to the electrode formulations given in Table 3-8. Then, 1mL of buffer pH 3 (0.1M solution prepared with KOH and citric acid) was added to 200mg of composite electrode material. The solid loading is thus ~17wt%. Three silicon nitride balls (9.5mm diameter) served as mixing media. A Fritsch

[11] C.C. Li, J.T. Lee, C.Y. Lo, M.S. Wu, Electrochem. Solid-State Lett. 8 (2005) A509.
[12] C.C. Li, J.T. Lee, X.W. Peng, J. Electrochem. Soc. 153 (2006) A809.
[13] C.C. Li, Y. Wang, T. Yang, J. Electrochem. Soc. 158 (2011) A828.
[14] Li J et al. J. Electrochem. Soc., 160 (2013) A201.

Pulverisette 7 mixer was used to mill the slurry at 500rpm for 60 minutes. The slurry was tape cast onto a 25µm thick copper foil and dried for 12h at room temperature and then at 2h at 100°C under vacuum. Citric acid and its salt, which are not eliminated by this vacuum treatment, remain in the composite tape. We verified that a film prepared by evaporating water from a pH 3 buffer solution is not soluble in the liquid electrolyte.

At the pilot scale, CMC was dissolved in the pH 3 buffer solution, prepared with KOH and citric acid at 0.1M. PAMA was added before introducing the conductive additive and the AM. The suspension is then dispersed using a high speed stirrer for 30 min. At the end of the dispersion, the SB latex is added and the slurry shortly homogenised. The slurries were coated using a semi industrial machine, with a comma bar system and an oven of 1m length onto a 10µm thick copper foil at a speed of $0.2 m.min^{-1}$. The transit time in the oven is so around 5 min.

Table 3-8. Composition, porosity, thickness and mean resistivity (measured with 2 probes) of composite electrodes. L and P mean an electrode prepared at the lab scale and at the pilot scale, respectively.

Electrode name	Si (wt%)	CB (wt%)	Latex (wt%)	CMC (wt%)	Buffer (wt%)	PAMA (wt%)	Porosity (%)	Thickness (µm)	Loading (mg/cm²)	Conductive additive volume fraction [a] (%)	2-probes resistivity with stand. dev. (ohm.cm)
La	-	51	-	16	33	-	-	-	-	-	-
Lb	-	49	-	15.7	31.8	3.5	-	-	-	-	-
Lc	-	47	-	15.2	31	6.8	-	-	-	-	-
Ld	-	43.2	-	14.4	29.5	12.9	-	-	-	-	-
L1	67.6	10.1	-	6.8	15.5	-	71-73	66-68	2.6-2.8	3.06	11.6 ± 0.5
L2	65.9	10.1	-	6.8	15.5	1.7	68-70	63-65		3.30	7.6 ± 0.5
L3	64.2	10.1	-	6.8	15.5	3.4	65-68	60-62		3.55	12.7 ± 0.5
P1	65.9	10.1	-	6.8	15.5	1.7	70-71	52-54	2.0-2.1	3.24	11.4 ± 0.5
P2	63.5	9.7	3.6	6.6	15	1.6	68-69	50-51		3.14	9.5 ± 0.5
P3	61.3	9.4	6.9	6.3	14.5	1.6	68-69	52-54		3.01	11.1 ± 0.5
P1	65.9	10.1	-	6.8	15.5	1.7	59-60	41-42	2.0-2.1	4.40	9.4 ± 0.5
P2	63.5	9.7	3.6	6.6	15	1.6				3.97	8.1 ± 0.5
P3	61.3	9.4	6.9	6.3	14.5	1.6				3.85	9.7 ± 0.5

[a] The volume fraction is calculated by taking into account the electrode porosity.

3.7.2 Optimization of the dispersant choice through sedimentation test

30mg of each material (Si, CB, Si+CB) was dispersed in pH 3 buffer solution by using ultrasons for 15 minutes. The volume of solution used is 15ml and contains different amount of additive. The dispersant quantity was adjusted in order that its concentration (mg/mL) is the same as for electrode preparation. The process of settling was observed as a function of time.

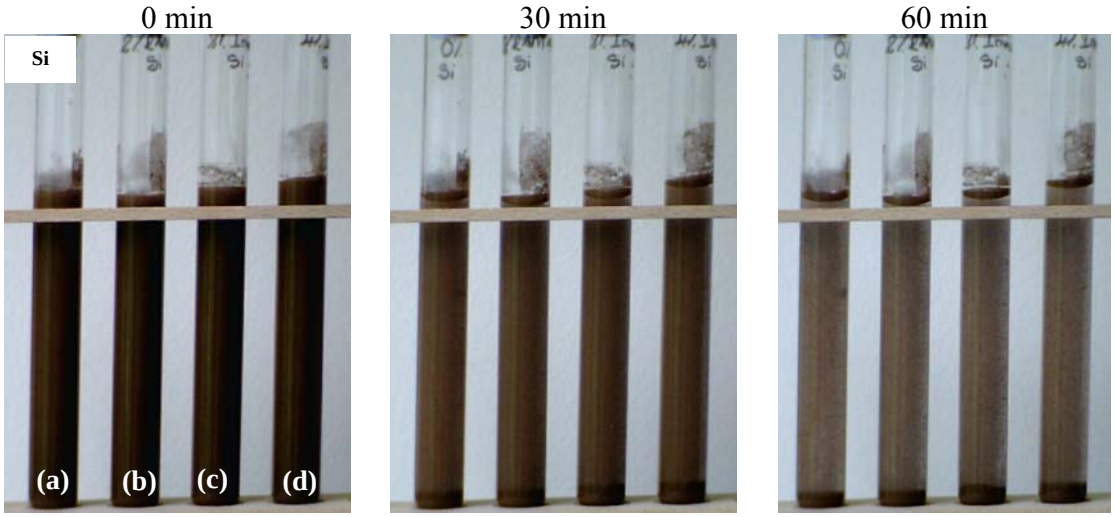

Figure 3-13. Settling test of Si and different dispersants as a function of time
(a) No dispersant (b)1.7wt%PAMA (c)1.7wt%PEI and (d)3.4wt%PEI

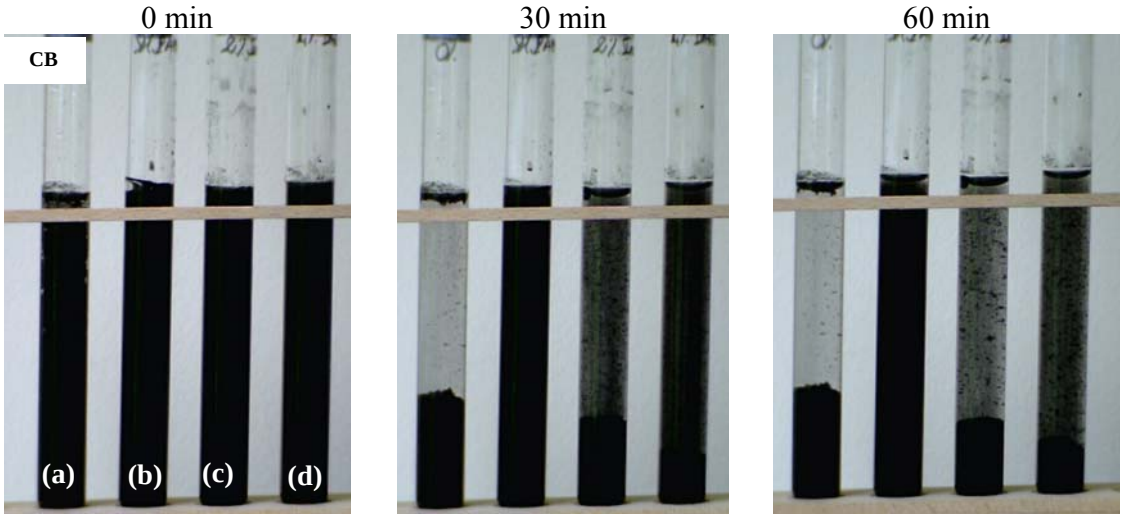

Figure 3-14. Settling test of AcB and different dispersants as a function of time
(a) No dispersant (b) 1.7wt%PAMA (c) 1.7wt%PEI and (d) 3.4wt%PEI

Figure 3-13 - Figure 3-15 show different pH 3 buffered suspensions of Si, CB, mixture of Si+CB in the presence of PAMA, PEI (with identical concentration in mg L^{-1} as in the electrode slurry of L2, L3) and without dispersant, respectively, after different time periods. In the initial state, Si, CB and mixture of them were homogeneously distributed in the suspension with addition of PAMA and PEI, while without dispersant the CB powder began to settle especially in the suspension of both Si+CB with the segregation into two separate phases (CB at the bottom and Si in the upper supernatant). After one hour, most of Si or CB powder settled to the bottom in the suspension without dispersant. In the suspension with PEI, most of Si and all mixture of Si+CB settle completely to the bottom while small quantity of CB still remains in the suspension. More amount of PEI used, better stability of CB observed. In contrast, the phenomena were apparently different in the suspension with PAMA. CB powder was still homogeneously distributed and mixture of Si+CB remained stable, although Si without CB settled to the bottom of the vial. From Figure 3-13, PAMA and PEI don't show obviously any effect on stability of Si in buffer solution. Concerning CB, Figure 3-14 shows practically an improvement of the stability of CB in buffer solution with addition of PAMA and PEI (3.4wt%) and the effect of PAMA is much stronger than PEI. Regarding the suspension of both Si+CB, PAMA remains an efficient dispersant as the settling phenomenon is very much decreased. (Figure 3-15).

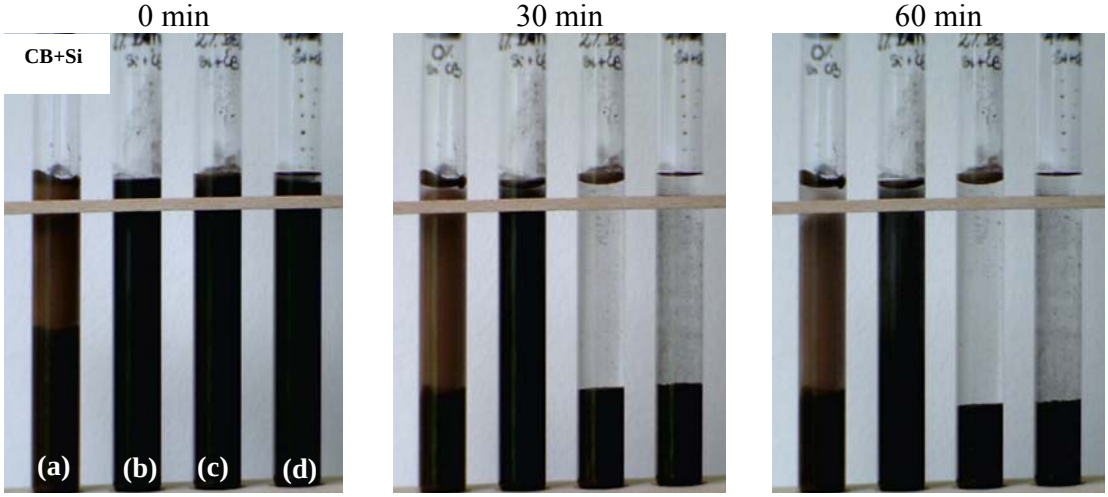

Figure 3-15. Settling test of Si, CB and different dispersants as a function of time
(a) No dispersant (b)1.7wt%PAMA (c)1.7wt%PEI and (d)3.4wt%PEI

For trials, I prepared composite tape with same formulation L2 and preparation conditions but replacing dispersant PAMA by PEI in the composition given in Table 3-8. After drying, the tape showed poor appearance with cavities (originating from bubbles) and cracks (Figure 3-16). In conclusion, PEI is not a suitable dispersant for the preparation of our composite electrodes while PAMA shows as an efficient one. I continued working with PAMA.

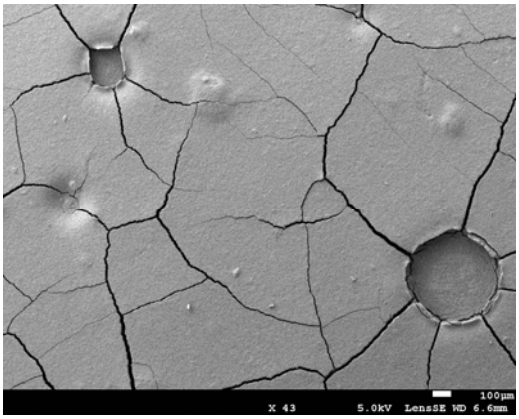

Figure 3-16. SEM observations of L2 electrode with dispersant PEI

3.7.3 Optimization of the dispersant quantity

This part is fully detailed in Paper I and here the results are briefly summarized. I tried to prepare electrodes with several quantities of PAMA, from 0 to 3.4wt% (more precisely, 0, 1.7 and 3.4wt%). I found 1.7wt% is an optimal PAMA quantity to achieve the best electrochemical performance. As can be observed from Figure 3-17a, the battery cycle life strongly depends on the amount of PAMA in the composite electrode. Without using PAMA (L1), the batteries can achieve around 200 cycles while with 1.7wt% of PAMA (L2), the cycle life increases more than 2 times (415 cycles). However, when 3.4wt% PAMA (L3) is used, the cycle life decreases sharply (30 cycles). Coulombic efficiencies over the first 50 cycles are 99.1, 99.3 and 91.4% for 0, 1.7 and 3.4wt% PAMA, respectively. In addition, when cycling at full capacity, significant improvement of capacity retention was observed with L2 compared to L1 and L3 (Figure 3-17b).

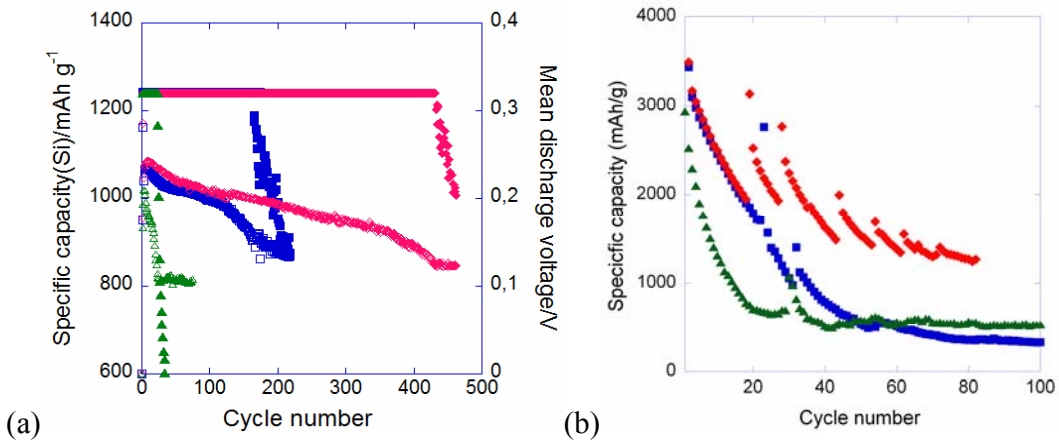

Figure 3-17. (a) Discharge capacity (■, ◆, ▲) and mean discharge voltage (□, ◇, △) versus number of cycle for electrode formulations with capacity limitation of 1200mAh per g of Si and different amount of PAMA: (■,□) 0 (L1), (◆,◇) 1.7 (L2) and (▲,△) 3.4wt% PAMA (L3). (b) Discharge capacity versus number of cycle for electrode formulations at full capacity: (■ L1), (◆ L2) and (▲ L3). The Si mass loading is 2.6mg cm^{-2}.

The interpretation of these results was obtained by combining several characterization techniques. EDX-SEM morphological analysis and mapping of the electrical resistivity of the dried tapes showed an improvement of the distribution of carbon black conductive additive (at the scale of tenths of micrometer squares), resulting in an improvement of the electrical resistivity (decrease of the electrical resistivity and better homogeneity of this property at the scale of centimetre squares) for 1.7wt% and more PAMA into the electrode formulation. However, very surprisingly, although the cycle life of the electrodes was significantly increased with 1.7wt% PAMA, it was dramatically decreased with 3.4wt% PAMA while the homogeneity and electrical resistivity were fairly similar to 1.7wt% PAMA. We then checked the electrochemical stability of PAMA by preparing carbon black/CMC/PAMA/Buffer tapes on copper foil with different PAMA contents. To prepare these L_a-L_d blends we kept the same ratio of the mass of PAMA vs. the CB powder surface area as in composite electrodes (Si+CB). These films were studied by cyclic voltammetry in the 0.05-2.5V range at the rate of 1 and 5 mV s^{-1}. Two-electrode Swagelok™ cells were used with lithium metal as counter and reference electrode and the electrolyte used is 88wt% LP30 2wt%VC 10wt%FEC. It's observed that whatever the PAMA content, the voltammograms are similar and do not evolve upon cycling (Figure 3-18). Thus we may conclude that there is no irreversible parasitic reaction associated with the presence of PAMA.

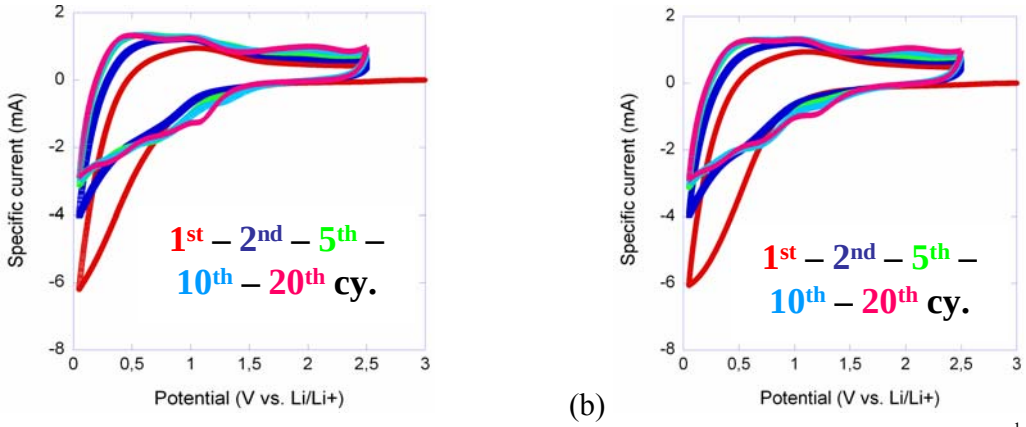

Figure 3-18. Cyclic voltamograms cycle of different tapes at different cycles (scan rate 5 $mV.s^{-1}$) (a) La (without PAMA) and (b) Lc (with 6.8wt%PAMA). The mass loading is 0.75-0.9mg/cm^2.

However, visual observations of the CB/CMC/PAMA/buffer composites shown in Figure 3-19 revealed that with increasing PAMA content, a demixing occurs between CB (dark zones) and one of the two polymers, CMC or PAMA. Thus, it might be hypothesized that by increasing the PAMA concentration in the CB/CMC/PAMA/buffer mixtures, the competition between CMC and PAMA resulted in the exclusion of the CMC from the CB particle surfaces [15]. A plausible interpretation of the very poor cycle life of L3 (3.4wt%PAMA) composite electrode is a lack of mechanical strength as a consequence of this competition between PAMA and CMC. The adsorption of PAMA to the CB surface likely impedes the adsorption of the CMC chains and thus the formation of bridges between the CB particles and the Si mass [6] which results in a catastrophic failure upon cycling.

[15] R. A. Jones and R. W. Richards, Polymers at Surfaces and Interfaces, Cambridge University Press, New York (1999).

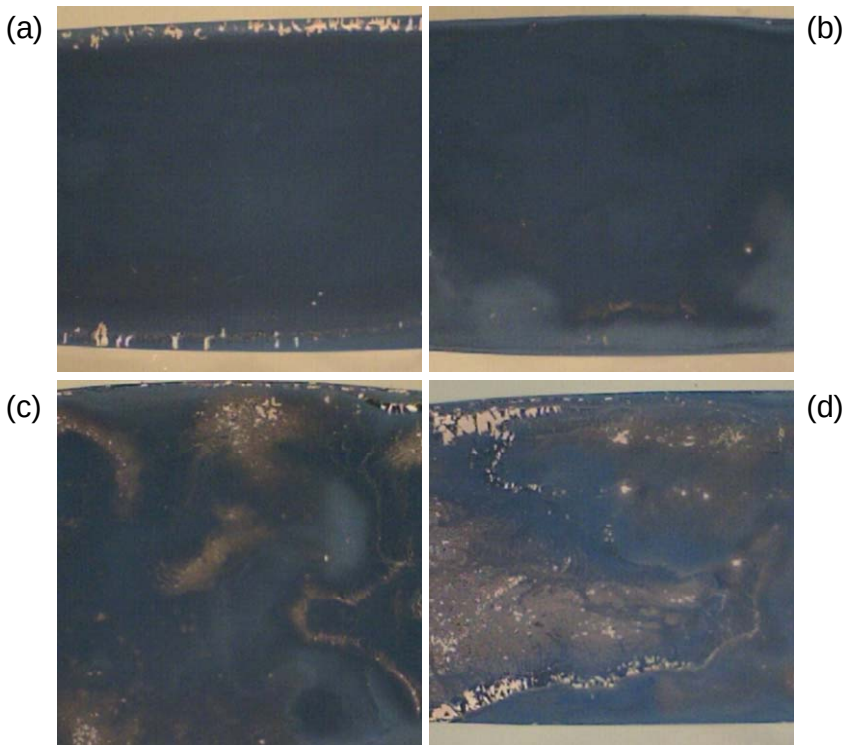

Figure 3-19. Camera pictures of CB/CMC/PAMA/Buffer tapes with varying amounts of PAMA: (a) La, (b) Lb, (c) Lc and (d) Ld tapes.

3.8 Transfer of optimized 1st formulation to the CEA pilot line

As a conclusion of this part, the electrode formulation L2 was selected for being processed at the pilot scale. Before the transfer we checked that the mechanical properties of the dried tape were good. As a matter of fact we found scrapping load higher than 500g. In order to check the homogeneity of AM loading along the tape, the evolution of the mass loading at different positions was determined (Figure 3-20). The mass loading of Si is higher than 2.5mgSi/cm^2 and it is rather homogeneous in the middle of the tape. However, it varies slightly at the end of the tape.

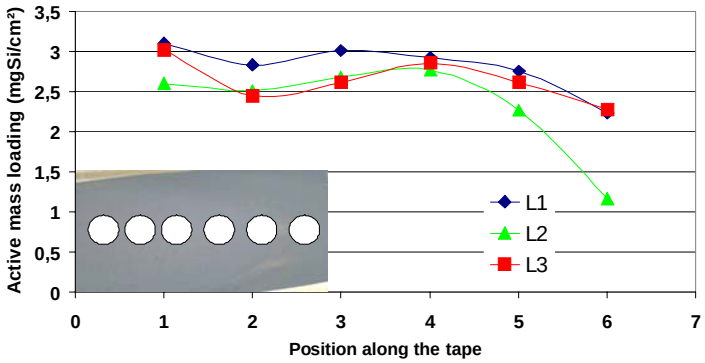

Figure 3-20. Evolution of active mass prepared at pH 3 at different positions along the tape

The rheological properties of L2 slurry were also measured and found suitable with the pilot line requirements: the viscosity is stable upon gentle stirring and the measurements of the viscoelastic moduli, under small-strain oscillatory shear, which allows to probe the structural state of the slurry at rest, demonstrate a favourable gel-like behaviour [16].

In CEA, the slurry was prepared with a total amount of 350g and a solid loading of 21%. The rheological properties of the slurry were found well adapted to a coating process with a comma bar system. However, the tape obtained after coating this slurry showed a low adhesion to the copper current collector. Moreover, the suppleness was not enough for winding the electrode to make lithium-ion cell prototype. Two complementary strategies to improve this adhesion were evaluated: the addition of a complementary elastomeric binder (a styrene-co-butadiene rubber copolymer in the form of a latex) and the calendaring of the electrode. The electrochemical performance of these P1-P3electrodes (Table 3-8) is shown in Figure 3-21. Cycling tests were done at capacity limitation of 1200mAh per g of Si. The P1 electrode which is non-calendared and contains no latex as L2 shows a lower cycle life than the latter, i.e. 100 vs. 450 cycles, a result which could be attributed to a poorer CB distribution in P1 vs. L2 (see later) and a lower adhesion of P1 to the Cu copper collector than L2. The cycle life is compared for P1, P2 and P3 for their different porosities in Figure 3-21b. Without calendaring and at high porosity (~69%), the cycle life increases with increasing the amount of latex, i.e. with increased adhesion. Another general trend is a shorter cycle life when the porosity is decreased (when the electrode is calendared).

[16] W. Porcher, B. Lestriez, S. Jouanneau, D. Guyomard, J. Electrochem. Soc. 156 (2009) A133.

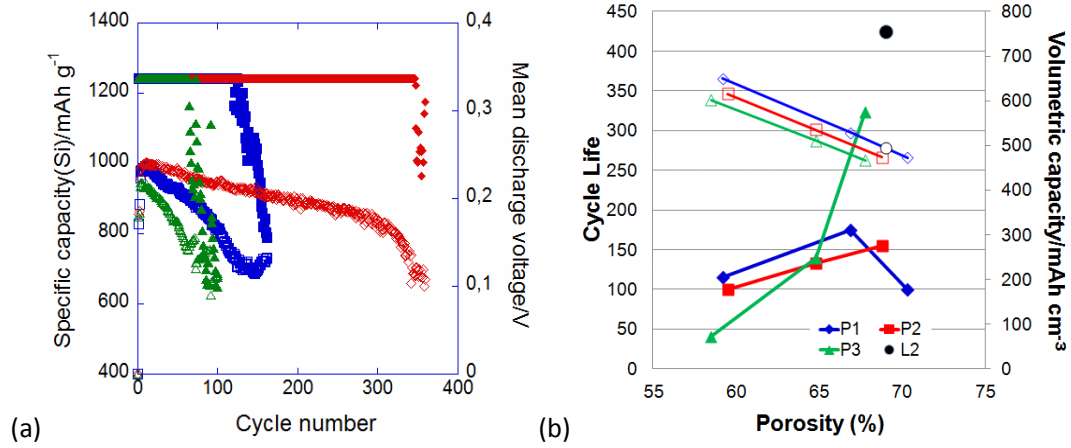

Figure 3-21. (a) Discharge capacity (■, ◆, ▲) and mean discharge voltage (□, ◇, △) versus number of cycle for electrode formulations with capacity limitation of 1200mAh per g of Si and different latex content or porosity: (■,□) P1 without calendaring, (◆,◇) P3 without calendaring, and (▲,△) P3 with calendaring down to 60% porosity. The Si mass loading is 2.0-2.1mg cm^{-2}. (b) Cycle life and the calculated volumetric capacity of the electrodes for L2, P1, P2 and P3 as a function of the porosity.

The reason of the poorer cycle life of the electrodes prepared on the pilot line compared to electrodes prepared in the lab could be interpreted based on morphological analysis and electrical resistivity measurement. The morphology of the tape cast electrodes were observed by SEM and analyzed by SEM-EDX chemical mapping (Figure 3-22). The CB appears less well distributed than in the composite electrodes prepared in the lab which could be ascribed to the different processing scales involved. Indeed, the preparation of electrodes at the lab scale implies small quantities and short mixing and casting durations, while at the pilot scale much larger quantities and much longer mixing and casting durations are implied. In particular, it is known that longer duration is detrimental to the stability of a slurry and thus to its homogeneity. The comparison of the electrical measurements in Table 3-8 quantitatively agrees with a poorer distribution of the CB as the electrical resistivity of P1-P3 are higher than L2, i.e. 9.5-11.4 vs. 7.6 ohm.cm for non-calendared P1-P3 vs. L2, respectively.

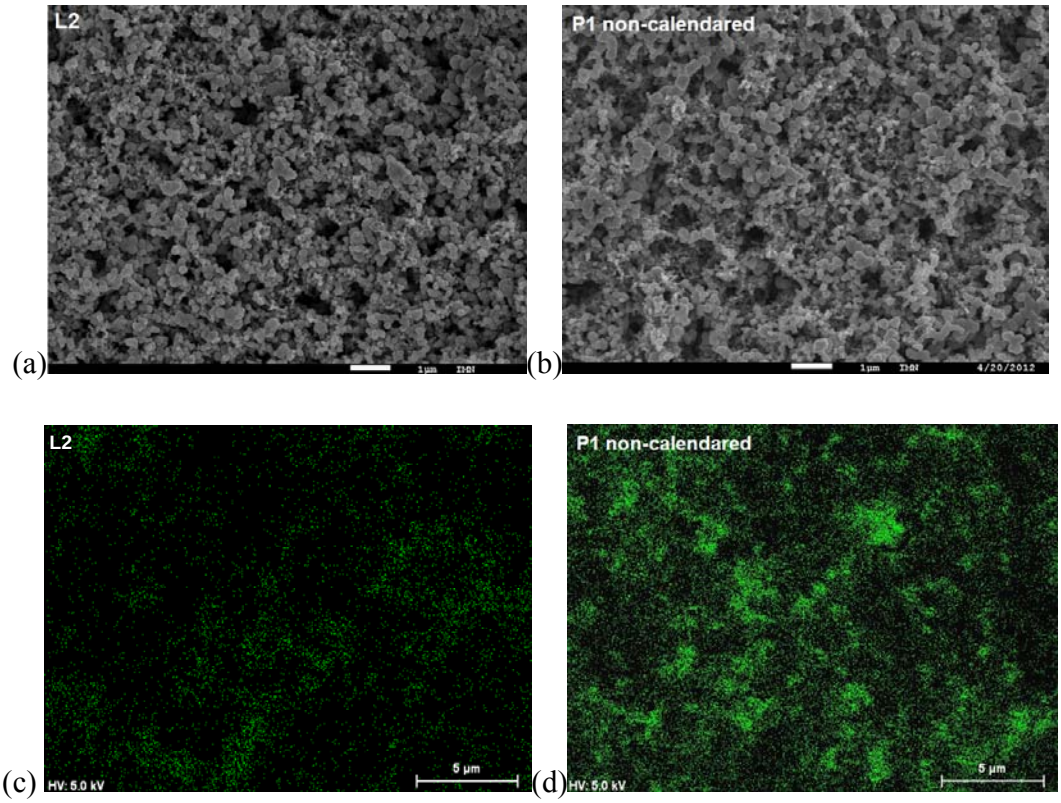

Figure 3-22. SEM images for electrode (a) L2 and (b) uncalendared P1. The EDX mapping image for Carbon in (a) L2 and in (b) uncalendared P1.

3.9 2nd formulation with exfoliated graphite as a conductive additive (paper II + III)

In order to move to 2nd formulation, different conductive additives were tested instead of acetylene black (CB): carbon nanofibres (VGCF-H from Showa Denko, 16m^2/g), carbon nanotubes (MWCNTs from Nanostructure & Amorphous Materials Inc., 110m^2/g), graphene (from CEA-INAC) and exfoliated graphite (GM15 from XG Sciences, 120-150m^2/g).

3.9.1 Study with VGCF and MWNTs instead of CB as a conductive additive

Concerning VGCF-H, pre-dissolving of CMC in buffer solution (0.1M, pH=3) prepared with KOH and citric acid was done by using ball miller at 500rpm for 30 minutes to have homogenous distribution of CMC into slurry. Measured amount of this mixture and corresponding mass of Si and VGCF-H (solid loading ~17wt.%) according to the L2 electrode formulation (VGCF instead of CB) were added and ball milled at 500rpm in 30 minutes. Regarding MWNTs, 1wt% of CMC and 8 wt% of MWNTs were ball milled in 1ml of buffer pH 3 for 15 hours at 700rpm in order to de-agglomerate the MWNTs. The rest of the composite

electrode material was added according to the L2 electrode formulation (MWNTs instead of CB) then ball milled in 2h at 500rpm (solid loading ~17wt%). Before ball milling, all constituents were hand mixed to achieve homogenous colour.

The homogeneity of the composite electrode with MWNTs is observed in Figure 3-23. Lots of cracks were observed after drying. We can calculate Γ for this electrode to be 3.3. This ratio is close to the critical value of 3.9mg/cm². Considering the latter value of 3.9mg/m², the theoretical amount of CMC to achieve good mechanical strength is 9.5mg. Furthermore, at a lower scale pronounced agglomeration of MWNTs can be observed. We also tried to adjust many factors like solid loading, ball milling time, amount of binder… in order to have better results. However, it's inefficient to disperse MWNTs in the composite electrode. As a conclusion, MWNTs is not an ideal candidate (instead of CB) in our case.

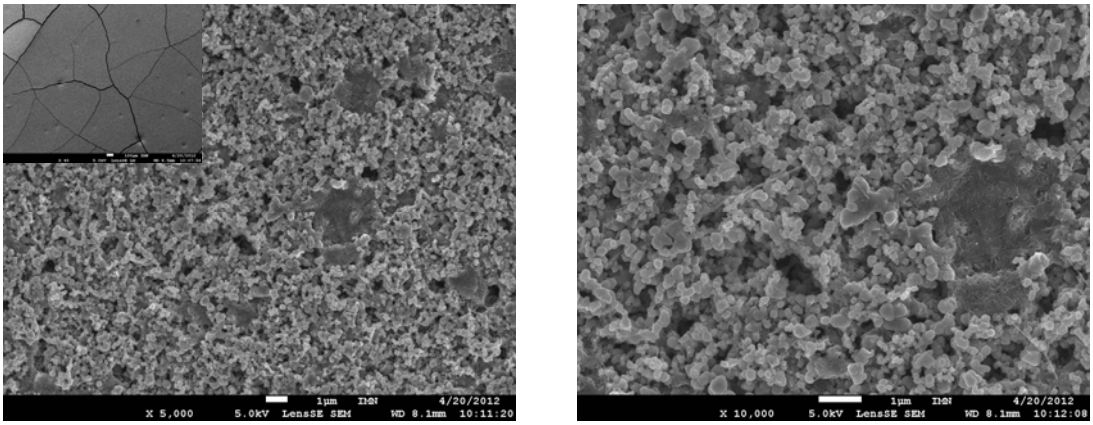

Figure 3-23. SEM images of composite electrode with MWNTs as a conductive additive

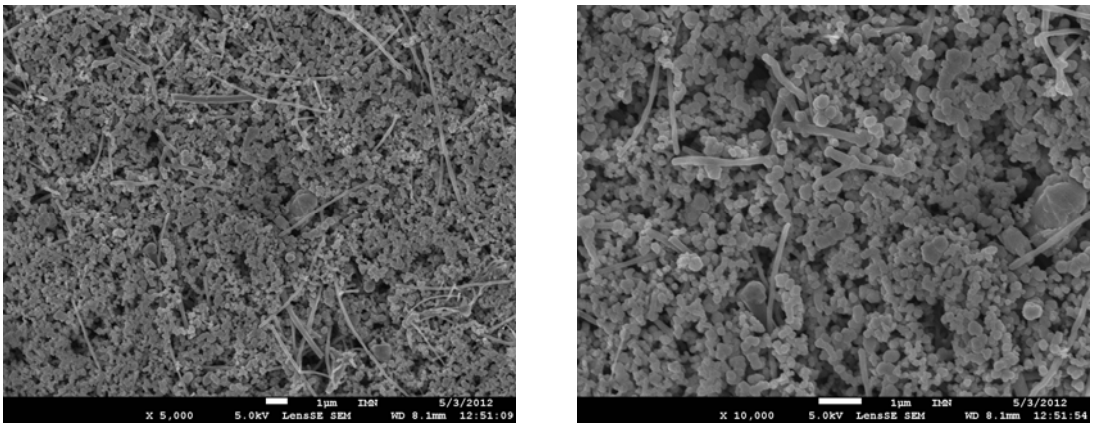

Figure 3-24. SEM observations of composite electrode with VGCF as a conductive additive

As can be seen from Figure 3-24, a fairly good distribution of VGCF among silicon particles was obtained. However, on can note that there are large zones of silicon particles without any conductive additive inside. Two batteries of this formulation were cycled with discharge capacity limitation to 1200mAh/g_Si and 88wt%LP30 2wt%VC 10wt%FEC electrolyte. The batteries could achieve less than 250 cycles (not shown). Contrarily to previous work with micrometric silicon [3], shorter cycle life is found for VGCF-based silicon electrode compared to CB-based ones. The difference observed between electrode based on CB and VGCF as a conductive additive could be due to coarser dispersion of VGCF in the composite electrode than CB, which can be more finely divided and distributed. Schematically, the morphology of the CB-based electrode can be described as a mosaic/patchwork of small silicon and small CB clusters, the smaller the CB clusters (L2 vs. L1) the longer the cycle life. The morphology of the VGCF-based electrode is closer to that of L1 with VGCF fibres segregated between large silicon clusters. As a conclusion, VGCF is not an ideal candidate (instead of CB) in our case.

3.9.2 Study with graphene instead of CB as a conductive additive

Aside to the EuroLiion project, I had an opportunity to collaborate with Nanjundan Ashok Kumar from CEA-LINAC during his stay for two weeks at IMN to evaluate graphene as a conductive additive. The results were spectacular with much better capacity retention, longer cyclability and higher Coulombic efficiency with reduced graphene oxide (rGO) compared to CB (paper II). In summary, the composite electrodes were prepared based on L2 formulation and according to same processing conditions but using graphene oxide (GO) or reduced GO (rGO) instead of CB. rGO was prepared from GO using hydrazine hydrate as a reductant [17]. Figure 3-25 shows high-resolution transmission electron microscopy (HRTEM) image of rGO, which exhibits typical wrinkled morphologies with a mixture of single to few-layered graphene structures. In the GO and rGO-based electrodes, graphene sheets are dispersed among Si aggregates thereby leading to partial wrapping of the nanoparticles by the carbon additives (Figure 3-26).

[17] N. A. Kumar, S. Gambarelli, F. Duclairoir, G. Bidan, L. Dubois, J. Mater. Chem. A 2013, 1, 2789.

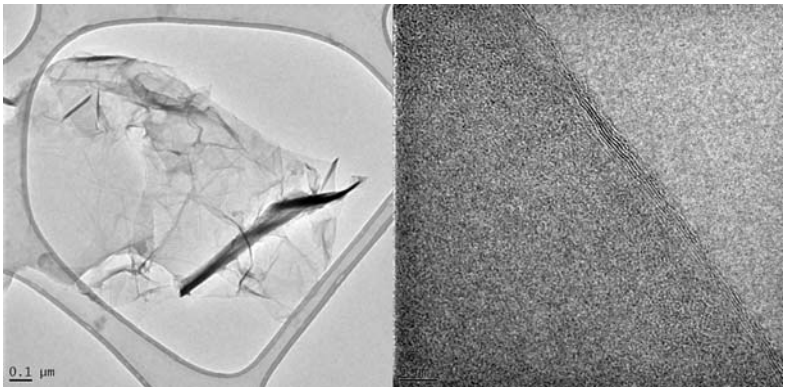

Figure 3-25. High-resolution TEM images of rGO (using a JEOL JEM-3010F microscope).

(a) 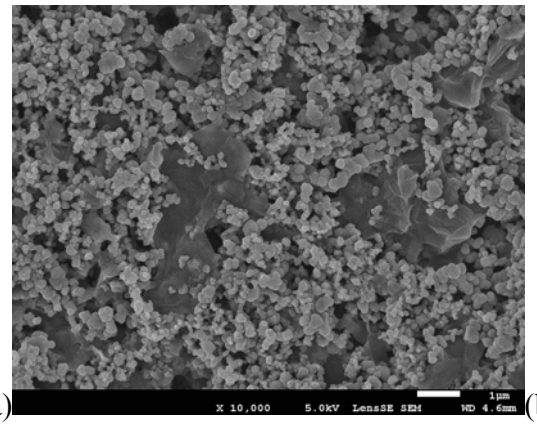

(b) 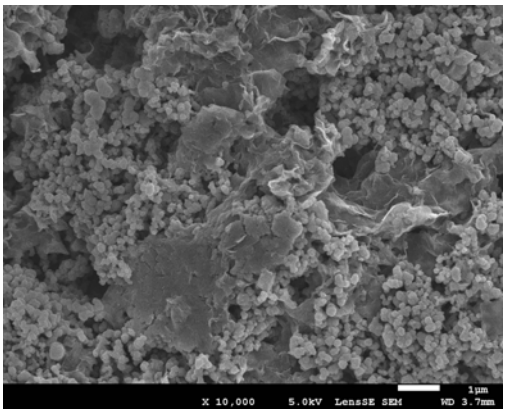

Figure 3-26. SEM images of the surface of (a) GO and (b) rGO based electrodes showing the distribution of Si nanoparticles in-between graphene sheets.

When cycling is performed with no capacity limitation, the rGO-based electrode displays a much better cycling behaviour than the CB-based one, with more than 2000 mAh/g_Si maintained after 100 cycles compared to less than 1000 mAh/g_Si, respectively (Figure 3-27). This is a fairly good result for nanoSi-based composite electrodes taking into consideration that the active mass loading is reaching 2.5 mg of Si/cm². In other words, a surface capacity of 3.3mAh/cm²_electrode is maintained after 100 cycles. After 200 cycles, the capacity retained is still 1500 mAh/g_Si (2.5 mAh/cm²_electrode). The GO-based electrode performs poorer than the rGO one, and similarly to the CB one. The analysis of the potential *vs*. composition curves indicated that the capacity fade is due to the loss of active mass through disconnection of the particles and that rGO does a much better job than CB or GO of maintaining the electrical contacts within the composite electrode.

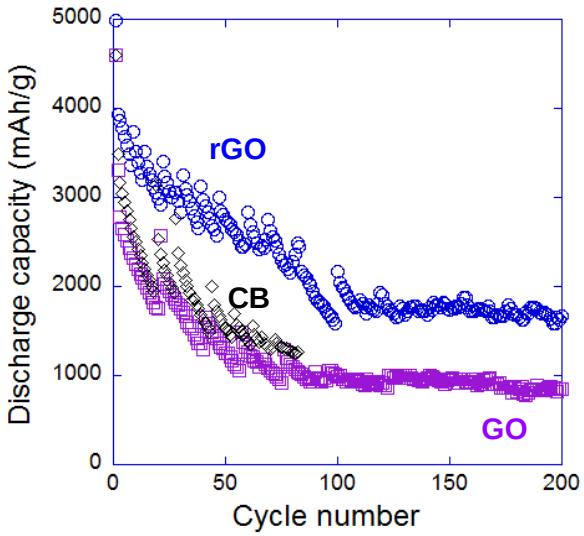

Figure 3-27. Discharge capacity in mAh/g of Si *vs*. Number of cycles for the different electrodes: (b) CB-based, (c) GO-based and (d) rGO-based electrodes.

The electrodes were also cycled with capacity limitations of 1200 mAh/g of Si. Table 3-9 gathers for all electrodes the cycle life, 1st cycle irreversible loss, and the coulombic efficiency over the 100 first cycles. Mean values are given for CB (the number of batteries cycled being 6), while for GO and rGO each value of the 2 sister electrodes is reported. The following trends can be observed from the results. With GO, a lower cycle life than with CB is observed. A much higher 1st cycle irreversible loss results likely from some in-situ electrochemical reduction of GO. The batteries cycled with rGO as a conductive additive show significantly improved electrochemical performance with longer cycle life and improved coulombic efficiencies of 99.3 and 99.9%, compared to a maximum of 99% for CB.

Table 3-9. Cycle life, 1st cycle irreversible loss, and the mean coulombic efficiency from the 2nd to the 100th cycle, for electrodes cycled with capacity limitations of 1200 mAh/g of Si.

Conductive additive	Cycle life	1st cycle irreversible loss (mAh/g_Si)	Coulombic efficiency (%)
CB	370 (+/-45)	413 (+/-54)	98.4 (+/-0.6)
GO	200 and 250	665 and 680	98.5 and 98.7
rGO	410 and 530	535 and 580	99.3 and 99.9

Using reduced graphene Oxide (rGO) instead of the standard acetylene black (CB) as the conductive additive for nanosilicon based negative composite electrodes allows thus a significant improvement of the electrochemical performance, whatever the cycling conditions. However, the synthesis of rGO is a costly process which uses dangerous chemicals (hydrazine for instance) and has a very low yield. rGO is thus not suitable for the EuroLiion project where the CEA must

produces meters of electrodes. Fortunately, a commercial and cheap material was found in large quantities with texture approaching rGO, which is exfoliated graphite GM15 from XG Sciences, which is thus suitable for semi-industrial production of silicon-based composite electrodes. GM15 nanoparticles consist of short stacks of several graphene sheets having a platelet shape with an average thickness in the 5-10 nanometer range and a diameter of 15µm. Electrodes were then prepared with GM15 as conductive additive. We found that this material allows to achieve similar performance as with rGO. The dry composition of the composite electrodes studied here is given in Table 3-10.

Table 3-10. Composition, porosity and electronic conductivity of composite electrodes

Electrode name	Si (wt%)	CB (wt%)	GM15 (wt%)	VGCF (wt%)	CMC (wt%)	Buffer (wt%)	PAMA (wt%)	Porosity (%)	2-probes resistivity with Stand. Dev. (ohm.cm)
L1	67.6	10.1	-	-	6.8	15.5	-	71-73	11.6 ± 0.5
L2	65.9	10.1	-	-	6.8	15.5	1.7	68-70	7.6 ± 0.5
L4	65.9	-	10.1	-	6.8	15.5	1.7	67-68	58.8 ± 2.9
L5	62.6	2.5	10.1	0.8	6.8	15.5	1.7	66-68	8.9 ± 0.8

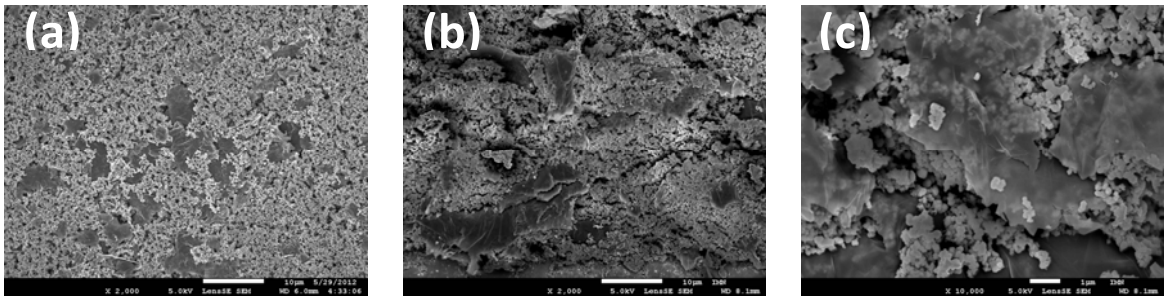

Figure 3-28. SEM observations of composite electrode L4 with GM15 as conductive additive: (a) on the surface, (b) (c) at the cross section

SEM images of cross-section and surface of GM15-based electrodes show fairly high homogeneous distribution of Si and Graphene GM15 (Figure 3-28). The composite electrode shows a lamellar-like morphology with Si nanoparticles distributed in-between graphene sheets. The conducting additives are not contacting each other, which is seen in the higher electronic resistivity of the GM15-based electrode compared to the CB one (discussed in following section). The addition of VGCF and CB was done to provide good connection between GM15 particles, which allows to increase the electronic conductivity and to reach values as high as that measured for L2 (Table 3-10).

Batteries were first cycled with discharge capacity limitation to 1800mAh/g of Silicon (1200mAh/g of electrode) (Figure 3-29). The batteries can achieve more than 200 cycles and coulombic efficiency over 150 cycles is 99.5+/-0.4%. Without capacity limitation, the cyclability of the electrode L4 prepared with GM15 is remarkably much better compared to L2 prepared with CB. With an active mass loading of more than 2.5 mg of Si per cm², the GM15 electrode shows a higher capacity compared to the CB one, i.e. a stable 1800 compared to 1200 mAh per g of Si, after 200 cycles.

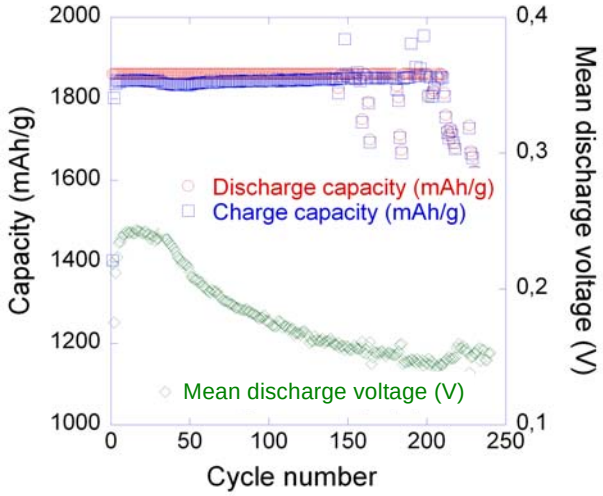

Figure 3-29. Charge/discharge capacity and mean discharge voltage versus number of cycle of electrode L4. The active mass loading is 2.6mg/cm^2. 1200mAh/g_electrode capacity limitation.

The 2nd formulation L4 based on GM15 was delivered to CEA for trials on the pilot line. As for 1st formulation, in order to increase the mechanical properties of the composite tape on copper current collector, a latex binder must be added (Table 3-11). The P4 and P5 composite electrodes also show a similar lamellar-like morphology like L4 electrode; however lower homogeneous distribution of active particle and conductive additive is observed as seen in the SEM images of the surface of these electrodes (compare Figure 3-30a-b and Figure 3-28a). The coarser distribution of GM15 in P4 and P5 compared to L4 is also consistent with the higher dry electronic resistivity of the former electrodes (Table 3-11). With addition of latex, agglomerations of Si particles form because of poor dispersion of latex added (Figure 3-30b). The latex, which is an insulating phase, increases the resistivity of P5 compared to P4.

Table 3-11. Composition, porosity and resistivity measured with 4 probes of composite electrodes. L and P mean an electrode prepared at the lab scale and at the pilot scale, respectively.

Electrode name	Si (wt%)	CB (wt%)	GM15 (wt%)	Latex (wt%)	CMC (wt%)	Buffer (wt%)	PAMA (wt%)	Porosity (%)	Loading (mg/cm²)	4-probes resistivity (ohm.cm)	Standard Deviation (%)
L2	65.9	10.1	-	-	6.8	15.5	1.7	68-70	2.6-2.8	30	6.04
L4	65.9	-	10.1	-	6.8	15.5	1.7	67-68		47	12.18
P4	65.9	-	10.1	-	6.8	15.5	1.7	74-76	1.9-2.0	142	28.8
P5	63.5	-	9.7	3.6	6.6	15	1.6	71-73		203	17.8

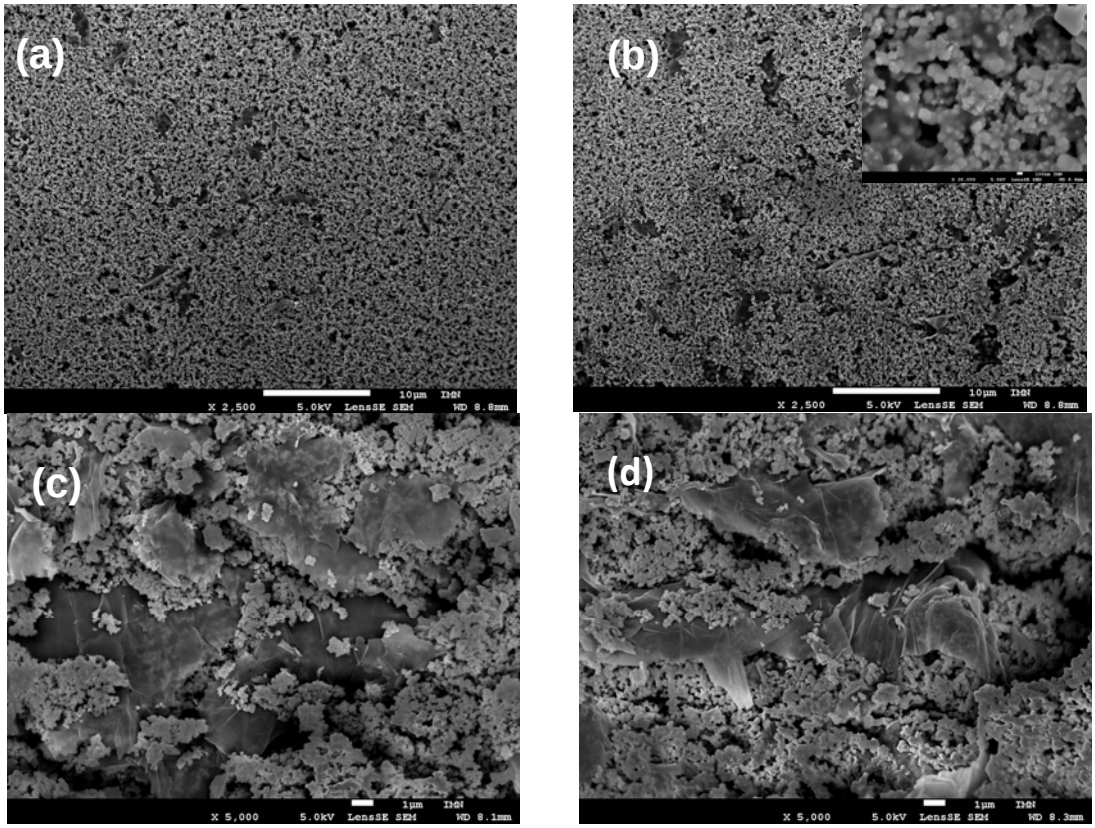

Figure 3-30. SEM observations of: the surface of electrode P4 (a) and P5 (b); the cross-sections of electrode P4 (c) and P5 (d).

Then cycling tests were done at capacity limitation of 1800mAh/g_Si and at full capacity for P4 and P5 composite electrodes prepared on the pilot line. The electrochemical performances are shown on Figure 3-31 and Figure 3-32. Addition of latex helps to increase slightly cycle life (cycling done with capacity limitation), and capacity retention (cycling done without capacity limitation), likely due to the increase of mechanical properties. However, the electrodes P4 and

P5 have poorer electrochemical properties (cyclability, capacity loss, capacity retention) than the ones prepared at the lab scale in IMN, whatever the cycling conditions. The results could be explained by SEM and electrical studies discussed before that highlight better homogeneity of the tapes prepared at the lab scale as a consequence of different mixing techniques used in IMN at the lab scale (high energy ball milling) and in CEA at the pilot scale (dissolver).

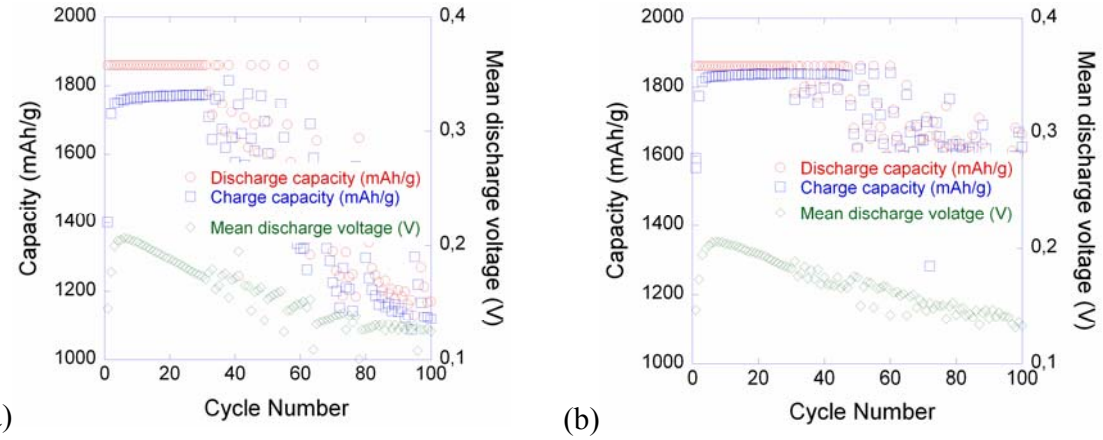

Figure 3-31. Charge/discharge capacity versus number of cycle for different electrodes at 1800mAh/g_Si limitation: P4 (a) and P5 (b).

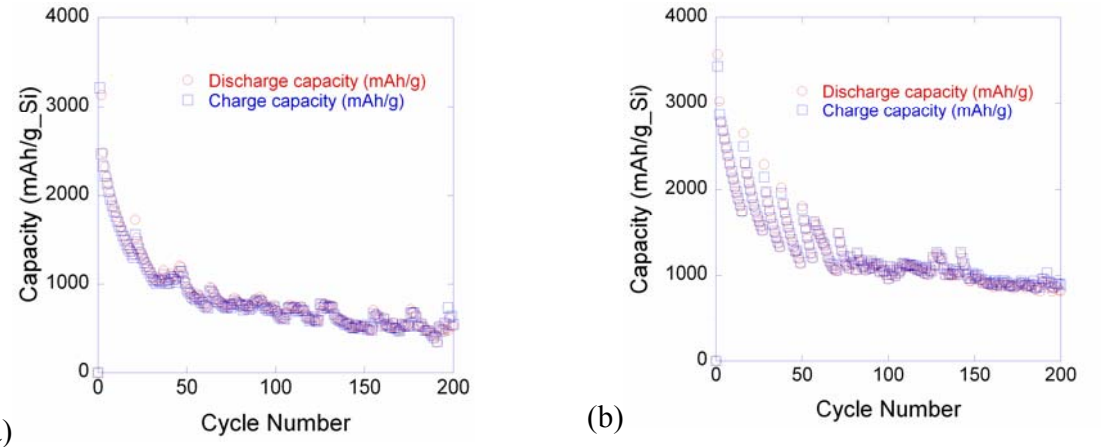

Figure 3-32. Charge/discharge capacity versus number of cycle for electrodes at full capacity: P4 (a) and P5 (b)

3.10 Analogy between electrochemical behaviour of silicon granular electrodes and fine soils micromechanics (paper III)

As a summary of previous parts, the cyclability of the four electrodes prepared in the lab, L1 (CB without PAMA), L2 (CB with PAMA), L4 (GM15 with PAMA), L5 (GM15+VGCF with PAMA) is compared in Figure 3-33a-b. The capacity of L1 steadily decreases and reaches a mere 250 mAh/g after 50 cycles. Adding the PAMA dispersant which improves the CB distribution in L2 is beneficial to the capacity retention. Indeed, the capacity is still approx. 1200 mAh/g after 80 cycles. The cyclability of L4 and L5 are remarkably much better than that of L2 since a nearly stable capacity of 1800mAh/g is retained after 200 cycles. It seems counter intuitive that performance of these electrodes does not reflect their electronic conductivity in the pristine state. Indeed, performance is improved by a better dispersion of CB in L2 vs. L1 (which is mirrored by a higher electronic conductivity) and by substituting GM15 for CB in L4 (which is associated with a decline of electronic conductivity). Similarly, in L5, VGCF and CB were mixed with GM15 to increase the electronic conductivity; however, the electrochemical performance was not improved vs. L4. Furthermore, an odd electrochemical behaviour was observed for those nanosilicon-based composite electrodes cycled without capacity limitations (Figure 3-17b, Figure 3-27, Figure 3-32b, Figure 3-33a,b). Steady decline followed by sharp recovery of the capacity are observed to repeat several times. This behaviour implies a dynamic variation in the quality of the electrical wiring and therefore of the activity of the Si particles during a given charge-discharge cycle. The better performing electrodes, which show higher capacity retention, also show the higher reversibility in this process.

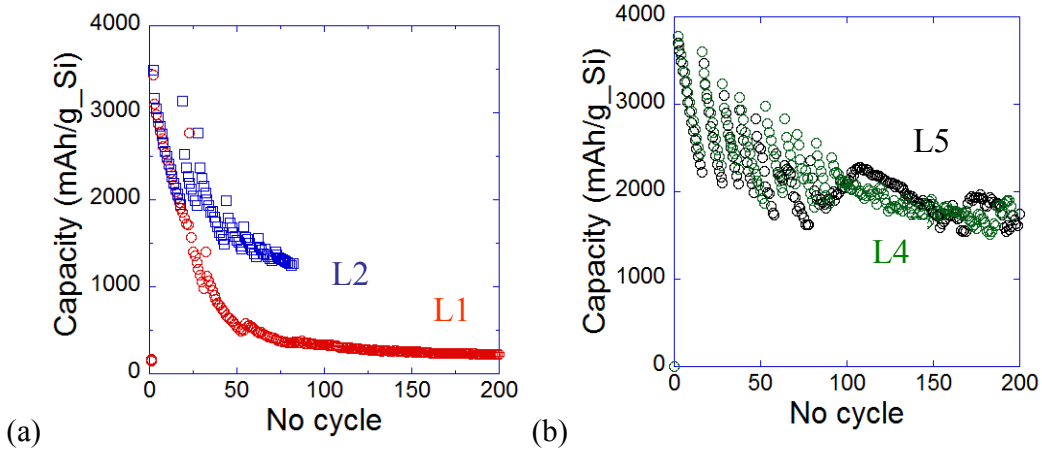

Figure 3-33. Discharge capacity versus number of cycle for electrodes L1 and L2 (a), and L4 and L5 (b).

This dynamic behaviour, as well as the lack of relationship between capacity retention and electronic conductivity in the pristine state, was interpreted in the background of the micromechanics of cohesive granular media such as fine soils. The build-up of an internal pressure as a consequence of the swelling of the Si particles' network within the confined space of the electrochemical cell would lead to a major geometrical change of granular texture with a vast redistribution of contacts assisted by adhesive CMC bridges and the concomitant recovery of the electrochemical capacity. However, the repetition of all these processes with frictional sliding of the particles must lead to a damaging of the SEI layer, and to the fragmentation of the CMC chains with a progressive loss of reversibility resulting in a decline of the mean capacity down to a plateau value (Figure 3-17b, Figure 3-27, Figure 3-32b, Figure 3-33a-b), which should correspond to a micromechanical equilibrium state.

We believe that the use of graphene or graphite nanoplatelets and a more homogeneous a finer distribution of the conductive additive favour a better resiliency of the electrodes, because the carbon additive likely plays on the stress intensity and distribution within the Si particles' network. Furthermore, the graphene-like materials with their electronically conducting large surface areas and/or finer and more homogeneous distribution of the conductive additives likely help the recovering and the maintaining of the electrical wiring within the moving Si mass.

3.11 Positive electrode formulation based on $LiNi_{0.5}Mn_{1.5}O_4$ (LNMO) (manuscript IV)

As the next step I moved to optimize the electrode formulation based on LNMO from Faculty of Applied Sciences, Delft University of Technology. This part is thoroughly described in draft of Paper IV and here the results are briefly summarized.

Electrode material synthesis - $LiNi_{0.5}Mn_{1.5}O_4$ (LNMO) powder was synthesized using a Carbon Combustion Method. Stoichiometric amount of Li_2CO_3, Mn_3O_4, and NiO together with carbon black (Li:C molar ratio=4:1) were mixed and ground manually for 10 minutes prior to ball milling in a planetary ball-mill (Fritsch P-0150) for 30 minutes at maximum speed. The mixture was first heated up to 950°C at 2ºC/min and kept there for 12 hours. A second heating step at the same temperature was used to force the powder to cool down slowly down to room temperature in 48 hours in order to ensure adequate oxygen uptake. The particles have a particle size of 1-10μm and a specific surface area of 0,32m^2/g.

Electrode preparation - Composite electrodes were composed of LNMO as an active material (AM), Super P carbon black (CB, Timcal, BET 65m²/g) and Carbon nanofibres (VGCF-S, BET 35m²/g) as a conductive additive (C), Polyvinylidene Fluorine (PVdF) from Solvay as a binder (B), and N-Methylpyrrolidone (NMP) as a solvent from Aldrich Chemical company. In aqueous solvent, Carboxylmethyl cellulose (CMC, DS=0.9, M_w=700.000 g/mol Sigma-Aldrich) and a copolymer of styrene, n-butylacrylate from PolymerLatex (X4020) were used as a binder (B). Pre-hand mixed of measured amount of AM/C/B was made in a mortar. The mixtures were introduced in: (i) a silicon nitride vial with three silicon nitride balls served as mixing media and a Fritsch Pulverisette 7 mixer was used to mill slurry at 700rpm for two hours with PVdF binder and for one hour with CMC binder (1 mL for 400mg), or (ii) a glass bottle with one magnetic stirrer bar then stir it in four days. The PVdF:C ratio was always kept constant at 5:3 following the studies of Battaglia and co-workers [18,19]. The powders and solvent were introduced according to the electrode formulations given in Table 3-12. After being blended in NMP, the slurries were tape-cast directly by using an automatic doctor blade onto aluminium foil in tape casting machine. By varying the height of the blade, the active mass loading of the electrode films was varied. Drying was primarily done at 60°C for 12h and then for 2h at 100°C under vacuum before battery assembly to remove the remaining solvent.

Table 3-12. Composition, porosity, theoretical BET, conductivity additive volume fraction and resistivity with standard deviation of the composite electrodes. B and M mean an electrode prepared in NMP by Ball milling and Magnetic stirring, respectively. BW means an electrode prepared in water by Ball Milling.

Electrode name	Electrode formulation (wt%)				Porosity (%)	Theoretical BET ** ($m^2\ g^{-1}$)	Conductive additive volume fraction*** (%)	Mean resistivity (4-probes) (ohm.cm)	Stand. Deviation (%)
	LNMO	CB	VGCF	Binder*					
B1	84	6	-	10	48-50	6,88	5.4	6.0	8
B2	84	4	2	10	50-53	6,28	5.2	0.5	7
B3	80	7.5	-	12.5	43-47	7,71	7.0	3.3	6
B4	80	5.5	2	12.5	45-48	7,11	6.8	0.4	5
B5	76	9	-	15	40-43	8,55	8.5	2.1	4
B6	76	7	2	15	42-43	7,95	8.4	0.3	5
M1	90.4	3.6	-	6	53-56	2,66	3.2	8.5	47
M2	90.4	2.6	1	6	58-61	2,36	2.8	1.2	15
M3	88	4.5	-	7.5	52-55	3,23	4.0	3.5	10
M4	88	3	1.5	7.5	54-58	2,78	3.7	0.6	15
BW1	92	2	1	5	61	4.90	2.2	2.6	5
BW2	90	4	1	5	57	6.13	4.1	1.1	4

[18] H. Zheng, G. Liu, X. Song, P. Ridgway, S. Xun, and V. S. Battaglia, J. Electrochemical Soc. 157 (2010) A1060.
[19] H. Zheng, R. Yang, G. Liu, X. Song, and V. S. Battaglia, J. Phys. Chem. C 116 (2012) 4875.

* PVdF in B and M electrodes. 4 parts of CMC and 1 part of X4020 in BW electrodes.
** Theoretical BET was calculated taking into account the BET surface area of the powders and their respective weight fraction in the electrode formulation: $BET = \sum_i \phi_{W,i} \times BET_i$

*** The volume fraction is calculated by taking into account the electrode porosity.

Electrochemical testing - Half cells: two-electrode Swagelok™ test cells comprise (i) a 0.78 cm^2 disc of composite positive electrode (ii) a porous glass paper as separator soaked in an electrolyte LP30 [1M $LiPF_6$ solution in dimethyl carbonate-ethylene carbonate (1:1)] and (iii) a 0.78 cm^2 Li metal disc as the negative and reference electrode. The LNMO/Li haft cells were assembled in a dry Ar-filled glove box. In order to evaluate the cycling performances of LNMO materials, cell cycling was performed at 20°C, monitored by a VMP™ system (Biologic) in a galvanostatic mode. Charge – discharge tests were carried out between 3.5 – 4.9V versus Li^+/Li. All composite electrodes were studied with the same rate (C/2.5 and D/2.5).

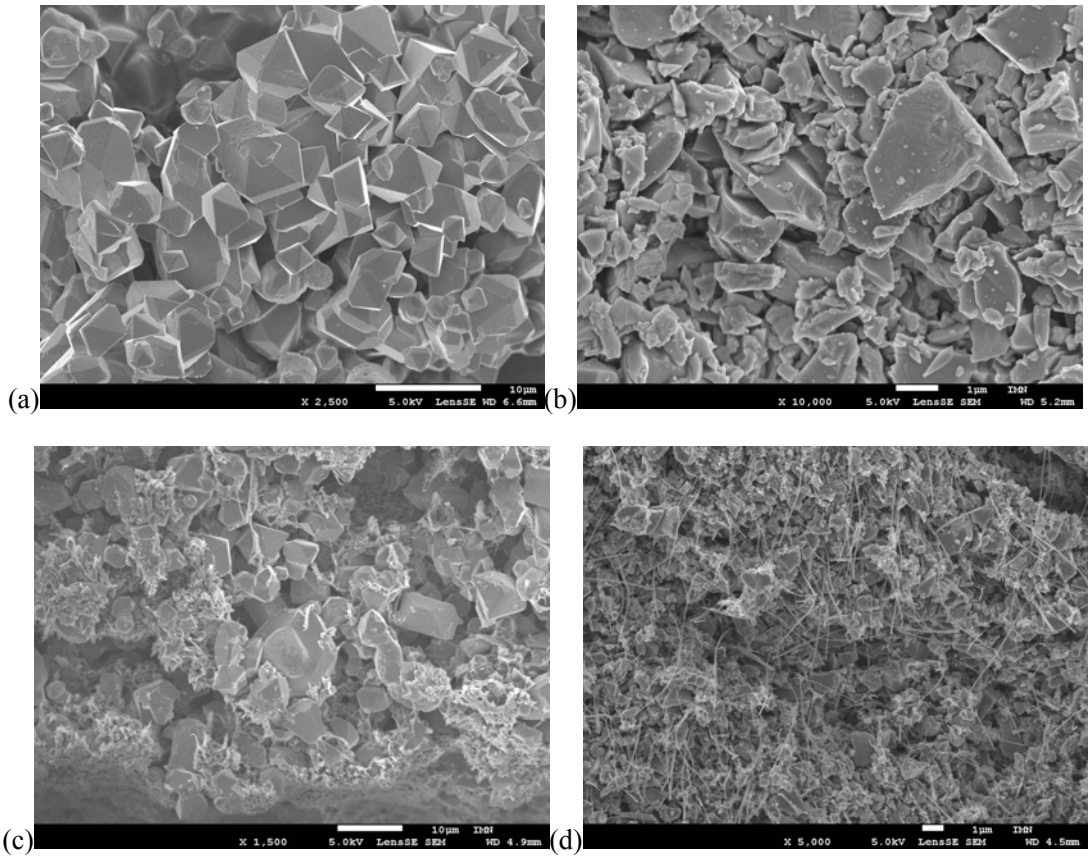

Figure 3-34. SEM observations of LNMO material and different composite electrodes: (a) pristine LNMO × 2,500, (b) ball milled (in NMP) LNMO × 10,000, (c) M1 × 1,500, (d) B2 × 5,000.

SEM images of LNMO before and after ball milling (BM) are shown in Figure 3-34. Well-crystallized particles of LNMO with average diameter of 3 to 8μm are observed in Figure 3-34a. Large LNMO particles were broken down into smaller ones under high mixing energy (Figure 3-34b) with significant increase of BET from 0.32 to 3.55 $m^2 g^{-1}$ compared to pristine material. However, there is no modification of the material crystallization after ball milling observed by XRD measurements. The typical textures of the electrodes are observed by SEM in Figure 3-34c-d, while the dry electronic resistivity and porosity are given in Table 3-12. First, the resistivity decreases when increasing the amount of conductive additive whatever mixing methods used (Table 3-12). In order to reach same dry electronic resistivity, the amount of conductive additive (and binder) needed is higher with BM electrodes than in MS ones. It is in agreement with the decrease in the LNMO particle size in BM electrodes.

On the whole, the electrodes show fairly good homogeneity, especially those prepared by using BM as demonstrated by the lower standard deviation of their electronic resistivity (Table 3-12). SEM images of electrodes prepared by MS (Figure 3-35) reveals the occurrence of some bundles of un-individualized VGCF, demonstrating that MS is not efficient enough to reach homogeneous distribution of such kind of conductive additives. This is quite consistent with electrical results.

(a) 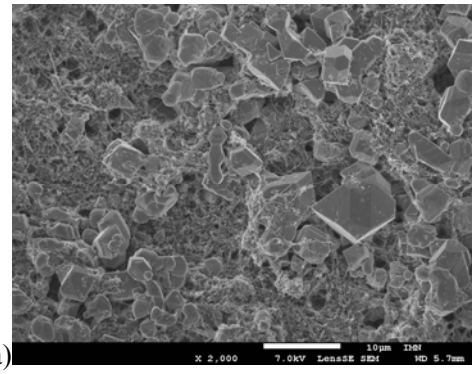 (b) 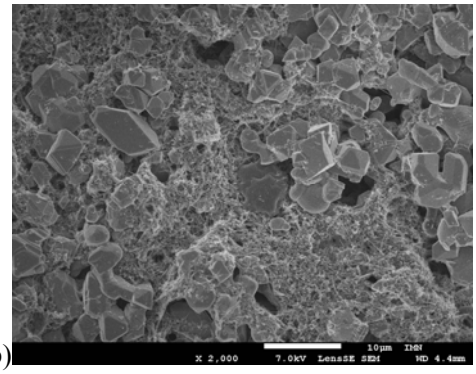

Figure 3-35. SEM observations of different composite electrodes on the surface: (a)M2 and (b)M4

Cycling tests were done with different electrode formulations. Electrode M1 shows poorest performance due to the defects in cohesion and insufficient C percolation, as observed on SEM images. All other electrodes showed a fairly high initial capacity that increases to a maximum value, Q_0, before showing a steady decline in the capacity. The fading could be

attributed to a loss of active mass likely through the loss of electrical connections with the carbon conductive network as a consequence of parasitic reactions occurring at high potentials. The retention in discharge capacity expressed in % of the maximum value, Q_0, at the 100th, 200th, 300th and 400th cycles is given versus the electronic resistivity of the LNMO electrodes in Figure 3-36a-c, for electrodes M1 to M4 prepared by magnetic stirring and LNMO loadings of 7-8 mg cm^{-2} (Figure 3-36a) and 20-28 mg cm^{-2} (Figure 3-36b), and for electrodes B1 to B6, prepared by ball milling and LNMO loadings of 15-18 mg cm^{-2} (Figure 3-36c).

At first sight, the retention in capacity increases when the electronic resistivity decreases. This trend is explained by a better maintain of electrical connections between the active mass and the conductive network in electrodes with higher amount of conductive additive or more well developed conductive network. The fading of the discharge capacity is less severe for composite electrodes with low active mass loading compared to the others with high AM (Figure 3-36a and b). Thicker electrode are more severely impacted by defects and non-homogeneities introduced during electrode fabrication, which result in inadequate connectivity within the electrode and partial isolation of some of the active material. Among all studied formulations, M3 electrode highlights the better performance of the electrode prepared by gentle stirring over that of electrodes prepared by high energy mixing. M3 exhibits high surface capacity up to ~ 3 mAh/cm^2, long cyclability and capacity retention after 300 cycles is ~80%. Such results can be attributed to lower specific surface of the bigger LNMO particles in M3 which results in less parasitic reactions. Finally, the optimized formulation M3 was transferred to CEA for trials on semi-industrial level. Electrochemical tests are presently on-going.

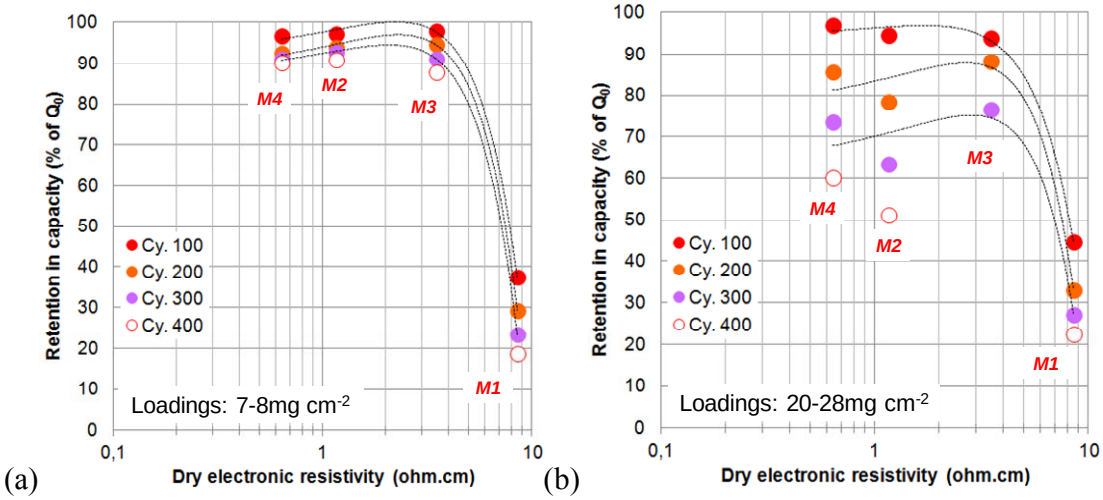

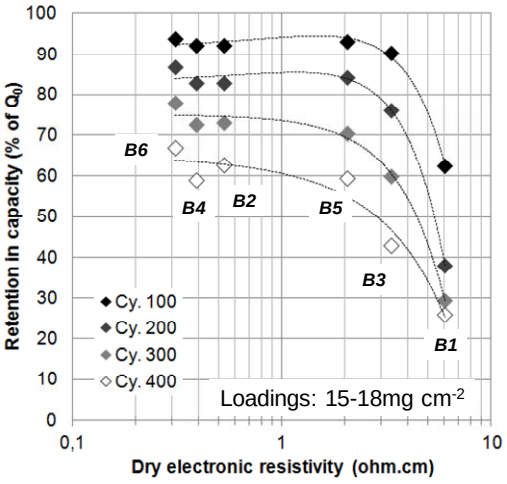

(c)

Figure 3-36. retention in discharge capacity expressed in % of the maximum value, Q_0, at the 100th, 200th, 300th and 400th cycles vs the electronic resistivity (a) LNMO loading of 7-8 mg cm^{-2}, (b) 20-28 mg cm^{-2} and (c) ball milling (15-18 mg cm^{-2}).

Aside from PVdF, I also studied CMC as a binder to prepare the LNMO based electrodes. Although electrodes BW1 and BW2 exhibit a fairly low dry electronic resistivity, their electrochemical results display poorer performance with strong fading at low AM loadings (6-7 mg cm^{-2}) compared to electrodes prepared with PVdF. This poor result is most likely a consequence of residual water left in the electrodes causing too much degradation of either of the electrode components.

3.12 The design of full cell using optimized formulations based on Si and LNMO materials

In this last section, a Si-based electrode (L4 formulation) as the negative and a LNMO-based electrode (M3 formulation) as the positive were used to make a Li-ion cell. Preliminary electrochemical studies were carried out for selection of the electrolyte. With respect to the selection of the electrolyte I used LP30 for evaluating LNMO and 88wt%LP30 10wt%FEC 2wt%VC for Si. As modifying LP30 with the FEC and VC additives is mandatory for the cycling behavior or silicon we checked the cyclability of LNMO with LP30 modified by these additives. It's found that VC must be removed from the electrolyte mix to achieve good cyclability of LNMO-based electrodes (Figure 3-37a). The detrimental influence of VC with respect to LNMO might be attributed to lack of electrochemical stability at 4.8-4.9V (Figure 3-37b). The composition of electrolyte selected was thus 90wt%LP30 10wt%FEC.

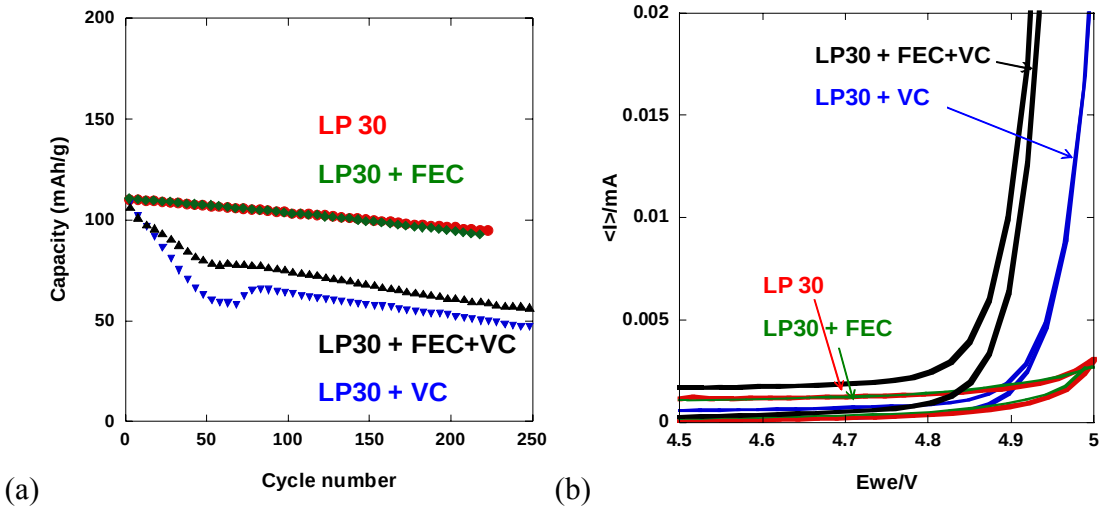

Figure 3-37. (a) Discharge capacity vs. cycle number for LNMO electrode (B2, Table 3-12) cycled at the C/2 rate in Swagelock test cell with lithium metal counter electrode and different electrolytes: LP30, or LP30 modified with 2wt%VC or 10wt%FEC or 2wt%VC+10wt%FEC. (b) Cyclic voltammetry evaluation of the same electrolytes.

Full cells were assembled as coin cells and two electrode Swagelok^{TM} cells with an active area of 0.78cm^2. The loadings of active material (anode:cathode) are presented in Table 3-13. As presented in previous parts, the Si based negative electrode has initial capacity of more than 3600mAh/g_Si and capacity retention of 1800mAh/g_Si after 200 cycles. The capacity of LNMO positive electrode decreases upon cycling and depends on the active mass loading. The capacity of 100mAh/g_LNMO was chosen for cell design. Three cells with different surface capacity, 1.0, 1.5 and 2 mAh/cm^2, were prepared for testing (Table 3-13). The surface capacity of full cell is determined by positive side. The voltage range used was 2.5-4.89V vs. Li/Li$^+$. All full cells prepared in coin cells were studied with 1st cycle at C/10 D/10, then C/2.5 D/2.5 with a limited charge capacity of 100mAh g^{-1}_LNMO. The results are shown in Figure 3-38. Noteworthy, similar results were obtained with Swagelok^{TM} cells.

Table 3-13. AM loadings of L4 and M3 electrodes and cell design

Electrode	Active mass loading (mg/cm^2)	Capacity used for calculations (mAh/g)	Surface capacity (mAh/cm^2)	Capacity ratio (anode:cathode)	Capacity limitation (mAh)
Negative	1.25	3600-1800	4.5-2.25	-	-
Positive	10	100	1	4.5-2.25	1
	15		1.5	3-1.5	1.5
	20		2	2.25-1.13	2

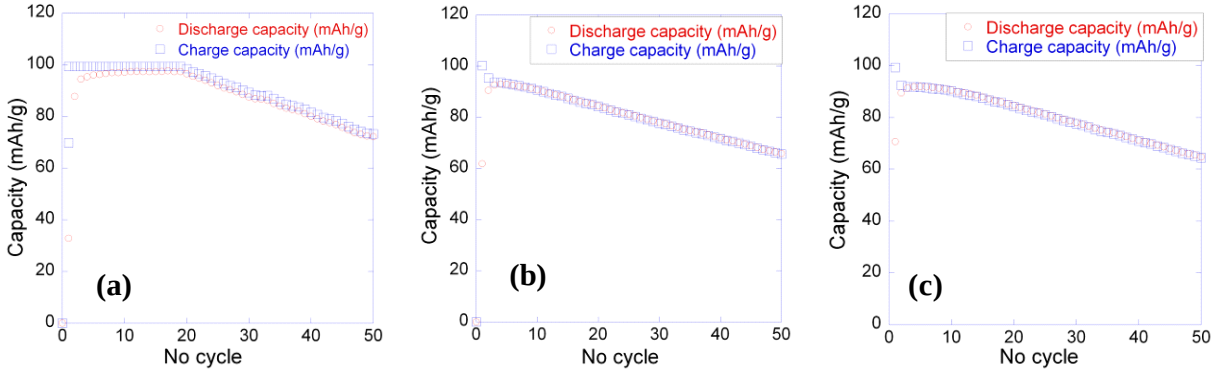

Figure 3-38. Charge/Discharge capacity vs. number of cycle for cells (Table 13) with different surface capacity (a) 1.0mAh/cm^2, (b) 1.5mAh/cm^2 and (c) 2.0mAh/cm^2

All full LMNO/Si cells showed a pronounced capacity fading of about 25% after 50 cycles. The mechanism at the origin of the end of life of $LiCoO_2$/Si full cells was studied recently into details by N. Delpuech in our group [20]. In short, for the first charge and following cycles, there are parasitic reactions occurring at the two electrodes, some electrolyte species being oxidized at the positive electrode and some electrolyte species being reduced at the negative one. These parasitic reactions produce an extra but irreversible capacity that results in the "shift" of the voltage versus capacity curves, the charge and discharge endpoints slip to higher absolute capacities (Figure 3-39 a-c). Parasitic reactions being more severe at the negative electrode, it is induced cycle after cycle a stronger "shift" compared to the positive electrode that results in a decrease of the number of electrons exchanged between the two active masses, i.e. a progressive decrease of the capacity of the battery (Figure 3-39d).

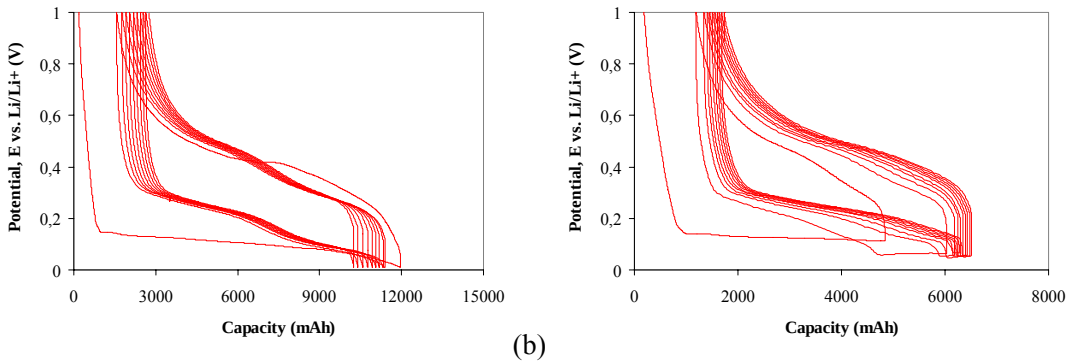

[20] N. Delpuech, « Origine de la perte de capacité et effet de l'oxyde de surface sur les performances électrochimiques d'électrodes à base de silicium pour accumulateurs lithium-ion », Thèse de l'Université de Nantes (2014).

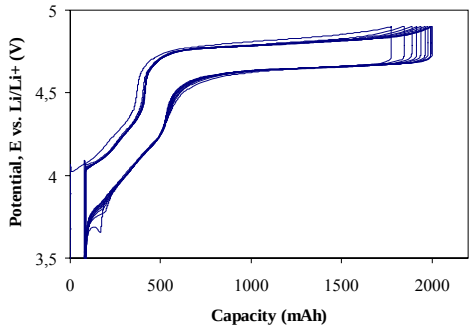

(c)

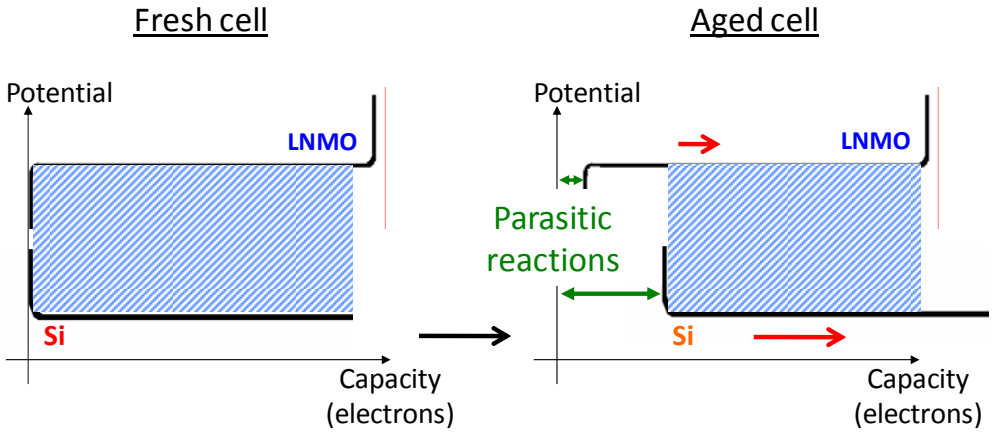

(d)

Figure 3-39. Voltage vs. capacity curves for ten first cycles of L4 (2.6mg_Si/cm²) cycled (a) at full capacity and (b) with 1800mAh/g_Si capacity limitation and (c) M3 (19.7mg_LNMO/cm²) when cycling is done in a half-cell with lithium metal as the counter electrode. (d) Schematic description of the different shifts of the LNMO and Si electrochemical curves resulting in a decrease of the capacity.

These results (Figure 3-38) can be compared with the literature. Bordes et al. studied a Silicon-Graphene/ $Li[Ni_{0.8}Co_{0.15}Al_{0.05}]O_2$ (Si-G/NCA) pouch cell. The design capacity of Si-G negative electrode is 1.15 times more than that of NCA positive electrode, resulting in a surface capacity of 2.2mAh/cm². The capacity fade ratio from 1st to 50th cycle was ~20% [21]. Elazari et al. studied a Silicon/TiS_2 button coin-type cell. The design capacity of Si negative electrode is 5 times more than that of TiS_2 positive electrode, resulting in a surface capacity of 0.5mAh/cm². The capacity fade ratio from 1st to 50th cycle was ~10% [22]. In the same group, Fridman et al. studied a Silicon/LNMO button coin-type cell. The design capacity of Si negative electrode is 12 times more than that of LNMO positive electrode, resulting in a surface capacity of 0.4mAh/cm².

[21] A. Bordes, K. Eom, T. F. Fuller, J. Power Sources 257 (2014) 163.
[22] R. Elazari, G. Salitra, G. Gershinsky, A. Garsuch, A. Panchenko, D. Aurbach, J. Electrochem. Soc., 159 (2012) A1440.

The capacity retention of the cell comprised 74.2% after 500 cycles [23]. However, in these two works from D. Aurbach group, the amorphous silicon thin film was fully pre-lithiated before battery assembly [22,23]. As the design capacity of silicon negative electrode is 5 or 12 times higher than that of the positive electrode, silicon is thus used with "charge capacity limited cycling" condition, working in between 3600 and 3000mAh/g in [22] and 3300 mAh/g in [23], respectively. E. Radyanvani showed the "charge capacity limited cycling procedure" results in much better cycling response of Si electrodes, due to the much better stability of the solid electrolyte interphase (SEI) film that is mechanically less strained than in "discharge capacity limited cycling procedure" because the variation in surface area of the silicon particles is less in the former condition than in the latter for geometrical reasons [24]. In all studies, FEC was pointed as a mandatory electrolyte additive to decrease the capacity fade in the full cells [21-24].

Here, we proceeded differently. The silicon-based electrode (active mass loading 1.25mg/cm²) was first fully lithiated and delithiated in a half-cell with Li metal at C/10 D/10. Then, the Li metal electrode was removed and replaced by LNMO based electrode (active mass loading 10 mg/cm²) and cycling of this full cell was done in the same conditions than above (90wt%LP30 10wt% FEC; voltage 2.5-4.89V vs. Li/Li^+; 1^{st} cycle at C/10 D/10, then C/2.5 D/2.5 with a limited charge capacity of 100mAh g^{-1}_LNMO). Interestingly, this LNMO/Si full cell showed a fully reversible cycling (at least 100 cycles) with mean coulombic efficiency of 99.1% (Figure 3-40).

[23] K. Fridman, R. Sharabi, R. Elazari, G. Gershinsky, E. Markevich, G. Salitra, D. Aurbach, A. Garsuch, J. Lampert, Electrochem. Commun., 33 (2013) 31.
[24] E. Radvanyi, "Compréhension des mécanismes de (dé)lithiation et de dégradation d'électrodes de silicium pour accumulateur Li-Ion et étude de facteurs influents", PhD at the University of Grenoble (2014).

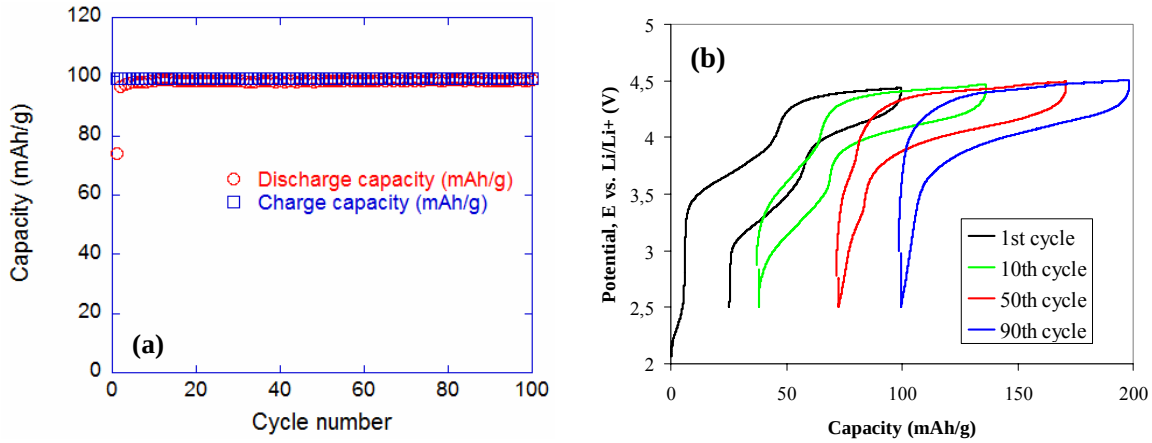

Figure 3-40. (a) Charge/Discharge capacity vs. cycle number and (b) voltage profile vs. specific capacity curves at different cycles for LNMO/Si full cell.

3.13 General conclusions and prospects

The work resumed in this dissertation aims to define the optimized formulations, first with nanometric Si and then for micrometric LNMO in order to make industry-relevant electrodes with a target-capacity of ~3mAh/cm². These formulations must possess good electrochemical performance and satisfactory properties for processing on semi-industrial coating machines of the CEA, which was the partner in charge of producing LNMO/Si prototype-cells for further evaluation of this technology by other partners within the EuroLiion project. My results could be summarized into three parts:

1. Optimized negative electrode formulation based on silicon (Si)

There is no satisfactory processing of commercial Si (70-80m²/g, 10-150nm) purchased from Alfa Aesar with high BET (low particle size) with conventional ball milling/tape casting process while with Si (14m²/g, 150nm) supplied by the CEA, it is opposite. I obtained suitable and stable rheological properties of the electrode slurry with respect to CEA expectations. The tapes display good adhesion/cohesion and good homogeneity at all scales (few µm up to few cm).

In agreement with previous work [4,6], a much better electrochemical performance for electrodes prepared at buffer pH 3 compared to water pH 7 is obtained with the carboxymethyl cellulose

(CMC) binder. Two optimized electrode formulations were successfully designed for Si CEA with following electrochemical performance:

- 1st formulation based on carbon black and Poly (acrylic-co-maleic) acid (PAMA) as dispersant, which could operate more than 400 cycles at 1200mAh/g_Si (800mAh/g_electrode) limitation (CE 99.3%) and at surface capacity ~2.1mAh/cm^2. In addition, the role of the PAMA dispersant has been investigated. This one could help not only to achieve higher homogeneity of the electrode at the lab scale, especially uniform carbon black distribution, which leads to improvement of cyclability and coulombic efficiency in half cell, but also facilitate the powder incorporation at the pilot scale. However, the amount of PAMA was optimized at 1.7wt% because a competitive adsorption occurs between PAMA and CMC versus the carbon black particles, which is detrimental to the mechanical bridging of the particles. When this 1st formulation was transferred to be processed at pilot scale it was found mandatory to add an elastomeric binder (a styrene-co-butadiene rubber copolymer (SBR) and to calendar the electrode to achieve enough mechanical strength of the electrode. While SBR plays an important role to achieve long cycle life, calendaring is very detrimental and significantly reduces the cycle life.

- 2nd formulation based on graphene instead of carbon black as the conductive additive allows a significant improvement of the electrochemical performance, whatever the cycling conditions. The surface capacity of 3.1mAh.cm^{-2}_electrode is maintained after 200 cycles (CE 99.5+/0.4%) when cycling was performed with capacity limitation. Without limiting capacity, the discharge capacity retained is still higher than 1800mAh/g_Si after 200 cycles (~3.1mAh.cm^{-2}). The electrochemical properties were not improved when mixing carbon nanofibres with graphene. SBR was added when 2nd formulation was processed at the pilot scale.

For both formulations prepared in CEA, poorer electrochemical performance was obtained compared to the one prepare in IMN. It could be ascribed to the different scales involved. At the IMN the electrodes are prepared at the lab scale which implies small quantities and short mixing

and casting durations, while at the CEA the electrodes are prepared at a larger scale which implies much larger quantities and longer mixing and casting durations that are detrimental to mastering the stability and thus the homogeneity of the slurries.

2. Optimized positive electrode formulation based on LNMO

The influence of the composite electrode formulation on the cyclability of LNMO electrodes was studied. Best result is retention of 80% of the capacity after 300 cycles and surface capacity of ~3 $mAh.cm^{-2}$. The fading of the capacity due to parasitic reactions at high voltage is minimized by increasing the amount of conductive additives or by substituting part of carbon black for carbon nanofibers. However, the cyclability of the electrodes with high active mass loading is severely decreased which could be attributed to more defects in terms of electronic percolation or adhesion and cohesion with thick electrodes. Furthermore, the electrodes prepared in water with carboxylmethyl cellulose (CMC) binder exhibit poorer cyclability compared to the ones prepared in N-Methylpyrrolidone (NMP) with Polyvinylidene Fluorine (PVdF) binder.

3. The design of Li-ion full cell – preliminary tests

Preliminary results of full cells base on my optimized formulations show promising future. Three full cells with different surface capacity (1.0, 1.5 and 2.0mAh/cm^2) could operate in 90wt% LP30 10wt%FEC and the electrochemical performance was improved significantly if the Si electrode is fully lithiated/delithiated versus lithium metal before assembly with LNMO electrode: more than 100 cycles with a reversible capacity of 100mAh/g_LNMO (CE 99.1%).

Finally, from the scientific point of view, this study proposed an interpretation of the electrochemical behavior of silicon electrodes from the micromechanics of granular materials. Such analogy might open new prospects for further interpretation of composite electrodes by considering how the mechanical stresses and strains transmit through an array of active material and conductive additive particles and influence the electronic wiring and charge transfer to the active mass.

It is interesting to calculate the gravimetric and volumetric energy densities for this new technology (Silicon/LNMO) and to compare it to a state-of-the-art (Graphite/$LiFePO_4$) for EV application. A stack with current collectors coated on both faces is considered (Figure 3-41). The equations used are taken from [25] and recalled in appendix. Values for some parameters of the calculations are given in Table 3-14. Results for one calculation (surface capacity of the stack 4 mAh/cm², by considering surface capacity of the tapes 2 mAh/cm²) are given in Table 3-15 and Table 3-16. The gravimetric and volumetric energy capacities are compared for different configurations in Figure 3-42. Noteworthy, we did not consider the additional weight and volume of the packaging of the cell.

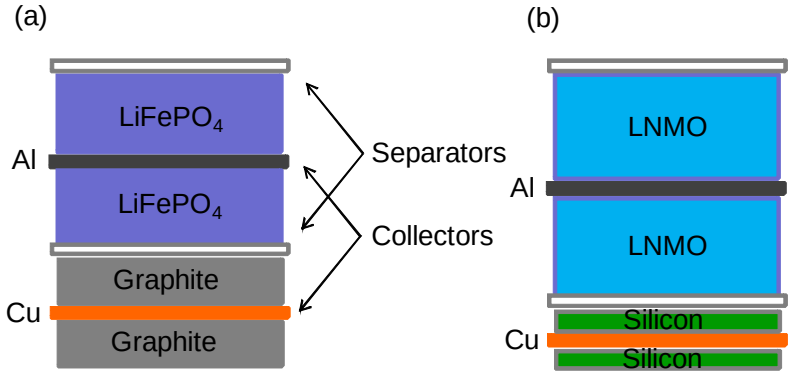

Figure 3-41. Scheme of the stacks considered for energy density calculations

Table 3-14. Values used in the calculations of energy densities.

	Negative electrode			Positive electrode			
	wt% in electrode	Specific capacity (mAh/g)	Porosity of electrode	wt% in electrode	Specific capacity (mAh/g)	Porosity of electrode	Potential difference (V)
Graphite/LFP	90	360	30	90	160	40	3.2
Silicon/LNMO	66	600-1800	60	88	100	40-50	4.2

Table 3-15. Table of results in the calculation of volumetric and gravimetric energy densities of a traditional lithium-ion $LiFePO_4$/Graphite cell with a stack surface area of 1000 cm^2.

SC	$m_{e,+}$	$m_{e,-}$	$h_{e,+}$	$h_{e,-}$	h_{stack}	V_{stack}	Q_{stack}	E_{vol}	m_{lyte}	$2m_{sep}$	m_{Al}	m_{Cu}	M_{stack}	E_{grav}
mAh/cm²	g	g	µm	µm	µm	cm^3	Ah	Wh/L	g	g	g	g	g	Wh/kg
4	27.8	12.3	73	42	320	32	4	410	13.9	2.6	5.4	17.8	78	165

Table 3-16. Table of results in the calculation of volumetric and gravimetric energy densities of a traditional lithium-ion LNMO/Silicon cell with a stack surface area of 1000 cm^2.

SC	$m_{e,+}$	$m_{e,-}$	$h_{e,+}$	$h_{e,-}$	h_{stack}	V_{stack}	Q_{stack}	E_{vol}	m_{lyte}	$2m_{sep}$	m_{Al}	m_{Cu}	M_{stack}	E_{grav}
mAh/cm²	g	g	µm	µm	µm	cm^3	Ah	Wh/L	g	g	g	g	g	Wh/kg
4	45.5	3.4	104	23	345	34.5	4	487	17.7	2.6	5.4	17.8	92	182

[25] D. Mazouzi, D. Reyter, M. Gauthier, P. Moreau, D. Guyomard, L. Roué, B. Lestriez, Adv. Energy Mater., 2014, DOI: 10.1002/aenm.201301718

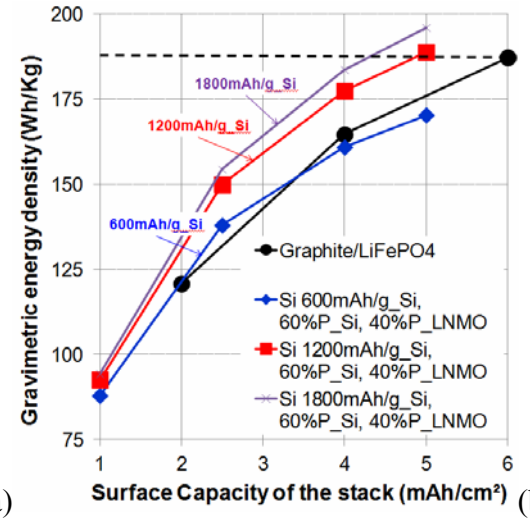
Gravimetric energy density (Wh/Kg)
200
175
150
125
100
75
1
2
3
4
5
6
Surface Capacity of the stack (mAh/cm²)
1800mAh/g_Si
1200mAh/g_Si
600mAh/g_Si
Graphite/LiFePO4
Si 600mAh/g_Si, 60%P_Si, 40%P_LNMO
Si 1200mAh/g_Si, 60%P_Si, 40%P_LNMO
Si 1800mAh/g_Si, 60%P_Si, 40%P_LNMO

(a)

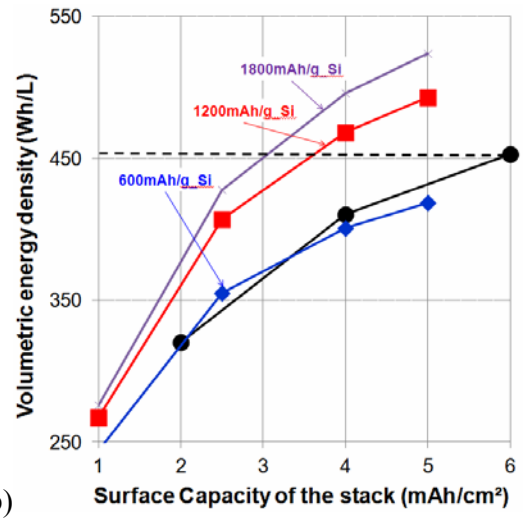
Volumetric energy density (Wh/L)
550
450
350
250
1
2
3
4
5
6
Surface Capacity of the stack (mAh/cm²)
1800mAh/g_Si
1200mAh/g_Si
600mAh/g_Si

(b)

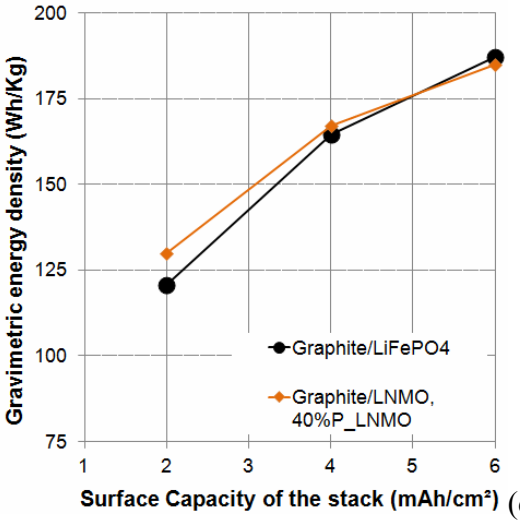
Gravimetric energy density (Wh/Kg)
200
175
150
125
100
75
1
2
3
4
5
6
Surface Capacity of the stack (mAh/cm²)
Graphite/LiFePO4
Graphite/LNMO, 40%P_LNMO

(c)

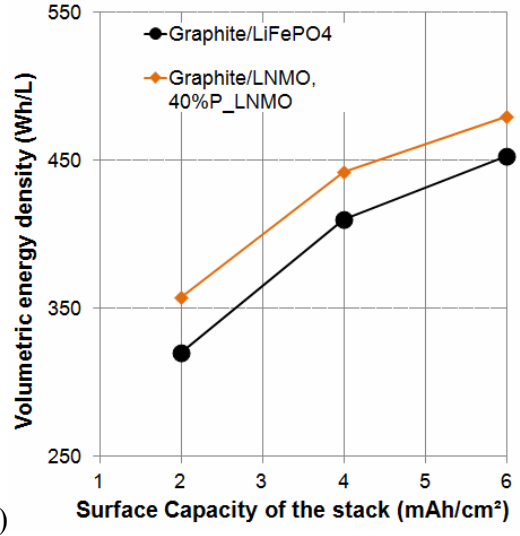
Volumetric energy density (Wh/L)
550
450
350
250
1
2
3
4
5
6
Surface Capacity of the stack (mAh/cm²)
Graphite/LiFePO4
Graphite/LNMO, 40%P_LNMO

(d)

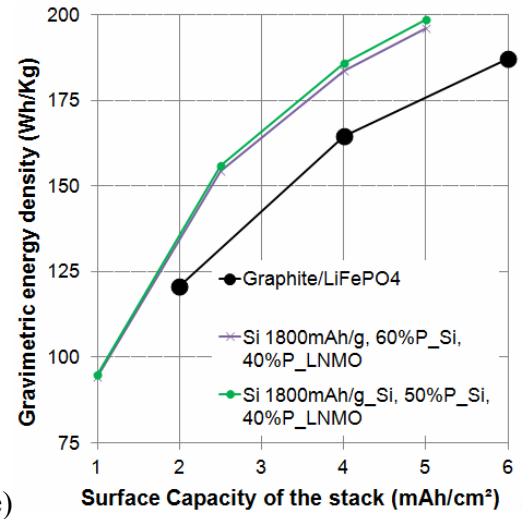
Gravimetric energy density (Wh/Kg)
200
175
150
125
100
75
1
2
3
4
5
6
Surface Capacity of the stack (mAh/cm²)
Graphite/LiFePO4
Si 1800mAh/g, 60%P_Si, 40%P_LNMO
Si 1800mAh/g_Si, 50%P_Si, 40%P_LNMO

(e)

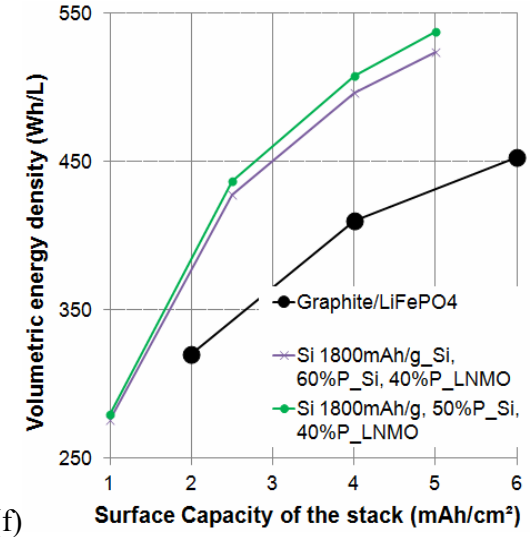
Volumetric energy density (Wh/L)
550
450
350
250
1
2
3
4
5
6
Surface Capacity of the stack (mAh/cm²)
Graphite/LiFePO4
Si 1800mAh/g_Si, 60%P_Si, 40%P_LNMO
Si 1800mAh/g, 50%P_Si, 40%P_LNMO

(f)

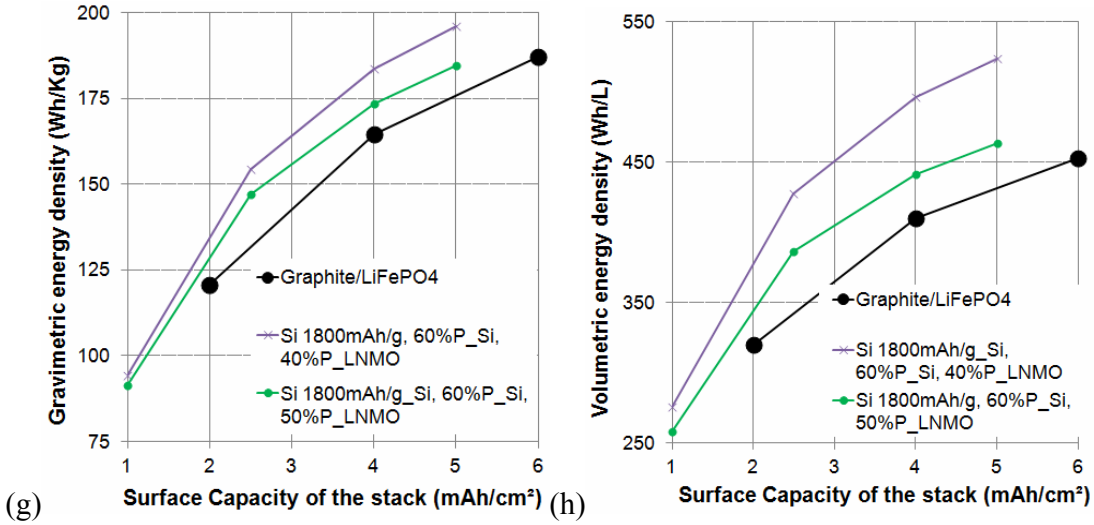

Figure 3-42. Gravimetric and volumetric energy densities calculated for different configurations: (a,b) comparison of Graphite/$LiFePO_4$ with different capacity limitations for silicon: 600, 1200 and 1800mAh/g_Si. (c,d) comparison of Graphite/$LiFePO_4$ with Graphite/LNMO (the two different positive electrodes have same porosity, 40%). (e,f) comparison of Graphite/$LiFePO_4$ with Silicon/LNMO with silicon electrode porosity of 60 or 50% (capacity limitation for silicon: 1800mAh/g_Si). (g,h) comparison of Graphite/$LiFePO_4$ with Silicon/LNMO with LNMO electrode porosity of 40 or 50% (capacity limitation for silicon: 1800mAh/g_Si).

The horizontal lines give a reference value for the state-of-the-art technology based on the Graphite/$LiFePO_4$ couple for electrodes with surface capacity of 3mAh/cm² (stack surface capacity of 6mAh/cm²). Indeed, such surface capacity is typically reached by common processing method in the industry. The plots show that the Silicon/LNMO couple can allows to reach higher energy densities, whatever the surface capacity of the stack, however to show better performance than the state-of-the-art (the horizontal line), it is mandatory to be able to produce silicon with good cycling behavior at surface capacity of 2.5mAh/cm² (Figure 3-42a,b). The superior energy density of the Silicon/LNMO couple is due to the higher gravimetric and volumetric capacity of silicon versus graphite. However, because the silicon electrode must have high porosity for good cyclability, it must be cycled at least at 1800mAh/g. Otherwise, e.g. at 600mAh/g, the extra porosity and lower capacity requires too thick electrodes for getting any improvement. Using LNMO does not increases the gravimetric energy density because of the low specific capacity, 100mAh/g versus 160mAh/g for $LiFePO_4$, which negatively counterbalance the higher voltage difference between the negative and the positive electrodes, 4.2V versus 3.2V, respectively. Indeed, one can see the same gravimetric energy densities for Graphite/$LiFePO_4$ and Graphite/LNMO (Figure 3-42c). However, the higher density of LNMO,

4.28g/cm^3 versus 3.6g/cm^3 for $LiFePO_4$, results in higher volumetric energy density (Figure 3-42d). If silicon is cycled at 1200 or 1800mAh/g, the calendaring of the silicon electrode results in negligible variation in energy densities (Figure 3-42e,f), as a consequence of the thinness of the silicon electrode with respect to the positive electrode. However, calendaring of the positive electrode is mandatory to achieve superior energy densities than the state-of-the-art technology (Figure 3-42g,h). In summary, the new technology (Silicon/LNMO) can surpass the state-of-the-art (Graphite/$LiFePO_4$) in both gravimetric and volumetric energy densities, if electrodes with industry-relevant active mass loading and good cyclability can be produced, which was achieved in this work. A main bottleneck toward their commercialization however remains, which is the liquid electrolyte that parasitic reactions toward both electrodes result in detrimental capacity fading.

Appendix

1 Study of polyacrylic acid as new binder to replace CMC

Recent works of Yushin and co-workers and Komaba and co-workers reported better performance of silicon-based electrode prepared with polyacrylic acid (PAA) instead of CMC as the binder [1,2]. Following these works the binder PAA instead of CMC was also tried to optimize the Si based electrode formulation at pH 3 and 7. Same preparation conditions corresponding to process of making composite electrode with CMC was followed. With same electrode formulation L1 prepared in 1ml of buffer (solid loading ~17%), poor homogeneity of the electrode is observed after drying (Figure 1). This can be explained that too much solvent used lead to settling of the materials during drying step.

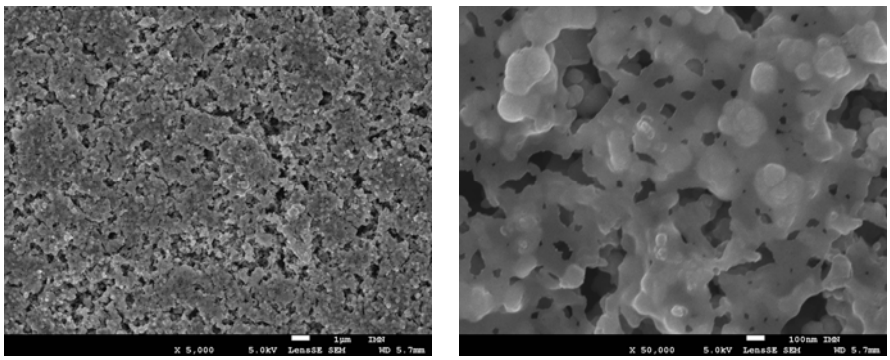

Figure 1. SEM observations of composite electrode L1 (PAA) prepared in 1ml pH=3

As the reason above, the amount of solvent was decreased from 1ml to 0.5ml in order to prepare the composite electrode. Figure 2 shows that settling phenomenon could be eliminated, however lots of cracks appeared after drying and especially the homogeneity is very poor.

[1] A. Magasinski, B. Zdyrko, I. Kovalenko, B. Hertzberg, R. Burtovyy, C. F. Huebner, T. F. Fuller, I. Luzinov, G. Yushin, J. Applied Materials and Interfaces, 2 (2010) 3004

[2] S. Komaba, K. Shimomura, N. Yabuuchi, T. Ozeki, H. Yui, K. Konno, J. Phys. Chem. C, 115 (2011) 13487.

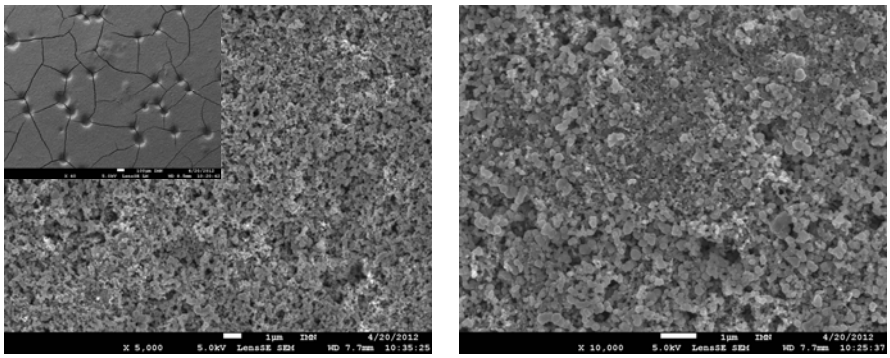

Figure 2. SEM observations of composite electrode L1 (PAA) prepared in 0.5ml pH=3

I also tried to prepare the composite electrode in distilled water using PAA as a binder. In order to prepare composite electrodes at pH 7, I first dissolved PAA in distilled water by using magnetic stirrer in one night to have homogenous distribution of PAA into slurry, LiOH was used to neutralize the pH of the slurry. Measured amount of this mixture and corresponding mass of Si and C (solid loading ~17wt.%) were introduced in a silicon nitride vial according to the electrode formulation 80wt%Si 12wt%CB and 8wt%PAA. Before ball milling, all constituents were hand mixed to achieve homogenous colour. Figure 3 shows the dispersion of all particles after drying. It's observed that an agglomeration of CB or Si formed and the homogeneity of all particles are not good compared to the composite electrode prepared with CMC at pH 7.

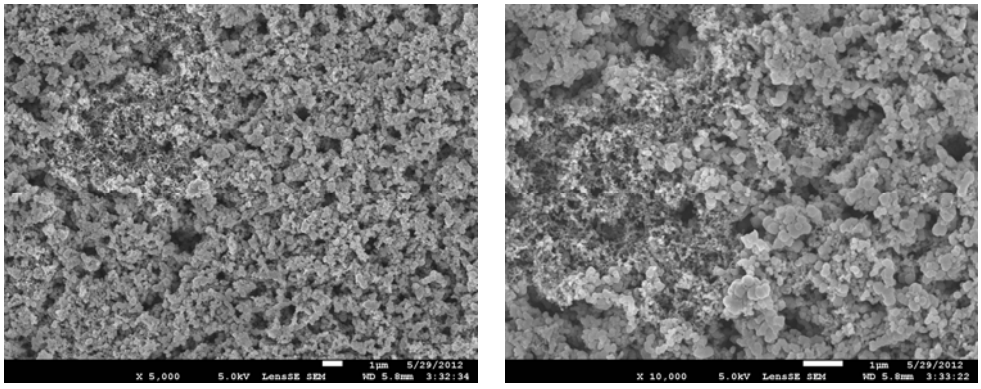

Figure 3. SEM observations of composite electrode 80%Si:12%AcB:8%PAA prepared at pH=7

In conclusion, PAA is not a good candidate in replacing of CMC binder.

2 Electrochemical studies with new salt LiTDI supplied from LPT Warsaw

Before electrolyte preparation, further drying of the salt (2^{nd} batch received in May) from Laboratory of Technological Processes – Warsaw (LPT) was done at 140^{o}C in 24 hours under vacuum (p<10mbar) according to recommendation. The electrolyte was prepared in the glove under argon atmosphere with different composition:

- 0.63mol/kg LiTDI in EC:DMC (1:2) (LiTDI)
- 88 wt% LiTDI 2wt% VC 10wt%FEC (LiTDI VCFEC)

The L2 batteries were cycled in two different ways:

(i) With discharge capacity limitation to 1200mAh/g_Si to minimize the mechanical breakdown of the composite electrode as a consequence of the huge volume variations of silicon particles upon alloying with lithium. This case, the cycle life is mostly determined by the growth of the SEI and thus strongly depends on the liquid electrolyte choice [3].

(ii) Without limitation. This case, the cycle life is strongly affected by the mechanical resiliency of the electrode.

Electrochemical performance was done with a first cycle at C/20, D/20 then at C/5, D/5 where C and D implies charge and discharge rate respectively. The active mass loading of Si is 2.5-2.6mg/cm^2.

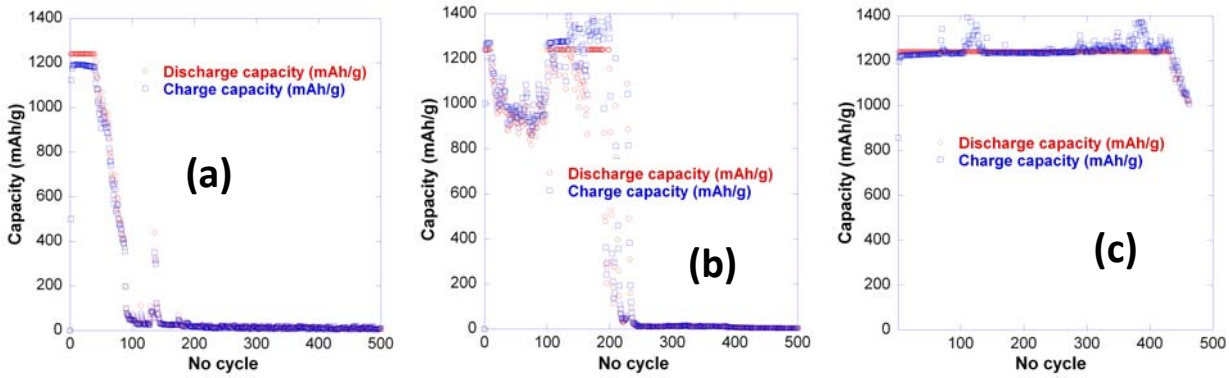

Figure 4. Charge/discharge capacity versus number of cycle for L2 electrodes at 1200mAh/g_Si limitation with different electrolytes (a) LiTDI, (b) LiTDI VCFEC and (c) LP30VCFEC

Figure 4-Figure 5 display charge and discharge capacity versus number of cycle of L2 electrodes which operate in different electrolyte compositions. Without VCFEC, LiTDI electrolyte shows poor performance in both cycling conditions (capacity limitation and without limitation). Adding additive VCFEC improves the LiTDI electrolyte performance. When L2 electrodes were cycled with capacity limitations, LiTDI is much worse than $LiPF_6$. When cycling at full capacity, LiTDI is slightly worse than $LiPF_6$.

[3] Y. Oumellal, N. Delpuech, D. Mazouzi, N. Dupré, J. Gaubicher, P. Moreau, P. Soudan, B. Lestriez and D. Guyomard, J. Mater. Chem., 21 (2011) 6201

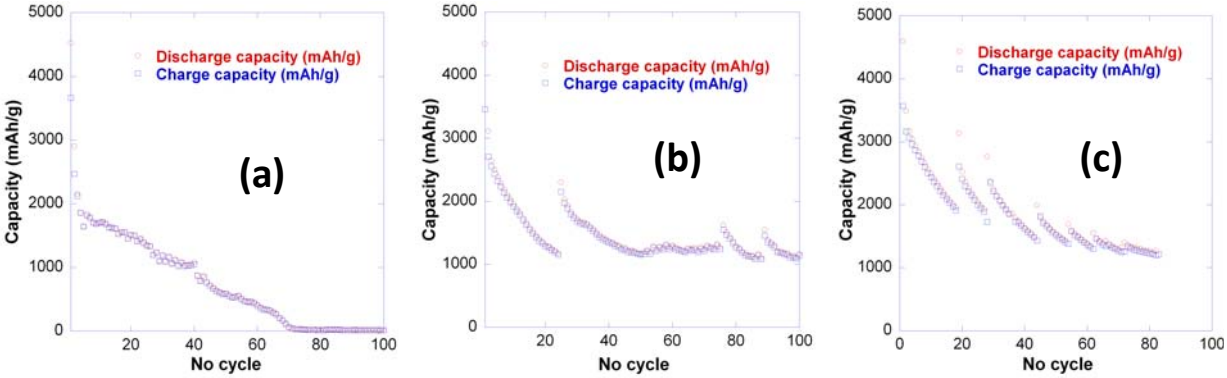

Figure 5. Charge/discharge capacity versus number of cycle for L2 electrodes at full capacity with different electrolytes (a) LiTDI, (b) LiTDI VCFEC and (c) LP30VCFEC.

3 Electrochemical studies with $LiNi_{0.42}Cr_{0.08}Mn_{1.5}O_4$ (LNMO-Cr) supplied from Faculty of Applied Sciences, Delft University of Technology

A major obstacle in applying LNMO is the compatibility with the electrolyte. In order to stabilize the LNMO material, new batch of LNMO with chromium doping ($LiNi_{0.42}Cr_{0.08}Mn_{1.5}O_4$ - LNMO-Cr) was synthesized in Delft University and sent to IMN for electrochemical testing. I prepared different composite electrodes with LNMO-Cr based on B6 and M3 formulations which exhibit best electrochemical performances. Cycling tests were done with same conditions as previous LNMO without doping. However, there was no difference observed between LNMO-Cr and undoped LNMO.

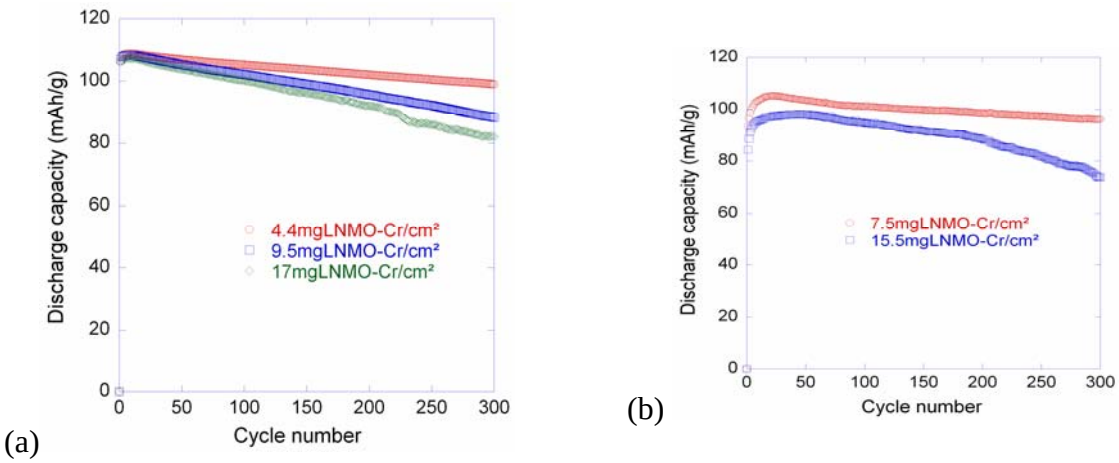

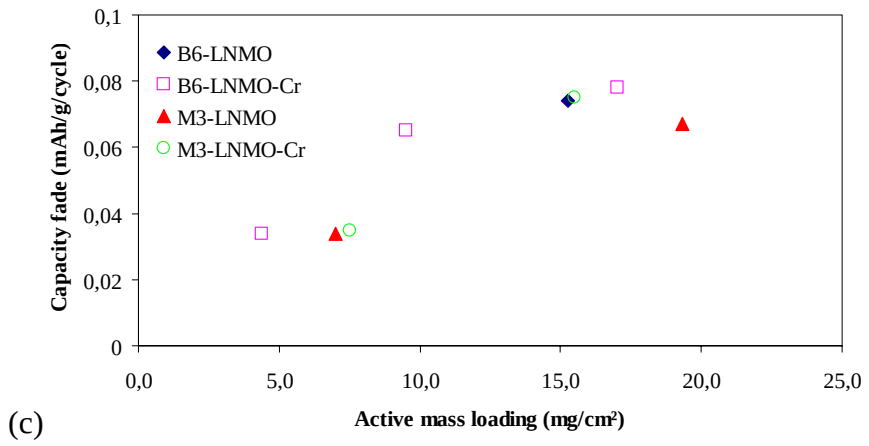

(c)

Figure 6. Discharge capacity vs. cycle number for B6 electrodes, (b) M3 electrodes at different LNMO-Cr mass loadings. (c) Capacity fade after 200 cycles from Q_0 as a function of the LNMO loadings for the different electrode formulations: B6 and M3 with undoped LNMO (close symbol) and Cr-doped LNMO (open symbol).

4 The cyclability data of calendared LNMO electrodes

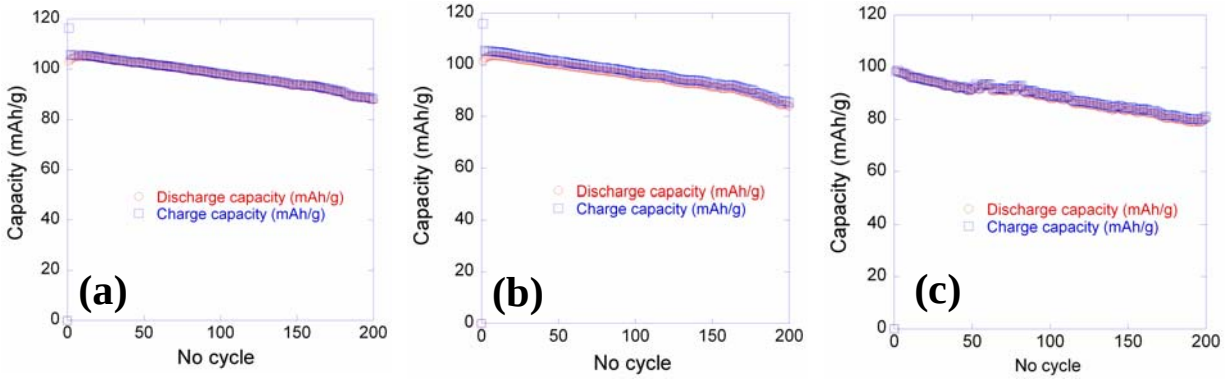

Figure 7. Charge/Discharge capacity vs. number of cycle of: B6 electrodes under calendaring (a) 4Tons (b) 8Tons and (c) M4 electrodes under calendaring at 2Tons.

Table 1. Capacity fade after 200cycles from Q_o of different B6, M4 electrodes with and without calendaring

Electrode name	Pressure (Tons)	Mean porosity (%)	AM loading (mg/cm^2)	Capacity lost after 200cy. from Q_o (mAh/g/cy.)
B6	0	42.5	15.3	0.074
	4	38	19.6	0.085
	8	32		0.1
M4	0	56	25-26	0.097
	2	45		0.093

The cyclability of different electrodes from B6 and M4 formulations were studied (shown in Figure 7 and Table 1). In general, both electrodes prepared by MS or BL under calendaring display same electrochemical behaviour as the one without calendaring. However, too high densification pressure may cause some cracks at the interface between the electrode and the current collector or block some pores to the liquid electrolyte, thereby increasing the value of capacity fade.

5 Calculation of the volumetric and gravimetric energy densities

The mass of the electrode m_e is first determined from the surface capacity, SC (in mAh/cm^2), summing both sides of the current collector, the specific capacity of the active material (160 mAh/g for $LiFePO_4$) and its weight fraction in the electrode composition, $\phi_{m,i}$. For example for the positive electrode, considering a stack surface area, S_{stack}, we obtain:

$$m_{e,+} = m_{LiFePO4} / \phi_{m,LiFePO4} \text{ with } m_{LiFePO4} = SC / 160 \times S_{stack} \qquad (a1)$$

The electrode thickness, h_e, is calculated from its bulk density, ρ_e, and its porosity, P_e. For the positive electrode we obtain:

$$h_{e,+} = [m_{e,+} / (\rho_{e,+} \times (1 - P_{e,+}))] / 2 S_{stack} \text{ with } \rho_e = 1 / (\Sigma (\phi_{m,i}/\rho_i)) \qquad (a2)$$

where *i* stands for $LiFePO_4$, binder and CB. The factor 2 takes into account that $m_{e,+}$ is the sum of the electrode masses from both side of the current collector. The same calculations are done for the negative electrode considering a specific capacity of 360mAh/g. Then the stack thickness, h_{stack}, is determined by summing the thicknesses of all the layers

$$h_{stack} = 2h_{e,+} + 2h_{e,-} + 2h_{sep} + h_{Al} + h_{Cu} \qquad (a3)$$

where h_{sep}, h_{Al} and h_{Cu} are the thicknesses of the separator, the aluminum and the copper current collectors, respectively. The factor 2 in front of $h_{e,+}$ and $h_{e,-}$ takes into consideration that the current collector has both faces coated by the electrode (Figure 3-41). The volume of the stack, V_{stack}, is simply given by

$$V_{stack} = h_{stack} \times S_{stack} \qquad (a4)$$

Considering a well balanced cell with the positive electrode capacity matching that of the negative electrode, the total capacity of the stack, Q_{stack}, is given by:

$$Q_{stack} = m_{LiFePO4} \times 160 \qquad (a5)$$

Then the volumetric energy density, E_{vol}, is given by:

$$E_{vol} = Q_{stack} \times (3.45 - 0.17) / V_{stack} \qquad (a6)$$

Where the term (3.45 – 0.17) is the average difference in potential of both active materials, $LiFePO_4$ and Graphite. Finally the mass of the stack, M_{stack}, is determined by summing the masses of all the layers as well as that of the electrolyte, m_{lyte}:

$$M_{stack} = m_{e,+} + m_{e,-} + 2\, m_{sep} + m_{Al} + m_{Cu} + m_{lyte} \qquad (a7)$$

$$m_{lyte} = S_{stack} \times \Sigma\, (n_i \times h_i \times P_i) / 1.28 \qquad (a8)$$

where i stands for separator, positive and negative electrode, n_i is the number of respective layers, h_i is the thickness of the layers, P_i is their porosities and 1.28 is the electrolyte density. Then the gravimetric energy density, E_{grav}, is given by

$$E_{grav} = Q_{stack} \times (3.45 - 0.17) / M_{stack} \qquad (a9)$$

Acknowledgements

It is important to take this opportunity to express my gratitude to all those that have contributed to my graduate education. Foremost, I would like to express my sincere appreciation towards my supervisors - Bernard Lestriez, Dominique Guyomard and Manuella Cerbelaud. Special thanks to Bernard Lestriez for his constant encouragement, endless inspiration, valuable guidance and also the correction of report. All of these have motivated me a lot.

I am grateful to financial support provided by the European Commission through the project EuroLiion for my PhD work during 3 years.

I am also thankful to Joël Gaubicher, Patrick Soudan, Nicolas Dupré, Philippe Moreau, Mauricette Chabot, Catherine Rochas, Kalid, Driss, Chon, Magali, Nathalie, Lenaic, Yassine, Pierre Emmanuel, Djamel, Margaud, Carole, Rémi, Nicolas, Elise, Stéphanie, Pablo, Henri, Léonard, Audrey, Marine, Cédric…and all those who gave me generous help and fruitful discussions.

Last but not least, I am greatly indebted to my family for their constant support and encouragement.

Published/to be submitted manuscripts

I. Manufacturing of industry-relevant silicon negative composite electrodes for lithium ion-cells, B. P. N. Nguyen, S. Chazelle, M. Cerbelaud, W. Porcher and B. Lestriez, Journal of Power Sources, 262 (2014) 112-122.

II. Nanosilicon-Based Thick Negative Composite Electrodes for Lithium Batteries with Graphene as Conductive Additive, B. P. N. Nguyen, N. A. Kumar, J. Gaubicher, F. Duclairoir, T. Brousse, O. Crosnier, L. Dubois, G. Bidan, D. Guyomard and B. Lestriez., Adv. Enery Mater., 3 (2013) 1351.

III. Analogy between electrochemical behaviour of thick silicon granular electrodes for lithium batteries and fine soils micromechanics, B. P. N. Nguyen, J. Gaubicher and B. Lestriez, Electrochimica Acta, 120 (2014) 319–326.

IV. Manufacturing of industry-relevant $LiNi_{0.5}Mn_{1.5}O_4$ positive composite electrodes for lithium ion-cells, B. P. N. Nguyen, N. Mariage, R. Fredon, E. Kelder, and B. Lestriez, written and to be submitted.

Paper I

“Manufacturing of industry-relevant silicon negative composite electrodes for lithium ion-cells”

Journal of Power Sources 262 (2014) 112–122

Contents lists available at ScienceDirect

Journal of Power Sources

journal homepage: www.elsevier.com/locate/jpowsour

Manufacturing of industry-relevant silicon negative composite electrodes for lithium ion-cells

B.P.N. Nguyen [a], S. Chazelle [b,c], M. Cerbelaud [a,c], W. Porcher [b,c], B. Lestriez [a,c,*]

[a] Institut des Matériaux Jean Rouxel (IMN), Université de Nantes, CNRS UMR 6502, F-44322 Nantes Cedex 3, France
[b] CEA/LITEN, Grenoble, France
[c] Réseau sur le Stockage Electrochimique de l'Energie (RS2E), FR CNRS 3459, France

HIGHLIGHTS

- PAMA dispersant improves the stability of electrodes slurries of Silicon based negative electrode.
- Amount of PAMA must be limited due to competition in adsorption with CMC at the surface of CB particles.
- SBR copolymer latex improves adhesion of the tape to the current collector and increases cycle life.
- Calendaring is detrimental to electrochemical properties.

ARTICLE INFO

Article history:
Received 15 January 2014
Received in revised form
6 March 2014
Accepted 24 March 2014
Available online 2 April 2014

Keywords:
Lithium-ion battery
Silicon
Electrode formulation
Dispersant
Latex

ABSTRACT

In this paper, Poly (acrylic-co-maleic) acid (PAMA) is used as a dispersant to improve the stability of electrodes slurries for large scale processing of Silicon based negative composite electrode. The stability and homogeneity of the slurries are characterized using different techniques. Sedimentation test, electrical measurement, SEM-EDX observations as well as rheological measurements show that a more homogeneous distribution of carbon black (CB) inside the stack of Si particles is reached with presence of PAMA. However, the amount of PAMA is limited due to the competition in the adsorption of PAMA and Carboxylmethyl cellulose (CMC) at the surface of the CB particles. Upon cycling with capacity limitation, the optimized electrode formulation at lab scale could achieve more than 400 cycles with surface capacity ~2.5–3.3 mAh cm^{-2}. At the pilot scale, the improvement of adhesion of the tape to the current collector by using Styrene-co-Butadiene rubber copolymer latex (SB) helps to maintain long cycle life while calendaring is detrimental to electrochemical properties.

1. Introduction

Nowadays, rechargeable lithium-ion battery is one of the most promising energy storage technologies to enable a various range of clean transportations (hybrid electric vehicles, electric vehicles, Plug-in Hybrid Electric Vehicles). To meet requirements of these automotive applications, it is necessary to find higher capacity electrode materials for Li-ion batteries. The current commercial lithium ion battery is based on the use of graphitic carbon anode which provides a low theoretical capacity of 372 mAh g^{-1} and energy density (779 mAh cm^{-3}) [1]. Compared with graphite, silicon is a favourable alternative candidate due to a high specific capacity (3572 mAh g^{-1}) and specific volumetric capacity (2081 mAh cm^{-3}) [2]. However, poor performance of Si electrodes (large capacity fading and low cyclability) is a major issue. This could be explained by two distinct reasons: (i) Silicon exhibits dramatic volume expansion and shrinkage during lithiation and delithiation, respectively. This volumetric variation results in mechanical breakdown of the composite electrode [3,4]. (ii) Formation of unstable solid electrolyte interphase (SEI) causes uninterrupted liquid electrolyte degradation at the surface of silicon [5–7].

Several strategies have been undertaken to overcome these problems. One way is optimising the binder in order to cope at the molecular scale with the expansion and contraction of Si upon alloying and dealloying with Li. Most studies of Si anodes have involved the use of carboxymethylcellulose (CMC) and polyvinylidene fluoride (PVDF) binders. The most conventional binder PVDF used for the batteries is likely attached to Si particles via weak

* Corresponding author. Institut des Matériaux Jean Rouxel (IMN), Université de Nantes, CNRS UMR 6502, F-44322 Nantes Cedex 3, France.
E-mail address: bernard.lestriez@cnrs-imn.fr (B. Lestriez).

http://dx.doi.org/10.1016/j.jpowsour.2014.03.119
0378-7753/

Van der Waals forces only (between its fluorine atoms and hydrogen atoms). Moreover, PVdF is significantly plasticized by the liquid electrolyte solvents (carbonates) and becomes an easily deformable material with small resistance to deformations [8]. PVdF thus fails to accommodate large changes in spacing between the particles during battery cycling and quickly becomes incompetent in keeping the particles together and maintaining electrical conductivity within the anode, which is required for battery operation. In the meantime, noteworthy amounts of improvement have been achieved for CMC binders, which typically display a better performance and can be considered to be the state of the art in this field. CMC favours both (i) a much more homogeneous distribution of the carbon black conductive additive particles, (ii) an efficient networking process of the carbon black and Si particles in the composite electrode slurry, due to its extended conformation in solution that enables the formation of bridges between particles, and (iii) the establishment of a covalent bond through the esterification of the SiOH surface groups by the COOH functional groups of CMC, which increases the cycle life [9,10]. Since early works on CMC, [11–14] several other works proposed alternative binders to CMC, most of them being polysaccharides and/or bearing COOH functional groups [15–18].

Another way to improve the cycle life is using electrolytes containing a film-forming agent. In the case of silicon, unstable layer is formed in the first cycles without utilising FEC/VC additives and cracks occur on this layer during volume expansion upon Li insertion of the particles which exposes new surfaces leading to additional liquid electrolyte degradation [19–25]. Flexible polycarbonates form in the surface film in FEC and VC-containing solutions, which allows a better ability to accommodate the volume variations of the Si phase, then limiting the contact between the silicon particles and the liquid electrolyte [26]. This results in reduction of the amount of SEI products precipitating and accumulating inside the electrode at each cycle [25].

Besides, electro-conductive additives also display an important influence for the performance of Si-based electrodes. Combining carbon nanotubes (multiwall carbon nanotubes (MWNTs)) and nanofibers (vapor-grown carbon nanofibers (VGCFs)) allows building a hierarchical and resilient 3D conductive network, which strongly improves the cyclability of micron-size Si in Si/C/CMC composite electrodes [27]. In the case of nano-size Si, no improvement was found by using these carbon additives when compared to the standard carbon black (CB). However, by using reduced graphene oxide (rGO) instead of CB as the conductive additive for nano silicon based negative composite electrodes, a significant improvement of the electrochemical performance was confirmed, whatever the cycling conditions [28,29].

In this work, we aim to design the formulation of nanosilicon-based negative composite electrodes to wind some cylindrical cells. To reach this goal we looked for: (i) homogeneous and stable slurry-state, (ii) suitable mechanical properties for calendaring and battery assembly steps, (iii) long cycle life, for high active mass loadings of about 2.5–3.3 mAh per cm^2.

2. Experimental

Electrode preparation – Composite electrodes were made of nanometric Si (particle size 150 nm, specific surface area 14 $m^2\ g^{-1}$) as an active material (AM), Super P carbon black (CB, Timcal) as a conductive additive (C), Carboxylmethyl cellulose (CMC, DS = 0.9, M_w = 700.000 g mol^{-1} Sigma–Aldrich) and a Styrene-co-Butadiene rubber copolymer latex (SB) as a binder (B) and Poly (acrylic-co-maleic) acid (PAMA M_w = 3000 g mol^{-1} Sigma–Aldrich) as a dispersant (D).

At the lab scale, powders were introduced in a silicon nitride vial according to the electrode formulations given in Table 1. Then, 1 mL of buffer pH 3 0.1 M solution prepared with KOH and citric acid was added to 200 mg of composite electrode material. The solid loading is thus 17 wt%. Three silicon nitride balls (9.5 mm diameter) served as mixing media. A Fritsch Pulverisette 7 mixer was used to mill the slurry at 500 rpm for 60 min. The slurry was tape cast onto a 25 μm thick copper foil and dried for 12 h at room temperature and then at 2 h at 100 °C under vacuum. Citric acid and its salt, which are not eliminated by this vacuum treatment, remain in the composite tape.

At the pilot scale, CMC was dissolved in the buffer pH 3 solution, prepared with KOH and citric acid at 0.1 M. PAMA was added before introducing the conductive additive and the AM. The suspension is then dispersed using a high speed stirrer for 30 min. At the end of the dispersion, the latex is added and the slurry shortly homogenised. The slurries were coated using a semi industrial machine, with a comma bar system and an oven of 1 m length onto a 10 μm thick copper foil at a speed of 0.2 m min^{-1}. The transit time in the oven is so around 5 min.

Sedimentation test – Small amount (30 mg) of each material (Si, CB) was dispersed in buffer solution pH 3 by using ultrasounds for 15 min. The dispersant quantity was adjusted in order that its concentration (mg mL^{-1}) is the same as for electrode preparation. The process of settling was observed visually as a function of time.

Rheological measurements – Rheological properties were measured on a controlled-stress rotating rheometer (Anton Paar,

Table 1
Composition, porosity, thickness and mean resistivity (measured with 2 probes) of composite electrodes. L and P mean an electrode prepared at the lab scale and at the pilot scale, respectively.

Electrode name	Si (wt%)	CB (wt%)	Latex (wt%)	CMC (wt%)	Buffer (wt%)	PAMA (wt%)	Porosity (%)	Thickness (μm)	Loading (mg Si cm^{-2})	Conductive additive volume fraction[a] (%)	2-probes resistivity with stand. dev. (ohm cm)
La	–	51	–	16	33	–	n.m.	n.m.	n.m.	n.m.	n.m.
Lb	–	49	–	15.7	31.8	3.5					
Lc	–	47	–	15.2	31	6.8					
Ld	–	43.2	–	14.4	29.5	12.9					
L1	67.6	10.1	–	6.8	15.5	–	71–73	66–68	2.6–2.8	3.06	11.6 ± 0.5
L2	65.9	10.1	–	6.8	15.5	1.7	68–70	63–65		3.30	7.6 ± 0.5
L3	64.2	10.1	–	6.8	15.5	3.4	65–68	60–62		3.55	12.7 ± 0.5
P1	65.9	10.1	–	6.8	15.5	1.7	70–71	52–54	2.0–2.1	3.24	11.4 ± 0.5
P2	63.5	9.7	3.6	6.6	15	1.6	68–69	50–51		3.14	9.5 ± 0.5
P3	61.3	9.4	6.9	6.3	14.5	1.6	68–69	52–54		3.01	11.1 ± 0.5
P1	65.9	10.1	–	6.8	15.5	1.7	59–60	41–42	2.0–2.1	4.40	9.4 ± 0.5
P2	63.5	9.7	3.6	6.6	15	1.6				3.97	8.1 ± 0.5
P3	61.3	9.4	6.9	6.3	14.5	1.6				3.85	9.7 ± 0.5

n.m. is for not measured.
[a] The volume fraction is calculated by taking into account the electrode porosity.

MCR 101) with a 50 mm diameter plane-and-plane geometry and the sample gap between the Pelletier plane and the geometry was fixed at 0.6 mm. Several types of rheological measurements were carried out: (i) Two measurements were done with continuous shear: a rate sweep measurement from 0.1 to 1000 s^{-1} to determine the viscosity of the slurries and sequence at constant rate measurement 10 s^{-1} for 900 s to simulate and follow what happens upon gentle mixing as in the reservoir of the slot die machine. (ii) The evolution of moduli at a frequency of 1 Hz and a strain of 1% after a preshear at 100 s^{-1} for 60 s to simulate and follow what occurs after casting.

Study of electrode's texture – Scanning electron microscopy (SEM) and Energy dispersive x-ray imaging was performed by using a JEOL JSM 7600 to investigate textural properties of composite electrodes.

Electrical measurements – Electronic resistivity measurements were carried out by impedance spectroscopy on dry Si electrode/current collector samples sandwiched in between two metallic plungers in a standard swagelok cell, using a VMP automatic cycling/data recording system (Biologic). The frequency range was scanned from 10 mHz to 189 kHz. Several compositions were studied at different thicknesses. Six samples were evaluated for each composition. The measure was repeated three times on each sample. The impedance diagrams were resumed in all cases to a single point on the real axis. A linear increase of the resistance, R, with the thickness, t, was found, with $R = 0$ for $t = 0$. The latter implies that the contact resistance between the copper foil used as current collector and the composite electrode is negligible in the dry state. The electrode resistivity, ρ, was thus determined from the well-known equation $\rho = (R \times S)/t$, where S is the contact surface area between the probe (metallic piston) and the sample, 0.283 cm^2.

In complement, a mapping of the electronic resistivity of dry Si composite tapes prepared on plastic film was also measured by using four-point probe mapping system (model 280SI-Microword) with computer controlled stepping motors to move the four-point probe. The spacing between each probe is 1 mm. Each probe has a contact area radius of 100 μm and the load applied on each probe is 60 g. The current source is a fixed-output, range-programmable constant-current generator, and provides an appropriate amount of test current to the sample under test. It is automatically selected by the measurement board during the measurement sequence.

Electrochemical testing – Half cells: two-electrode Swagelok™ test cells comprise (i) a 0.78 cm^2 disc of composite positive electrode (ii) a porous glass paper as separator soaked in an electrolyte consisting of 88 wt% LP30 [1 M $LiPF_6$ solution in dimethyl carbonate-ethylene carbonate (1:1)] 2 wt% vinylene carbonate and 10 wt% fluoroethylene carbonate mixture and (iii) a 0.78 cm^2 Li metal disc as the negative and reference electrode. The cells were assembled in the glove box under argon atmosphere. Cell cycling was performed at 20 °C, monitored by a VMP™ system (Biologic) in a galvanostatic mode. The voltage range used was 0.01–1 V versus Li^+/Li. All composite electrodes were studied with the same rate (C/5 and D/5) with a limited discharge capacity of 1200 mAh g^{-1}_Si (850 mAh g^{-1}_electrode).

3. Results

3.1. Elaboration at the lab scale: selection of a dispersant

Our previous works show that preparing the electrode in a pH 3 buffer is mandatory to achieve the grafting of the CMC binder which strongly improves the cycle life [30]. However, at pH 3, the zeta potential of the Si particles is equal to zero and the slurries are not stable and flocculate through the attractive Van der Waals interactions [31]. Thus we looked for a dispersant to improve the stability of the electrode slurries for large scale processing. In the aqueous-processing of $LiFePO_4$, poly(4-styrene sulfonic acid) (PSSA), poly(acrylic acid-co-maleic acid) (PAMA), polyethyleneimine (PEI) and the isooctylphenylether of polyoxyethylene (Triton X-100) were considered as highly efficient dispersants to have good dispersion property [32–35]. While in non-aqueous processing, the study of C–C. Chang et al. demonstrated improvement of $LiFePO_4$ and KB electrode by using polyacrylate based dispersant [36]. In aqueous-processing of $LiCoO_2$, it's found that both $LiCoO_2$ and carbon powders can be well-dispersed by using ammonium polyacrylic acid (PAA-NH_4), resulting in a decrease of powder aggregation and an increase in the contact area between $LiCoO_2$ and the conductive additives [37,38]. In addition, J.T. Patey el al. proved the role of Triton X-100 in improvement of distribution of the suspensions of TiO_2 and CB, leading to improved electrical contact between particles [39]. With respect to the use of dispersants, no study concerned Si-based negative composite electrodes. Here, different dispersant were tried and we will report the results achieved with PAMA.

In order to identify the dispersing efficiency of PAMA on Si and CB, dilute suspensions in pH 3 buffer were prepared and their dispersion stabilities were observed by sedimentation tests. Fig. 1 shows different buffer suspensions of Si, CB, mixture of Si + CB in the presence of PAMA (with identical concentration in mg L^{-1} as in the electrode slurry of L2) and without PAMA, respectively, after different time periods. In the initial state, Si, CB and mixture of them were homogeneously distributed in the suspension with addition of PAMA, while without PAMA the CB powder began to settle especially in the suspension of both Si + CB with the

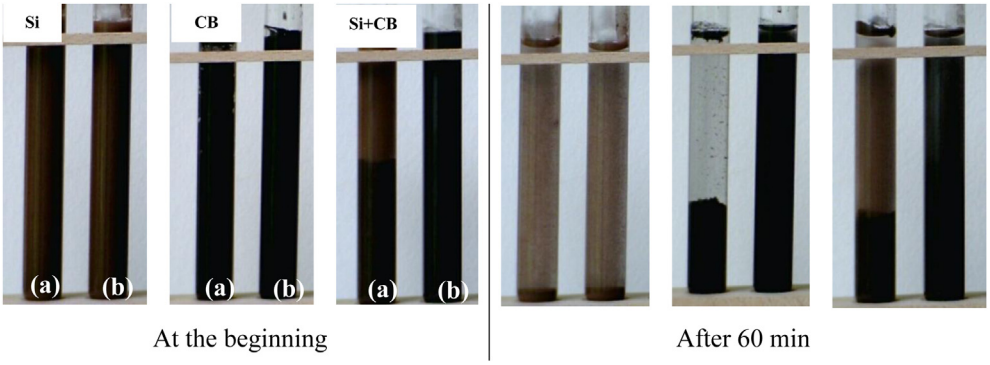

Fig. 1. Settling test of different suspensions (Si, CB, Si + CB in pH3 buffer) as a function of time: (a) without PAMA, (b) with 4 mg mL^{-1} of PAMA (which is the same concentration as in the slurry of electrode L2).

segregation into two separate phases (CB at the bottom and Si in the upper supernatant). After 1 h, most of Si or CB powder settled to the bottom in the suspension without PAMA and only small amount of Si powder was suspended in the upper supernatant. In contrast, the phenomena were apparently different in the suspension with PAMA. CB powder was still homogeneously distributed and mixture of Si + CB remained stable, although Si without CB settled to the bottom of the vial. From the above sedimentation results, it clearly indicates that PAMA doesn't provide better stability of Si in buffer solution while an improvement of stability of CB was displayed practically. Regarding the suspension of both Si + CB, PAMA remains an efficient dispersant as the settling phenomenon is very much decreased.

Complementary visual observations of CB/CMC/PAMA/buffer composites (without Si) are shown in Fig. 2. To prepare these blends we kept the same ratio of the mass of PAMA vs. the powder surface area (Si + CB) as in composite electrodes. One can observe in Fig. 2 that with increasing PAMA content, a demixing occurs between CB (dark zones) and one of the two polymers, CMC or PAMA. Such a demixing between a powder and a polymer generally occurs when a polymer does not adsorb at the surface of the particles. Non adsorbed polymers are excluded from the particle surfaces and the particles may flocculate by the mechanism of depletion [40–42]. The settling tests clearly shows a stabilization of the CB suspensions by PAMA which must results from the adsorption of PAMA and the establishment of repulsive electrostatic forces between the CB particles. The adsorption of PAMA on carbon surface has been shown elsewhere [33]. On another hand, CMC is also known to show attractive interactions with carbon surfaces and generally strongly adsorbs on it [43–45]. It is well known that when more than one polymer is present in a suspension, some competitive absorption can occur between the different polymers [46]. Thus, we may hypothesize that by increasing the PAMA concentration in the CB/CMC/PAMA/buffer mixtures (Fig. 2) the competition between CMC and PAMA resulted in the exclusion of the CMC from the CB particle surfaces. Whatever it is, a competition between CMC and PAMA with respect to adsorption on CB is evidenced. Same kind of visual observations show however no difference between L1 (0), L2 (1.7) and L3 (3.4 wt% PAMA) composite electrodes. L2 tape is shown in Fig. 3. It can be noted some detachments from the copper current collector, as for most of the lab-made tapes studied here.

Further SEM observations exhibit the morphology of composite electrodes with and without PAMA. After ball milling, all particles are fairly well dispersed at micro scale (Fig. 4(a)–(c)). The electrodes prepared with PAMA show visually a higher compactness (and a lower porosity, Table 1), which is another evidence of the better stability of their slurries. Larger agglomerates are formed in

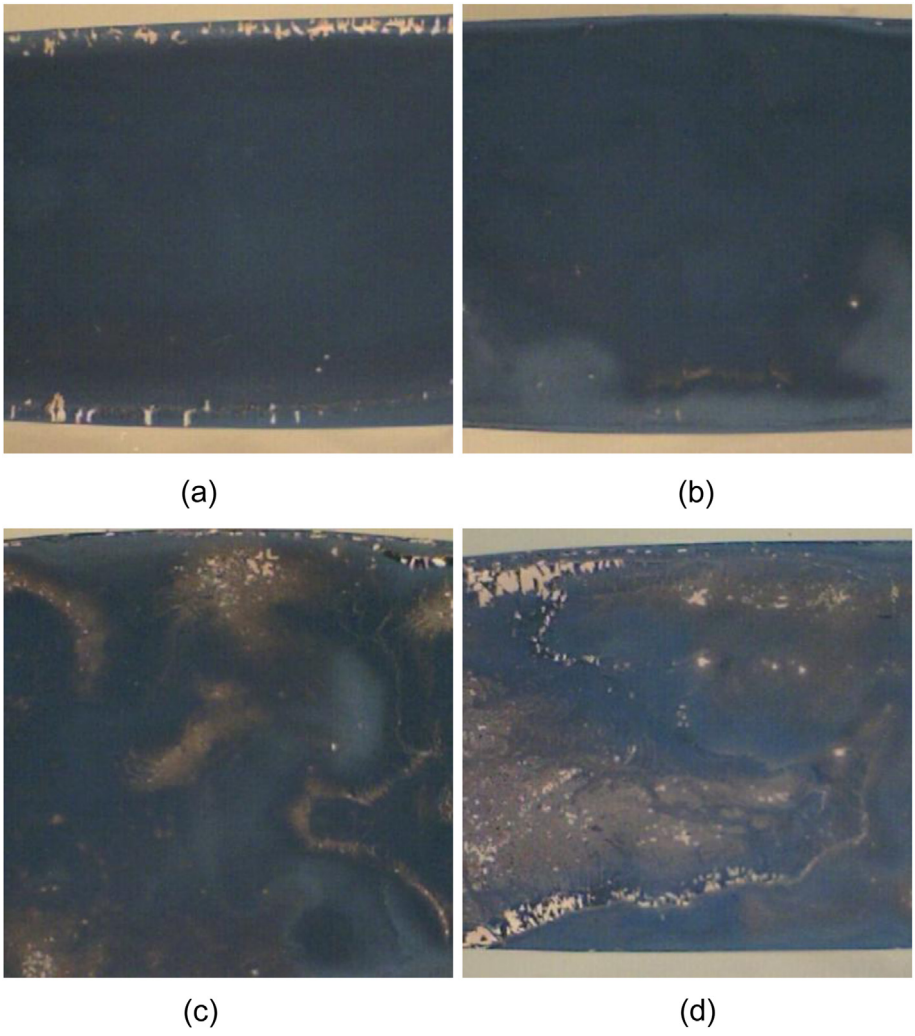

Fig. 2. Camera pictures of CB/CMC/PAMA/Buffer tapes with varying amounts of PAMA: (a) La, (b) Lb, (c) Lc and (d) Ld tapes.

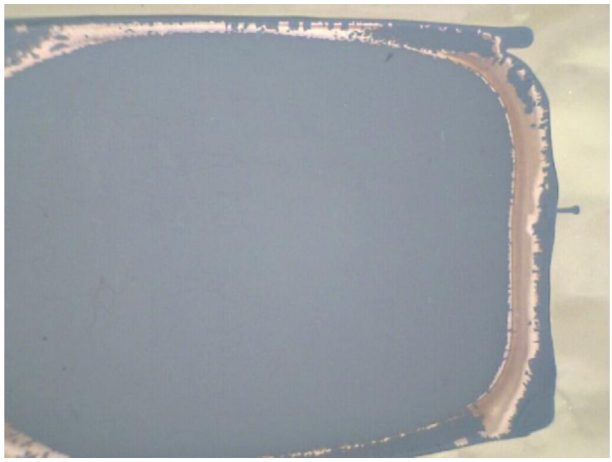

Fig. 3. Camera pictures of L2 tape.

less stable slurry which results in a higher porosity. EDX measurements at high magnification were utilized in order to more finely characterize the distribution of CB and Si in the electrodes. It can be seen from Fig. 4(d)–(i) that the dispersion within the composite electrodes seems to be better with presence of PAMA with less area which has rich carbon than without PAMA.

In order to verify the role of PAMA in dispersion of CB particles within the dried composite electrodes, two types of electrical measurements were carried out (Fig. 5(a)). Fig. 5(b) shows the resistance, R, of L2 electrode/current collector samples sandwiched in between two metallic pistons as a function of the Si electrode thickness, t. One can observe a linear increase of R with t, with $R = 0$ for $t = 0$. The latter implies that the contact resistance between the copper foil used as current collector and the composite electrode is negligible in the dry state. Average values of the electrode resistivity with different PAMA compositions are given in Table 1. There is variation of the resistivity with the amount of PAMA. It starts decreasing when PAMA is used and reaches the minimum at 1.7 wt% for L2 then increases for L3. It confirms that PAMA could help in the dispersion of the conductive additive leading to a decrease of resistivity by nearly a factor of 2. However, at high amount of PAMA (3.4wt%), it contributes to the increase of the resistivity as it also increases the electrically insulating organic matter content [37,38]. In complement, Fig. 5(c) shows resistivity scans on the different composite tapes L1-L2 using four-probes measurement technique on samples that were tape cast on plastic film. The results are displayed as values of resistivity (in ohm square) along lines at different positions as schematized in the drawing of Fig. 5(a). Without addition of PAMA, the spatial distribution of sheet resistance in L1 is large and mean value of resistivity is higher than for others. One can see that the presence of PAMA in L2 helps to lower the distribution in resistivity through the sheet, likely due to improved CB powder dispersion. In fact a fairly homogeneous value of resistivity is observed. We believe that the spatial distribution of sheet resistance in L1 reflects the size of variations in the homogeneity of this electrode.

Finally, cycling tests were done in order to evaluate the electrochemical behaviour of the different electrodes. As can be observed from Fig. 6(a), the battery cycle life strongly depends on the amount of PAMA in the composite electrode. Without using PAMA (L1), the batteries can achieve around 200 cycles while with 1.7 wt% of PAMA (L2), the cycle life increases more than 2 times (415 cycles). However, when 3.4 wt% PAMA (L3) is used, the cycle life decreases sharply (30 cycles). Coulombic efficiencies over the first

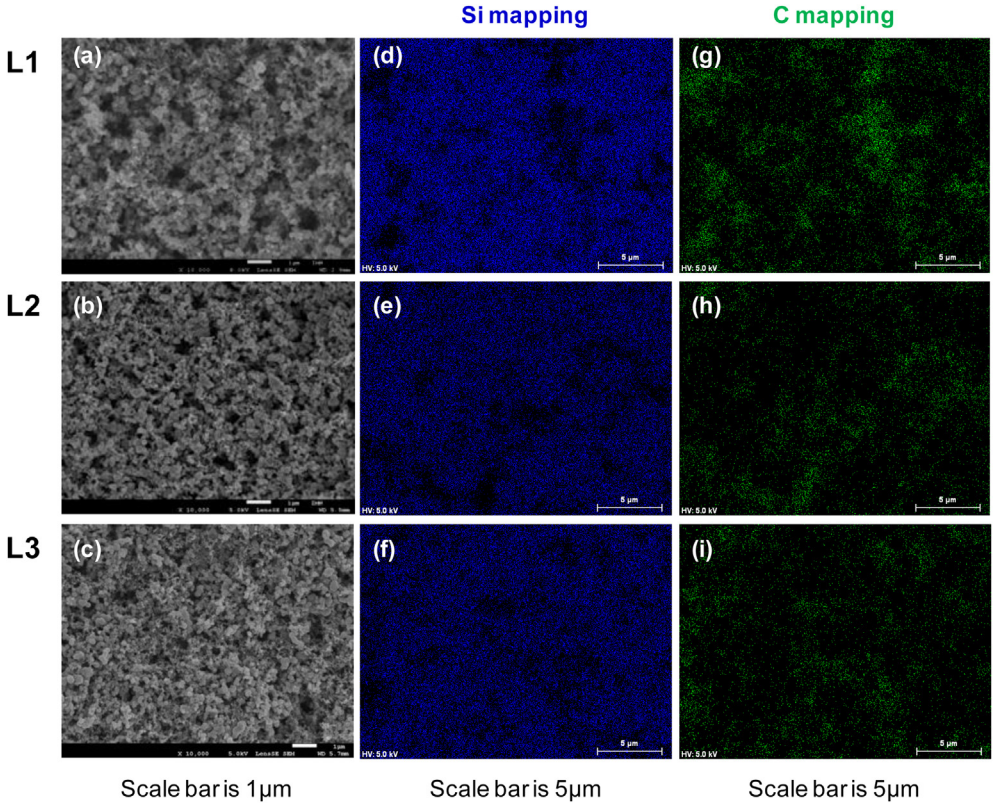

Fig. 4. (a–c) SEM observations and (d–i) EDX mappings (Si and C) of (from top to bottom) L1, L2 and L3 electrodes.

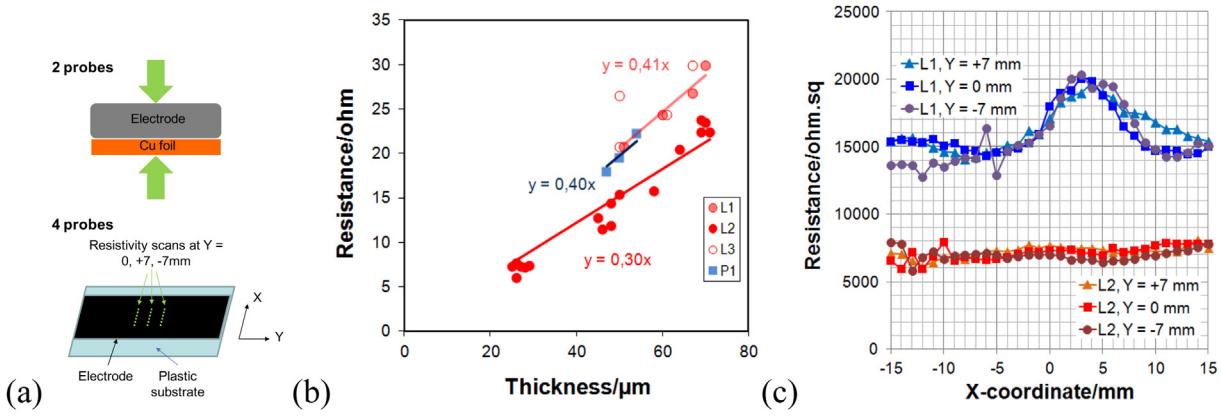

Fig. 5. (a) Schematic drawings of the 2-probes and 4-probes electrical resistance set-up. (b) Resistance of dry electrode/current collector samples sandwiched in between two metallic pistons as a function of the electrode thickness (2-probes). (c) Variation in the resistivity through the tape width (over 3 cm) at different position along the tape (at +7 and −7 mm above and behind a central line) (4-probes).

50 cycles are 99.1, 99.3 and 91.4% for 0, 1.7 and 3.4 wt% PAMA, respectively. The incremental capacity curves are shown in Fig. 6(b)–(d) for L1 to L3. Let's remind that electroactivity of Si is characterized by two major steps, A and B, which have been ascribed to Li reactions with amorphous Si [47]. Li_xSi alloys formed in step B are lithium rich compared to step A. The capacity which corresponds to step A is ca 1875 mAh g^{-1}. Thus, when cycling is done with a capacity limitation of 1200 mAh g^{-1}, only step A must be involved if all the Si particles are active, i.e. are electrically wired to the current collector. The curves at the 2nd cycle show that initially there is an activation step of the electrode as the capacity is sought from both steps A and B. However, after 100 cycles one can see only step A in the incremental capacity curves for L1 and L2. With higher number of cycles, for example 160, one can see the appearance of step B in L1 which shows that the number of Si particles which remain electrically wired has decreased and that

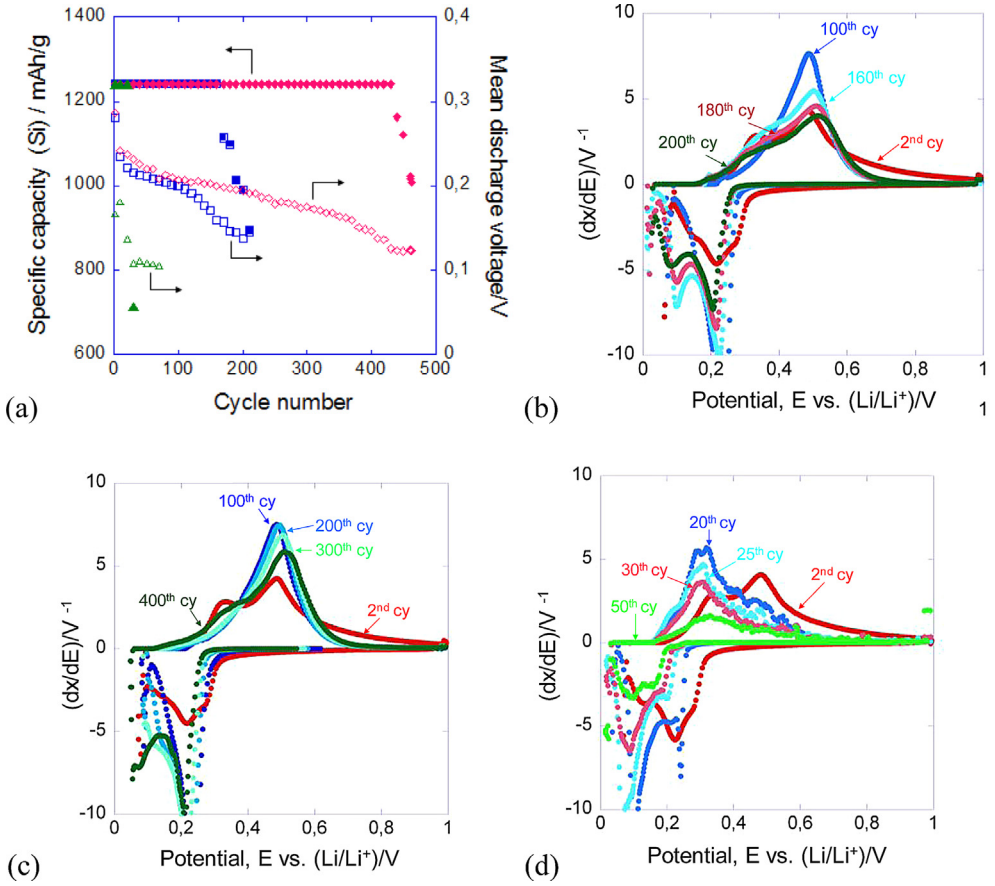

Fig. 6. (a) Discharge capacity (■, ◆, ▲) and mean discharge voltage (□, ◇, △) versus number of cycle for electrode formulations with capacity limitation of 1200 mAh per g of Si and different amount of PAMA: (■, □) 0 (L1), (◆, ◇) 1.7 (L2) and (▲, △) 3.4 wt% PAMA (L3). The Si mass loading is 2.6 mg cm^{-2}. Incremental capacity curves at selected cycles for electrode formulations with different amounts of PAMA: L1 (b), L2 (c) and L3 (d).

Table 2
Mass and thickness of electrodes, mass of Si, mass gained Δm and thickness variation, cumulative capacity loss after cycling, number of electrons n (e_{lost}), average weight M_{srp} of side reaction products.

$m_{electrode}$ (mg)	m_{Si} (mg)	Thickness (μm)	Mass gained Δm (mg)	Thickness variation (μm)	Cummulative Capa. loss (mAh/g)	n(e_{lost}) (mol)	M_{srp} (g mol^{-1} e^- loss)
3.45	2.28	65	6.40	56 ± 3	1472	$1{,}24.10^{-4}$	51
3.45	2.28	65	6.91	58 ± 3	1696	$1{,}44.10^{-4}$	48

only a fraction of the total Si mass remains electrochemically active. Contrarily, for L2 with 1.7 wt% PAMA and up to 300 cycles, only step A is involved for delivering the 1200 mAh g^{-1} capacity, which shows that a much larger Si mass remains electrochemically active in L2 compared to L1. In the case of L3, the incremental capacity curves show that the capacity is sought from a minor part of the Si active mass as both steps A and B are involved all along the short cycle life.

Here, as already observed, [25] there is a relationship between the cycle life and the coulombic efficiency. When silicon is cycled with capacity limitations, the first cause of fading is the liquid electrolyte degradation rather than the mechanical disintegration if the electrode is properly formulated [25,48,49]. Higher the coulombic efficiency, then lower the liquid electrolyte degradation, and thus longer the cycle life is. We note that as in previous work [25] a post-mortem analysis reveal a thickness increase and a mass-uptake of the composite electrodes. The weight and thickness variations of different electrodes L2 were followed (ex-situ measurements) after 100 cycles and correlated to the cumulative irreversible capacity loss which is defined as the sum over all cycles of the excess discharge versus charge capacity at each cycle (Table 2). The results are in agreement with D. Mazouzi's work. They highlight the occurrence of the liquid electrolyte degradation which products precipitate within the electrode porosity. One can see that improving the CB distribution with PAMA (from L1 to L2) slightly improves the coulombic efficiency and significantly improves the cycle life. We believe this better stability upon cycling (more uniform functioning of the Si active mass) is due to a more uniform mechanical stress distribution and more uniform electronic conductivity within the composite electrode as a consequence of the more uniform carbon black distribution [29]. L3 has dramatically short cycle life and very poor coulombic efficiency. The SEM-EDX pictures show a rather homogeneous distribution of the CB particles within the composite electrode and the electrical properties of the pristine L3 electrode are at the level of L1. A plausible interpretation is a lack of mechanical strength in this composite electrode as a consequence of the competition between PAMA and CMC which would result in less CMC bridging [14] between the different particles when the PAMA content increases. Another interpretation could be a parasitic reaction between the PAMA additive and the liquid electrolyte. This hypothesis was checked by cyclic voltammetry in the 0.05–2.5 V range at the rate of 1 and 5 mV s^{-1} on the CB/CMC/PAMA/Buffer tapes of Fig. 2. Whatever the PAMA content (from 0 to 12.9 wt%) the

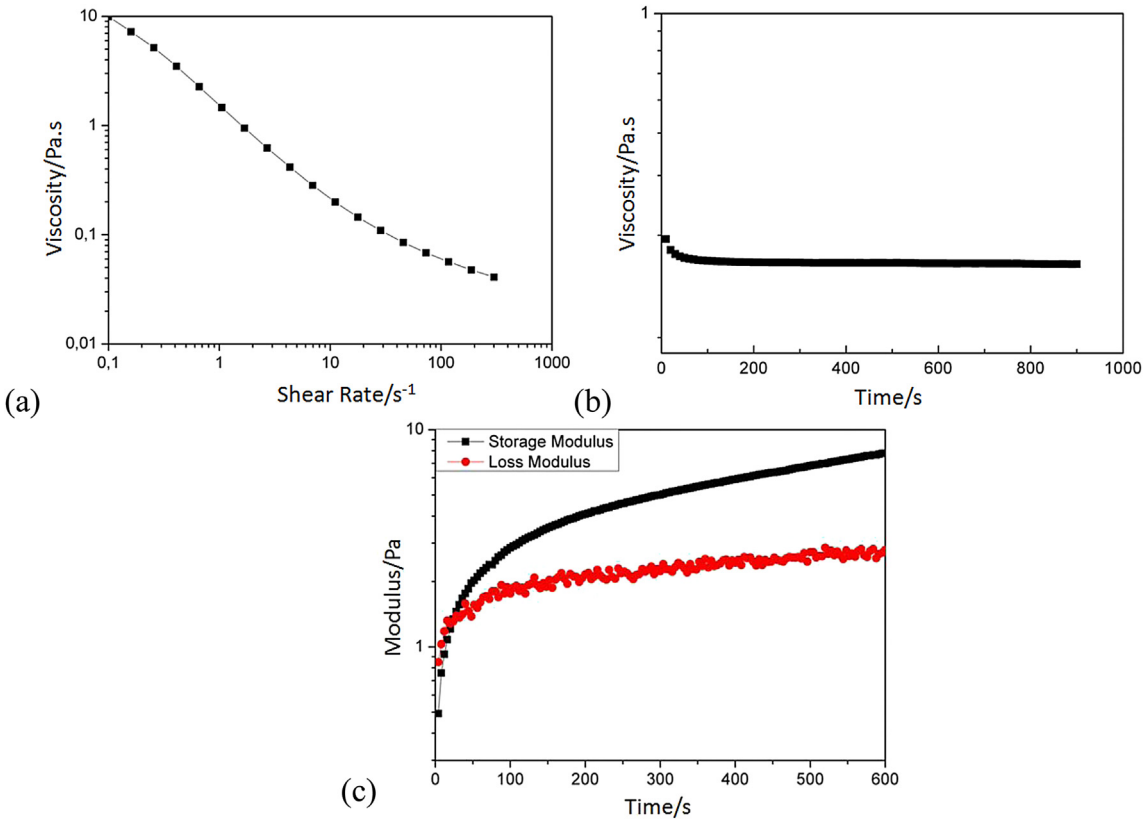

Fig. 7. Rheological properties of L2 slurry: (a) The evolution of viscosity as a function of shear rate. (b) The evolution viscosity as a function of time at a shear rate 10 s^{-1}. (c) The storage modulus and loss modulus as a function of time at a frequency of 1 Hz and a strain of 1% after pre-shear at 100 s^{-1} for 60 s.

voltammograms are similar and do not evolve upon cycling (not shown). Thus we may conclude that there is no parasitic reaction associated with the presence of PAMA.

In summary, the results obtained by sedimentation test, electrical measurements and SEM-EDX observations show that a more homogeneous distribution of CB inside the stack of Si particles is reached with PAMA. Two scales of heterogeneity are disclosed when no dispersant is added. At the microscale (EDX observations on 500 μm^2) larger CB clusters of about 5 μm diameter are detected while at the macroscale (resistivity mapping on 9 cm^2) zones of about 1 cm diameter with much higher (33% higher) resistivity are observed. As a consequence of the more uniform CB dispersion, a much better electrochemical behaviour is displayed with significantly improved coulombic efficiency and cycle life. However, if PAMA is added in too large concentration (3.4 wt% here), a very poor coulombic efficiency and cycle life are observed, which could be attributed to the competition in the adsorption of PAMA and CMC at the surface of the particles. The adsorption of PAMA to the CB surface likely impedes the adsorption of the CMC chains and thus the formation of bridges between the CB particles and the Si mass which results in a catastrophic failure upon cycling. As a conclusion of this part, the electrode formulation L2 was selected for being processed at the pilot scale.

Before the transfer from the lab to the pilot scale, the rheological properties of L2 slurry were checked. The viscosity vs. shear rate is given in Fig. 7. A shear-thinning behaviour is observed (i.e., a decrease of the viscosity with increasing shear rate). Fig. 7(b) display viscosity versus time at constant shear rate. There is a small decrease of the viscosity at the beginning; nevertheless the plateau seen after 60 s depicts the stability of slurry upon gentling mixing as in the reservoir of coating machine. In order to model the process after coating, the electrode slurry was preliminary sheared at 100 s^{-1} for 60 s. Then the evolution of the storage G′ and loss modulus G″ vs time was recorded [50]. Under very small strain

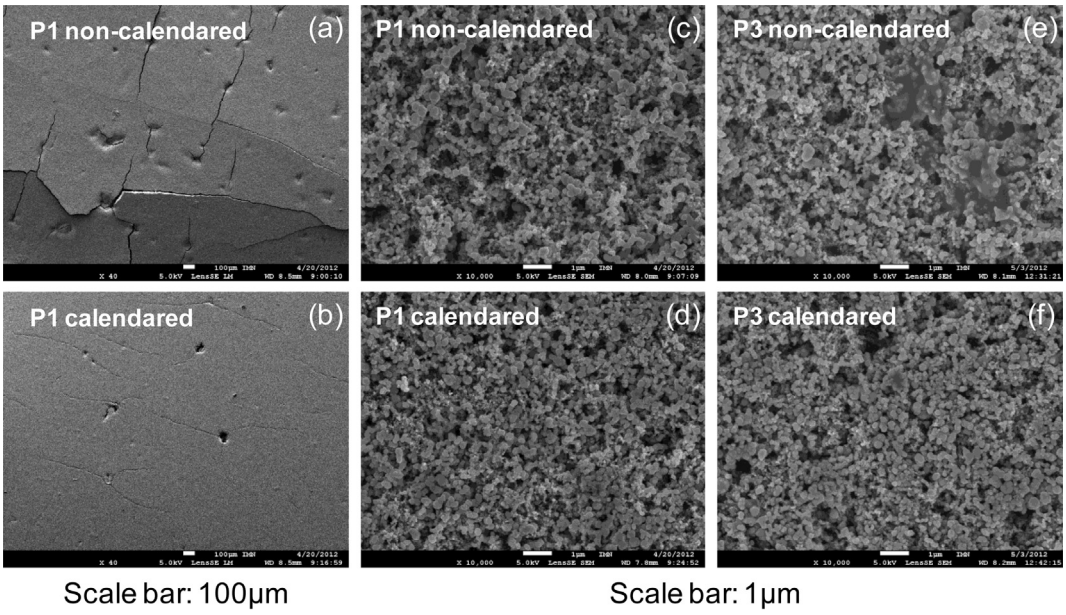

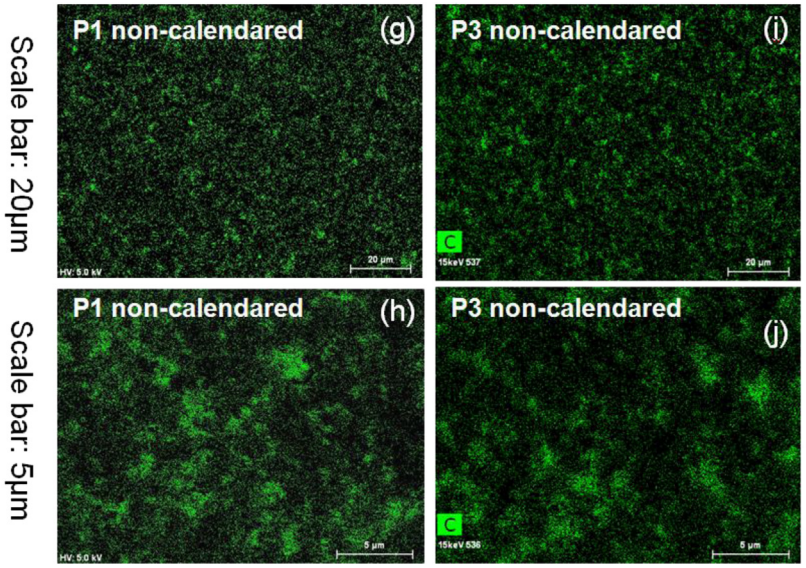

Fig. 8. SEM images for electrode P1 (a,c) uncalendared and (b,d) calendared down to 60% porosity; electrode P3 (e) uncalendared and (f) calendared down to 60% porosity. The EDX mapping image for Carbon at two different magnifications in P1 (g, h) and in P3 (i,j).

amplitude applied, the variation with time of the moduli reflects the spontaneous rearrangements or relaxations into the slurry at rest. As can be seen from Fig. 7(c) a solid like behaviour is rapidly reached and G′ dominates G″ after 60 s. This means that after short time, settling is virtually stopped by the mechanical percolation throughout the sample of the solid network of particles. After shear the moduli keep increasing upon time as a function of internal reorganization within the slurry. According to these measurements, the rheological properties of the slurry with PAMA dispersant are then suitable with the pilot line requirements.

3.2. Elaboration at the pilot scale: addition of an elastomeric latex binder and calendaring

The slurry was prepared with a total amount of 350 g and a solid loading of 21%. Its rheological properties were also characterized to validate that they were in the process window of the coating machine. Results (not shown) give a viscosity between 1 and 10 Pa s for shear rate of 1–100 s^{-1} in the range of the coating machine. There is a factor 10 between the viscosity of the slurry prepared in the lab and the one prepared at the pilot scale, a consequence of the higher solid loading of the latter compared to the former, i.e. 21 vs. 17 wt%. The slurry is observed to be stable at rest, with G′ which is superior to G″ in the low frequency range. These data show that the rheological properties of the slurry are well adapted to a coating process with a comma bar system.

However, the tape obtained after coating this slurry showed a low adhesion to the copper current collector (Fig. 8(a)). Moreover, the suppleness was not enough for winding the electrode. Two complementary strategies to improve this adhesion were evaluated: the addition of a complementary elastomeric binder (a styrene-co-butadiene rubber copolymer in the form of a latex) and the calendaring of the electrode (Fig. 8(b)). Indeed, it is known that to improve the adhesion to the current collectors of aqueous processed electrodes, mixture of CMC and emulsion polymerized styrene-butadiene copolymer latex (SB) could be used [11,12,51–53]. SB is a flexible polymer with large breakage elongation, which improves the mechanical stability of the electrode. Interestingly, a latex does not perturb the rheological properties of the slurry. It was added in the end of the mixing step to avoid any competitive adsorption with CMC [54].

Adhesion was evaluated qualitatively, using a scotch and making a peeling test manually; the suppleness was estimated by winding electrodes around mandrels of different diameters. Results are grouped in Table 3. If the electrode is not calendared, then the suppleness is fairly low. Cracking and eventually debonding of the electrode is seen when one try to wind it around a mandrel of 30 mm or less diameter. The calendaring step allows enhancing significantly the electrode suppleness. In complement, adding SB (in P2 and P3) allows to completely fold the electrode and to handle it.

Table 3
Adhesion and suppleness (min diameter at which the electrode can be wound before cracking and detaching from the current collector) of the electrode following the latex proportion (P2: 3.6 wt% and P3: 6.9 wt%) and the electrode porosity.

Electrode name	Porosity (%)	Adhesion	Suppleness (mm)
P1	70	Bad	>30
P2		Good	>30
P3		Good	>30
P1	65	Bad	10
P2		Good	2
P3		Good	0
P1	60	Bad	5
P2		Good	0
P3		Good	0

The morphology of the tape cast electrodes were observed by SEM (Fig. 8(c–f)). The images suggest a similar morphology than the electrodes prepared at the lab scale. Rather good homogeneous distribution of Si and CB were observed with P1 and P2. Nevertheless, at the highest SB content (P3), it could be observed some rich SB zones (Fig. 8(e)), a possible consequence of SB migration during the drying step [55,56]. With and without calendaring step, the dispersion of all particles in composite tape is identical. Calendaring reduces the porosity (Compare Fig. 8(c),(e) to (d),(f)). As can be seen from SEM-EDX chemical mapping (Fig. 8(g–j)), the CB appears less well distributed than in the composite electrodes prepared in the lab (Fig. 4) which could be ascribed to the different processing scales involved. Indeed, the preparation of electrodes at the lab scale implies small quantities and short mixing and casting durations, while at the pilot scale much larger quantities and much longer mixing and casting durations are implied. In particular, it is known that longer duration is detrimental to the stability of a slurry and thus to its homogeneity. The comparison of the electrical measurements in Fig. 5(b) and in Table 1 agrees with a poorer distribution of the CB as the electrical resistivity of P1–P3 are higher than L2, i.e. 9.5–11.4 vs. 7.6 Ω.cm for non-calendared P1–P3 vs. L2, respectively. Calendaring decreases the electrical resistivity to 8.1–9.7 Ω.cm for calendared P1–P3.

Finally, to evaluate the electrochemical behaviour of the electrodes prepared at the pilot scale, cycling tests were done at capacity limitation of 1200 mAh per g of Si. The same behaviour was observed as for L1-L2 in all cases, i.e. a first activation period where the mean discharge voltage is seen to increase and then a steady decrease of the latter (Fig. 9(a)). At some point of the battery life, the mean discharge voltage shows a faster decrease which is preceding the end of life. In fact, the capacity is observed to drop from the 1200 mAh per g when steps B starts to be involved as seen on the incremental capacity curves (Fig. 9(b–d)). Thus, we may conclude that the same degradation mechanism operates than in L1-L2. The slow mechanical disintegration of the composite electrode and the continuous precipitation of liquid electrolyte degradation products within the composite electrode porosity progressively disconnect the active particles. When one compares the different electrodes, a longer cycle life is mirrored in a slower polarization drop in mean discharge voltage.

The P1 electrode which is non-calendared and contains no latex as L2 shows a lower cycle life than the latter, i.e. 100 vs. 450 cycles, a result which could be attributed to a poorer CB distribution in P1 vs. L2 and a lower adhesion of P1 to the Cu copper collector than L2. The cycle life is compared for P1, P2 and P3 for their different porosities in Fig. 10(a). Without calendaring and at high porosity (~69%), the cycle life increases with increasing the amount of latex, i.e. with increased adhesion. In other work it was shown that the improvement of the adhesion by roughening of the copper current collector was strongly increasing the cycle life by decreasing the rate of active mass disconnection [57]. A possible interpretation is that the electrode, being swollen by the liquid electrolyte degradation products, an internal stress grows which results in the detaching of parts of the electrode from the current collector. A higher adhesion keeps the electrode attached and electronically wired to the current collector for a higher number of cycles. Another general trend is a shorter cycle life when the porosity is decreased (when the electrode is calendared). Several causes may individually or altogether explain this result. A lower porosity implies more mechanical constraints within the composite electrode upon alloying of the Si particles [58]. Moreover, a lower porosity means less volume to accommodate the precipitation of the liquid electrolyte degradation products. Furthermore, the calendaring step could damage the CMC bridges between the Si and CB particles, decreasing the mechanical strength at this molecular level.

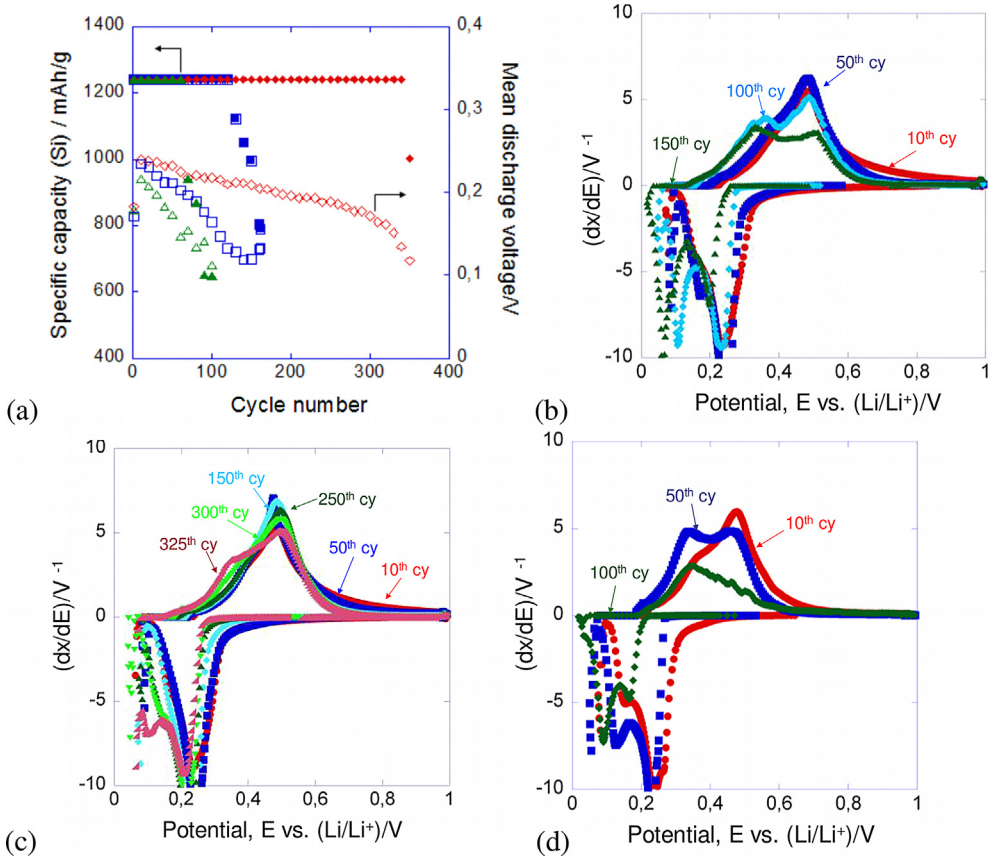

Fig. 9. (a) Discharge capacity (■, ◆, ▲) and mean discharge voltage (□, ◇, △) versus number of cycle for electrode formulations with capacity limitation of 1200 mAh per g of Si and different latex content or porosity: (■, □) P1 without calendaring, (◆, ◇) P3 without calendaring, and (▲, △) P3 with calendaring down to 60% porosity. The Si mass loading is 2.0–2.1 mg cm^{-2}. (b) Incremental capacity curves at selected cycles for (b) P1 without calendaring, (c) P3 without calendaring, and (d) P3 with calendaring down to 60% porosity.

This way, an interesting feature is observed in Fig. 10(b). One can see that the maximum mean discharge potential (reached at the end of the electrode activation step) shows a clear decrease with a decrease in porosity. The mean discharge voltage is influenced by both the (i) electrode resistance and the (ii) fraction of active mass that is electrochemically active. A lower mean discharge voltage means either or both (i) more resistive electronic and/or ionic wiring of the active mass; (ii) a lower fraction of active mass that is electrochemically active, with in the case of Si cycled with capacity limitations, a deeper extent of lithiation of the active mass to deliver the capacity, and as a consequence a lower discharge voltage. Thus the results in Fig. 10(b) confirm that calendaring has a detrimental effect of the composite electrode architecture efficiency with respect to its electrochemical behaviour.

A disappointing conclusion from the applied point of view is that to achieve long cycle life, Si-based composite electrodes must be highly porous (or the Si volume fraction must be kept low [58]) which results in low volumetric capacity. We can calculate for

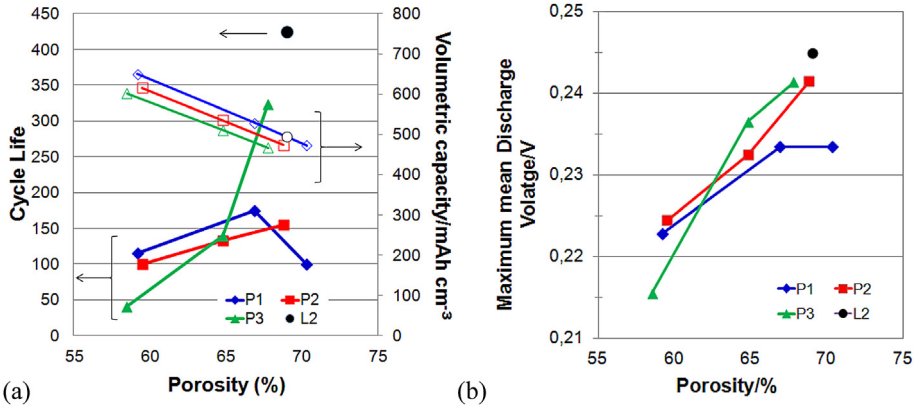

Fig. 10. (a) Cycle life and the calculated volumetric capacity of the electrodes for L2, P1, P2 and P3 as a function of the porosity. (b) Maximum value taken by the mean discharge voltage for L2, P1, P2 and P3 as a function of the porosity.

typical graphite-based electrodes with 30% porosity and 80 wt% graphite in the dried electrode composition (which gives a volume fraction of 60% for graphite), by considering a specific capacity of 350 mAh g^{-1}, that the volumetric capacity is 475 mAh per cm^3 of composite electrode. Here, higher values are achieved only if the Si-based composite electrodes are calendared down to 65% and less. However in such a case the cycle life of electrodes prepared at the pilot scale is decreased down to 150 cycles.

4. Conclusion

We have successfully designed the formulation of nano-silicon based negative composite electrodes with homogeneous morphology which could operate more than 400 cycles at 1200 mAh g^{-1} of Si limitation and a surface capacity is ~3.3 mAh cm^{-2} when prepared at the lab scale. In addition, the role of the PAMA dispersant has been investigated. This one could help not only to achieve high homogeneity of the electrode, especially uniform carbon black distribution prepared at the lab scale which leads to improvement of cyclability and coulombic efficiency in half cell, but also facilitate the powder incorporation at the pilot scale. However, the amount of PAMA was optimized at 1.7 wt% because a competitive adsorption occurs between PAMA and CMC versus the CB particles. At too high content (3.4 wt%) the adsorption of PAMA to the CB surface impedes the adsorption of the CMC chains and thus the formation of bridges between the CB particles and the Si mass which results in a catastrophic failure upon cycling. At the pilot scale, in order to wind cylindrical cells, the adhesion of the tape to the copper current collector needs to be improved by calendaring and adding the latex SB. Our electrochemical study of different electrode formulations prepared at pilot scale indicates that to achieve long cycle life, SB plays an important role while calendaring is detrimental to electrochemical behaviour. Long cycle life is only achieved for non-calendared electrodes with high SB loading which results in lower volumetric capacity than Graphite-based electrodes.

Acknowledgements

Financial support provided by the European Commission (EC), through the project EuroLiion (NMP3-SL-2010-265368) is gratefully acknowledged.

References

[1] T. Tran, J. Feikert, X. Song, K. Kinosbita, J. Electrochem. Soc. 142 (1995) 3297.
[2] M.N. Obrovac, L. Christensen, Electrochem. Solid State Lett. 7 (2004) A93.
[3] J.H. Ryu, J.W. Kim, Y.-E. Sung, S.M. Oh, Electrochem. Solid State Lett. 7 (2004) A306.
[4] L.Y. Beaulieu, K.W. Eberman, R.L. Turner, L.J. Krause, J.R. Dahn, Electrochem. Solid State Lett. 4 (2001) A137.
[5] C.C. Nguyen, S.W. Song, Electrochim. Acta 55 (2010) 3026.
[6] L. Baggetto, R. Niessen, P. Notten, Electrochim. Acta 54 (2009) 5937.
[7] M. Winter, Z. Phys. Chem. 223 (2009) 1395.
[8] A. Magasinski, B. Zdyrko, I. Kovalenko, B. Hertzberg, R. Burtovyy, C.F. Huebner, T.F. Fuller, I. Luzinov, G. Yushin, J. Appl. Mater. Interfaces 2 (2010) 3004.
[9] B. Lestriez, C.R. Chimie 13 (2010) 1341.
[10] N.S. Hochgatterer, M.R. Schweiger, S. Koller, P.R. Raimann, T. Wohrle, C. Wurm, M. Winter, Electrochem. Solid State Lett. 11 (2008) A76.
[11] W.R. Liu, M.H. Yang, H.C. Wu, S.M. Chiao, N.L. Wu, Electrochem. Solid State Lett. 8 (2005) A100.
[12] H. Buqa, M. Holzapfel, F. Krumeich, C. Veit, P. Novak, J. Power Sources 161 (2006) 617.
[13] J. Li, R.B. Lewis, J.R. Dahn, Electrochem. Solid State Lett. 10 (2007) A17.
[14] B. Lestriez, S. Bahri, I. Sandu, L. Roué, D. Guyomard, Electrochem. Commun. 9 (2007) 2801.
[15] I. Kovalenko, B. Zdyrko, A. Magasinski, B. Hertzberg, Z. Milicev, R. Burtovyy, I. Luzinov, G. Yushin, Science 334 (2011) 75.
[16] B. Koo, H. Kim, Y. Cho, K.T. Lee, N.-S. Choi, J. Cho, Angew. Chem. Int. Ed. 51 (2012) 8762.
[17] Z.-J. Han, N. Yabuuchi, K. Shimomura, M. Murase, H. Yui, S. Komaba, Energy Environ. Sci. 5 (2012) 9014.
[18] M.-H. Ryou, J. Kim, I. Lee, S. Kim, Y.K. Jeong, S. Hong, J.H. Ryu, T.-S. Kim, J.-K. Park, H. Lee, J.W. Choi, Adv. Mater. 25 (2013) 1571.
[19] M. Ulldemolins, F. Le Cras, B. Pecquenard, V.P. Phan, L. Martin, H. Martinez, J. Power Sources 206 (2012) 245.
[20] H. Nakai, T. Kubota, A. Kita, A. Kawashima, J. Electrochem. Soc. 158 (2011) A798.
[21] N.-S. Choi, K.H. Yew, K.Y. Lee, M.S. Sung, S.-S. Kim, J. Power Sources 161 (2006) 1254.
[22] N.-S. Choi, Y. Lee, S. Kim, S.-C. Shin, Y.-M. Kang, J. Power Sources 195 (2010) 2368.
[23] L. Chen, K. Wang, X. Xie, J. Xie, J. Power Sources 174 (2007) 538.
[24] R.R. Garsuch, D.-B. Le, A. Garsuch, J. Li, S. Wang, A. Farooq, J.R. Dahn, J. Electrochem. Soc. 155 (2008) A721.
[25] D. Mazouzi, N. Delpuech, Y. Oumellal, M. Gauthier, M. Cerbelaud, J. Gaubicher, N. Dupré, P. Moreau, D. Guyomard, L. Roué, B. Lestriez, J. Power Sources 220 (2012) 180.
[26] V. Etacheri, O. Haik, Y. Goffer, G.A. Roberts, I.C. Stefan, R. Fasching, D. Aurbach, Langmuir 28 (2012) 965.
[27] B. Lestriez, S. Desaever, J. Danet, P. Moreau, D. Plée, D. Guyomard, Electrochem. Solid State Lett. 12 (2009) A76.
[28] B.P.N. Nguyen, N.A. Kumar, J. Gaubicher, F. Duclairoir, T. Brousse, O. Crosnier, L. Dubois, G. Bidan, D. Guyomard, B. Lestriez, Adv. Energy Mater. 3 (2013) 1351.
[29] B.P.N. Nguyen, J. Gaubicher, B. Lestriez, http://dx.doi.org/10.1016/j.electacta.2013.12.126.
[30] D. Mazouzi, B. Lestriez, L. Roué, D. Guyomard, Electrochem. Solid State Lett. 12 (2009) A215.
[31] M. Cerbelaud, B. Lestriez, D. Guyomard, A. Videcoq, R. Ferrando, Langmuir 28 (2012) 10713.
[32] C.C. Li, X. Peng, J. Lee, F. Wang, J. Electrochem. Soc. 157 (2010) A517.
[33] C.C. Li, Y. Wang, T. Yang, J. Electrochem. Soc. 158 (2011) A828.
[34] J. Li, B. Armstrong, J. Kiggans, C. Daniel, D. Wood, Langmuir 28 (2012) 3783.
[35] W. Porcher, B. Lestriez, S. Jouanneau, D. Guyomard, J. Power Sources 195 (2010) 2835.
[36] C.-C. Chang, L.-J. Her, H.-K. Su, S.-H. Hsu, Y. Te Yen, J. Electrochem. Soc. 158 (2011) A481.
[37] C.C. Li, J. Lee, C. Lo, M. Wu, Electrochem. Solid State Lett. 8 (2005) A509.
[38] C.C. Li, J. Lee, X. Peng, J. Electrochem. Soc. 153 (2006) A809.
[39] T.J. Patey, A. Hintennach, F. La Mantia, P. Novák, J. Power Sources 189 (2009) 590.
[40] W.B. Russel, D.A. Saville, W.R. Schowalter, Colloidal Dispersions, second ed., Cambridge University Press, Cambridge, 1991.
[41] R. Hunter, Foundations of Colloid Science, vol. I, Clarendon Press, Oxford, 1992.
[42] J. Israelachvili, Intermolecular and Surface Forces, third ed., Academic Press, London, 1997.
[43] J.-H. Lee, U. Paik, V.A. Hackley, Y.-M. Choi, J. Electrochem. Soc. 152 (2005) A1763.
[44] M. Pawlik, Colloids Surf. A 266 (2005) 82.
[45] T. Ueno, S. Yokota, T. Kitaoka, H. Wariishi, Carbohydr. Res. 342 (2007) 2593.
[46] R.A. Jones, R.W. Richards, Polymers at Surfaces and Interfaces, Cambridge University Press, New York, 1999.
[47] M.N. Obrovac, L.J. Krause, J. Electrochem. Soc. 154 (2007) A103.
[48] Y. Oumellal, N. Delpuech, D. Mazouzi, N. Dupré, J. Gaubicher, P. Moreau, P. Soudan, B. Lestriez, D. Guyomard, J. Mater. Chem. 21 (2011) 6201.
[49] N. Delpuech, N. Dupré, D. Mazouzi, J. Gaubicher, P. Moreau, J.S. Bridel, D. Guyomard, B. Lestriez, Electrochem. Commun. 33 (2013) 72.
[50] W. Porcher, B. Lestriez, S. Jouanneau, D. Guyomard, J. Electrochem. Soc. 156 (2009) A133.
[51] J.H. Lee, U. Paik, V.A. Hackley, Y.M. Choi, J. Electrochem. Soc. 152 (2005) 1763.
[52] J.H. Lee, S. Lee, U. Paik, Y.M. Choi, J. Power Sources 147 (2005) 249.
[53] A. Guerfi, M. Kaneko, M. Petitclerc, M. Mori, K. Zaghib, J. Power Sources 163 (2007) 1047.
[54] C.-C. Li, Y.-S. Lin, J. Power Sources 220 (2012) 413.
[55] C.-C. Li, Y.-W. Wang, J. Electrochem. Soc. 158 (2011) A1361.
[56] S. Lim, K.H. Ahn, M. Yamamura, Langmuir 29 (2013) 8233.
[57] D. Reyter, S. Rousselot, D. Mazouzi, M. Gauthier, P. Moreau, B. Lestriez, D. Guyomard, L. Roué, J. Power Sources 239 (2013) 308.
[58] S.D. Beattie, D. Larcher, M. Morcrette, B. Simon, J.-M. Tarascon, J. Electrochem. Soc. 155 (2008) A158.

Paper II

“Nanosilicon-Based Thick Negative Composite Electrodes for Lithium Batteries with Graphene as Conductive Additive”

ADVANCED ENERGY MATERIALS
www.advenergymat.de

Nanosilicon-Based Thick Negative Composite Electrodes for Lithium Batteries with Graphene as Conductive Additive

*Binh Phuong Nhan Nguyen, Nanjundan Ashok Kumar, Joël Gaubicher, Florence Duclairoir, Thierry Brousse, Olivier Crosnier, Lionel Dubois, Gérard Bidan, Dominique Guyomard, and Bernard Lestriez**

Reduced graphene oxide (rGO) is used as a conductive additive for nanosilicon-based lithium battery anodes with the high active-mass loading typically required for industrial applications. In contrast to conventional Si electrodes that use acetylene black (AcB) as an additive, the rGO system shows pronounced improvement of electrochemical performance, irrespective of the cycling conditions. With capacity limitation, the rGO system results in improved coulombic efficiency (99.9%) and longer cycle life than conventional electrodes. Upon cycling without capacity limitation, much higher discharge capacity is maintained (2000 mAh g^{-1} after 100 cycles for 2.5 mg of Si cm^{-2}). Used in conjunction with the bridging carboxymethyl cellulose binder, the crumpled and resilient rGO allows highly reversible functioning of the electrode in which the Si particles repeatedly inflate and deflate upon alloying and dealloying with lithium.

1. Introduction

The recent cost escalation of petroleum fuel and increased concern over pollution from combustible power sources has turned the attention of researchers towards cleaner and better electrochemical energy systems.[1] Among these systems, lithium-ion batteries (LIB) show promise of meeting both energy and power requirements and hence are considered prime candidates for hybrid-electric-vehicle (HEV) and electric-vehicle (EV) applications.[2] Existing lithium-ion batteries rely on anodes made from graphitic carbon that, at full lithiation, offer a theoretical capacity nearing 372 mAh g^{-1}, which is unable to meet the colossal energy requirements. In the search for high-capacity anode materials, silicon-based anodes have received attention as they theoretically offer as much as a tenfold capacity improvement over graphite (3579 mAh g^{-1}) along with a low discharge potential and natural abundance.[3] Although substituting silicon (Si) for graphite and the subsequent gain of higher capacity have been explored previously, these anodes have so far not been stable enough for practical use since they exhibit large volume changes (ca. 328%) during Li insertion and extraction; these lead to internal cracks and result in loss of electrical contact and increased impedance, which results in short cycle life. Similar arguments hold true for other types of anodes, namely, tin-based anodes.

Various efforts have been made to circumvent this stability problem to enhance the electrochemical performance of Si-based anode materials. Among such efforts, miniaturization and control of morphology of the Si particles are known to effectively improve cycling stability and rate capability, for example, silicon nanocrystal and nanowire architectures can withstand volume changes.[3a] Another simple approach is dispersion of the Si particles in carbon matrix to form a carbon coating[4] that can act as a stress-buffer during volume expansions, which will improve the electronic and ionic conductivities and also the stability of the anodes. Recent studies reveal that the rapid fading of capacity is limited or prevented to a large extent by modifying Si anodes with carbon,[5] or by constructing other types of electrode architectures based on Si and carbon coating on the nanoscale, which have been explored in great detail.[6] Long-term stability of such anodes, however, depends on additional components in the battery that include electrically conducting additives, binder, and electrolyte.[7]

With the aim of further advancing the anode performance and stability, two-dimensional (2D) graphene could be used as a conductive matrix as, in this, it is superior to other carbon materials, namely zero or 1D ones. In addition, graphene with its heavily crumpled nature is a good absorber for accommodating the Si volume change, and is also electrically conductive,

B. P. N. Nguyen,[†] Prof. J. Gaubicher, Prof. T. Brousse, Prof. O. Crosnier, Prof. D. Guyomard, Prof. B. Lestriez
Institut des Matériaux Jean Rouxel (IMN)
Université de Nantes
CNRS, 2, rue de la Houssinière–B.P. 32229 - 44322
Nantes cedex 3, France
E-mail: bernard.lestriez@cnrs-imn.fr

Dr. N. A. Kumar,[†] Dr. F. Duclairoir, Dr. L. Dubois, Dr. G. Bidan
Laboratoire de Chimie Inorganique et Biologique
UMR-E CEA-UJF
Institute for Nanoscience and Cryogenics Commissariat à l'énergie atomique (CEA)
17 rue des martyrs, 38054, Grenoble, cedex 9, France

Prof. J. Gaubicher, Prof. T. Brousse, Prof. D. Guyomard, Prof. B. Lestriez
Réseau sur le Stockage Electrochimique de l'Energie (RS2E)
FR CNRS 3459, France

[†]These authors contributed equally to this work

DOI: 10.1002/aenm.201300330

facilitating charge-transfer reactions. Interestingly, graphene oxide (GO) and reduced GO (rGO) based composites have been used as LIB hosts for a variety of metal oxide nanocrystals, which in most cases showed pronounced capacity increase along with stability.[8] Furthermore, graphene can be produced in significant quantities by various reduction techniques from exfoliated GO.[9] In short, using graphene as a conductive additive in battery anodes is an interesting approach, not only because of its high electrical conductivity and chemical stability, but also because its large surface area could facilitate in storing/adsorbing more Li into its ubiquitous cavities than graphite. Such studies have rarely been reported in the past.[10]

In contrast to prior work on mixing silicon/graphene as composites,[11] herein, we report the preparation and performance of rGO as a conductive additive for nanosilicon-based LIB anodes and identify the important parameters that govern the performance. In addition, cycling stability along with cell performance was scrutinized and it was found that using rGO can greatly enhance the cycling stability of the electrodes at full capacity due to the crumpled nature of the rGO which preserves and maintains the percolations in the anode structure. In addition, with no capacity limitation, significantly better coulombic efficiency was observed when rGO was used rather than acetylene black (AcB).

2. Results and Discussion

Composite electrodes were prepared from Si nanoparticles of typically 100 nm diameter, different conductive additives, and carboxymethyl cellulose (CMC) as the binder in a pH 3 buffered aqueous solution. The structural morphologies of the electrodes were observed by using scanning electron microscopy (SEM) as in **Figure 1**. The nanoparticles of Si have 100–200 nm diameters and form small aggregates of a few particles. In the AcB-based electrodes, aggregates of Si nanoparticles and aggregates of AcB coexist and are point-contacted. In the GO and rGO-based electrodes, graphene sheets are dispersed among Si aggregates, which thereby leads to partial wrapping of the nanoparticles by the carbon additives (Figure 1b,c, Figure S3).

The dry electronic resistance of the composite electrode/current collector bilayer was measured with two stainless-steel probes sandwiching the sample with a small pressure applied, typical of the Swagelok™ cells used to evaluate the battery performance. The electronic resistance of the rGO-based electrodes was always higher than of the AcB-based ones, 90–175 vs. 25 Ω respectively. We attribute this result to the lamellar-like morphology of the rGO-based electrodes, where resistive layers of Si nanoparticles limit the current flow in the dry state.

The electrochemical performance of the electrodes was evaluated by galvanostatic charge/discharge cycling of the cells using the commercial LP30 liquid electrolyte, modified with vinylene carbonate (VC) and fluoroethylene carbonate (FEC) additives. When cycling was performed with no capacity limitation, the rGO-based electrode displayed a much better cycling behavior than the AcB-based one, with discharge capacity of more than 2000 mAh g^{-1} maintained after 100 cycles, compared to less than 1000 mAh g^{-1}, respectively (**Figure 2**a). As far as we know, this is the best result ever reported for nano-Si-based composite electrodes taking into consideration that the active-mass loading is nearly 2.5 mg of Si cm^{-2}. In other words, a surface capacity of 5 mAh cm^{-2} is maintained after 100 cycles. After 200 cycles, the discharge capacity retained is still 1500 mAh g^{-1} (3.75 mAh cm^{-2}). The GO-based electrode performs poorer than the rGO one, and similarly to the AcB one. The potential vs. composition curves, $V(x)$ vs. x in Li_xSi (Figure 2b–d), show that the capacity is not limited by a polarization process whatever the conducting additive is, as the potential is well above the 10 mV cut-off even at the end of the material's lithiation. With an increasing number of cycles, the mean number of inserted lithium x decreases while the electrode polarization (difference between the charge and discharge potentials) increases. However, the former phenomenon (decrease in capacity) cannot be ascribed to the latter one (increase of the polarization). This observation suggests that the capacity fade is due to the loss of active mass through disconnection of the particles and that rGO plays a more efficient role than AcB or GO in maintaining the electrical contacts within the composite electrode. We note that the cycling behavior of all three types of electrodes is characterized by repeated decrease, followed by sharp jumps in capacity (see the first 100 cycles in Figure 2a). Such original behavior has never been reported, and was not observed for thin electrodes made from AcB with active mass loadings typically lower than or equal to 1 mg of Si cm^{-2} and cycled in the same conditions to those reported here. The amplitude of this effect is however, less pronounced for rGO-based electrodes.

The typical evolution of incremental capacity curves is reported in **Figure 3**. The electroactivity of Si is characterized by two major steps, A and B (Figure 3c,d), which have been ascribed to Li reactions with amorphous Si.[12] Li_xSi alloys formed in step B are lithium-rich compared to those in step A. More precisely, the B peak can be attributed to the compositional equilibrium (biphasic process) $Li_{15}Si_4/Li_2Si$ and the A peak to the transformation of the Li_2Si/amorphous Si (via a solid solution).[13] Figure 3 clearly shows that the loss of capacity between two consecutive jumps is associated with both a preferential decrease of step B vs. A and a clear increase of its polarization. Interestingly, just after the jump of capacity, the initial capacity and polarization of step B are almost fully recovered, which implies that some reversible modification of the electrodes took place. Looking at the capacity jumps for AcB by using the $V(x)$ representation (Figure 3d) confirms that this modification arises through a large recovery of step B. After

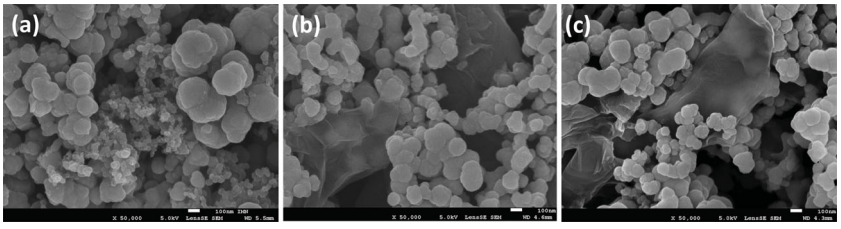

Figure 1. SEM images of Si-based composite electrodes using graphene as a conductive additive a) AcB, b) GO, and c) rGO.

Adv. Energy Mater. **2013**,
DOI: 10.1002/aenm.201300330

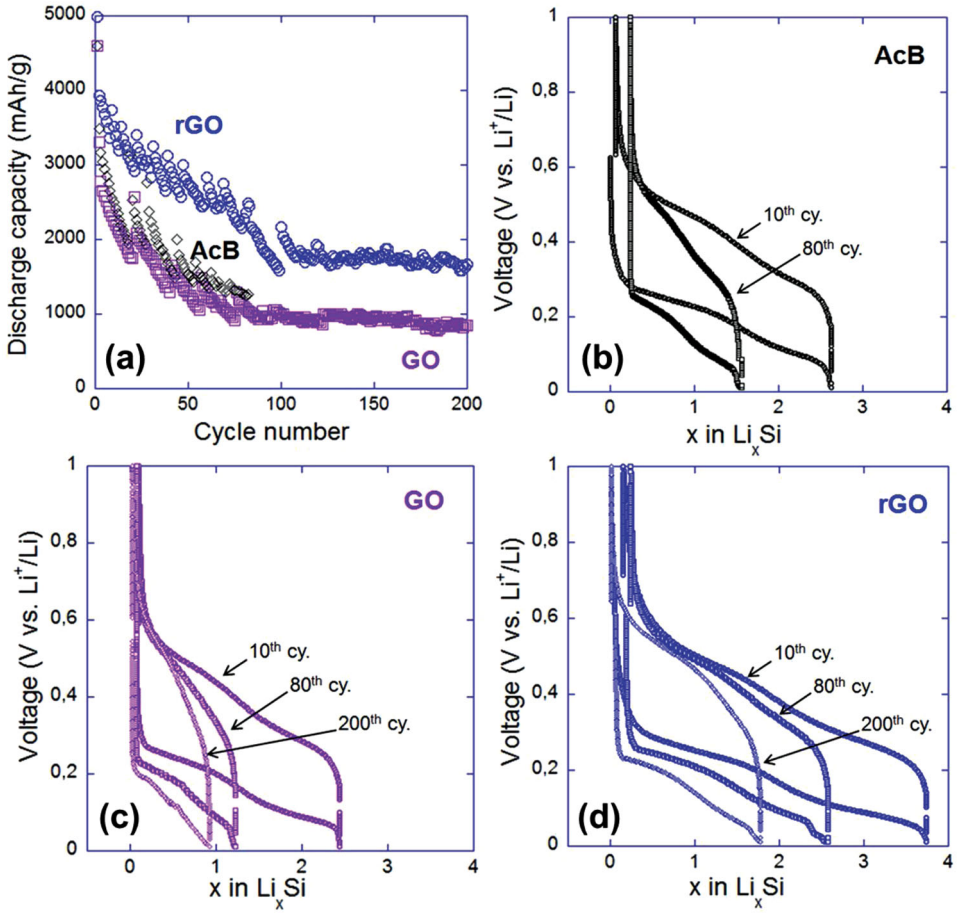

Figure 2. a) Discharge capacity of Si vs. number of cycles for the different electrodes. Corresponding voltage vs. composition curves: b) AcB-based, c) GO-based, and d) rGO-based electrodes.

reaching a threshold of 15 mV vs. Li^0, the potential increases back up to 50 mV, as for a nucleation and growth process, before the capacity is recovered by discharging down to 10 mV. In contrast to step B, Figure 3a–c show that the amplitude of step A is barely modified, which demonstrates that Si grains of the three types of electrodes remain connected to the electrical circuit during this process.

Although pinning down physical phenomenon underneath these capacity jumps requires more characterization, it can be highlighted that step B is associated with larger volume variations of Si grains than step A. The volume increase of step A is twofold for the Li_2Si composition compared to 3.7 for step A for $Li_{15}Si_4$.[14] Noteably, it has been reported that the electrode porosity acts as a buffer against the Si particles' expansion up to the Li_2Si composition (corresponding to step A), a limit beyond which this buffering effect stops.[15] Beyond this limit (corresponding to step B), the internal organization of the electrode has to adapt in response to the particles' swelling and displacement. Here, we postulate that beyond this limit it occurs either a loss of particle contact and reversibility because of definitive breaking of the Si–AcB contacts,[16] or a preservation of the network thanks to shape and flexibility of the rGO sheets herein. Therefore one plausible hypothesis would be that a reversible disconnection of active grains takes place during step B. Such a process would be less pronounced for the rGO sample owing to the platelet shape of graphene sheets. Although the GO-based electrode displays the same texture as the rGO one, it displays the same fading as the AcB-based electrode. More or less the same mechanical properties are expected for GO- and rGO-based electrodes as both fillers have the same shape and flexibility. However, GO has lower intrinsic electronic conductivity due to extensive sp^3 hybridization of carbon atoms. Although mechanical contacts must be preserved thanks to the platelet shape of GO, this filler has poorer ability than rGO to supply electrons to the Si particles.

We can note that a self-healing process of the Si–CMC hydrogen bonding, which can accommodate textural stresses and can evolve during cycling, has been hypothesized to be critical for Si-based electrode performances.[17] Our results support and illustrate this quite new picture of a breathing composite electrode due to the repetition of the Si particles' inflating and deflating upon alloying and dealloying with lithium, rolling on the rGO sheets but sticking to them by the adsorbed or grafted CMC bridging polymeric chains (**Figure 4**).[18] Comparatively, this self-healing effect would be harder to observe with AcB as Si nanoparticles and AcB have only point contacts, which can

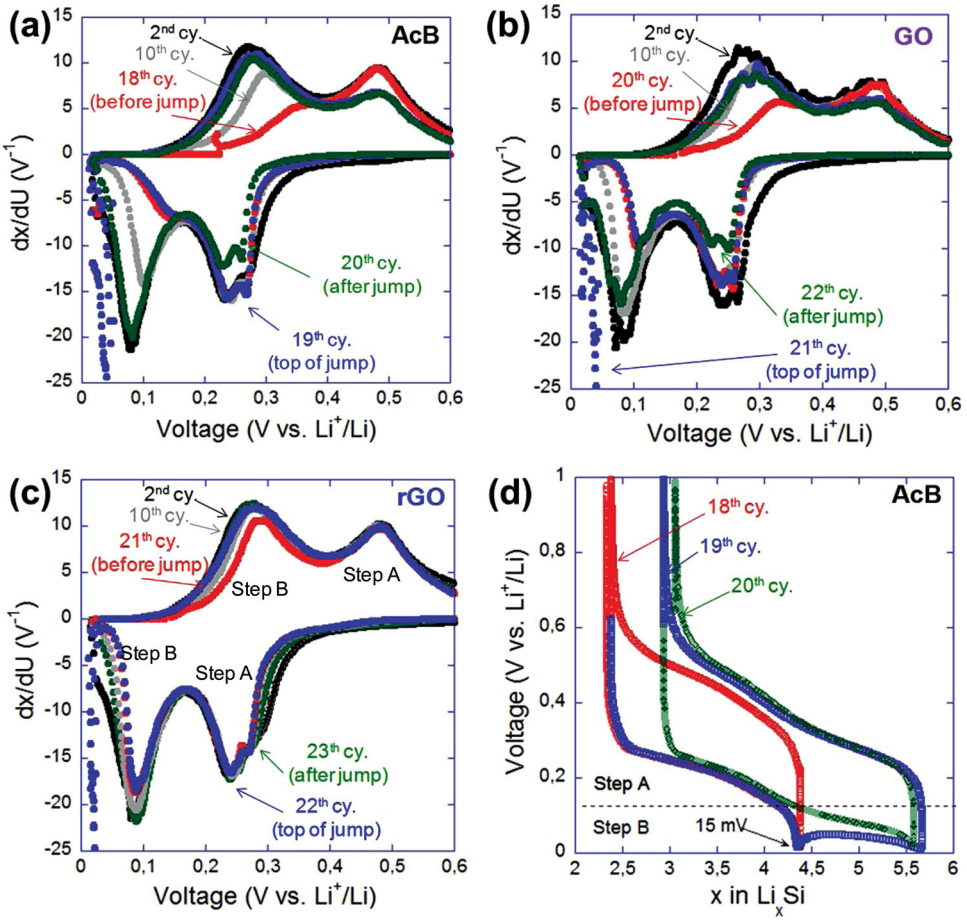

Figure 3. Incremental capacity curves at selected cycles: a) AcB-, b) GO-, and c) rGO-based electrodes. d) Voltage vs. composition curve showing capacity recovery after first jump for AcB-based electrodes.

be more easily disconnected because CMC can less easily stick to small surfaces and play the role of a bridging spring between the two components (Figure 4).

Figure 5 compares the incremental capacity curves for selected cycles systematically after the capacity jump. One can note that the capacity difference between AcB- and rGO-based electrodes is homogeneously distributed over the two lithiation steps. This observation confirms that the capacity difference is due to a difference in the quantity of active Si mass wired to the current collector. rGO favors a better functioning of the electrode than does GO, as the rGO sheets can better withstand the volume variations from Li–Si alloying and dealloying processes, supply electrons for the Si nanoparticles, and maintain an integrated structure. This conclusion is in-line with recent electrochemical impedance spectroscopy measurements[11a] and other works.[6c,e]

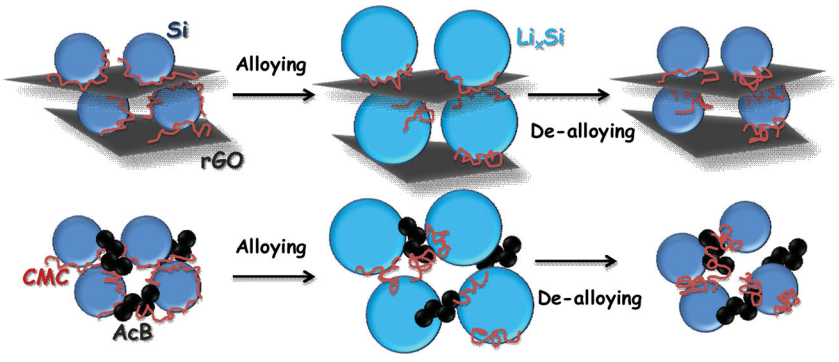

Figure 4. Schematic of lithium insertion and deinsertion in silicon electrodes with CMC binder and different conductive additives, rGO, or AcB. The Si particles are bound to the flexible rGO platelets through the soft and dynamic CMC bridges, which allows and excellent reversibility of the alloying process in the Si–rGO–CMC electrode.

In the second part of the study the electrodes were cycled with capacity limitations of 1200 mAh g^{-1} of Si, meaning that the discharge is stopped at the theoretical composition $Li_{1.2}Si$. In this condition, the favored source of fading is not mechanical disintegration of the composite electrode but liquid electrolyte degradation.[19] In this case, a relationship between the cycle life and the extent of electrolyte degradation, as measured by the coulombic efficiency (CE) or the mean irreversible loss per cycle, is found: the higher the extent of electrolyte degradation,

Adv. Energy Mater. 2013,
DOI: 10.1002/aenm.201300330

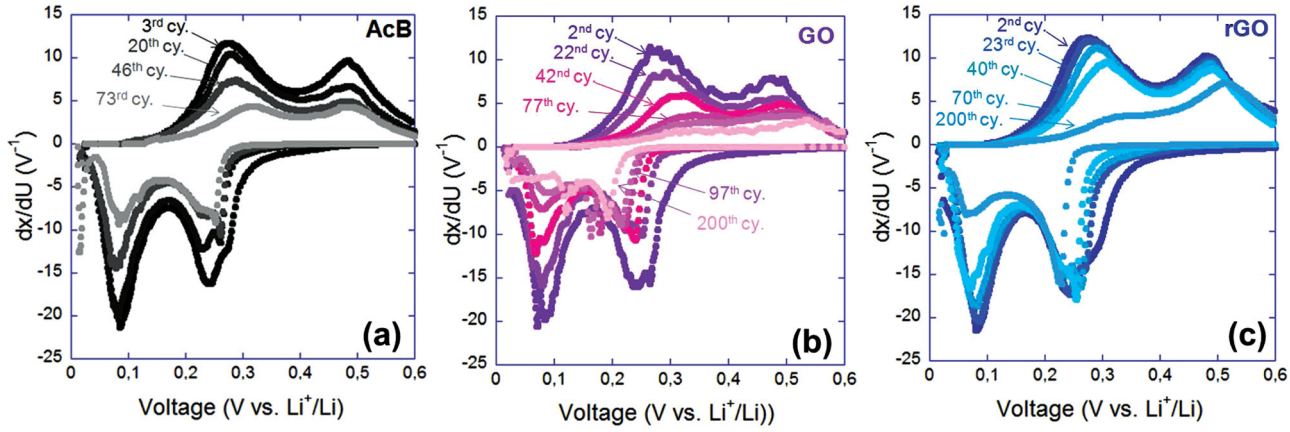

Figure 5. Incremental capacity curves at selected cycles (after jumps): a) AcB-based, b) GO-based, and c) rGO-based electrodes.

the poorer the CE and the lower the cycle life.[20] The grafting of the CMC binder at the Si surface, or the use of liquid electrolyte additives such as FEC and VC, result in less electrolyte decomposition, higher CE, and longer cycle life. For the electrodes that meet these criteria, we have shown that end of life is mainly controlled by the adhesion toward the current collector.[21]

Here, we compare the electrodes prepared with either pristine GO or rGO to the reference containing AcB. **Figure 6** shows typical cycling curves and **Table 1** presents for all electrodes the cycle life, first-cycle irreversible loss, and the coulombic efficiency over the first 100 cycles. Mean values are given for AcB (the number of batteries cycled was six), while for GO and rGO each value of the two sister electrodes is reported. The data in Figure 6 are intentionally not reproduced after the 100th cycle as the charge capacity starts overpassing the discharge capacity, a phenomenon which can be attributed to the formation of temporary microdendrites popping up from the lithium metal counter-electrode. This phenomenon is observed particularly for thick Si electrodes, as herein, with the FEC-VC additives cycled with a capacity limitation.

The following trends can be observed from the results: With GO, a lower cycle life than with AcB is observed. A much higher first-cycle irreversible loss results likely from some in situ electrochemical reduction of GO. The batteries cycled with rGO as a conductive additive show significantly improved electrochemical performance with longer cycle life and improved coulombic efficiencies of 99.3% and 99.9%, compared to a maximum of 99% for AcB. As far as we know, such a coulombic efficiency of 99.9% has never been reported for Si-based electrodes with high active-mass loading and high Si content in the composite electrode formulation. Figure 6 shows the discharge capacity vs. cycle number for an AcB, a GO, and an rGO battery, as well as the variation of their mean discharge voltage and their coulombic efficiency over the first 100 cycles.

Table 1. Cycle life, first-cycle irreversible loss, and mean coulombic efficiency from the second to the 100th cycle.

Conductive additive	Cycle life	First-cycle irreversible loss [mAh g^{-1}]	Coulombic efficiency [%]
AcB	370 (+/–45)	413 (+/–54)	98.4 (+/–0.6)
GO	200 and 250	665 and 680	98.5 and 98.7
rGO	410 and 530	535 and 580	99.3 and 99.9

One can note the higher and more stable value of the mean discharge voltage of the rGO-based electrode compared to the others, which is in agreement with a higher coulombic efficiency.[20] In complement, **Figure 7** allows the comparison of the potential vs. composition curves, $V(x)$ vs. x, and of the incremental capacity curves $dx/dV(x)$ vs. $V(x)$ for the different conductive additives at the 10th and 80th cycles. A better reversibility is observed for rGO than for AcB.

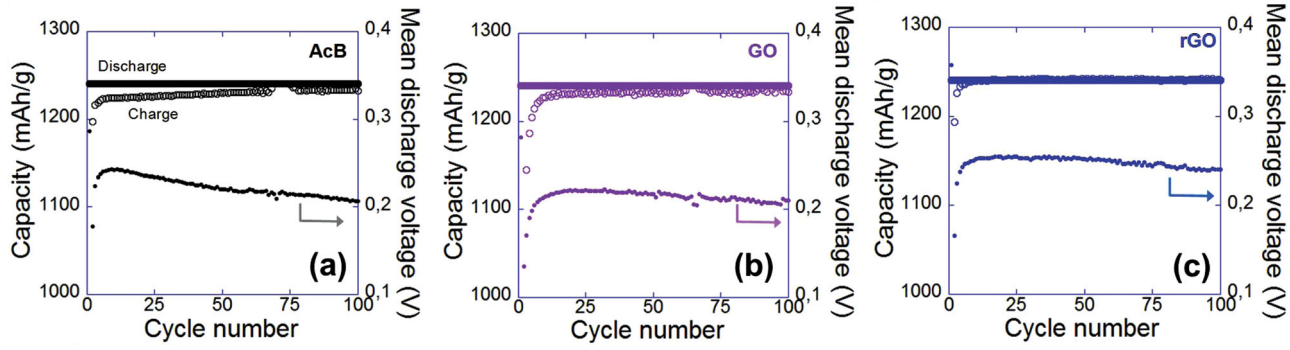

Figure 6. Discharge capacity vs. cycle number for a) AcB, b) GO, and c) rGO batteries as well as the variation of their mean discharge voltage.

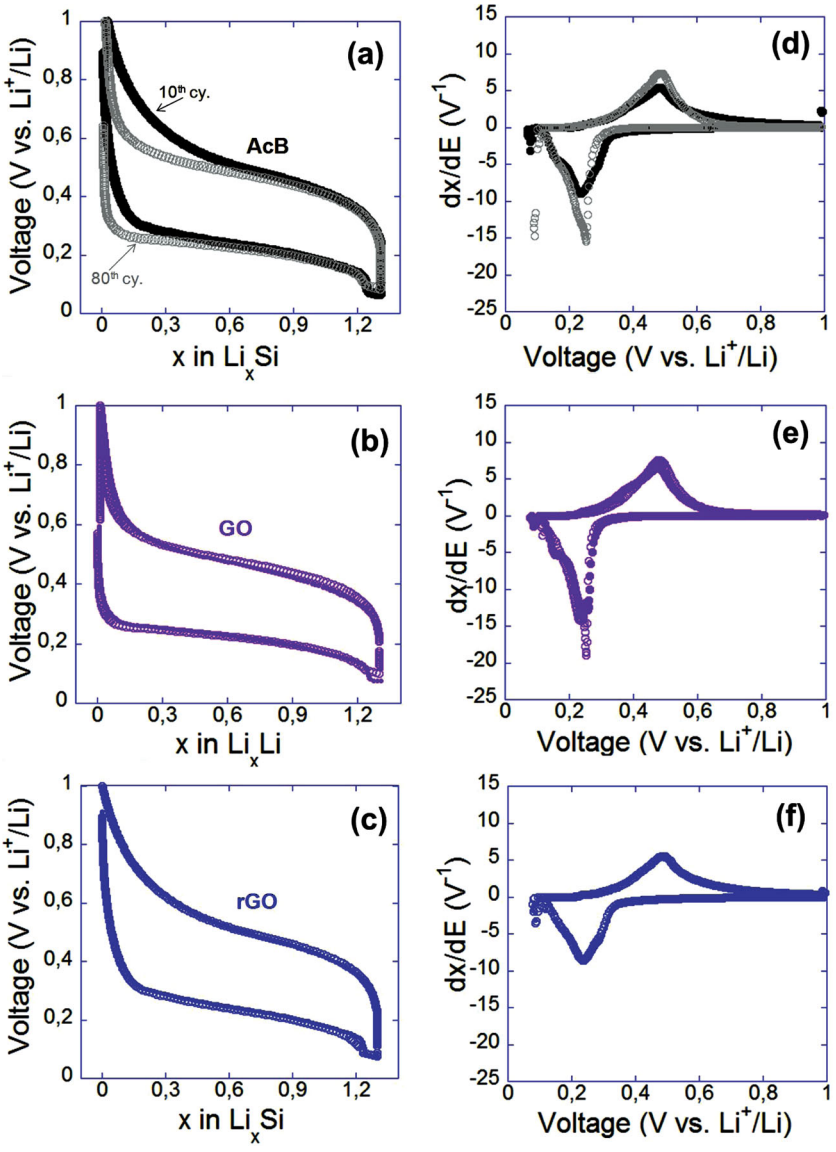

Figure 7. Potential vs. composition curves, $V(x)$ vs. x, and incremental capacity curves $dx/dV(x)$ vs. $V(x)$ for the different conductive additives at the 10th (●) and 100th (○) cycles. a,d) AcB, b,e) GO, c,f) rGO.

For better understanding, one needs to recall in detail the failure mechanism of nano-Si-based electrodes cycled with capacity limitations.[20] The liquid electrolyte degradation occurs at low potential through reduction at the surface of the active particles. In the well-known case of graphite,[22] the degradation products precipitate at the surface of the active particles forming a stable electronically insulating but ionically conducting layer called SEI (solid electrolyte interphase) which allows Li^+ ions to transfer through it but prevents further reduction of the liquid electrolyte on successive cycles. In the case of silicon, the layer built in the first cycles is unstable unless FEC/VC additives are used and the volume variations occurring upon Li insertion of the particles produce cracks in this SEI layer[23] exposing new surfaces which result in additional liquid electrolyte degradation. The insoluble liquid electrolyte degradation products precipitate in the composite electrode pores, obtruding the pores and causing loss of active material due to ionic or electronic insulation. The results obtained in this study show that using rGO improves the coulombic efficiency, i.e., reduces the liquid electrolyte degradation. It can simply be assumed that the wrapping of the Si nanoparticles by the rGO may prevent the former surfaces from contacting the liquid electrolyte and thus reduces its degradation. Here, only parts of the Si nanoparticles were wrapped by the rGO sheets. We may assume that better performance could be achieved by increasing the rGO content.

3. Conclusion

Using reduced graphene oxide (rGO) instead of the standard acetylene black (AcB) as the conductive additive for nanosilicon-based negative composite electrodes allows a significant improvement of the electrochemical performance, whatever the cycling conditions. When the cycling is done at full capacity, rGO allows a much higher capacity over hundreds of cycles. In the situation where the Si particles show strong volume variations and displacements within the composite electrode, this result can be attributed to a much better ability of rGO to maintain the electronic percolation and supply electrons to the moving active mass. When the cycling is done with capacity limitation, in the situation where the main cause of fading is the liquid electrolyte degradation, rGO also improves the cycling behavior, with an increased coulombic efficiency, which results in a longer cycle life. The improvement could be attributed to the wrapping of the Si particles by the rGO sheets, which likely decreases the contact surface area between Si and the liquid electrolyte, and minimizes the degradation of the latter. These results, which were achieved for nano-Si-based composite electrodes with much higher active-mass loading than usually studied in academic studies but which are of clear interest from the practical industrial point of view, show that rGO has significant advantages compared to the standard carbon black as a conductive additive for improving battery cycle life. This conclusion is particularly true for negatively active materials that show volume variations and/or for active materials plagued with low coulombic efficiency.

4. Experimental Section

Material Synthesis: Graphene oxide (GO) was prepared from flaky graphite by a modified Hummers and Offemans method as reported previously.[24] Reduced graphene oxide (rGO) was obtained using hydrazine hydrate as a reductant.[9b] As-prepared GO and rGO samples

DOI: 10.1002/aenm.201300330

were formulated with nanosized silicon by ball-milling and were used as electrodes as described below (see Supporting Information for detailed experimental procedures for GO and rGO synthesis).

Electrode Preparation: Composite electrodes were made of 78 wt% commercially available nanometric Si as an active material (AM), with 12 wt% of rGO, GO, or acetylene black (AcB) as a conductive additive, 8 wt% of carboxymethyl cellulose (CMC, DS = 0.9, M_w = 700.000 Sigma-Aldrich) as a binder, and 2 wt% of a dispersant. First, rGO and nanosized silicon particles were homogeneously mixed in ethanol solution followed by drying the sample for 1 h at 100 °C in the oven to remove the solvent. The dispersant CMC was predissolved in buffer solution (0.1 M, pH = 3) prepared with KOH and citric acid by using a roller tank overnight. A measured amount of this mixture and corresponding mass of silicon and graphene with a solid loading of about 17 wt% were introduced in a silicon nitride vial, according to the electrode formulation. Three silicon nitride balls served to mix the components. A Fritsch Pulverisette 7 mixer was used to mill slurry at 500 rpm for 1 h. Before ball-milling, all constituents were hand-mixed to achieve homogenous color. The slurry was tape-cast directly after ball-milling by using an automatic doctor blade onto 25-µm-thick copper foil in the tape-casting machine. The gap between the blade and the current collector was fixed to reach an active-mass loading of 2.5 mg of Si cm^{-2}, whatever the conductive additive. Drying was primarily done at room temperature for a night and then for 2 h at 100 °C under vacuum before battery assembly to remove the remaining water. The as-prepared electrode samples were analyzed for morphological changes using field-emission scanning electron microscopy (FE-SEM).

Electrochemical Testing: Half-cell tests were conducted using a two electrode Swagelok™ cell assembled in an argon-filled glove box with Li metal discs (0.785 cm^2) as the negative and reference electrode. A porous glass paper used as a separator was soaked in LP30 electrolyte consisting of 88 wt% LP30 [$LiPF_6$–EC/DMC] 1 M electrolyte with 2 wt% vinylene carbonate and 10 wt% fluoroethylene carbonate mixture provided by Novolyte. Electrochemical experiments were performed at 20 °C by galvanostatic charge/discharge cycling of the cells in the range of 0.01 to 1 V vs. Li^+/Li, monitored by a VMP™ system (Biologic). All composite electrodes were studied at the same rate (C/5 and D/5) with a limited discharge capacity of 1000 mAh g^{-1} for each electrode. Here, a C/5 rate refers to a discharge in 5 h.

Supporting Information

Supporting Information is available from the Wiley Online Library or from the author.

Acknowledgements

Financial support provided by *the Agence Nationale de la Recherche (ANR)*, France through the project *Graph'N'Stock* and by the *European Commission (EC)*, through the project EuroLion are gratefully acknowledged. The authors thank Eric Prestat for his assistance with TEM microscopy (Supporting Information). NAK wishes to thank the CEA-Eurotalents program for the postdoctoral fellowship and special thanks to Dr. Pascale Maldivi, at the INAC, CEA Grenoble, for her continued support and encouragement.

Received: March 21, 2013
Published online:

[1] L. Dai, D. W. Chang, J.-B. Baek, W. Lu, *Small* **2012**, *8*, 1130.
[2] a) B. Dunn, H. Kamath, J. M. Tarascon, *Science* **2011**, *334*, 928; b) A. Manthiram, *J. Phys. Chem. Lett.* **2011**, *2*, 176; c) R. Marom, S. F. Amalraj, N. Leifer, D. Jacob, D. Aurbach, *J. Mater. Chem.* **2011**, *21*, 9938; d) J.-M. Tarascon, *Phil. Trans. Royal Soc. A* **2010**, *368*, 3227.
[3] a) C. K. Chan, H. Peng, G. Liu, K. McIlwrath, X. F. Zhang, R. A. Huggins, Y. Cui, *Nat. Nanotechnol.* **2008**, *3*, 31; b) A. Magasinski, P. Dixon, B. Hertzberg, A. Kvit, J. Ayala, G. Yushin, *Nat. Mater.* **2010**, *9*, 353.
[4] J. Saint, M. Morcrette, D. Larcher, L. Laffont, S. Beattie, J. P. Pérès, D. Talaga, M. Couzi, J. M. Tarascon, *Adv. Funct. Mater.* **2007**, *17*, 1765.
[5] a) C. Martin, M. Alias, F. Christien, O. Crosnier, D. Bélanger, T. Brousse, *Adv. Mater.* **2009**, *21*, 4735; b) C. Martin, O. Crosnier, R. Retoux, D. Bélanger, D. M. Schleich, T. Brousse, *Adv. Funct. Mater.* **2011**, *21*, 3524.
[6] a) R. Mukherjee, R. Krishnan, T.-M. Lu, N. Koratkar, *Nano Energy* **2012**, *1*, 518; b) J. R. Szczech, S. Jin, *Energy and Environ. Sci.* **2011**, *4*, 56; c) K. Evanoff, A. Magasinski, J. Yang, G. Yushin, *Adv. Energy Mater.* **2011**, *1*, 495; d) X. Zhao, C. M. Hayner, M. C. Kung, H. H. Kung, *Adv. Energy Mater.* **2011**, *1*, 1079; e) X. Zhou, Y.-X. Yin, L.-J. Wan, Y.-G. Guo, *Adv. Energy Mater.* **2012**, *2*, 1086.
[7] N. Yabuuchi, K. Shimomura, Y. Shimbe, T. Ozeki, J.-Y. Son, H. Oji, Y. Katayama, T. Miura, S. Komaba, *Adv. Energy Mater.* **2011**, *1*, 759.
[8] Z.-S. Wu, G. Zhou, L.-C. Yin, W. Ren, F. Li, H.-M. Cheng, *Nano Energy* **2012**, *1*, 107.
[9] a) N. A. Kumar, H. Nolan, N. McEvoy, E. Rezvani, R. L. Doyle, M. E. G. Lyons, G. S. Duesberg, *J. Mater. Chem. A* **2013**; *1*, 4431; b) N. A. Kumar, S. Gambarelli, F. Duclairoir, G. Bidan, L. Dubois, *J. Mater. Chem. A* **2013**, *1*, 2789.
[10] a) A. Abouimrane, O. C. Compton, K. Amine, S. T. Nguyen, *J. Phys. Chem. C* **2010**, *114*, 12800; b) A. M. Chockla, M. G. Panthani, V. C. Holmberg, C. M. Hessel, D. K. Reid, T. D. Bogart, J. T. Harris, C. B. Mullins, B. A. Korgel, *J. Phys. Chem. C* **2012**, *116*, 11917; c) N. Zhu, W. Liu, M. Xue, Z. Xie, D. Zhao, M. Zhang, J. Chen, T. Cao, *Electrochimica Acta* **2010**, *55*, 5813; d) W. Guo, Y.-X. Yin, S. Xin, Y.-G. Guo, L.-J. Wan, *Energy & Environ. Sci.* **2012**, *5*, 5221; e) L. Wang, X. Deng, P.-X. Dai, Y.-G. Guo, D. Wang, L.-J. Wan, *Phys. Chem. Chem. Phys.* **2012**, *14*, 7330.
[11] a) S.-L. Chou, J.-Z. Wang, M. Choucair, H.-K. Liu, J. A. Stride, S.-X. Dou, *Electrochem. Commun.* **2010**, *12*, 303; b) J. K. Lee, K. B. Smith, C. M. Hayner, H. H. Kung, *Chem. Commun.* **2010**, *46*, 2025.
[12] M. N. Obrovac, L. J. Krause, *J. Electrochem. Soc.* **2007**, *154*, A103.
[13] M. Gauthier, J. Danet, B. Lestriez, L. Roué, D. Guyomard, P. Moreau, *J. Power Sources* **2013**, *227*, 237.
[14] M. N. Obrovac, L. Christensen, D. B. Le, J. R. Dahn, *J. Electrochem. Soc.* **2007**, *154*, A849.
[15] J.-S. Bridel, T. Azaïs, M. Morcrette, J.-M. Tarascon, D. Larcher, *J. Electrochem. Soc.* **2011**, *158*, A750.
[16] S. D. Beattie, D. Larcher, M. Morcrette, B. Simon, J.-M. Tarascon, *J. Electrochem. Soc.* **2008**, *155*, A158.
[17] J. S. Bridel, T. Azaïs, M. Morcrette, J. M. Tarascon, D. Larcher, *Chem. Mater.* **2009**, *22*, 1229.
[18] M. Cerbelaud, B. Lestriez, D. Guyomard, A. Videcoq, R. Ferrando, *Langmuir* **2012**, *28*, 10713.
[19] Y. Oumellal, N. Delpuech, D. Mazouzi, N. Dupre, J. Gaubicher, P. Moreau, P. Soudan, B. Lestriez, D. Guyomard, *J. Mater. Chem.* **2011**, *21*, 6201.
[20] D. Mazouzi, N. Delpuech, Y. Oumellal, M. Gauthier, M. Cerbelaud, J. Gaubicher, N. Dupré, P. Moreau, D. Guyomard, L. Roué, B. Lestriez, *J. Power Sources* **2012**, *220*, 180.
[21] S. R. D. Reyter, D. Mazouzi, M. Gauthier, P. Moreau, B. Lestriez, D. Guyomard, L. Roué, *J. Power Sources* **2013**, *239*, 308.
[22] M. Winter, *Z. Phys. Chem.* **2009**, *223*, 1395.
[23] X. H. Liu, L. Zhong, S. Huang, S. X. Mao, T. Zhu, J. Y. Huang, *ACS Nano* **2012**, *6*, 1522.
[24] a) N. A. Kumar, H. J. Choi, A. Bund, J.-B. Baek, Y. T. Jeong, *J. Mater. Chem.* **2012**, *22*, 12268; b) N. A. Kumar, H.-J. Choi, Y. R. Shin, D. W. Chang, L. Dai, J.-B. Baek, *ACS Nano* **2012**, *6*, 1715.

Paper III

“Analogy between electrochemical behaviour of thick silicon granular electrodes for lithium batteries and fine soils micromechanics”

Electrochimica Acta 120 (2014) 319–326

Contents lists available at ScienceDirect

Electrochimica Acta

journal homepage: www.elsevier.com/locate/electacta

Analogy between electrochemical behaviour of thick silicon granular electrodes for lithium batteries and fine soils micromechanics

B.P.N. Nguyen[a], J. Gaubicher[a,b], B. Lestriez[a,b,*]

[a] Institut des Matériaux Jean Rouxel (IMN), Université de Nantes, CNRS UMR 6502, F-44322 Nantes Cedex 3, France
[b] Réseau sur le Stockage Electrochimique de l'Energie (RS2E), FR CNRS 3459, France

ARTICLE INFO

Article history:
Received 5 October 2013
Received in revised form
20 December 2013
Accepted 23 December 2013
Available online 4 January 2014

Keywords:
silicon
composite electrodes
micromechanics
electrochemistry

ABSTRACT

In this paper we study the influence of the distribution and the shape of the carbon conductive additives on the cyclability of thick silicon based composite electrodes. Results pinpoint the influence of carbon additives is not only to play on the electronic conductivity but also to play on the micromechanics (stress distribution) of the composite films. The lack of correlation between electrochemical performance and the macroscopic electronic conductivity of the pristine electrodes and the observation of repeated drops and jumps in capacity during cycling brought us to make an analogy between the silicon composite electrodes and cohesive granular materials such as fine soils media. Considering the collective mechanical behavior of a stack of silicon particles upon repeated volume variations shed a novel understanding to the electrochemical behavior of composite electrodes based on silicon and alloying materials and tells us how critically important is the design at the different scales (the particle, a few particles, the composite electrode, the cell) to engineer the mechanical stress and strain and improve cycle life.

1. Introduction

Nowadays, rechargeable lithium battery is one of the most promising energy storage technologies to enable a various range of clean electric transportations which are essential to reduce the fossil oil dependency. To meet requirements of these applications, it is necessary to find higher capacity electrode materials. For a few years, great attention has been paid to silicon as negative electrode material for Lithium ion batteries, due to its very high gravimetric and volumetric capacities (3572 mAh g^{-1} and 2144 mAh cm^{-3}) in comparison to those of graphite (372 mAh g^{-1} and 843 mAh cm^{-3}) [1]. However, unoptimized Si electrodes suffer from poor cyclability due to the large volumetric expansion of Si particles upon cycling [2], resulting in their pulverization and electrical disconnection after the breakdown of the electronically conductive polymeric binder-carbon matrix [3–6], and also to the formation of an unstable solid electrolyte interphase (SEI) leading to low coulombic efficiencies [7–9]. With respect to the mechanical issue, the research directions have been focused only at the scale of one or two particles with: (i) the study of the microscopic deformation mechanism of silicon particles [10–17], (ii) the study of the bridging of the silicon particles by the polymeric binder chains [18–22]. However, the collective mechanical behaviour of a stack of particles has rarely been discussed in depth [23], although the electrochemical behaviour of composite electrodes is obviously strongly dependent on it [24].

In this paper we study the influence of the distribution and the shape of the carbon conductive additives on the cyclability of silicon based composite electrodes. The lack of correlation between electrochemical performance and the macroscopic electronic conductivity of the pristine electrodes and the observation of repeated drops in capacity during cycling brought us to make an analogy between the silicon composite electrodes and fine soils media. It then appeared that the extrapolation of the micromechanics of such granular materials to composite electrodes looks relevant to the understanding of the mechanical strength of the latter and of the cyclability of alloying materials such as silicon.

2. Experimental

Composite electrodes were made of nanometric Si (particle size 150 nm, specific surface area 14 m^2/g) as an active material (AM), Super P carbon black (CB, particle size 10-50 nm Timcal), Carbon nanofibres (VGCF) or exfoliated graphite nanoplatelets (GM15, XG Science) as a conductive additive, Carboxylmethyl cellulose (CMC, DS = 0.9, M_w = 700.000 g/mol Sigma-Aldrich) as a binder (B) and Poly (acrylic-co-maleic) acid (PAMA M_w = 3000 g/mol Sigma-Aldrich) as a dispersant. The electrodes preparation is already

* Corresponding author.
E-mail address: bernard.lestriez@cnrs-imn.fr (B. Lestriez).

0013-4686/$ – see front matter © 2014 Elsevier Ltd. All rights reserved.
http://dx.doi.org/10.1016/j.electacta.2013.12.126

Table 1
Composition, porosity and electronic conductivity of composite electrodes.

Electrode name	Si (wt%)	CB (wt%)	GM15 (wt%)	VGCF (wt%)	CMC (wt%)	Buffer (wt%)	PAMA (wt%)	Porosity (%)	Conductivity (S/m)
A	67.6	10.1	-	-	6.8	15.5	-	71-73	0.037 + - 0.004
B	65.9	10.1	-	-	6.8	15.5	1.7	67-69	0.108 + - 0.005
C	65.9	-	10.1	-	6.8	15.5	1.7	67-68	0.017 + - 0.001
D	62.6	2.5	10.1	0.8	6.8	15.5	1.7	66-68	0.112 + - 0.010

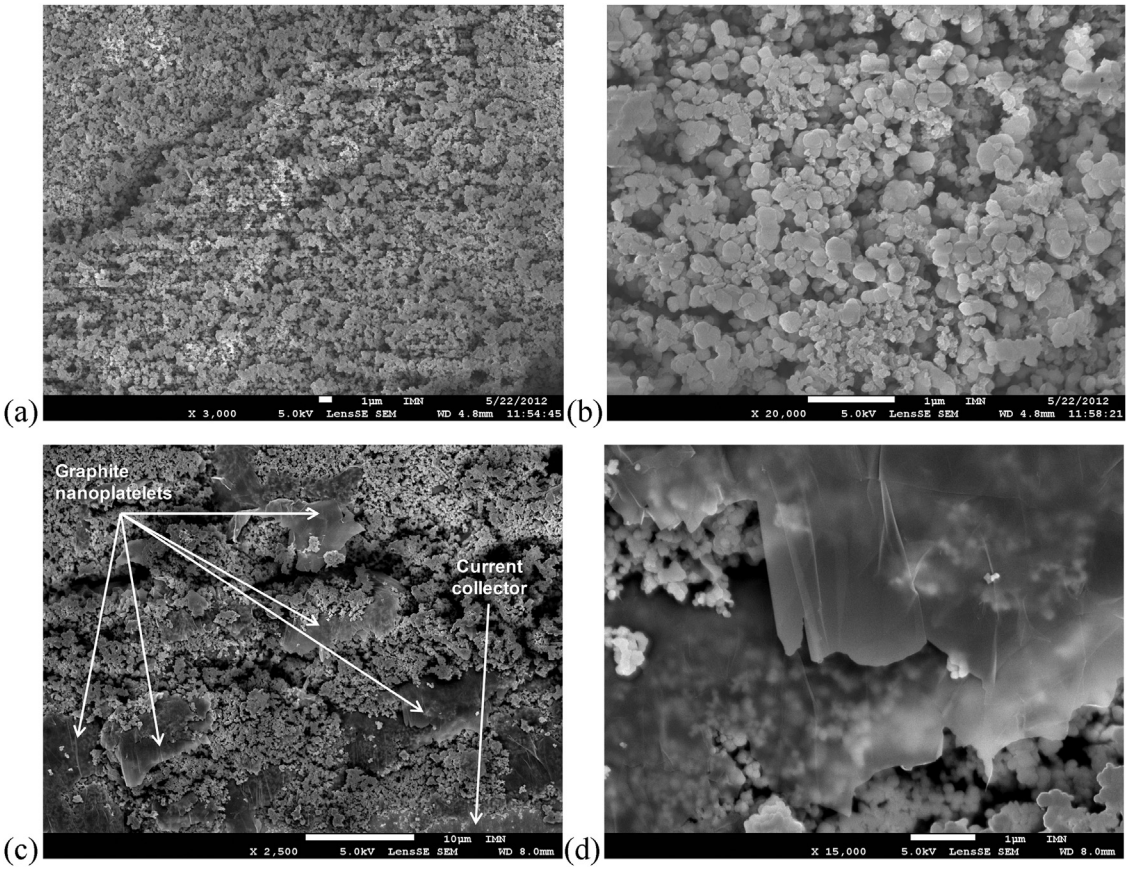

Fig. 1. SEM cross-sections of composite electrodes B (a;b) and C (c;d).

described in our previous works [9,26]. The Si mass loading is close to 2.6 mg cm^{-2} in all cases and the electrodes thicknesses are in the range of 60-62 μm.

Scanning electron microscopy (SEM) imaging was performed by using a JEOL JSM 7600. Electronic resistivity measurements were carried out by impedance spectroscopy on dry Si electrode/current collector samples sandwiched in between two metallic pistons in a standard swagelok cell, using a VMP automatic cycling/data recording system (Biologic). The frequency range was scanned from 10 mHz to 189 kHz. Each composition was studied at three different thicknesses. Six samples were evaluated for each composition. The measure was repeated three times on each sample. The impedance diagrams were resumed in all cases to a single point on the real axis. A linear increase of the resistance, R, with the thickness, t, was found, with R = 0 for t = 0. The latter implies that the contact resistance between the copper foil used as current collector and the composite electrode is negligible in the dry state. The electrode conductivity, σ, was thus determined from the well-known equation $\sigma = t/(R \times S)$, where S is the contact surface area between the probe (metallic piston) and the sample, 0.283 cm^2.

For electrochemical testing we used two-electrode Swagelok test cells with (i) a 0.78 cm^2 disc of composite positive electrode (ii) a porous glass paper as separator soaked in an electrolyte consisting of 88 wt% LP30 [1 M $LiPF_6$ solution in dimethyl carbonate-ethylene carbonate (1:1)], 2 wt% vinylene carbonate and 10wt% fluoroethylene carbonate mixture and (iii) a 0.78 cm^2 Li metal disc as the negative and reference electrode. The cells were assembled in the glove box under argon atmosphere. Cell cycling was performed at 20 °C, monitored by a VMP system (Biologic) in galvanostatic mode. The voltage range used was 0.01-1 V versus Li^+/Li^0. All composite electrodes were studied with the same rate (C/5 and D/5) at full capacity.

3. Results

The dry composition of the composite electrodes studied here is given in Table 1. SEM images show their morphology (Fig. 1). Comparing the morphology of electrodes A and B, both prepared with carbon black (CB), clearly showed (elsewhere) that a more homogeneous distribution of CB is obtained thanks to the use of the Poly (acrylic-co-maleic) acid (PAMA) dispersant [25]. This result falls in line with the fact that a higher electronic conductivity is measured for B compared to A (Table 1). The cross-section of B is shown in Fig. 1a-b. At the lowest magnification cracks can be observed, that were likely formed during the sample preparation for SEM imaging, but highlight a typical deformation mechanism for this kind

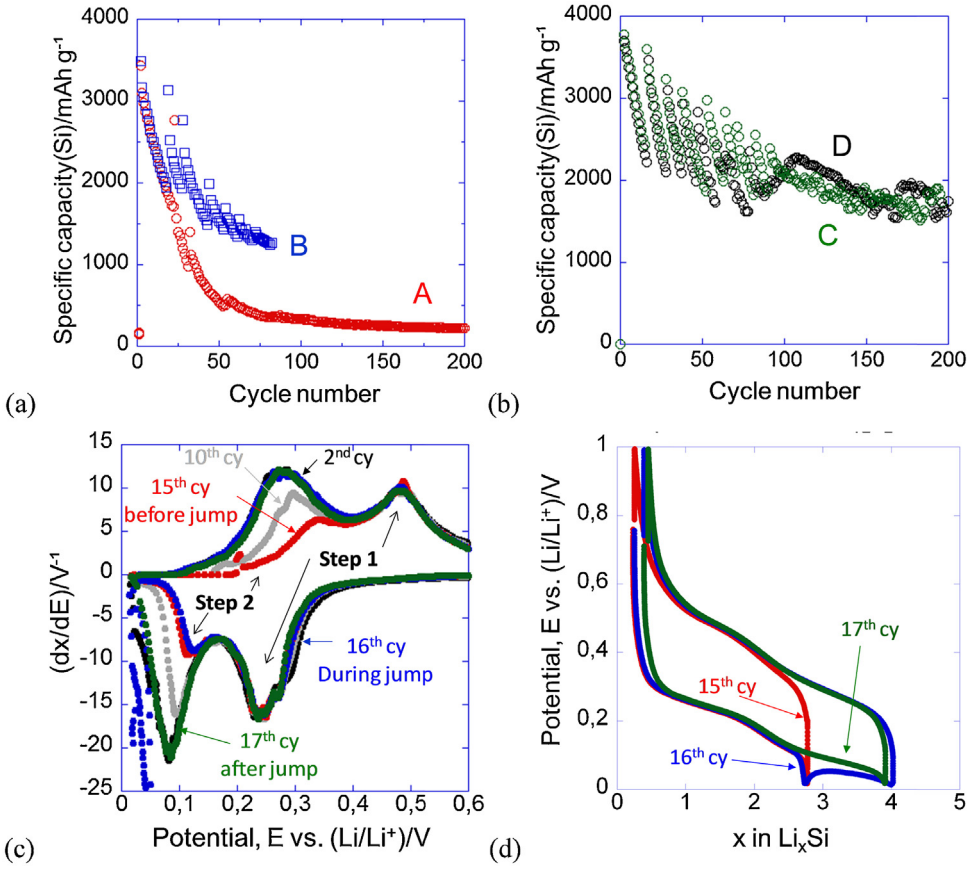

Fig. 2. Discharge capacity versus number of cycle for electrodes A and B (a), and C and D (b). Incremental capacity curves at selected cycles for C (c). Voltage composition curves showing capacity recovery after first jump for **C** (**d**).

of granular material. The cross-section of C is shown in Fig. 1c-d. In a previous work, we showed that using reduced graphene oxide instead of CB gives much better electrochemical performance for thick nanosilicon-based composite electrodes (2.5 mg of Si per cm^2) [26]. We used in this work exfoliated graphite nanoplatelets, a commercially available cheap graphene-like product (GM15). These nanoparticles consist of short stacks of several graphene sheets having a platelet shape with an average thickness in the 5–10 nanometer range and a diameter of 15 μm. The GM15 graphite nanoplatelets are found mostly orientated parallel to the current collector surface, giving a lamellar or multilayered morphology to the C electrode with stacks 3–5 μm thick of silicon nanoparticles piled over graphite nanoplatelets. Transparency of the latter to the electron beam demonstrates they are thin. They provide large contact surface area to the silicon nanoparticles. However these GM15 nanoplatelets do not contact each other, which explains the lower electronic conductivity of C compared to B (Table 1). In D, addition of supplementary CB and carbon nanofibres (VGCF) allows to increase the electronic conductivity and to reach values as high as that measured for B (Table 1).

The cyclability of the four electrodes is compared in Fig. 2a-b. The capacity of A steadily decreases and reaches a mere 250 mAh/g after 50 cycles. Adding the PAMA dispersant which improves the CB distribution in B is beneficial to the capacity retention. Indeed, the capacity is still approx. 1200 mAh/g after 80 cycles. The cyclability of C and D are remarkably much better than that of B since a nearly stable capacity of 1800mAh/g is retained after 100 cycles. It seems counter intuitive that performance of these electrodes does not reflect their electronic conductivity in the pristine state. Indeed, performance is improved by a better dispersion of CB in B vs. A (which is mirrored by a higher electronic conductivity) and by substituting GM15 for CB in C (which is associated with a decline of electronic conductivity). Similarly, in D, VGCF and CB were mixed with GM15 to increase the electronic conductivity; however, the electrochemical performance was not improved vs. C.

Interestingly, the cycling behaviour of B, C and D is characterized by the repetition of capacity jumps, the amplitude of which decreases on cycling. It is significant that such phenomenon is not seen in the previous literature, including our work on electrode with same composition. However, an early paper of Dahn and co-workers pinpointed that a CMC-based electrode showed some oscillating behaviour, with the specific capacity changing between 1300 and 1100 mA h/g during 70 cycles, but no interpretation was proposed [27]. Furthermore, in the large majority of published studies (including our previous work) [8,9,18] the active mass loading is low (lower than 0.7 mg/cm^2) and electrodes are thin. Here, the active mass loading is 5 times higher. The lack of capacity jumps in thin electrodes vs. thicker ones maybe a consequence of a different stress field. Indeed, it is known that there are effects of geometric confinement on the stress distribution within layers of material [28,29].

These unexpected processes are studied in more details in Fig. 2c-d. Typical incremental capacity curves are shown in the case of electrode C before, during, and after a capacity jump (Fig. 2c). These curves were found to be representative of all observed capacity jumps. Electroactivity of Si is characterized by two major steps, 1 and 2, ascribed to Li reactions with amorphous Si [1]. Li_xSi alloys formed during step 2 are lithium rich compared to step 1. Comparing cycle 2 to 15th in Fig. 2c shows that the loss of capacity occurring before the jump (cycle 16) corresponds to a strong alteration of the amplitude and profile of step 2 whereas that of step 1 are barely modified. Accordingly, it appears that the volume of Si connected

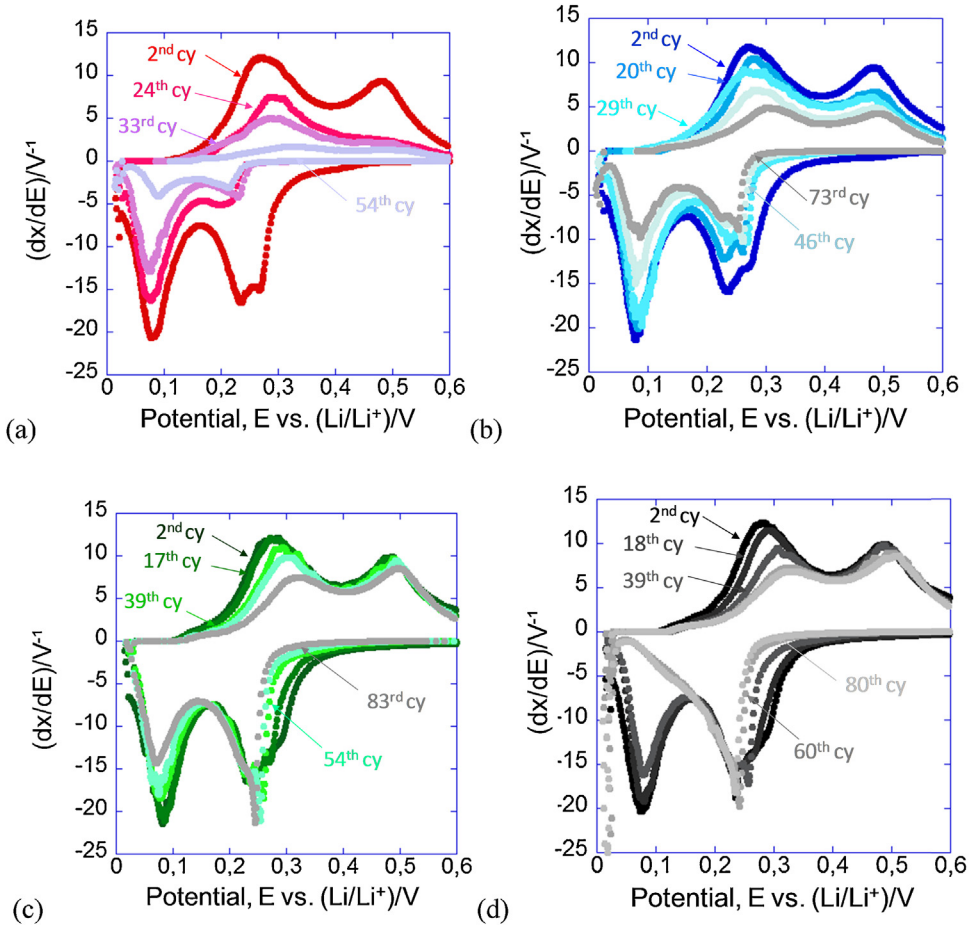

Fig. 3. Incremental capacity curves at selected cycles after capacity jumps for the A (a), B (b), C (c) and D (d) electrodes.

to the electrical circuit varies reversibly with the degree of alloying with Li. Just after the jump of capacity (cycle 17), the capacity of step 2 is remarkably recovered since cycle 17 and cycle 2 are strikingly similar. This implies that some reversible modification of the electrode took place during the jump (cycle 16) and lead to a quasi-total refreshing of the electrochemical behaviour. Focusing on the capacity jump by using a Voltage-x representation (Fig. 2d) confirms that discharge and charge remain unchanged above 0.1 V and that the sole alteration actually stems from below 0.1 V, that is during step 2. As a matter of fact, during the 16th discharge, just before the potential reached the 10 mV cut off, it suddenly reverses back to 50 mV after having hit a threshold of nearly 15 mV vs. Li^0. This process therefore enables the system to gain a significant amount of additional capacity which corresponds to the observed jump of capacity.

Given these peculiar electrochemical features, in order to compare the influence of the conductive additive on the electrochemical profiles, we have focused in the following on cycles that are only those just after the capacity jumps (Fig. 3). Comparison of the incremental capacity curves for such cycles clearly shows that the difference in capacity observed between A, B, C and D electrodes in Fig. 2 is homogeneously distributed over the two lithiation steps.

We are now left with two questions: what are the underlying physical processes accounting for the capacity jumps? How interpreting the performance improvement brought by the PAMA dispersant in B vs. A and by the graphite nanoplatelets in C vs. A, given the fact that there is no apparent correlation between the overall capacity retention and the electronic conductivity of these electrodes in their pristine state; despite the fact that cycle performance of large volume variation materials obviously rely on the sustainability of the electronic wiring. We found that possible answers are nested in the field of micromechanics of cohesive granular materials [30]. Indeed, an analogy can be made between these ones and composite electrodes.

4. Discussion

The term “cohesive granular media” covers a vast spectrum of granular materials in which rigid grains are bound together by direct surface forces of various chemico-physical origins or from the presence of a binding phase filling fully or partially the interstitial space [30]. Well-known example is the wet sand. The liquid bridges result in a capillary force keeping the grains together. When a stress or a strain is imposed onto a granular material, it generates broad and highly heterogeneous contact force distributions [30]. This heterogeneity is often described in terms of force chains spanning several particles organized in strong and weak networks; and some contacts are screened in these networks as a result of arching (i.e. formation of arches). When geometrical change of granular texture occurs, as a consequence of imposed stress or strain, it is highly non-linear, involving creation and loss of contacts, rotation frustration and frictional sliding. The geometrical changes depend on the contact interactions and steric exclusions among particles. The displacements result in transition to new equilibrium states. An interesting example is observed in fine soils, where particle swelling (or shrinkage) happens as a result of humidification (or drying) [31]. The particle size changes lead to a bulk strain, some contacts being under tensile stress whereas others are under compressive one. This build up of strain leads to initiation of cracks as soon as the strongest tensile contacts begin to fail. Cracks can form either when the particle size increases or decreases [32].

Composite electrodes are obviously granular media endowed with a cohesion that stems from the presence of the binder [33]. Here, the carboxymethyl cellulose binder (CMC) is forming adhesive bridges between silicon and carbon particles [18,19]. Furthermore, the Li/Si alloying reaction produces particles swelling [34], which results from a simple geometrical point of view in displacements and rearrangements of the particles [23]. The formation of cracks through the composite electrode parallel to the current collector surface has been observed. [35–37]. The type of bonding between the CMC binder and the particles influences the force and the interaction range between the particles bridged by the polymer chains [20]. Atomic force microscopy measurements showed covalent Si–CMC bonding results in up to an order of magnitude larger surface forces and wider interaction distances than Si–CMC complexes resulting from simple adsorption. The former is also associated with much longer cycle life of the composite electrode [18,38]. Very interestingly, one can note that in both cases (adsorption or covalent bonding) the reversibility of the adhesion between the particle–CMC complex and the nearby solid phase was proved, i.e. the repetitions of the establishment of bridges upon the repetitions of approach/retract cycles. Such reversibility could be ascribed to some self-healing character of the CMC-Si interaction. The hydrogen bonds between SiOH and COOH groups may be at the origin of this reversibility by being temporarily broken and reformed from one anchorage site to the neighbouring ones [21,39,40]. Nevertheless, reversible adhesion is a typical feature of polymer/solid interfaces where polymer segments can adsorb through soft Van der Waals or acide-base interactions [41]. However, upon repeated disruption and establishment of bridged contact, the adhesion between the surfaces is reduced. Indeed, during contact disruption, the polymer chains bridging the two surfaces are stretched leading to chain scission. On the re-establishment of contact, these fragmented polymer chains are unable to fully re-establish the adhesion [41].

Let's try to interpret the characteristic features of the capacity jumps. Remind that between two consecutive jumps the capacity loss is associated with a preferential alteration of the profile (intensity and shape) of step 2 vs. 1. Just after the jump of capacity, the profile of step 2 is recovered. Differential particle-size change upon lithium insertion is a plausible hypothesis in regard to the distribution in electrical wirings of the Si particles or as a natural consequence of granular disorder. Thus, considering a network of Si particles, one can imagine that upon lithium insertion, the heterogeneity in force distribution will grow from step 1 to step 2, leading to the formation of a network of particles engaged into strong and weak force chains, some contacts being under compressive stress whereas others are under tensile one, some particles being even disconnected from the network as they could be expelled from it for geometrical reasons (but possibly still sticking to it thanks to the CMC bridges). Let's remind that in a stack of particles the electrons are transferred between particles by a hopping or tunnelling mechanism with contact resistivity depending exponentially with the gap in between the particles, the gap being dependent on the stress distribution [42–44]. A 8-10 nm gap makes a contact electronically insulating. Thus, depending on the state of stress a particle is engaged in, this particle would be more or less well wired to the network and thus shows a different electrochemical activity. Whether a particle is engaged into (i) a compressive force chain, or (ii) weak force chain (small gap), or (iii) strong tensile force chain (large gap), its electronic wiring is (i) good, (ii) poor, or (iii) very bad. In the first situation (i), such particle could effectively participate to step 2, while in the second and third situation such particle would have difficulties to accomplish step 2 as a consequence of higher interparticle electrical contact resistance and local polarization.

Only numerical simulation could give the real picture of the stress and strain distributions in a composite electrode where the active particles show volume variations upon lithium insertion. However, making simple drawings, trying to visualize the growth of a set of Si particles upon lithium insertion from the unlithiated state to step 1, and then to step 2 (Fig. 4), it appears that accomplishing step 1 would not create a lot of stress in the network while accomplishing step 2 requires a lot of displacement of the particles with numerous losses or variations in the contacts. To get this picture we simply considered a square filled with nine particles with a void corresponding to about 65-70% porosity (Fig. 4). The particles where individually grown in size with a ratio between their radii of 1.32 between unlithiated and end of step 1 states (the volume variation is 130%, thus $V_{Li1.8Si} = 2.3\,V_{Si}$ and $R_{Li1.8Si}/R_{Si} = (2.3)^{1/3}$) and 1.55 between unlithiated and end of step 2 states (the volume variation is 270%, thus $V_{Li3.75Si} = 3.7\,V_{Si}$ and $R_{Li1.8Si}/R_{Si} = (3.7)^{1/3}$). The particles were randomly selected to grow in size only one at a time. Drawing 0 corresponds to the pristine state; 1-9 to step 1; and 10-14 to step 2 but only for some particles. The changes in the texture are evidenced by dotted circles which show the previous position or size of the particles that have moved or grown in size. The blue arrows highlights where gaps have been created between particles previously in contact. It appears that these gaps are mainly created during step 2, for geometrical reasons. This simulation by hands is in agreement with experimental in-situ visualisations that show thickness's variation of Si-based composite electrode does not occur during step 1 but when step 2 starts [21]. Thus, this set of drawings where the growth of Si particles upon lithium insertion is analyzed from simple geometrical constraints could explain the odd electrochemical behaviour seen in the incremental capacity curves in Fig. 2c. During step 2 the growth of some particles generates gaps within the network that disconnect and prevent other particles to further lithiate. However, on charge thanks to the adhesive CMC bridges, these gaps are likely closed allowing delithiation during step 1 of the previously disconnected particles; indeed, as can be seen in Fig. 2c, step 1 is fully reversible. In addition, we can also pinpoint that the occurrence of step 2 implies numerous frictions between the particles that might induce damage to the SEI layer. These frictions, or the sliding of two particles on each other are highlighted by green stars in the drawings 10-14, that have been duplicated for the sake of clarity. Some contacts (blue squares in drawings 13 and 14) are also created after one particle has grown in size or moved. However, the contact resistance at these spots is likely to be large due to the presence of the SEI layer on the surface of the two particles that are brought in contact.

Now, how to explain that at some point capacity jump occurs, with a large recovery of the number of Si particles that are again able to lithiate during step 2? Only numerical simulations could unambiguously address this issue. Considering the micromechanics of a granular material under stress, these capacity jumps likely involve some geometrical changes in the granular texture, to release the elastic mechanical energy that builds up, due to finite-volume constraints, during the volume variations of the silicon particles. Within the Swagelok lab cells that were used during this study, both the separator and the current collector oppose a reaction force (equivalent to approx. 2 Bars) to the thickness increase of the electrode. As a consequence, the internal pressure in the electrode should increase, resulting at some point in some break-down of the composite electrode architecture with the formation of cracks and some internal reorganization within the network formed by contiguous Si particles leading to a vast redistribution of contacts and a recovery of the electrochemical capacity. The hypothesized correlation between the variations in capacity and in the mechanical elastic energy is depicted in Fig. 5. Let's note that the repetition of such events as well as the repetition of the opening and closing of gaps between particles or their frictional sliding, involves a repetition of disruption and re-establishment of the Si-CMC-Si (and Si-CMC-Carbon) bridges [20]. Such repetition must lead to the

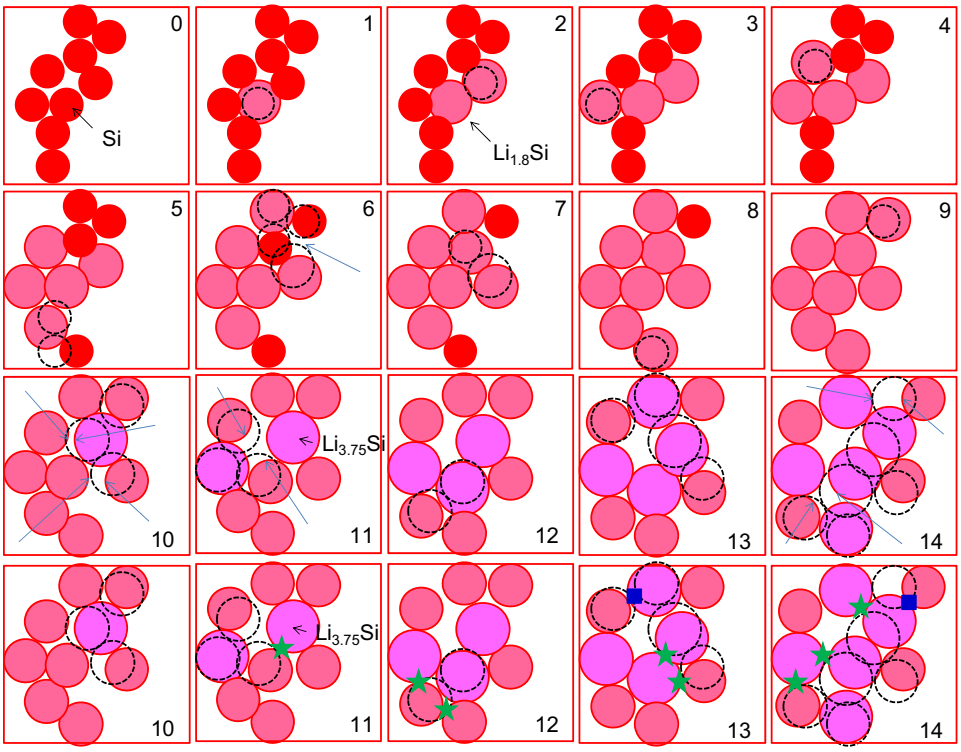

Fig. 4. Schematization of a Si-based granular composite electrode where the Si particles grow in size as a consequence of lithium insertion. Drawing 0 corresponds to the pristine state; 1-9 to step 1; and 10-14 to step 2. Drawings 10-14 have been duplicated for the sake of clarity. Dotted circles show the previous position or size of the particles that have moved or grown in size. Blue arrows highlight where gaps have been created between particles previously in contact. Green stars highlight friction or sliding of two particles on each other. Blue squares highlight the contacts that have been created after one particle has grown in size or moved.

fragmentation of the CMC chains with a progressive loss of reversibility resulting in a decline of the mean capacity (identified by the red dotted line in Fig. 5) [41]. The decrease of the cyclability of Si-based electrodes with a decrease of the molecular weight of the CMC binder is another indirect proof of the latter interpretation [22]. Another origin of the decline in the mean capacity is the continuous growth of the liquid electrolyte decomposition products [7–9] as a consequence of the SEI damaging that stems from frictional sliding of the particles.

Finally, how to understand the influence of the dispersion state of the conductive additive (coarse or fine distribution) or of its shape factor (particle, fibre, and platelet) on the overall capacity retention? A more homogeneous distribution of small CB clusters (in B compared to A) likely favours a more homogeneous stress distribution because the CB clusters do not vary in size and therefore act as buffering zones with respect to the strain and the stress. Smaller and thus less critical cracks would form as a consequence of the Si volume variations with a more homogeneous distribution of the CB clusters, resulting in a better resiliency of the composite

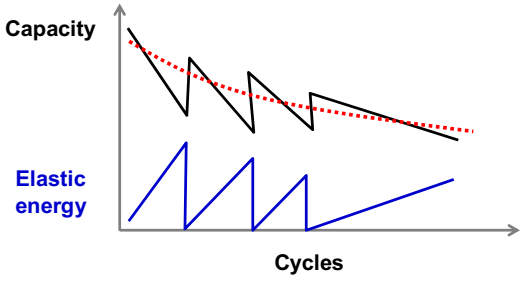

Fig. 5. Proposed correlation between the variations in electrochemical capacity and in the mechanical elastic energy stored into the granular Si-based electrode. Red dotted line highlights the decline of the mean capacity.

electrode to the volume variations of the Si particles. This interpretation is supported by the knowledge of the toughening mechanisms of another class of materials, namely polymer blends and composites. Indeed, glassy and brittle polymers can be reinforced by the incorporation of a second phase consisting of dispersed particles [45]. In glassy polymers, the imposition of a strain leads to a stress which concentrates on the biggest defect and leads to propagation of a large crack resulting in a catastrophic failure. In toughened glassy polymers, the dispersed particles lead to a distributed stress over a large zone. As a consequence, such materials can sustain much larger strains before breaking. Furthermore, in Si-based composite electrodes the CB clusters make electronically conducting bridges between the Si particles favouring more sustainable connections to the electrical network.

With all these thoughts in mind, one can note that significantly higher levels of glassy polymer toughening are obtained with particles which show high aspect ratios [45]. Therefore, we believe that the graphite nanoplatelets would also act in favour of a more homogeneous stress and strain distribution (within C and D compared to CB in B), which in turn would allow a more reversible breathing of the stacks of particles. Depending on their stiffness (associated with their thickness), large contact areas provided by graphite nanoplatelets may play the same role as the lintels do in the house's which walls are made of stones, or may provide sliding surfaces to the silicon particles improving the medium plasticity and resiliency to cracking. Furthermore, the large electronically conducting surface areas of graphite nanoplatelets likely offer a more efficient local electronic wiring to Si particles than CB. Let's note that two other works pinpoint the possible influence of the carbon conductive additives on the mechanical stress distribution within Si-based composite electrodes upon cycling [46,47].

According to in-situ electrochemical dilatometry, CB appears to act as a buffering system, mitigating the electrode expansion [47].

On another hand, increasing the CB content into Si-based composite electrodes has the disadvantage of possibly increasing the first cycle irreversible capacity loss due to excessive formation of a solid electrolyte interface (SEI) on poorly graphitized carbons.

5. Conclusion

In this work, an odd electrochemical behavior was observed for thick nanosilicon-based composite electrodes cycled without capacity limitations. Steady decline followed by sharp recovery of the capacity were observed to repeat several times. This behavior implies a dynamic variation in the quality of the electrical wiring and therefore of the activity of the Si particles during a given charge-discharge cycle. This odd behavior can be interpreted in the background of the micromechanics of cohesive granular media such as fine soils. The build-up of an internal pressure as a consequence of the swelling of the Si particles' network within the confined space of the electrochemical cell would lead to a major geometrical change of granular texture with a vast redistribution of contacts assisted by adhesive CMC bridges and a recovery of the electrochemical capacity. However, the repetition of all these processes with frictional sliding of the particles must lead to a damaging of the SEI layer, and to the fragmentation of the CMC chains with a progressive loss of reversibility resulting in a decline of the mean capacity down to a plateau value which should correspond to a micromechanical equilibrium state.

The influence of the carbon additives' distribution and shape on the electrochemical behaviours of the nanosilicon-based composite electrodes was investigated. The use of graphene or graphite nanoplatelets and a more homogeneous distribution favor a better resiliency of the electrodes, likely because the carbon additive plays on the stress intensity and distribution within the Si particles' network. Furthermore, the graphene-like materials offer electronically conducting large surface areas which likely help maintaining the electrical wiring within the moving Si mass.

Let's note that these conclusions are in line with the large work in the literature about silicon-based electrodes. Indeed, it has been shown that the dilution of the Si particles within a CMC/CB [23,48] or flexible cellulose/CB [47] porous matrix, allows to mitigate the volume changes undergone by the Si particles during insertion (deinsertion) of Li and to improve cyclability, although at the expense of gravimetric and volumetric energy density. As observed recently, slurries of Si and CB nanoparticles suspended in a liquid electrolyte shows a reversible cycling [49]. In such electrode, contact forces are highly reversible thanks to attractive interparticle interactions induced by the Van der Waals forces and all particles can move freely without permanently damaging the network.

The extrapolation of the micromechanics of granular cohesive materials to composite electrodes seems fairly relevant and offers novel understanding of the mechanical strength of the latter, which is so important with respect to their processing and electrochemical behavior, in particular for the cyclability of alloying materials. Such extrapolation must be relevant also when one turns toward the understanding of the charge transport properties and in particular the electronic charge transfer mechanism. Numerical simulation studies are required in this direction and will likely help in smarter designing of new composite electrode with improved performance.

In previous works, most of the research focused on the selection of the binder to improve interparticles contact forces. New macromolecular architectures could be designed to allow a better reversibility of the contacts. A recent advance lies in the development of elastic and conductive binders [50]. The engineering of electrode's architectures with a controlled stress distribution upon particle swelling (and shrinkage) is an important prospect. This way, using silicon materials in the form of flexible nanostructures such as wires looks appealing [51]. Micrometric silicon particles embedded into a resilient electronically conducting hierarchical network of carbon nanofibres and nanotubes also give fairly interesting cyclability [6,52].

Finally, the internal cell pressure is pinpointed here as a significant parameter playing on the stress distribution and its variation within the granular Si-based electrode upon cycling. The engineering of the stress distribution appears critical to the cycle life of silicon- and alloying-based electrodes. Then the search for new cell design appears to be at the industrial level as a possible path of performance improvement.

Acknowledgements

Financial support provided by the *European Commission (EC)*, through the project EuroLiion is gratefully acknowledged.

References

[1] M.N. Obrovac, L.J. Krause, J. Electrochem. Soc 154 (2007) A103.
[2] L.Y. Beaulieu, K.W. Eberman, R.L. Turner, L.J. Krause, J.R. Dahn, Electrochem. Solid-State Lett. 4 (2001) A137.
[3] W.R. Liu, M.H. Yang, H.C. Wu, S.M. Chiao, N.L. Wu, Electrochem. Solid-State Lett. 8 (2005) A100.
[4] J.H. Ryu, J.W. Kim, Y.E. Sung, S.M. Oh, Electrochem. Solid-State Lett. 7 (2004) A306.
[5] S. Park, T. Kim, S.M. Oh, Electrochem. Solid-State Lett. 10 (2007) A142.
[6] B. Lestriez, S. Desaever, J. Danet, P. Moreau, D. Plée, D. Guyomard, Electrochem. Solid-State Lett 12 (2009) A76.
[7] M. Winter, Z. Phys. Chem 223 (2009) 1395.
[8] Y. Oumellal, N. Delpuech, D. Mazouzi, N. Dupre, J. Gaubicher, P. Moreau, P. Soudan, B. Lestriez, D. Guyomard, J. Mater. Chem 21 (2011) 6201.
[9] D. Mazouzi, N. Delpuech, Y. Oumellal, M. Gauthier, M. Cerbelaud, J. Gaubicher, N. Dupré, P. Moreau, D. Guyomard, L. Roué, B. Lestriez, J. Power Sources 220 (2012) 180.
[10] X.H. Liu, L. Zhong, S. Huang, S.X. Mao, T. Zhu, J.Y. Huang, ACS Nano 6 (2012) 1522.
[11] K. Zhao, M. Pharr, Q. Wan, W.L. Wang, E. Kaxiras, J.J. Vlassak, Z. Suo, J. Electrochem. Soc 159 (2012) A238.
[12] I. Ryu, J.W. Choi, Y. Cui, W.D. Nix, J. Mech. Phys. Solids 59 (2011) 1717.
[13] B. Hertzberg, A. Alexeev, G. Yushin, J. Am. Chem. Soc. 132 (2010) 8548.
[14] K. Zhao, W.L. Wang, J. Gregoire, M. Pharr, Z. Suo, J. Vlassak, E. Kaxiras, Nano Lett. 11 (2011) 2962.
[15] M.J. Chon, V.A. Sethuraman, A. McCormick, V. Srinivasan, P.R. Guduru, Phys. Rev. Lett. 107 (2011) 045503.
[16] M.T. McDowell, S.W. Lee, J.T. Harris, B.A. Korgel, C. Wang, W.D. Nix, Y. Cui, Nano Lett. 13 (2013) 758.
[17] J. Rohrer, K. Albe, J. Phys. Chem. C 117 (2013) 18796.
[18] B. Lestriez, S. Bahri, I. Sandu, L. Roué, D. Guyomard, Electrochem. Commun. 9 (2007) 2801.
[19] M. Cerbelaud, B. Lestriez, D. Guyomard, A. Videcoq, R. Ferrando, Langmuir 28 (2012) 10713–10724.
[20] U. Maver, A. Znidarsic, M. Gaberscek, J. Mater. Chem. 21 (2011) 4071.
[21] J.S. Bridel, T. Azaïs, M. Morcrette, J.M. Tarascon, D. Larcher, J. Electrochem. Soc 158 (2011) A750.
[22] J.-S. Bridel, T. Azaïs, M. Morcrette, J.-M. Tarascon, D. Larcher, Chem. Mater. 22 (2010) 1229.
[23] S.D. Beattie, D. Larcher, M. Morcrette, B. Simon, J.M. Tarascon, J. Electrochem. Soc 155 (2008) A158.
[24] M. Smith, R.E. García, Q.C. Horn, J. Electrochem. Soc. 156 (2009) A896.
[25] B. P. N. Nguyen, S. Chazelle, M. Cerbelaud, W. Porcher and B. Lestriez, unpublished results.
[26] B.P.N. Nguyen, N.A. Kumar, J. Gaubicher, F. Duclairoir, T. Brousse, O. Crosnier, L. Dubois, G. Bidan, D. Guyomard, B. Lestriez, Adv. Energy Mater. 32 (2013) 1351.
[27] J. Li, R.B. Lewis, J.R. Dahn, J. Electrochem. Soc. Lett. 10 (2007) A17.
[28] R.E. Webber, K.R. Shull, A. Roos, C. Creton, Physical Review E 68 (2003) 021805.
[29] J.W. Landry, G.S. Grest, L.E. Silbert, S.J. Plimpton, Phys. Rev. E 67 (2003) 041303.
[30] B. Cambou, M. Jean et F. Radjai (2009), Micromechanics of granular materials.(Wiley- Iste, Berlin).
[31] J.K. Mitchell, Fundamentals of Soil Behavior, Wiley, New York, 1993.
[32] M.S. El Youssoufi, J.Y. Delenne, F. et, Radjai, Phys. Rev. E 71 (2005) 051307.
[33] S. Babinec, H. Tang, A. Talik, S. Hughes, G. Meyers, J. Power Sources 174 (2007) 508.
[34] M.N. Obrovac, L. Christensen, D. Ba Le, J.R. Dahn, J. Electrochem. Soc. 154 (2007) A849.
[35] S. Komaba, N. Yabuuchi, T. Ozeki, Z.-J. Han, K. Shimomura, H. Yui, Y. Katayama, T. Miura, J. Phys. Chem. C 116 (2012) 1380–1389.
[36] A. Magasinski, B. Zdyrko, I. Kovalenko, B. Hertzberg, R. Burtovyy, C.F. Huebner, T.F. Fuller, I. Luzinov, G. Yushin, ACS Appl. Mater. Interf 2 (2010) 3004.

[37] B. Koo, H. Kim, Y. Cho, K. Tae Lee, N.-S. Choi, J. Cho, Angew. Chem. Int. Ed 51 (2012) 8762–8767.
[38] D. Mazouzi, B. Lestriez, L. Roué, D. Guyomard, Electrochem. Solid-State Lett 12 (2009) A215.
[39] I. Kovalenko, B. Zdyrko, A. Magasinski, B. Hertzberg, Z. Milicev, R. Burtovyy, I. Luzinov, G. Yushin, Science 334 (2011) 75.
[40] M.-H. Ryou, J. Kim, I. Lee, S. Kim, Y.K. Jeong, S. Hong, J.H. Ryu, T.-S. Kim, J.-K. Park, H. Lee, J.W. Choi, Adv. Mater. 25 (2013) 1571.
[41] P.S. Bhosale, J.C. Berg, Langmuir 28 (2012) 16807.
[42] D. Guy, B. Lestriez, R. Bouchet, D. Guyomard, J. Electrochem. Soc. 153 (2006) A679.
[43] A. Awarke, S. Lauer, S. Pischinger, M. Wittler, J. Power Sources 196 (2011) 405.
[44] K. Seid, J.-C. Badot, O. Dubrunfaut, S. Levasseur, D. Guyomard, B. Lestriez, J. Mater. Chem. 22 (2012) 2641.
[45] R.J. Young, P.A. Lovell, Introduction to Polymers, Chapman & Hall, New York, 1991.
[46] J. Guo, A. Sun, X. Chen, C. Wang, A. Manivannan, Electrochim. Acta 56 (2011) 3981.
[47] J.L. Gómez Cámera, J. Morales, L. Sánchez, P. Ruch, S.H. Ng, R. Kötz, P. Novák, Electrochimica Acta 54 (2009) 6713.
[48] J. Guo, C. Wang, Chem. Commun. 46 (2010) 1428.
[49] S. Hamelet, D. Larcher, L. Dupont, J.-M. Tarascon, J. Electrochem. Soc. 160 (2013) A516–A520.
[50] G. Liu, S. Xun, N. Vukmirovic, X. Song, P. Olalde-Velasco, H. Zheng, V.S. Battaglia, L. Wang, W. Yang, Advanced Materials 23 (2011) 4679.
[51] J.R. Szczech, S. Jin, Energy Environ. Sci. 4 (2011) 56.
[52] M. Gauthier, D. Mazouzi, D. Reyters, B. Lestriez, P. Moreau, D. Guyomard, L. Roué, Energy Environ. Sci. 6 (2013) 2145.

Paper IV

“Manufacturing of industry-relevant $LiNi_{0.5}Mn_{1.5}O_4$ positive composite electrodes for lithium ion-cells”

Manufacturing of industry-relevant $LiNi_{0.5}Mn_{1.5}O_4$ positive composite electrodes for lithium ion-cells

B. P. N. Nguyen,[1] N. Mariage,[2] R. Fredon,[3] E. Kelder,[3] and B. Lestriez[1*]

[1] *Institut des Matériaux Jean Rouxel (IMN), Université de Nantes, CNRS UMR 6502, F-44322 Nantes Cedex 3, France*

[2] *CEA/LITEN, Grenoble, France*

[3] *Technichal University of Delft (TUD), Netherlands*

[1,2] *Réseau sur le Stockage Electrochimique de l'Energie (RS2E), FR CNRS 3459, France*

* bernard.lestriez@cnrs-imn.fr

Abstract

The composite electrodes usually consist of a mixture of active material and non-electro active additives (polymeric binder and conductive carbon additives). In this paper, the influence of the composite electrode formulation on the cyclability of $LiNi_{0.5}Mn_{1.5}O_4$ (LNMO) electrodes was studied for industry-relevant surface capacities (i.e. up to ~3 mAh cm^{-2}) with two mixing methods (ball milling and magnetic stirring). The inactive binder and carbon additives content were varied, as well as the type of carbon additive and binder. SEM observations and electrical measurement show more homogeneous distribution of non-electro active additives in ball milled electrodes than stirred ones. The cycle life of the former electrodes is degraded with lower coulombic efficiency at first cycle, as a consequence of higher specific surface area of the electrodes and increased parasitic reactions. Coulombic efficiency stabilizes upon cycling at 99.25% whatever the formulation. The fading of the capacity is minimized by increasing the amount of conductive additives or by substituting part of carbon black for carbon nanofibers whatever mixing methods. However, the cyclability of the electrodes with high active mass loading is severely decreased which could be attributed to more defects in terms of electronic percolation or adhesion and cohesion with thick electrodes. Best result is retention of 85% of the capacity after 300 cycles. In addition, the electrodes prepared in water with carboxylmethyl cellulose (CMC) binder exhibits poorer cyclability compared to the ones prepared in N-Methylpyrrolidone (NMP) with Polyvinylidene Fluorine (PVdF) binder.

Keywords: Lithium-ion battery, $LiNi_{0.5}Mn_{1.5}O_4$, electrode formulation, cyclability.

Introduction

$LiNi_{0.5}Mn_{1.5}O_4$ (LNMO) shows very good structural stability upon cycling. [1,2,3,4,5,6,7] As a positive electrode active material, its large reversible capacity of ca 135 mAh/g and high working voltage results in higher specific energy than that of $LiFePO_4$, undoped-$LiMn_2O_4$ and $LiCoO_2$. Moreover, LNMO can be a high rate electrode material even in the form of micron-size particles. [8] This material is thus envisioned for electric vehicles as it meets the performance/cost requirements needed. Its advantages are, however, largely counter-balanced by the instability of several of the cell constituents at the high working voltage of this positive electrode, which is beyond the thermodynamic stability window of common organic electrolytes. As a consequence, parasitic reactions occur at the surface of the active material with the electrolyte that decompose and form surface films deposit including lithium salts and organic carbonates. [9] As a result, large irreversible capacity at the first cycle and low coulombic efficiency (CE) are usually observed for LNMO with conventional electrolytes, which prohibit the use of LNMO for electric vehicle application. [10] Through accurate measurements, Dahn and co-workers showed the CE decreases proportionally to the increase in charge-discharge cycle time indicating that parasitic reactions at the positive electrode occur at a fixed rate at a given temperature. Time and temperature, not the cycle count, impact the parasitic reactions as well as calendar life for LNMO-based cells. [11] In this regard, the influence of the particle size has been studied, in general by varying the temperature of the material's synthesis. [9,11,12,13] The trend systematically observed is a decrease in the extent of electrolyte degradation, decrease of first cycle irreversible loss and increase of the coulombic efficiency with a decrease in the surface area/increase of the particle size. Upon cycling, the surface film formed from the electrolyte degradation becomes thicker, which leads to the resistance increase. The charge/discharge reaction becomes sluggish due to polarization increase, which eventually leads to capacity fading. [14]

A very few works, however, looked at the influence of the engineering of the composite electrode (binder and conductive additive content, calendaring, active mass loading) on the cyclability of LNMO. High operating voltages also lead to parasitic reactions with inactive components of the cell such as the carbon conductive additives, the metallic parts of the can and the separator. [15,16,17,18] These parasitic reactions affect the CE of the cell and the electrochemical performance of the LNMO electrodes. Indeed, the growing of electrolyte degradation products at the surface of the active mass, the degradation of the carbon conductive additive with the loss of LNMO/CB electrical contacts, all lead to increase

of the polarization and loss of active mass utilization. [14] Vidal et al. evaluated the influence of sonication and densification but on the rate performance of electrode with active mass loading up to 17mg/cm². [19] Except the study of Vidal et al., all other works considered low active mass loading electrodes, about 3-5 mg/cm² of LNMO, or model electrodes without binder and carbon additives.

Here, we looked at the influence of the composite electrode formulation on the cyclability of LNMO electrodes, with active mass loading up to 28 mg cm $^{-2}$ (surface capacity up to ~3 mAh cm^{-2}), i.e. for industry-relevant active mass loading. Two different mixing methods were used to make the electrodes: a high energy one, ball milling and a low energy one, stirring. In the latter method, the particle size of the pristine material (3-8 µm) was unaffected while in the former method it was much decreased to 1µm and less. The inactive binder and carbon additives content were varied, as well as the type of carbon additive. Most of the results reported here were achieved for electrodes with Polyvinylidene fluorine (PVdF) as a binder and prepared with N-Methylpyrrolidone (NMP) as a solvent. However, a few electrodes were also prepared with water as the solvent and with Carboxymethyl cellulose (CMC) as the binder.

Table 1. Composition and porosity of the composite electrodes. B and M mean an electrode prepared in NMP by Ball milling and Magnetic stirring, respectively. BW means an electrode prepared in water by Ball Milling.

Electrode name	Electrode formulation (wt%)				Porosity (%)	Theoretical BET ** ($m^2 g^{-1}$)	Conductive additive volume fraction*** (%)	Mean resistivity (ohm.cm)	Stand. Deviation (%)
	LNMO	CB	VGCF	Binder*					
B1	84	6	-	10	48-50	6,88	5.4	6.0	8
B2	84	4	2	10	50-53	6,28	5.2	0.5	7
B3	80	7.5	-	12.5	43-47	7,71	7.0	3.3	6
B4	80	5.5	2	12.5	45-48	7,11	6.8	0.4	5
B5	76	9	-	15	40-43	8,55	8.5	2.1	4
B6	76	7	2	15	42-43	7,95	8.4	0.3	5
M1	90.4	3.6	-	6	53-56	2,66	3.2	8.5	47
M2	90.4	2.6	1	6	58-61	2,36	2.8	1.2	15
M3	88	4.5	-	7.5	52-55	3,23	4.0	3.5	10
M4	88	3	1.5	7.5	54-58	2,78	3.7	0.6	15
BW1	92	2	1	5	61	4.90	2.2	2.6	5
BW2	90	4	1	5	57	6.13	4.1	1.1	4

* PVdF in B and M electrodes. 4 parts of CMC and 1 part of X4020 in BW electrodes.

** Theoretical BET was calculated taking into account the BET surface area of the powders and their respective weight fraction in the electrode formulation: $BET = \sum_i \phi_{W,i} \times BET_i$

*** The volume fraction is calculated by taking into account the electrode porosity.

Experimental

Electrode preparation - Composite electrodes were composed of $LiNi_{0.5}Mn_{1.5}O_4$ (particle size 1-10µm, specific surface area 0,32m^2/g) as an active material (AM) which was supplied from Delft University, Super P carbon black (CB, Timcal, BET 65m^2/g) and Carbon nanofibres (VGCF-S, BET 35m^2/g) as a conductive additive (C), Polyvinylidene Fluorine (PVdF) from Solvay as a binder (B), and N-Methylpyrrolidone (NMP) as a solvent from Aldrich Chemical company. In aqueous solvent, Carboxylmethyl cellulose (CMC, DS=0.9, M_w=700.000 g/mol Sigma-Aldrich) and a copolymer of styrene, n-butylacrylate from PolymerLatex (X4020) were used as a binder (B).

Pre-hand mixed of measured amount of AM/C/B was made in a mortar. The mixtures were introduced in: (i) a silicon nitride vial with three silicon nitride balls served as mixing media and a Fritsch Pulverisette 7 mixer was used to mill slurry at 700rpm for two hours with PVdF binder and for one hour with CMC binder (1 mL for 400mg), or (ii) a glass bottle with one magnetic stirrer bar then stir it in four days. The PVdF:C ratio was always kept constant at 5:3 following the studies of Battaglia and co-workers.[20,21] For micrometric active particles, such a composition seems the best compromise in terms of mechanical strength of the electrode, electronic and ionic wirings of the active mass with the PVdF binder and carbon black as conductive additive. A higher PVdF content would results in some limitation in the ionic wiring by pores obstruction, and a higher C content would results in some limitations in the electronic wiring as a consequence of insufficient adhesion of the PVdF/C matrix on the active particles.

The powders and solvent were introduced according to the electrode formulations given in Table 1. After being blended in NMP, the slurries were tape-cast directly by using an automatic doctor blade onto aluminium foil in tape casting machine. By varying the height of the blade, the active mass loading of the electrode films was varied. Drying was primarily done at 60°C for 12h and then for 2h at 100 °C under vacuum before battery assembly to remove the remaining solvent.

Study of electrode's texture - Scanning electron microscopy (SEM) was performed by using a JEOL JSM 7600 to investigate textural properties of composite electrodes. The specific surface area was determined by multipoint Brunauer-Emmett-Teller treatment (BET method) from the volumetric adsorption isotherms at 77K of nitrogen gas (instrument ASAP 2010 Physisorption Analyzer). Taking into account the mass and density of each component within the composite electrode, it was possible to calculate the theoretical electrode volume ($V_{calc.}$). Then, the electrode porosity in percent was calculated according to the equation: Porosity (%)

= ($V_{exp.}$ − $V_{calc.}$) × 100/$V_{exp.}$ The value of $V_{exp.}$ was determined from the circular surface area and the thickness of the tested electrode.

Electrical measurements - Electrical measurements were carried out by impedance spectroscopy on dry LNMO electrode/aluminum current collector samples (disks of 0.785 cm²) sandwiched in between two metallic plungers in a standard swagelok cell, using a VMP automatic cycling/data recording system (Biologic). The frequency range was scanned from 10 mHz to 189 kHz. Several compositions were studied at different thicknesses. Six samples were evaluated for each composition. The measure was repeated three times on each sample. The impedance diagrams were resumed in all cases to a single point on the real axis. The resistance, R, was found invariant with the thickness, t, with R ~ 13 ohm. This result implies that the contact resistance between the aluminum foil used as current collector and the composite electrode is dominating the LNMO electrode/aluminum current collector electrical resistance in the dry state. Thus, the electronic resistivity of the dry LNMO composite electrodes was measured on tapes cast on plastic film by using four-point probe mapping system (model 280SI-Microword) with computer controlled stepping motors to move the wafer chuck and the four-point probe. The spacing between each probe is 1mm. Each probe has a contact area radius of 100µm and the load applied on each probe is 60g. The current source is a fixed-output, range-programmable constant-current generator, and provides an appropriate amount of test current to the sample under test. It is automatically selected by the measurement board during the measurement sequence.

Electrochemical testing - Half cells: two-electrode Swagelok™ test cells comprise (i) a 0.78 cm^2 disc of composite positive electrode (ii) a porous glass paper as separator soaked in an electrolyte LP30 [1M $LiPF_6$ solution in dimethyl carbonate-ethylene carbonate (1:1)] and (iii) a 0.78 cm^2 Li metal disc as the negative and reference electrode. The LNMO/Li haft cells were assembled in a dry Ar-filled glove box. In order to evaluate the cycling performances of LNMO materials, cell cycling was performed at 20°C, monitored by a VMP™ system (Biologic) in a galvanostatic mode. Charge – discharge tests were carried out between 3.5 – 4.9V versus Li^+/Li. All composite electrodes were studied with the same rate (C/2.5 and D/2.5).

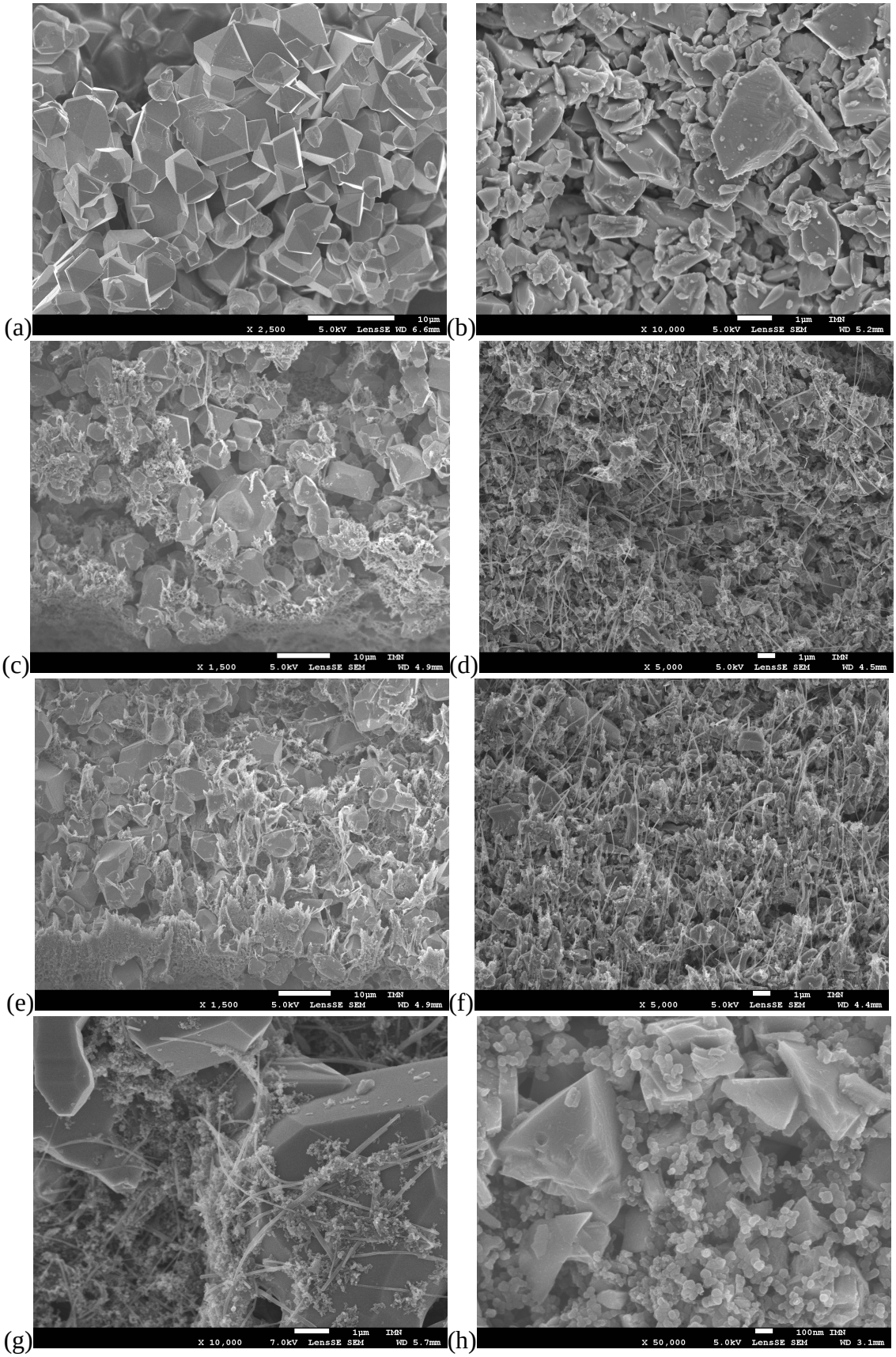

Figure 1. SEM observations of LNMO material and different composite electrodes (cross-section except noted): (a) pristine LNMO × 2,500, (b) ball milled (in NMP) LNMO × 10,000, (c) M1 × 1,500, (d) B2 × 5,000, (e) M3 × 1,500, (f) B6 × 5,000, (g) M2 surface × 10,000 and (h) B3 surface × 50,000.

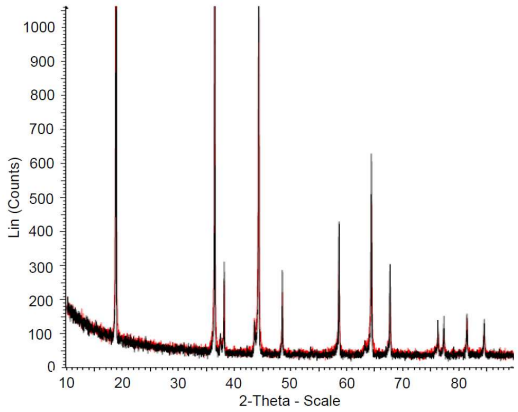

Figure 2. XRD diagram of LNMO powders before (black line) and after ball milling (red line) in NMP.

Results and discussion

The results achieved with electrodes prepared with the PVdF binder in NMP are first described, while those achieved aqueous binders in water are discussed with less details at the end.

Texture and electrical properties - SEM images of LNMO before and after ball milling (BM) are shown in Figure 1a-b. Well-crystallized particles of LNMO with average diameter of 3 to 8µm are observed in Figure 1a. Ball milling breaks the large LNMO particles down into smaller ones (Figure 1b) with significant increase of BET from 0.32 to 3.55 $m^2 g^{-1}$ compared to pristine material. However, X-Ray diffraction (Figure 2) points out no modification of the material crystallization after ball milling.

The typical textures of the electrodes are observed by SEM in Figure 1c-h, while the dry electronic resistivity and porosity are given in **Table 1**. On the whole, the electrodes show fairly good homogeneity, especially those prepared by using BM as demonstrated by the lower standard deviation of their electronic resistivity (**Table 1**), which is lower than 8% compared to more than 10% for MS. As generally observed with the PVdF binder, CB aggregates are well mixed with the polymer. [20,21] Indeed, in the electrodes prepared by MS, the CB/PVdF masses form soft adhesive and conductive connections between LNMO particles (Figure 1c,e). Moreover, these CB/PVdF masses tend to form a network, which degree of percolation increases with increasing the CB+PVdF content (compare Figure 1c and e: in electrode M1, there are zones of LNMO particles without any CB+PVdF in between them, contrarily to M3). In some electrodes, part of the CB content was substituted for carbon nanofibres (VGCF). The latter conductive additive, thanks to its fibrous shape, tends to form conductive bridges through and between the CB/PVdF masses (Figure 1g), which improves the electrical connectivity, as discussed later with Figure 3a. However, careful examination of

the SEM images of electrodes prepared by MS (not shown in Figure 1) reveals the occurrence of some bundles of un-individualized VGCF, demonstrating that MS is not efficient enough to reach homogeneous distribution of such kind of conductive additives. A better homogeneity would be reached by using a stirring device with higher mixing energy such as a dissolver. However, small volumes (typically 0.75mL) cannot be processed with dissolvers. The electrodes prepared by ball milling (Figure 1d,f,h) show visually higher compactness with lower porosity. Higher porosity of the electrodes prepared with magnetic stirring (MS) (Figure 1c,e,g) compared to BM is likely due to the preservation with the former mixing method of the angular shape and large size of the pristine LNMO particles, which can hardly pack without a calendaring step of the composite electrode, and to the lower content of binder and carbon additives in their compositions. As a consequence of the smaller size of LNMO particles in BM electrodes, one can also note the more homogeneous mixing of the LNMO and CB particles, altogether bridged by the PVdF binder (Figure 1h). Furthermore, in electrodes prepared by BM, a very good distribution of VGCF could be achieved (Figure 1d,f).

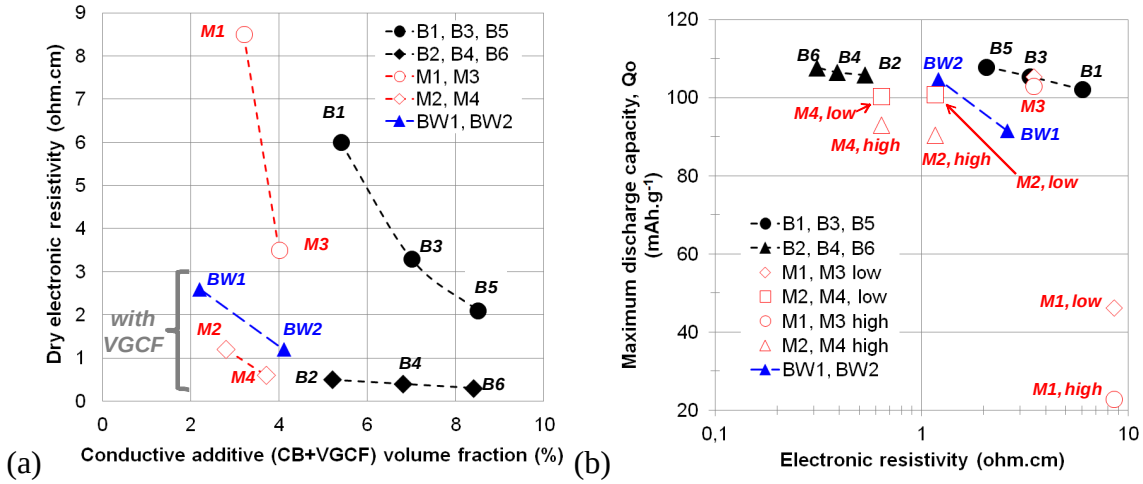

Figure 3. (a) Dry electronic resistivity as a function of volume fraction of conductive additive for different electrodes. (b) Maximum discharge capacity as a function of the dry electronic resistivity (log scale) for the different electrodes. For twin batteries there is less than 1% difference, except for M1 (10% and 20% for low and high loadings, respectively).

The dry electronic resistivity decreases with increasing the amount of conductive additive whatever mixing method used (Figure 3a), as generally observed. [22,23,24] With same conductive additive volume fraction, the resistivity decreases sharply by substituting VGCF for small amount of CB. It is well known, indeed, that as a consequence of their shape factor, conductive fibers allow forming better connected conducting network and therefore provides

higher conductivity than CB particles. [25,26,27] CB and VGCF thus fulfill complementary electrical functions in the electrode: CB improves the contact between the particles of the active electrode material whereas VGCF creates the conductive path through the electrode. In addition, Figure 3a and Table 1 show that in order to reach same dry electronic resistivity, the amount of conductive additive (and binder) needed is higher with BM electrodes than in MS ones (for example compare B3 and M3 or B2 and M4). It is consistent with the decrease in the LNMO particle size in BM electrodes. Larger active particles need less conductive additive [28] and less binder [29] to ensure percolation of the conductive network and reach good mechanical properties.

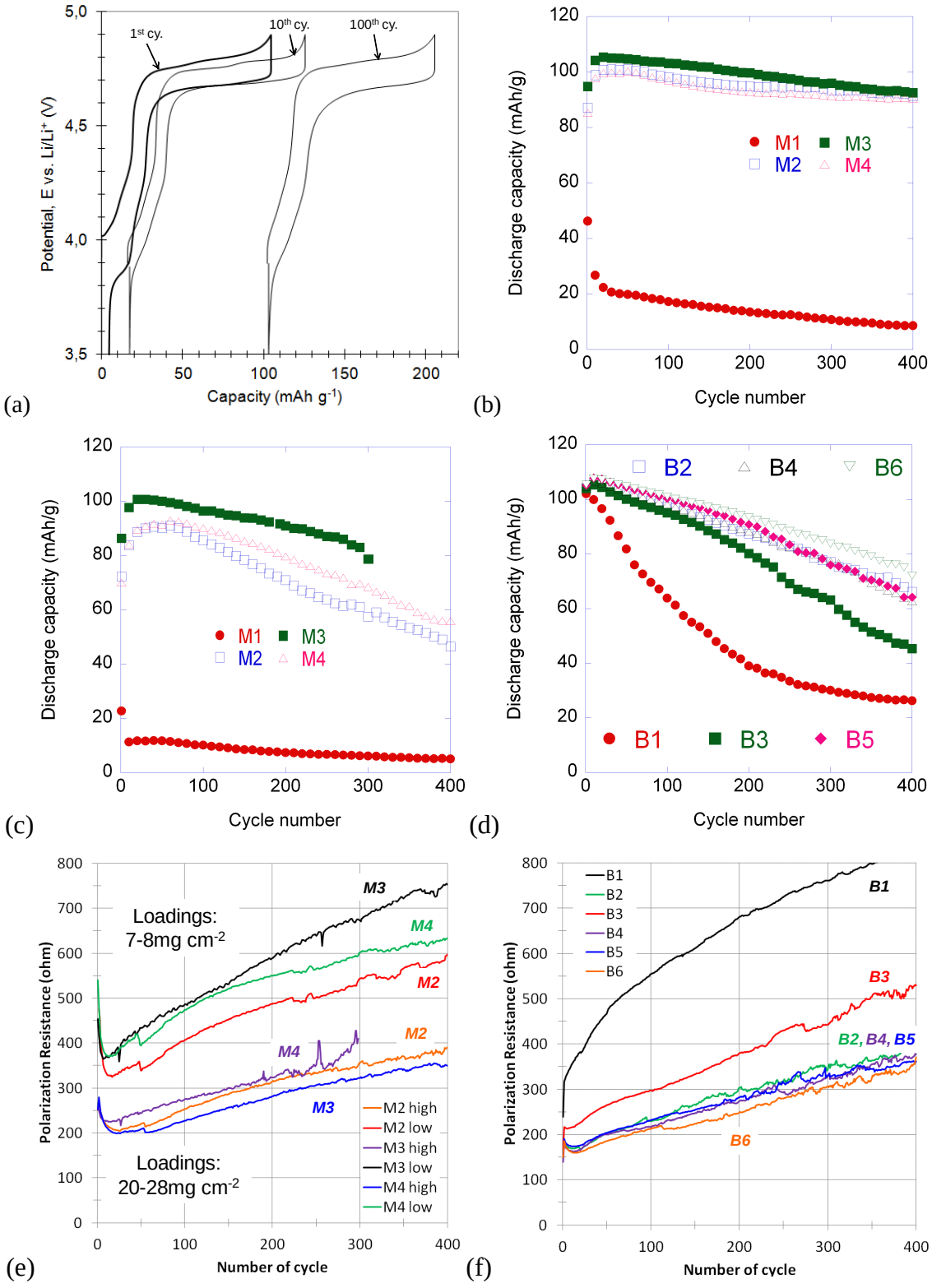

Figure 4. (a) voltage profile versus specific capacity for LNMO/Li cell with M3 electrode (LNMO loading of 7-8 mg cm^{-2}), cycled between 3.5 and 4.9 V with LP30 electrolyte at C/2.5 and D/2.5 rate and at room temperature. (b-d) Discharge versus cycle number of different electrode formulation prepared by stirring (b) LNMO loading of 7-8 mg cm^{-2}, (c) 20-28 mg cm^{-2} (close symbol: without VGCF, open symbol with VGCF) and (d) ball milling (15-18 mg cm^{-2}). Polarization resistance versus cycle number for different electrode formulation prepared by (e) stirring and (f) ball milling.

Electrochemical properties - Charge (de-lithiation) and discharge (lithiation) voltage profile versus specific capacity at several selected cycles for LNMO/Li cell with electrode M3 (LNMO loading of 7-8 mg cm^{-2}) is shown in Figure 4a. It was cycled between 3.5 and 4.9 V with 1M $LiPF_6$ solution in dimethyl carbonate-ethylene carbonate (1:1) electrolyte (LP30) at C/2.5 and D/2.5 rate and at room temperature. The major charge/discharge reaction occurs at more than 4.6 V ($Ni^{2+} \leftrightarrow Ni^{4+}$ redox reaction) while a minor redox reaction occurs below 4.4 V ($Mn^{3+} \leftrightarrow Mn^{4+}$ redox reaction by Mn^{3+} impurities). [30,31,32] At the first cycle, the specific charge, Q_c, and discharge capacity, Q_d, is 104.5 and 99.5 mAh g^{-1}, respectively, from which a coulombic efficiency (CE) is calculated to be 95.4% ($CE = Q_d/Q_c$). This poor CE is due to parasitic reactions at high potentials that consume electric charges from the oxidative decomposition of electrolyte on LNMO and carbon additives, partially reversible PF_6^- (de)insertion into the carbon additives and corrosion of the stainless steel parts of the electrochemical cell. [9-18] At the 10^{th} cycle one can note an increase of the reversible capacity up to 108.5 mAh g^{-1} and an improvement of the CE at 98.9%. The former phenomenon could be due to the better wetting of the LNMO particles by the liquid electrolyte that progressively swells the C/PVdF masses and penetrates into the smallest pores of the composite electrode. The improvement of CE is explained by the formation during the first cycle of a film at the surface of LNMO and C particles from the decomposition products of the electrolyte. This surface film likely decreases the contact between the electrode and cell materials and the electrolyte and then decreases to some extent the parasitic reactions. After 100 cycles, the reversible capacity has decreased to 102.6 mAh g^{-1} and the CE is stabilized at 99.2%. Moreover, a slight but appreciable increase in the polarization is observed, which is generally accounted for by the steady growth of organic-rich surface films. Finally, the charge and discharge endpoints slipped to higher absolute capacities, because of the parasitic reactions in the cells. [10] With number of cycles (not shown), all these phenomena are enlarged (lower reversible capacity, larger polarization and stronger slippage), indicating parasitic reactions continue causing degradation of the composite electrode. The capacity fade is generally explained by the loss of active particles that are disconnected from the C/PVdF network as a consequence of formation of thick insulating surface films at contact spots between C and LNMO and/or C degradation. [9-18]

Discharge capacity versus cycle number for LNMO/Li cells is shown in Figure 4c-e, for electrodes M1 to M4 prepared by magnetic stirring and LNMO loadings of 7-8 mg cm^{-2} (Figure 4b) and 20-28 mg cm^{-2} (Figure 4c), and for electrodes B1 to B6, prepared by ball milling and LNMO loadings of 15-18 mg cm^{-2} (Figure 4d). First, we can note that electrode

M1 show very poor performance. The initial polarization was high (not shown) and the initial capacity is only a fraction of the nominal value. Such poor performance can be explained by defects in cohesion and insufficient C percolation, as observed on SEM images for these electrodes (see Figure 1c for M1). All other electrodes showed a fairly high initial capacity that increases to a maximum value, Q_0, before showing a steady decline in the capacity (Figure 4b-d). Q_0 values are plotted in Figure 3b versus the dry electronic resistivity of the same electrodes. The former value gives an insight about the fraction of LNMO particles that are truly electrochemically active and the latter measures the quality of electronic percolation in the electrode. [33] Main facts shown in Figure 3b is that a fraction of LNMO particles (~20%) is not electronically wired in the thicker electrodes prepared by stirring, M2 and M4, which contain VGCF, although these electrodes show very low electronic resistivity. Discrepancy between the quality of the wiring of the active mass and the dry electronic resistivity has already been reported. The wiring of the active mass depends on the electronic percolation and area density of contact points between the active mass and the electronically conductive network. [34,35] This result is consistent with the SEM observations of these electrodes showing some bundles of un-individualized VGCF, i.e. non-homogeneous dispersion of the latter conductive additive. Thicker electrode are more severely impacted by defects and non-homogeneities introduced during electrode fabrication, which result in inadequate connectivity within the electrode and partial isolation of some of the active material. [36] All other electrodes show a Q_0 value between 100 and 108 mAh g^{-1}.

The fading of the discharge capacity is less severe for composite electrodes with low active mass loading (Figure 4b and c). Indeed, for M2 to M4 with 7-8 mg cm^{-2}, the fading is less than 0.035 mAh g^{-1} per cycle, while for M2 to M4 with 20-28 mg cm^{-2}, the fading is more than 0.070 mAh g^{-1} per cycle, i.e. two times larger. This fading of the capacity likely finds its origin in the parasitic reactions. [9-18] The coulombic efficiency, CE, at the 1st cycle of the different electrodes is plotted in Figure 5a as a function of the theoretical specific surface area of the electrodes, which was calculated from the specific surface area of the different powders and their respective weight fractions in the composition of the composite electrode (see Table 1). Noteworthy, no difference was measured for low and high active mass loadings in the case of M2 to M4. In agreement with previous works, [9-13] the 1st cycle CE is found to increase when the specific surface area increases, the most significant increase in specific surface area and 1st cycle CE being seen for ball milled electrodes compared to stirred ones. However, after the initial cycles, the CE stabilizes to a mean ~99.25%, rather independent on the different parameters of the electrode (i.e. preparation method, formulation, active mass

loading), as can be seen in Figure 5b. Nevertheless, it is possible that by using high precision chargers the influence of the parameters of the electrode could be highlighted. [10,11]

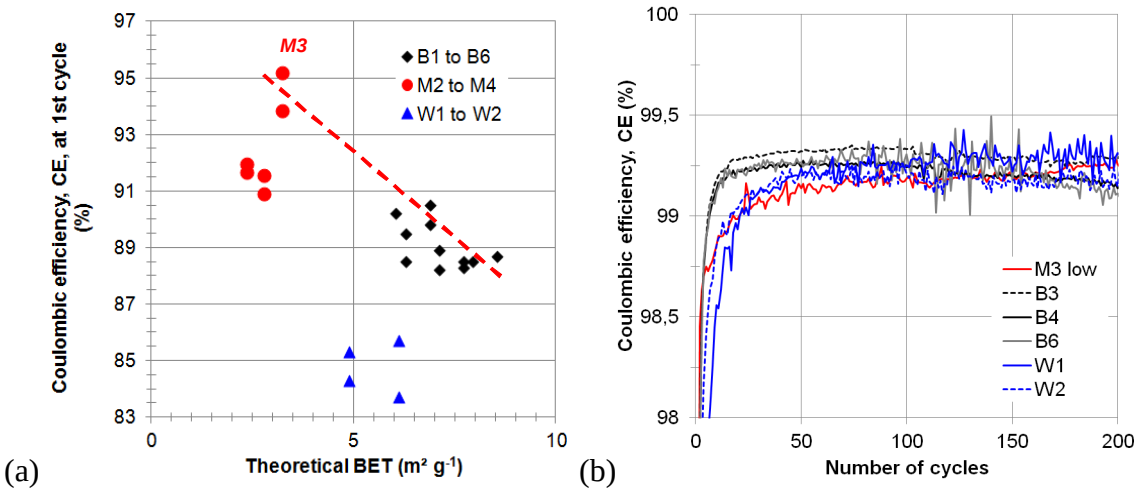

Figure 5. (a) Coulombic efficiency at 1st cycle for the different kinds of electrodes as a function of the theoretical BET (see Table 1). The line (- - -) is drawn to guide the eyes about the best electrodes. (b) Coulombic efficiency for selected electrodes as a function of cycle number (colour on line).

In Figure 4e and f is shown the variation in the electrode polarization resistance, R_{pol}, as a function of the number of cycles for all electrodes, except M1 that displayed very poor performance. It was determined from the difference in the mid-charge and mid-discharge potentials, $E_{ch} - E_{disch}$, and the current, I, as

$$R_{pol} = (E_{ch} - E_{disch}) / I \quad (1)$$

All electrodes show a steady increase in R_{pol} with cycling, which can be attributed to the growth of electrolyte degradation surface films at contact spots between C and LNMO and/or C degradation. [9-18] In the case of MS prepared electrodes, one can note the larger R_{pol} of thin versus thick electrodes, a classical trend when R_{pol} is dominated by the charge transfer resistance at the surface of the active mass. If R_{pol} was dominated by the electronic or ionic wiring of the active mass, through the carbon network or the porous network filled by the electrolyte, R_{pol} would be higher for the thicker electrodes. [37,38] The steady increase of R_{pol} upon cycling is consistent with the continuous occurrence of parasitic reactions upon cycling, as detected by the low CE of about 99%, and the thickening of resistive film at the LNMO particles/electrolyte interface and/or at the contact spots between the LNMO active mass and the C conductive network. One can note that R_{pol} does not grow faster for thick than for thin electrodes, although the fading is accentuated for the former electrodes compared to the latter.

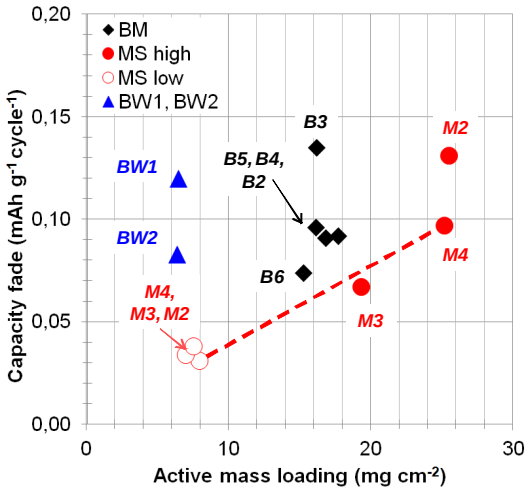

Figure 6. Capacity fade after 200 cycles from Q_0 as a function of the LNMO loadings for the different electrode formulation prepared by MS with (○) LNMO loading of 7-8 mg cm^{-2}, (●) 20-28 mg cm^{-2}, (◆) BM (15-18 mg cm^{-2}) and (▲) BW (6-7 mg cm^2). The line (- - -) is drawn to guide the eyes about the best electrodes. For twin batteries there is less than 5% difference, except for BW1 (22%), B3 (16%).

The capacity lost per cycle (capacity fade) over 200 cycles (after the maximum in discharge capacity) is given for all electrodes as a function of the LNMO loading in Figure 6. The worse formulations (B1 and M1) however are not considered here. A line is drawn to guide the eyes through the best electrodes that show the lowest fading at a given active mass loading. The comparison between electrodes with same formulation and same preparation method (M2, M3 and M4) clearly illustrates the critical influence of the active mass loading on the fading of the capacity. Such kind of relationship is also observed for silicon-based negative electrodes that similarly suffer from parasitic reactions of the electrolyte at low potential in addition to mechanical disintegration of the electrode. [39] A dramatic increase of the capacity fade is seen with increase of the active mass loading. Thicker electrodes are more severely impacted by defects and non-homogeneities introduced during electrode fabrication, which result in inadequate connectivity within the electrode [36], adhesion problems, [40] and poorer cyclability. [41,42,43]

Some electrodes with different formulations have same active mass loading and can thus be directly compared in Figure 6. Formulation M2 is clearly worse than M4, which could be attributed to the higher content in conductive additive in M4. Similarly, formulation B3 is clearly worse than B2, B4, B5 and B6, which could also be attributed to the higher content in conductive additive in B5 and in B6 or to the lower electronic resistivity in B2 and B4 (as a consequence of the presence of VGCFs in the latter electrodes). Similarly, the superiority of B6 over B2, B4 and B5 could also be attributed to the higher content in conductive additive in

B6 compared to B2 and B4 or to the lower electronic resistivity in B6 than in B5 (as a consequence of the presence of VGCFs in the former electrode). Also mentioning the very poor cyclability of B1 and M1 electrodes, all these results pinpoint the influence of the conductive additive content and/or of the electronic resistivity, i.e. of the electronic wiring, on the capacity fading of the LNMO-based electrodes. Increasing the carbon conductive additive content is a standard strategy to improve the cyclability of both negative and positive electrodes. [44,45] Finally, the comparison of M3 with B2, B4, B5 and B6 highlights the better performance of the electrode prepared by gentle stirring over that of electrodes prepared by high energy mixing. Such result can be attributed to lower specific surface of the bigger LNMO particles in M3. As illustrated in Figure 5a, the higher specific surface area of the smaller LNMO particles in B2, B4, B5 and B6 results in more parasitic reactions at the first cycle.

Noteworthy, calendaring has been reported to improve the cyclability of some composite electrodes. [46,47] Trials were made with B6 electrode that was calendared below 4 or 8 tons cm^{-2}, however they were not successful in decreasing the capacity fading (not shown).

Aqueous processed LNMO electrodes were prepared with the carboxymethyl cellulose (CMC) binder. However, the results show poorer performance of aqueous formulations. The electrode BW1 and BW2 show a fairly low dry electronic resistivity of 2.6 and 1.15 ohm cm (Figure 3a), respectively, but a strong fading of 0.165 and 0.085 mAh g^{-1} $cycle^{-1}$ (Figure 6), respectively, considering their low active mass loadings of 6-7 mg cm^{-2}. Such poor performance can be attributed to significantly lower CE in the first 50 cycles (Figure 5), which could be a consequence of the presence of trace impurities of water driving detrimental HF formation from $LiPF_6$ decomposition. [48] Figure 7 illustrates the occurrence of the parasitic reactions by showing SEM pictures with high-magnification of BW1 electrode before and after 10 cycles. After 10 cyles a glue is covering not only the LNMO particles but also the C ones.

(a) 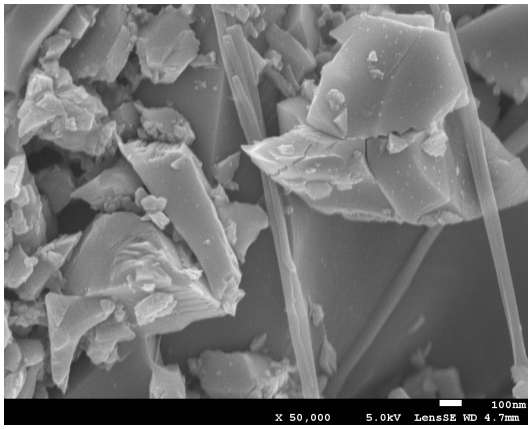

(b) 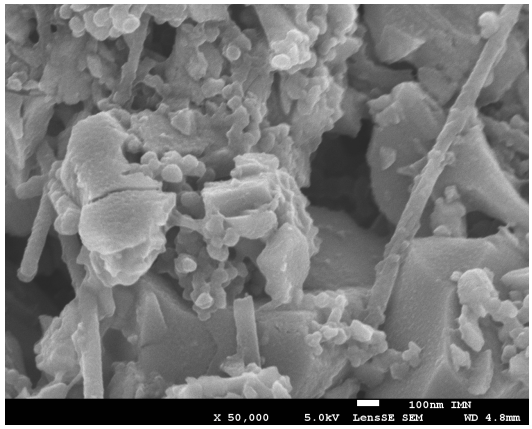

Figure 7. SEM (× 50,000) of BW1 electrode (a) before and (b) after 10 cycles between 3.5 and 4.9 V with LP30 electrolyte at C/2.5 and D/2.5 rate and at 20°C. The cell was disassembled and the electrode soaked into DMC.

Conclusion

In this work, the influence of the composite electrode formulation on the cyclability of LNMO electrodes was studied, for industry-relevant active mass loadings, i.e. up to 28 mg cm^{-2} (surface capacity up to ~3 mAh cm^{-2}).

Two different mixing methods were used to make the electrodes: a high energy one, ball milling and a low energy one, stirring. In the latter method, the particle size of the pristine material (3-8 µm) was unaffected while in the former method it was much decreased to 1µm and less. The inactive PVdF binder and conductive C contents was varied, but the PVdF:C ratio was always kept constant at 5:3. Carbon black (CB) or mixture of carbon nanofibres (VGCF) were used as C. To reach same levels of conductivity, electrodes prepared by ball milling required higher contents of PVdF+C additives than electrodes prepared by stirring. The former electrodes show a more homogeneous distribution of PVdF+C additives than the latter ones.

Parasitic reactions with the electrolyte are evidenced by the poor CE, which value at first cycle is ~85-95% and then stabilizes at ~99.25%. These parasitic reactions lead to continuous increase of the electrode polarization and capacity fade, likely through the loss of electrical connections between the active mass and the C network. The cyclability of the electrodes is degraded for ball milled electrodes, as seen in lower CE at first cycle, as a consequence of higher specific surface area of the electrodes and increased parasitic reactions. The cyclability of the electrodes was severely decreased by increasing the active mass loading, more heavily loaded (thicker) electrodes having more defects in terms of electronic percolation or adhesion and cohesion. Whatever the preparation method, cyclability is

improved by increasing the amount of C additives or by substituting part of CB for VGCF. However, this strategy does not succeed in improving the CE.

Electrodes prepared in water with aqueous CMC binder showed poorer cyclability.

Acknowledgements

Financial support provided by the *European Commission (EC)*, through the project EuroLiion (NMP3-SL-2010-265368) is gratefully acknowledged.

References

[1] Q. Zhong, A. Bonakclarpour, M. Zhang, Y. Gao, J.R. Dahn, J. Electrochem. Soc. 144 (1997) 205–213.
[2] M. Kunduraci, G. G. Amatucci, J. Electrochem. Soc. 153 (2006) A1345.
[3] S. Patoux, L. Sannier, H. Lignier, Y. Reynier, C. Bourbon, S. Jouanneau, F. Le Cras, S. Martinet, Electrochim. Acta 53 (2008) 4137.
[4] E. S. Lee, K. W. Nam, E. Y. Hu, A. Manthiram, Chem. Mater. 24 (2012) 3610.
[5] J. Cabana, M. Casas-Cabanas, F. O. Omenya, N. A. Chernova, D. L. Zeng, M. S. Whittingham, C. P. Grey, Chem. Mater. 24 (2012) 2952.
[6] J. Xiao, X. L. Chen, P. V. Sushko, M. L. Sushko, L. Kovarik, J. J. Feng, Z. Q. Deng, J. M. Zheng, G. L. Graff, Z. M. Nie, D. W. Choi, J. Liu, J. G. Zhang, M. S. Whittingham, Adv. Mater. 24 (2012) 2109.
[7] L. Wang, H. Li, M. Courty, X. Huang, E. Baudrin, J. Power Sources 232 (2013) 165.
[8] X. H. Ma, B. Kang, and G. Ceder, J. Electrochem. Soc. 157 (2010) A925.
[9] Y. Talyosef, B. Markovsky, R. Lavi,G. Salitra, D. Aurbach, D. Kovacheva, M. Gorova, E. Zhecheva, and R. Stoyanova, J. Electrochem. Soc. 154 (2007) A682.
[10] S. R. Li, C. H. Chen, X. Xia, J. R. Dahn, J. Electrochem. Soc. 160 (2013) A1524.
[11] S. R. Li, C. H. Chen, J. Camardese, and J. R. Dahn, J. Electrochem. Soc. 160 (2013) A1517.
[12] J. Cabana, H. H. Zheng, A. K. Shukla, C. Kim, V. S. Battaglia, and M. Kunduraci, J. Electrochem. Soc. 158 (2011) A997.
[13] J. Mao, K. Dai, Y. Zhai, Electrochim. Acta 63 (2012) 381.
[14] T. Yoon, D. Kim, K. H. Park, H. Park, S. Jurng, J. Jang, J. H. Ryu, J. J. Kim, and S. M. Oh, J. Electrochem. Soc. 161 (2014) A519.
[15] X. Li, Y. Chen, C. C. Nguyen, M. Nie, and B. L. Lucht, J. Electrochem. Soc. 161 (2014) A576.
[16] J. Syzdek, M. Marcinek, R. Kostecki, J. Power Sources 245 (2014) 739.
[17] N.N. Sinha, J.C. Burns, R.J. Sanderson, J. Dahn, J. Electrochem. Soc. 158 (2011) A1400.
[18] X. Chen, W. Xu, J. Xiao, M.H. Engelhard, F. Ding, D. Mei, D. Hu, J. Zhang, J.-G. Zhang, J. Power Sources 213 (2012) 160.
[19] E. Vidal, J. M. Rojo, M. C. García-Alegre, D. Guinea, E. Soto, J. M. Amarilla, Electrochim. Acta 108 (2013) 175.
[20] H. Zheng, G. Liu, X. Song, P. Ridgway, S. Xun, and V. S. Battaglia, J. Electrochemical Soc. 157 (2010) A1060.
[21] H. Zheng, R. Yang, G. Liu, X. Song, and V. S. Battaglia, J. Phys. Chem. C 116 (2012) 4875.
[22] S. Mandal, J. M. Amarilla, J. Ibanez, J. M. Rojo, J. Electrochem. Soc. 148 (2001) A24.
[23] Dominko, R., Gaberscek, M., Drofenik, J., Bele, M., and Jamnik, J., Electrochim. Acta 48 (2003) 3709.
[24] D. Guy, B. Lestriez, R. Bouchet, V. Gaudefroy, D. Guyomard, J. Electrochem. Soc. 153 (2006) A679.
[25] C. W. Wang, K. A. Cook, A. M. Sastry, J. Electrochem. Soc. 150 (2003) A385.
[26] M. S. Wu, J. T. Lee, P. C. J. Chiang, J. C. Lin, J. Mater Sci. 42 (2007) 259.
[27] F. Mizuno, A. Hayashi, K. Tadanaga, M. Tatsumisago, J. Electrochem Soc. 152 (2005) A1499.
[28] D. He and N.N. Ekere, J. Phys. D: Appl. Phys., 37 (2004) 1848.
[29] B. Lestriez, C. R. Chimie 13 (2010) 1341.
[30] Y. Terada, K. Yasaka, F. Nishikawa, T. Konishi, M. Yoshio, I. Nakai, J. Solid State Chem. 156 (2001) 286.
[31] X. H. Ma, B. Kang, and G. Ceder, J. Electrochem. Soc. 157 (2010) A925.

[32] T. Yoon, S. Park, J. Mun, J. H. Ryu, W. Choi, Y.-S. Kang, J.-H. Park, S. M. Oh, J. Power Sources 215 (2012) 312.
[33] C. Fongy, A.C. Gaillot, S. Jouanneau, D. Guyomard, B. Lestriez, J. Electrochem. Soc. 157 (2010) A885.
[34] R. Dominko, M. Gaberscek, J. Drofenik, M. Bele, and S. Pejovnik, Electrochem. Solid-State Lett. 4 (2001) A187.
[35] D. Guy, B. Lestriez, R. Bouchet, D. Guyomard, J. Electrochem. Soc. 153 (2006) A679.
[36] G. Chen, T. J. Richardson, J. Power Sources 195 (2010) 5387.
[37] M. Gaberscek and J. Jamnik, Solid State Ionics 177 (2006) 2647.
[38] C. Fongy, S. Jouanneau, D. Guyomard, J-C. Badot, B. Lestriez, J. Electrochem. Soc. 157 (2010) A1347.
[39] D. Mazouzi, , D. Reyter, M. Gauthier, P. Moreau, D. Guyomard, L. Roué, B. Lestriez, "Very high surface capacity with Si negative electrodes embedded in copper foam as 3D current collector", Adv. Energy Mater. (2014) DOI: 10.1002/aenm.201301718
[40] C-C. Li, Y-W. Wang, J. Electrochem. Soc. 158 (2011) A1361.
[41] J. H. Lee, U. Paik, V. A. Hackley, Y. M. Choi, J. Power Sources 161 (2006) 612.
[42] Z. Zhang, T. Zeng, C. Qu, H. Lu, M. Jia, Y. Lai, J. Li, Electrochim. Acta 80 (2012) 440.
[43] K. C. Kil, M. E. Lee, G. Y. Kim, C-W. Cho, K. Kim, G. Kim, U. Paik, J. Phys. Chem. C 115 (2011) 16242.
[44] Michael E. Spahr, "Carbon-Conductive Additives for Lithium-Ion Batteries" in Lithium-Ion Batteries (2009).
[45] D.H. Jang, S.M. Oh, Electrochim. Acta 43 (1998) 1023.
[46] K.A. Striebel, A. Sierra, J. Shim, C.W. Wang, A.M. Sastry, J. Power Sources 134 (2004) 241.
[47] C-C. Li, Y-S. Lin, J. Power Sources 220 (2013) 413.
[48] M. Moshkovich, M. Cojocaru, H. E. Gottlieb, D. Aurbach, J. Electroanal. Chem. 497 (2001) 84.

Résumé

Formulation d'électrode à base de Si et $LiNi_{0.5}Mn_{1.5}O_4$ pour batteries lithium ion appliquées à la traction électrique

La batterie lithium-ion est l'une des technologies de stockage de l'énergie les plus prometteuses pour permettre le développement des transports propres. Dans ce but il est cependant nécessaire de rechercher des matériaux d'électrode de batterie lithium-ion adaptés et qui satisfont différentes conditions de : (i) fortes capacités spécifique ($Ah.kg^{-1}$) et volumétrique ($Ah.L^{-1}$); (ii) grande différence de potentiel entre les deux électrodes ; (iii) haute sécurité et respect de l'environnement. Ainsi, une transition du graphite au silicium de forte capacité et des composés à base de cobalt ou de fer au matériau à haut potentiel $LiNi_{0.5}Mn_{1.5}O_4$ (LNMO) est examinée ici.

Dans cette étude, nous avons identifié des formulations d'électrodes optimisées, premièrement pour un Si nanométrique avec de la carboxymethyl cellulose (CMC), de l'acide poly(acrylique-co-maléique) et du graphene à la négative ; deuxièmement pour un LNMO micrométrique avec du polyfluorure de vinylidène (PVdF) et des nanofibres de carbone (CNF) à la positive. Ces formulations possèdent de bonnes performances électrochimiques et ont des propriétés appropriées à leur mise en œuvre sur des machines d'enduction industrielles. Pour atteindre ces buts, nous avons fait des investigations sur les encres d'électrode (comportement rhéologique, granulométrie, potentiel zéta, tests de sédimentation) et des caractérisations sur les électrodes (analyse de leur texture par MEB-EDX, porosité, comportements mécanique, électrique, et électrochimique).

Mots-clés: Batterie lithium-ion; silicium; $LiNi_{0.5}Mn_{1.5}O_4$; Formulation d'électrode.

Electrode formulation of Si and $LiNi_{0.5}Mn_{1.5}O_4$ for Li-ion battery applied to electric traction

Rechargeable lithium-ion battery is one of the most promising energy storage technologies to enable a various range of clean transportations. To meet requirements of these automotive applications, it is necessary to find suitable electrode materials which satisfy several conditions: (i) high specific capacity ($Ah.kg^{-1}$) and volumetric capacity ($Ah.L^{-1}$); (ii) high difference of potential between positive and negative electrodes; (iii) high safety and environmental standards. This way, a shift from graphite to much higher capacity silicon-based and from cobalt or iron-based to high voltage $LiNi_{0.5}Mn_{1.5}O_4$ (LNMO) is examined here.

This study successfully defined the optimized electrode formulations first with nanometric Si coupled with carboxymethyl cellulose (CMC), poly (acrylic-co-maleic) acid (PAMA) and graphene at the negative side; then for micrometric LNMO material coupled with polyvinylidene fluorine (PVdF) and carbon nanofibres (CNF) at the positive side. These formulations possess good electrochemical performance and satisfactory properties for processing on industrial coating machine. In order to achieve this purpose, characterization of electrode slurries (e.g., rheological behaviour, particle size distribution, zeta potential measurements, settling tests) were investigated together with elaboration (e.g., tape casting, calendaring, drying) and characterization of the electrodes (e.g., texture analysis through SEM, EDX observations, measurements of porosity, mechanical, electrical and electrochemical behaviours).

Keywords: Lithium-ion battery; Silicon; $LiNi_{0.5}Mn_{1.5}O_4$; Electrode formulation.